STUDIES ON THE SYNTHESIS AND SINTERING OF NANOCRYSTALLINE B_4C AND YSZ

By

SOJA K VIJAY

CHEM02201304007

Indira Gandhi Centre for Atomic Research,
Kalpakkam, Tamil Nadu, India

A thesis submitted to the
Board of Studies in Chemical Sciences
In partial fulfillment of requirements
for the Degree of

DOCTOR OF PHILOSOPHY

of

HOMI BHABHA NATIONAL INSTITUTE

April, 2018

Homi Bhabha National Institute

Recommendations of the Viva Voce Committee

As members of the Viva Voce Committee, we certify that we have read the dissertation prepared by Ms. Soja K Vijay entitled "Studies on the synthesis and sintering of nanocrystalline B_4C and YSZ" and recommend that it may be accepted as fulfilling the thesis requirement for the award of Degree of Doctor of Philosophy.

Chairman - Dr. K. Ananthasivan		Date: 7/3/19
Guide / Convener - Dr. S. Anthonysamy	S. Anthonysamy	Date: 7/3/19
Examiner - Prof. Govind S. Gupta	G.S. Gupta	Date: 07/03/19
Member 1 - Dr. N.V. Chandra Shekar	N.V. Chandra Shekar	Date: 7/3/19
Member 2 - Dr. Saroja Saibaba	S. Sai	Date: 07/03/2019
Member 4 - Dr. V. Chandramouli (Technology Advisor)	Chandramouli	Date: 07/03/19

Final approval and acceptance of this thesis is contingent upon the candidate's submission of the final copies of the thesis to HBNI.

I/We hereby certify that I/we have read this thesis prepared under my/our direction and recommend that it may be accepted as fulfilling the thesis requirement.

Date:

Place: 7.3.'19

S. Anthonysamy

Dr. S. Anthonysamy
(Guide)

STATEMENT BY AUTHOR

This dissertation has been submitted in partial fulfillment of requirements for an advanced degree at Homi Bhabha National Institute (HBNI) and is deposited in the Library to be made available to borrowers under rules of the HBNI.

Brief quotations from this dissertation are allowable without special permission, provided that accurate acknowledgement of source is made. Requests for permission for extended quotation from or reproduction of this manuscript in whole or in part may be granted by the Competent Authority of HBNI when in his or her judgment the proposed use of the material is in the interests of scholarship. In all other instances, however, permission must be obtained from the author.

Soja K Vijay

DECLARATION

I, hereby declare that the investigation presented in the thesis has been carried out by me. The work is original and has not been submitted earlier as a whole or in part for a degree / diploma at this or any other Institution / University.

Soja K Vijay

List of Publications arising from the thesis

I. Published:

1. Soja K. Vijay, R. Krishna Prabhu, V. Chandramouli, S. Anthonysamy, Synthesis of nanocrystalline boron carbide by sucrose precursor method-optimization of process conditions, Ceram. Int., 44 (5) (2018) 4676-4684.
2. Soja K. Vijay, V. Chandramouli, Shabana Khan, P.C. Clinsha, S. Anthonysamy, Microwave-assisted gel-combustion synthesis of 8 mol.% YSZ: A study of the effect of fuel on the ionic conductivity, Ceram. Int., 40 (10) B (2014) 16689-16699.

II. Communicated:

1. Soja K Vijay, D. Annie, V. Chandramouli, R. Krishna Prabhu, G.V. Suresh, S. Anthonysamy, Freeze-drying: An effective technique to improve the homogeneity of the precursor for the synthesis of boron carbide (Under Review-Trans. Indian. Ceram. Soc.).
2. Soja K Vijay, R. Krishna Prabhu, V. Chandramouli, D. Annie, S. Anthonysamy, Microwave-assisted preparation of precursor for the synthesis of nanocrystalline boron carbide (Ceram. Int.).

III. Manuscripts under preparation:

1. Soja K Vijay, R. Krishna Prabhu, V. Chandramouli, S. Anthonysamy, Spark plasma sintering of nanocrystalline boron carbide synthesized by precursor method.
2. Soja K Vijay, V. Chandramouli, R. Krishna Prabhu, S. Anthonysamy, Sintering of nanocrystalline boron carbide by hot pressing.

IV. Conference presentations:

1. Soja K Vijay, R. Krishnaprabhu, V. Chandramouli, S. Anthonysamy, A novel method for the synthesis of nanocrystalline boron carbide, Theme Symposium on Materials for Inclusive Development, MRSI-AGM 2015, February 9-11, University of Rajasthan, Jaipur.

2. Soja K Vijay, R. Krishna Prabhu, V. Chandramouli, S. Anthonysamy, Improving the homogeneity of the precursor for the synthesis of nanocrystalline B_4C using freeze-drying, 9th National Conference on Thermo-physical Properties-NCTP2017, November 6-8, SRI Convention Centre, Anupuram.
3. Soja K. Vijay, V.Chandramouli, S. Anthonysamy, Microwave-assisted gel combustion synthesis of yttria-stabilized zirconia: A study of effect of combustion fuel on the ionic conductivity, Symposium on Electronic Materials for Energy and Environment, MRSI-AGM2014, February 12-14, IISc, Bangalore.
4. Soja K Vijay, V. Chandramouli, S. Anthonysamy, Gel combustion synthesis of yttria-stabilized zirconia, Recent Trends in Materials Chemistry-RTMC2013, VIT University, Vellore.

Soja K Vijay

DEDICATED

To

My dear husband Ahish

ACKNOWLEDGEMENT

I take this opportunity to thank all those who have contributed to this thesis and supported me throughout this wonderful journey.

I would like to express my sincere gratitude to my research supervisor, Dr. S. Anthonysamy. I am deeply indebted to him for the continuous support for my PhD study and related research, for his patience, motivation and immense knowledge. I am also thanking him, for patiently going through the thesis, and for his critical comments, that helped me a lot to improve my writing skills.

I am deeply grateful to my technical advisor, Dr. V. Chandramouli who helped me throughout my PhD life. His deep insights helped me at various stages of my research. I am very thankful to him for the patience he has shown in correcting the manuscript and he has taught me how to write a research paper. I express my sincere gratitude for the moral support, inspirational talks and generous care during my carrier.

I would like to thank my doctoral committee chairman, Dr. K. Ananthasivan, former chairman Dr. K. Nagarajan, members, Dr. N.V. Chandra Shekar and Dr. Saroja Saibaba and former member Dr. Bharathi for their valuable suggestions, support and useful discussions.

I am indebted to Mr. R. Krishna Prabhu, without his help and support my PhD would not have come to this form. His technical knowledge helped me a lot during the period of my PhD work.

I thank Dr. N. Sivaraman, Dean, Chemical Sciences, HBNI for his constant support and help. I am thankful to Dr. P. Muralidaran for permitting me to concentrate on my PhD work.

I would like to express my gratitude to Mr. T. Haribabu, who has helped me a lot during my PhD and because of that I could complete the work at the earliest. He has helped me a lot without any hesitation.

I would like to thank Dr. Dibyendu Chakravarty, ARCI, for doing spark plasma sintering of boron carbide samples. I thank Dr. R. Subasri, ARCI, for introducing him.

I am thankful to Dr. Tammana S.R.Ch. Murthy, Materials Processing and Corrosion Engineering Division, BARC, for hot pressing the boron carbide samples.

I would like to thank Dr. Ashish Jain for TG analysis, for giving me the experimental set up for conductivity measurement and chemicals/materials without any hesitation, whenever needed.

I am grateful to Dr. Rani P. George for helping me to carry out the microhardness measurement and for the silicon carbide papers for grinding the samples. I am extremely thankful for the motivation, affection and care she has provided during the journey to the office. She is always an inspiration for me.

I sincerely acknowledge Dr. R. Sudha, Dr. Arup Dasgupta, Dr. R. Mythili, Mr. G.V Suresh, Dr. G Thirupathy and Mr. Sai Kumaran for characterizing B_4C and YSZ by SEM and EDX. I sincerely thank Mrs. D. Annie for the wet chemical analysis of B_4C samples. I thank Mr. Raja Madhavan for XRD analysis during initial days of PhD work. I wish to express special thanks to Mr. P. Ravishankar and G. Saravanan for helping me during the initial days of my PhD work. I also thank Mr. Jogeswara Rao for helping me in the particle size distribution measurement. I am thankful to Mr. Abhiram Senapati for the specific surface area analysis. I thank Dr. T.R. Ravindran for recording the Raman spectra of the samples. I am grateful to Mrs. Jaysree and Mrs. Dinu for helping me to make pellets of precursors during the bulk synthesis of boron carbide for the sintering studies. I express my gratitude to Mrs. Shabhana Khan for the TEM analysis of the YSZ samples. I would like to thank Mrs. Clinsha for helping me to carry out conductivity measurement of YSZ. I thank Mr. Ravi Shankar Anne and Mr. Srinivas Mannepalli, for microhardness measurement. I thank Mr. V. Paramasivam for all the helps he has provided during the PhD period.

I deeply thank each and every member of MFPS for their support in conducting my research.

It is a pleasure to thank my friends, Mrs. Meera and Mrs. Aiswarya for the beautiful times we shared and unforgettable moments we cherished. I cannot forget the help provided by Aiswarya during the toughest time, in the final stage of my PhD life. I thank my friend, Mrs. Rasmi, for helping me during the initial days of my PhD work. I thank Reshmi chechi and Deepu ettan for helping during the toughest time. I also thank Lalichechi and Dinu for the helping me at the needful times. I am thankful to my friend Liju, for drawing the schematic of experimental assemblies. I also thank Mrs. Chithra Chandramouli, for the support she has given me to take the right decision at the critical time.

I also place on record, my sense of gratitude to one and all who, directly or indirectly, have lent their helping hand in this venture.

I am forever thankful to my dear husband, Mr. Ahish, for being with me as a constant source of strength and encouragement for fulfilling my dream. I deeply thank him for giving me the freedom to concentrate on my career, beyond the family commitments. I am very much grateful to God for gifting me such a loving husband.

Words cannot express how grateful I am to my mother, Sumala, for taking care of me like a small child until now. She has given me the freedom to explore new directions in life and seek my own choices. I am grateful to my mother-in-law, father-in-law and relatives for all the support they have made. I thank my brother Visakh for being with me during the toughest time.

Finally, I thank God, for letting me through all the difficulties. I have experienced his guidance every day and I will keep on trusting him for my future.

Soja K Vijay

CONTENTS

CHAPTER 3 97

STUDIES ON THE SYNTHESIS OF nc-B_4C BY PRECURSOR METHOD

CHAPTER 4 139

STUDIES ON THE SINTERING OF nc-B_4C BY SPARK PLASMA SINTERING TECHNIQUE

CHAPTER 5 155

STUDIES ON THE SINTERING OF nc-B_4C BY HOT PRESSING TECHNIQUE

CHAPTER 6 167

STUDIES ON THE SYNTHESIS OF YTTRIA-STABILIZED ZIRCONIA

SYNOPSIS

India is a developing nation and its energy requirement presently is at its peak. Conventional sources are not sufficient to meet the ever increasing demand. Nuclear energy is one never depleting source that can augment the conventional and renewable energy sources. Nuclear Power is the fourth-largest source of electricity in India after the thermal, hydroelectric and other renewable sources [1]. The limited uranium reserves of India cannot sustain the nuclear energy programme with thermal reactors for long. Due to the availability of large thorium reserves, India has adopted a three stage nuclear programme [2]. The first stage is based on the Pressurized Heavy Water Reactors (PHWRs) which use natural uranium dioxide (^{235}U–0.7%, fissile isotope and ^{238}U-99.3%, fertile isotope) as the fuel. The second stage is fast reactors in which utilization of uranium is enhanced and also fresh fuel in the form of ^{239}Pu is produced. The ^{233}U will also be produced in the fast reactors from the ^{232}Th blanket material. In the third stage, ^{233}U produced in the second stage will be used as fuel for thermal breeder reactor. India has already entered into the second stage of the nuclear power programme with the construction of a prototype fast breeder reactor at Kalpakkam, which is now at an advanced stage of commissioning [2-3]. There is a demand to develop materials with superior properties compared to the conventional ones to accomplish the requirements of the growing indigenous nuclear technology. It necessitates R&D on the materials relevant to the nuclear technology.

Control rod is one of the major components in any nuclear reactor. Owing to the high neutron absorption cross section of ^{10}B in the fast neutron region, boron in the form of boron carbide is proposed as the control rod material in fast reactors. B_4C is also an important ceramic in many industries due to its excellent combination of properties such as high hardness, low density, high melting point, high elastic modulus, chemical inertness, excellent thermoelectric properties etc. [4]. Commercially available boron carbide is synthesized by carbothermic reduction of boric oxide or boric acid at very high temperatures greater than 2200 K. This is an energy intensive process and often results in a coarse grained product. This necessitates grinding which results in contamination from the grinding media [4]. Recently polymer precursor based synthesis of boron carbide ceramics is being carried out as an alternate to the high temperature synthesis [4]. The precursor method yields nanocrystalline boron carbide as compared to the conventional synthesis which gives microcrystalline product [5-9]. Nanocrystalline materials exhibit superior physical and chemical properties compared to the microcrystalline materials [10-11]. Nanocrystalline materials show enhanced sinterability at relatively lower temperatures as compared to their microcrystalline counterparts [12].

Consolidation of B_4C is difficult due to high melting point, low self diffusion coefficient and the presence of covalent bonding [4]. In recent years, spark plasma sintering (SPS) technique has been widely used for the sintering of boron carbide ceramics. SPS brings about densification at relatively lower temperature in shorter time with limited grain growth as compared to the conventional sintering techniques. Hot pressing is the most common method for the fabrication of dense B_4C without sintering additives [4]. The B_4C can be densified to near theoretical density by hot pressing by the application of load $\geq$30 MPa.

Yttria-stabilized zirconia (YSZ) is another important ceramic in nuclear industry. YSZ is used as a solid electrolyte for thermochemical property measurements, oxygen sensor and as an oxygen probe for the measurement of oxygen potentials of oxides. YSZ is one of the promising candidates for the inert matrix fuel due to its structural similarity with UO_2 and low absorption cross section for neutrons [13]. YSZ finds extensive applications in the field of solid oxide fuel cells, electrolytic support in catalytic applications using solid electrolyte cell reactors, carrier for metallic nanoparticles etc., due to its unique characteristics and enhanced chemical stability compared to other ceramic conductors [14]. Combustion synthesis of materials using microwave energy is a novel method for the synthesis of nanocrystalline materials [15]. The method involves a self sustained reaction containing a metal nitrate and an organic fuel. Microwave heating produces materials with improved properties, lowers the processing temperatures and reduces the time required for the processing.

Scope of the study

This thesis mainly deals with the research and development related to the synthesis and sintering of nanocrystalline boron carbide and yttria-stabilized zirconia. The present study aims at developing novel methods for the synthesis of sinteractive B_4C and YSZ powders suitable for fabricating high-density compacts at a relatively low sintering temperature, since the conventional methods use very high temperatures which are energy and cost intensive processes. The sintering of boron carbide ceramic compacts is generally influenced by the powder characteristics such as surface area, particle size distribution, free carbon content etc. The present study has been carried out to optimize process parameters to obtain nanocrystalline boron carbide with desired powder characteristics for sintering at relatively low temperatures using advanced sintering techniques. The nanocrystalline boron carbide thus prepared in the present study was sintered using two advanced techniques viz., spark plasma sintering and hot pressing.

A new method based on microwave-assisted combustion synthesis was also developed to prepare nanocrystalline yttria-stabilized zirconia in the present study.

Organization of the thesis

The thesis consists of 7 chapters. Chapter 1 gives a brief introduction to the present work. Experimental methods and characterization techniques used in the present study are described in Chapter 2. Chapter 3 discusses the results obtained in the present study on the synthesis and characterization of nanocrystalline boron carbide using the precursor method. Chapter 4 describes spark plasma sintering studies carried out on the nanocrystalline boron carbide prepared using precursor method. Sintering of nanocrystalline boron carbide by hot pressing method was attempted and the results of the studies on sintering using hot pressing are discussed in Chapter 5. Chapter 6 discusses the synthesis of nanocrystalline 8 mol.% yttria-stabilized zirconia. Chapter 7 provides the summery and conclusions from the present work and also presents the scope for future work.

Chapter 1

Chapter 1 discusses the importance of nuclear energy in India and the three-stage nuclear power programme with emphasis on fast reactors. A brief introduction highlighting the importance of the present work is given in this chapter. The components of nuclear reactor and materials relevant to nuclear technology are described. Information on various control rod materials employed in thermal and fast reactors are provided emphasizing the importance of boron carbide as the control rod material for fast reactors. This chapter also describes the synthesis and sintering methods available for the fabrication of boron carbide. The application of YSZ in nuclear industry and different methods of synthesis, sintering and conductivity measurement of 8 mol.% yttria-stabilized zirconia are described. The advantages of microwave heating for the synthesis of ceramics and advanced sintering techniques such as hot pressing and spark plasma sintering are discussed.

Chapter 2

Chapter 2 provides the details of materials used, experimental methods and characterization methods used in the present study. The design of the furnace made in-house for the synthesis of boron carbide powder is discussed. The method of synthesis of boron carbide using precursor method is described. The nanocrystalline boron carbide synthesized in the present work is sintered using spark plasma sintering and hot pressing. Methods of characterization of boron carbide powder and sintered boron carbide compacts are described in this chapter. The analytical techniques for the analysis of boron, total carbon and free carbon in the synthesized powders are explained. Methods used in the microstructural characterizations of these powders (Scanning electron microscopy, SEM and Transmission electron microscopy, TEM) and sintered compacts are given in detail. The methods used for the synthesis of 8YSZ and its electrical conductivity measurements are described.

Chapter 3

Chapter 3 deals with studies on the synthesis of nanocrystalline boron carbide using a precursor method. The precursor was prepared using boric oxide and sucrose. A homogeneous mixture of boric oxide and sucrose with a carbon to B_2O_3 mole ratio (CBMR) of 3.38 was heat treated at various temperatures ranging from 373 to 973 K. The optimized temperature for the preparation of precursor is found to be 873 K. The precursor prepared at each temperature was heat-treated from 1273 to 1873 K. The products thus obtained at each temperature were characterized for their boron, total carbon and free carbon content. It was found that the formation of boron carbide commences at 1273 K. The boron carbide obtained by this method was found to be nanocrystalline and the average X-ray crystallite size was found to be ~33 nm. The boron carbide formed at 1873 K from the precursor prepared at 873 K was found to contain a free carbon content less than 3 wt.% . The free carbon content in the boron carbide synthesized by a precursor method depends on the homogeneity of the precursor, heating rate and particle size of the reactants. In order to improve the homogeneity of precursor, wet mixing and freeze-drying was used. Boric oxide and sucrose were made into a slurry using water and ethanol. The slurry was frozen and the slurry media was subsequently removed by freeze-drying. The freeze-dried product was heated at 873 K under flowing argon. The precursor prepared by this method was heat-treated at different temperatures ranging from 1273 to 1873 K. The boron carbide formed from the precursor prepared using water as medium of mixing at 1873 K was found to contain a lower free carbon content of 1.6 wt.%, whereas the formation of boron carbide was incomplete when the precursor prepared using ethanol as the medium of mixing was heat treated even at 1873 K for 10 min. Synthesis of boron carbide was also carried out by taking boric acid as the boron source and mannitol as the carbon source. The precursor was prepared by microwave-assisted heating of the boric acid-mannitol solution by maintaining CBMR equal to 3.38. The product obtained was heat-treated at 673 to 873 K. The precursor obtained at each temperature was ground into fine powder and compacted. These compacts were heat treated at 1273 to 1873 K. The microwave-assisted synthesis of precursor was also carried out by taking excess mannitol by fixing the CBMR is equal to 6. All these products were characterized for their phase purity and chemical composition. Microstructural examination of selected samples was also carried out.

Chapter 4

Chapter 4 deals with studies on sintering of nanocrystalline boron carbide prepared by precursor method by spark plasma sintering. Conventional sintering requires very high temperature for sintering boron carbide compacts due to the low diffusivities of both B and C in the B_4C lattice which is predominantly covalent. Nanocrystalline boron carbide synthesized in the present study was sintered using SPS technique. The fully characterized nanocrystalline boron carbide samples were sintered at 1873, 1973 and 2073 K using SPS technique with a heating rate of 100 K min^{-1} at each run. 50 MPa was applied at the start of the run. The duration of heating was 5 min at each run. In order to compare the densification, a commercial sample (Make: M/s. Sigma Aldrich, Germany) was also sintered at 1973 K. The sintered samples were characterized for their phase purity, microstructure and hardness.

Chapter 5

Chapter 5 describes studies on sintering of nanocrystalline boron carbide using hot pressing method. The sintering was carried out at two temperatures, 1973 and 2073 K and the results of sintering were compared with those reported in literature. The hot pressing of the commercial sample was also carried out at the same temperature in order to compare the densification of the sample prepared in the present study.

Chapter 6

Chapter 6 discusses the results of the synthesis of nanocrystalline 8 mol.% yttria-stabilized zirconia. Two different heating methods were used for the synthesis by taking three different fuels- citric acid, glycine and urea. Microwave-assisted combustion synthesis of 8YSZ was carried out by fixing the fuel to oxidant ratio equal to 1. Conventional heating using hot plate was also carried out by fixing the fuel to oxidant ratio as 1. The powder synthesized was fully characterized for phase purity, specific surface area, particle size distribution and microstructural analysis. The powder samples were sintered at 1873 K. The sintered compacts were also characterized. The ionic conductivity of sintered compacts were measured by ac-impedance spectroscopy.

Chapter 7

The main findings and the results of the present study are highlighted in Chapter 7. Scope for further studies is also discussed.

References

[1] M.R. Kolhe P.G. Khot, India’s Energy Scenario-current and future, Int. J. Manage., 6 (2015) 47-66.

[2] S. Banerjee, H.P. Gupta, The evolution of the Indian nuclear power programme, Prog. Nucl. Energy, 101 (2017) 4-18.

[3] P. Puthiyavinayagam, P. Selvaraj, V. Balasubramanian, S. Raghupathy, K. Velusamy, K. Devan, B.K. Nashine, G.P. Kumar, K.V.S. kumar, S. Varatharajan, P. Mohanakrishnan, G. Srinivasan, A.K. Bhaduri, Development of fast breeder reactor technology in India, Prog. Nucl. Energy, 102 (2017) 19-42.

[4] A.K. Suri, C. Subramanian, J.K. Sonber, T.S.R. Ch. Murthy, Synthesis and consolidation of boron carbide: a review, Int. Mater. Rev., 55 (2010) 4-40.

[5] T.R. Pilladi, Studies on the synthesis and characterization of nanocrystalline boron carbide, THESIS, HBNI, August 2012.

[6] Rafi-ud-din, G.H. Zahid, E. Ahmad, M. Maqbool, T. Subhani, W.A. Syed, S. Z. Hussain, Effect of cellulose-derived structural homogeneity of precursor on the synthesis and morphology of boron carbide, J. Inorg. Organomet. Polym., 25 (2015) 995-999.

[7] M. Maqbool, Rafi-ud-din, G.H. Zahid, E. Ahmad, Z. Asghar, T. Subhani, M. Shahzad, I. Kaleem, Effect of saccharides as carbon source on the synthesis and morphology of B_4C fine particles from carbothermal synthesis precursors, Mater. Express, 5 (2015) 390-400.

[8] M. Kakiage, N. Tahara, I. Yanase, H. Kobayashi, Low-temperature synthesis of boron carbide powder from condensed boric acid-glycerin product, Mater. Lett., 65 (2011) 1839-1841.

[9] K. Zakharova, A. Mednikova, V. Rumyantsev, T. Genusova, Proc. Int. Conf. Nanomater., Appl. Prop., 2 (3) (2013) (03AET09) (4pp).

[10] C.S. Pande, K.P. Cooper, Nanomechanics of Hall–Petch relationship in nanocrystalline materials, Prog. Mater.Sci., 54 (2009) 689-706.

[11] H. Gleiter, Nanocrystalline Materials, Prog. Mater. Sci., 33 (1989) 223-315.

[12] K. Lu, Sintering of nanoceramics, Int. Mater. Rev., 53 (2008) 21-38.

[13] H. Kleykamp, Selection of materials as diluents for burning of plutonium fuels in nuclear reactors, J. Nucl. Mater., 275 (1999) 1-11.

[14] M.N. Tsampas, F.M. Sapountzi, P. Vernoux, Applications of yttria-stabilized

zirconia in catalysis, Catal. Sci. Technol., 1-3 (2015) 1-18.

[15] R.V. Mangalaraja, J.Mouzon, P. Hedstorm, C.P. Camurri, S. Ananthakumar, M. Oden. Microwave-assisted combustion synthesis of nanocrystalline yttria and its powder characteristics, Powder Technol., 191 (2009) 309-314.

LIST OF FIGURES

LIST OF TABLES

List of Abbreviations

BET	Brunauer-Emmett-Teller
CA	Citric Acid
CBMR	Carbon to B_2O_3 mole ratio
CSR	Control and Safety Rod
CSRDM	Control and Safety Rod Drive Mechanism
DLS	Dynamic Light Scattering
DSR	Diverse Safety Rod
DSRDM	Diverse Safety Rod Drive Mechanism
EDX	Energy Dispersive X-Ray
FBRs	Fast Breeder Reactors
FBTR	Fast Breeder Test Reactor
ICDD	International Centre for Diffraction Data
KHP	Potassium Hydrogen Phthalate
MOX	Mixed Oxide
nc	Nanocrystalline
PHWR	Pressurized Heavy Water Reactor
PFBR	Prototype Fast Breeder Reactor
SAED	Selected Area Electron Diffraction
SEM	Scanning Electron Microscopy
SHS	Self Propagating High Temperature Synthesis
SPS	Spark Plasma Sintering
SSA	Specific Surface Area
TEM	Transmission Electron Microscopy
T.D	Theoretical Density
TG	Thermo gravimetric
XRD	X-ray Diffraction
XCS	X-ray Crystallite Size
YSZ	Yttria-Stabilized Zirconia

Chapter 1

Introduction

This chapter gives an introduction to the importance of nuclear energy and the fast reactor programme in India, major components of a nuclear reactor and the need for control systems in nuclear reactors. This chapter describes various control rod materials available and the characteristics of neutron absorber materials. The importance of boron as control rod material in fast reactors is presented. A brief description of properties of boron carbide, crystal structure and B-C phase diagram is also given. The thesis mainly consists of two parts. Part I deals with studies on the synthesis and sintering of boron carbide. Methods available for the synthesis of boron carbide are given in detail. The main focus of the first part of this chapter is to highlight the importance of synthesis and sintering of nanocrystalline boron carbide. Part II deals with the studies on the synthesis of yttria-stabilized zirconia and its conductivity measurements.

1.1 Nuclear power programme in India

India is a developing nation and its energy requirement presently is at its peak. Conventional sources are not sufficient to meet the ever-increasing energy demand in the country. Nuclear energy is one never depleting source that can augment conventional and renewable energy sources. Nuclear power is the fourth-largest source of electricity in India after the thermal, hydroelectric and other renewable sources [1]. The current contribution of nuclear energy to the total electricity generation is only 3% and aims to supply 25% of electricity from nuclear power by 2050 [2]. At present, the total nuclear power plant capacity is 6780 MWe with 22 operating nuclear power plants [3].

With limited reserves of uranium (natural uranium reserves ~70,000 tonnes), the nation cannot sustain the nuclear energy programme with only thermal reactors for long. Due to the availability of vast thorium reserves (~3,60,000 tonnes), India has adopted a three-stage nuclear power programme [4-6] as shown pictorially in Fig. 1.1 [7]. India's three-stage nuclear power programme was envisioned by Dr. Homi Jehangir Bhabha in 1950 to secure the country's long-term energy requirements. The objective of this program is to use the mined uranium and thorium reserves of the nation judiciously. The first stage is based on Pressurized Heavy Water Reactors (PHWRs) which use natural uranium (0.7 at.% of fissile[1] isotope ^{235}U and 99.3 at.% ^{238}U, a fertile[2] isotope) as the fuel to produce electricity. Apart from this, ^{238}U is converted to fissile ^{239}Pu through neutron capture ($^{238}_{92}U + {}^{1}_{0}n \rightarrow {}^{239}_{92}U \xrightarrow{\beta^-} {}^{239}_{93}Np \xrightarrow{\beta^-} {}^{239}_{94}Pu$) in the reactor. In the second stage, fast breeder reactors (they produce fissile material by the fast neutrons at a faster rate than it consumes fissile material) produce energy by utilizing the ^{239}Pu generated in the first stage. At the same time, these reactors will also be used for converting another naturally occurring fertile isotope ^{232}Th through neutron capture into a fissile isotope ^{233}U ($^{232}_{90}Th + {}^{1}_{0}n \rightarrow {}^{233}_{90}Th \xrightarrow{\beta^-} {}^{233}_{91}Pa \xrightarrow{\beta^-} {}^{233}_{92}U$). The main aim of the second stage is breeding and utilization of uranium. In the third stage, ^{233}U produced in the second stage will be used as fuel for thermal breeder reactor[3] (^{233}U has breeding potential in the thermal region). Hence, by employing a three-stage nuclear power programme, an effective

---

[1] *Fissile material (nuclide) is a material that is capable of undergoing fission reaction after absorbing thermal neutron (energy 0.025 eV). Typical fissile isotopes are ^{235}U, ^{239}Pu and ^{233}U*

[2] *Fertile material consists of isotopes that are not fissionable by thermal neutrons but can be converted into fissile isotopes (after neutron absorption and subsequent nuclear decay). Typical fertile isotopes are ^{238}U and ^{232}Th.*

[3] *A breeder reactor in which the thermal neutrons sustain the fission chain reaction.*

utilization of uranium and thorium is achieved, thereby meeting the increasing energy demands of the country.

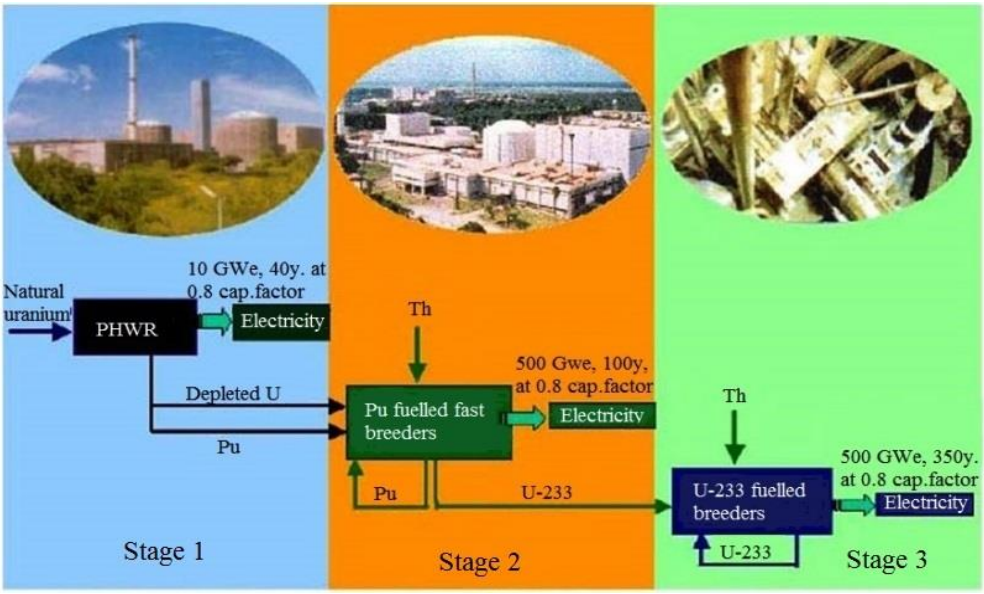

Figure 1.1. Schematic of the three-stage nuclear power programme in India (Reproduced from Ref. 7)

1.2 Major components of a nuclear reactor

Different types of reactors have some common general features. The nuclear reactor core is the critical component of a nuclear reactor. A reactor core consists of four essential components, namely, fuel, coolant, moderator and control rods [8, 9] as shown schematically in Fig. 1.2.

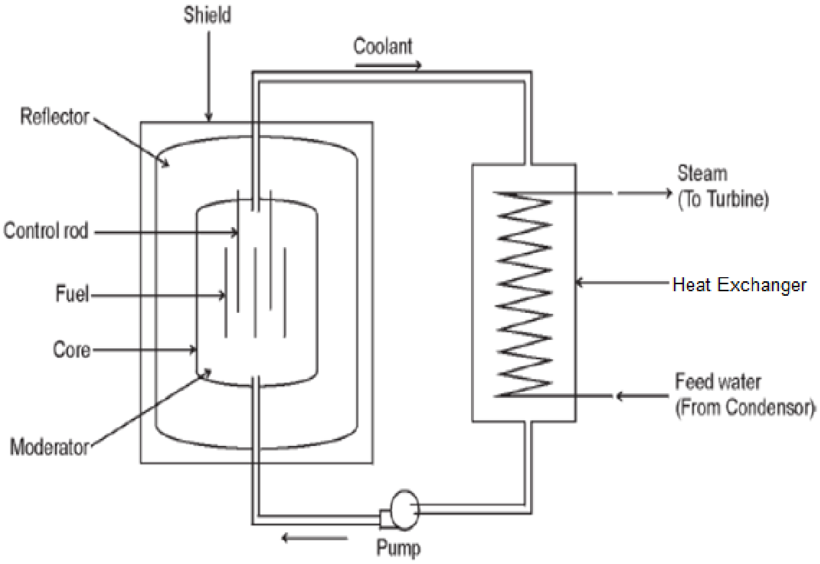

Figure 1.2. Schematic representation of nuclear reactor

1.2.1 Nuclear fuel

Nuclear fuel is the fuel used in the nuclear reactor to produce electricity as a result of nuclear fission. The chemical forms of nuclear fuel employed in nuclear reactors are oxide/carbide/metal/alloy of U/Pu/Th. The fuel is usually made into small pellets (in the case of oxide or carbide fuels) or rods (in the case of metallic fuels) and is sealed in a clad typically made up of zirconium alloys, magnesium alloy, stainless steel or its variants depending on the type of the reactors. The fuel loaded into a clad tube is called a fuel pin/rod. The fuel rods are arranged into fuel subassemblies. The reactor core contains many such fuel subassemblies arranged in a particular way. The cladding ensures the retention of fission products.

1.2.2 Coolant

The heat energy generated in the reactor core needs to be transported to the steam generator to run a turbine. A coolant circulating through the core transfers heat from the core to steam generator directly or to the secondary cooling system through the heat exchangers. The steam is produced in the steam generator and it transfers energy to the turbine generator to produce electricity. The coolant can be light water, heavy water, liquid metal or a gas, depending on the type of the nuclear reactor.

1.2.3 Moderator

Moderator is an essential constituent only in thermal reactors. The function of the moderator is to slow down the high energy neutrons liberated in the fission reaction. The neutrons generated in fission have energy up to 10 MeV. These high energy neutrons are called fast neutrons. Moderator slows down the fast neutrons so that the probability of absorption of the neutron by the fissile nuclide is increased. The moderator can be either liquid (light water or heavy water) or solid (graphite).

1.2.4 Control rods

Nuclear reaction is a source of tremendous energy. The nuclear fission chain reactions that produce this energy need to be controlled predictably. It is here that the control rods come into the picture and play an important role in the operation of nuclear reactors. Control rods are rods, plates or tubes made with neutron absorbing materials (boron, cadmium, hafnium, etc.) and are used to control the nuclear chain reaction by inserting into or withdrawing from the reactor core. When control rod assemblies are inserted into the reactor core, they absorb neutrons thereby slowing the rate of the fission reaction and decreasing the power produced. Conversely, if the control rods are removed, fewer neutrons are consumed and the fission rate and energy production increases. In an emergency, the chain reaction can be stopped by fully inserting all of the control rods into the nuclear reactor core between the fuel subassemblies.

***1.3 Fast Breeder Reactors* (FBRs)**

The chain reaction in a fast reactor is sustained by fast neutrons produced during the nuclear fission reaction. A nuclear reactor which produces more fuel than it consumes is a breeder reactor. Breeding is possible in the case of fast reactors where chain reaction is sustained by fast neutrons; hence these are called fast breeder reactors. In order to achieve a high breeding ratio[4], the neutron flux[5] in the fast reactors needs to be kept as flat as possible. In the fast flux, more number of neutrons are produced per neutron absorbed in the fissile isotope and hence the breeding ratio is high. The fission cross-sections (probability to undergo nuclear fission) of the

---

[4]. *The ratio of fissile material obtained to spent fissile material after the use of a fuel mixture of fissile and fertile material in a nuclear reactor.*

[5] *Number of neutrons incident /cm^2/sec on target material is called flux*

fissile material and the neutron energy are inversely related. To compensate for small cross-sections in the fast energy region, highly enriched fuel (enriched in fissile isotope) is used in the core from reactor criticality considerations. The high enrichment in the core requires high power ratings and leads to high flux. High power ratings are needed to reduce fuel inventory and this makes the reactor core small size. A blanket of thorium or natural uranium is used to capture the neutrons leaking from the core thereby producing fissile material ^{233}U and ^{239}Pu. The blanket also acts as a reflector of neutrons and thus reduces the critical mass[6]. Fast reactors use liquid sodium coolant because of its favourable nuclear, chemical and physical properties. The driving force behind the development of a fast reactor is the realization that fast reactors could be used for breeding fissile material (^{233}U and ^{239}Pu) from fertile material (^{232}Th and ^{238}U).

1.4 Fast reactor programme in India

The driving force behind the development of fast reactors is that, it could be used to breed the fissile material from fertile material and thereby utilize the limited uranium resources and vast thorium resources available judiciously.

Fast reactor programme in India emerged with the commissioning of Fast Breeder Test Reactor (FBTR) at Kalpakkam in October 1985 [10]. FBTR is the only operational sodium-cooled fast reactor with (U, Pu) carbide as the driver fuel. Mark I fuel is (U, Pu) carbide with Pu/(U + Pu) = 0.7. This is a biphasic fuel containing (U, Pu) monocarbide with 5 to 15 vol.% (U, Pu) sesquicarbide. Mark II fuel is (U, Pu) monocarbide with Pu/(U + Pu) = 0.55. This is also a biphasic fuel containing (U, Pu) monocarbide with 5 to 15 vol.% (U, Pu) sesquicarbide. India has already entered into

---

[6] *A critical mass is the smallest amount of fissile material needed for a sustained chain reaction.*

the second stage of nuclear power programme with the construction of a Prototype Fast Breeder Reactor (PFBR) at Kalpakkam, which is in the advanced stage of commissioning [4]. PFBR is a 500 MWe, sodium-cooled, pool-type fast reactor which uses (U, Pu) mixed oxide (MOX) fuel. The active core in which most of the heat is generated by controlled fission consists of 181 fuel subassemblies. A homogenous core concept with two fissile enrichment zones is adopted for power flattening. The reactor core contains (U, Pu) mixed oxide fuel with Pu/(U + Pu) = 0.21 at the centre and (U, Pu) mixed oxide fuel with Pu/(U + Pu) = 0.28 at the periphery of the core. Radial blanket subassemblies are placed in 2 rows. 12 absorber rods viz., 9 Control and Safety Rods (CSR) and 3 Diverse Safety Rods (DSR) are arranged in two rings. Boron carbide enriched in ^{10}B isotope (^{10}B ~65 at. %) is used as absorber material for reactor control and shutdown. The radial shielding is provided by boron carbide subassemblies. One of the major requirements of fast reactors is a proper control system for the fast neutrons produced as a result of the fission chain reaction.

1.5 Reactor control

A sustained chain reaction between neutrons and fissile isotopes is essential for the continuous operation of a nuclear reactor [11]. During these reactions, approximately 2.5 neutrons are produced per neutron absorbed. This process is self-sustaining as long as one of the neutrons involves in the fission reaction. Neutron loss also occurs by leakage and parasitic captures in structural components of the reactor core. The neutron balance in a reactor is expressed by infinite multiplication factor, k_∞, which is defined as the ratio of the number of fissions in any one generation to the number of fissions in the immediately preceding generation in a system of infinite size [11]. In the real situation, the reactors are not infinite in size. Hence in such a case, the “criticality” is expressed by the effective multiplication factor, k_{eff} [11]. The condition for criticality is that, k_{eff} should be equal to one. Then the chain reaction proceeds at a constant rate. When it is greater than one, the uncontrolled chain reaction leads to super-criticality. When it is less than one, the chain reaction decreases and eventually ends. A reactor is considered to be critical when $k_{eff} = 1$; supercritical when $k_{eff} > 1$; and subcritical when $k_{eff} < 1$.

In order to compensate for fuel burn up and neutron loses, reactors are designed in such a manner that k_{eff} is slightly greater than one. In order to prevent the reactor from super criticality, even though the effective multiplication factor is greater than one, neutron absorbers are introduced into the reactor core as a part of the control system. The effectiveness of these absorbers is measured as control rod worth and it is the amount of reactivity they can control. The reactivity is defined as the fractional departure of the system from criticality (Reactivity = $\frac{k_{excess}}{k_{eff}}$), where k_{excess} is the excess reactivity. Reactivity is commonly expressed in decimal or percentage or per cent mille (pcm).

The nomenclature used to designate various types of control rods are [11]: (1) safety rods, those which are kept above the reactor core during operation and are dropped for emergency shutdown (i.e. scram); (2) regulating rods, which are partially inserted and are moved to adjust power and (3) shim rods, which provide adjustment over long-term cycles.

Control rods when placed at the lowest elevation in the core, the reactor is in shut down state. The rods should be raised to a certain elevation to make the reactor critical. The rods should be raised further to bring to the desired power level. Raising of the control rods by their drive mechanisms removes the neutron absorbing material from the active core region resulting in controlled multiplication of the neutronic population thereby reaching the desired power level. In case of rapid shut down, the rods should be dropped suddenly.

Neutron absorbers are elements in which the nuclei capture neutrons without generating or emitting new neutrons. Two most common type of reactions involving neutron absorption by the target nuclei are: 1) (n, α) and 2) (n, γ) reactions. The rate at which the nuclear reactions proceed is determined by nuclear cross-section, σ. It is a measure of the probability of the occurrence of the nuclear reaction. It is the property of the nucleus and defined for neutron of a particular energy. The unit of the nuclear cross-section is cm^2. The absolute value of the cross-section is small, so the unit barn (1 barn = 1×10^{-24} cm^2) is used. Cross-sections are high for slow neutrons and it decreases as the energy of neutron increases. Effective absorber materials have cross-sections of at least 1000 barns in the neutron energy range below one electron volt (eV) [11]. However in the fast neutron range (0.1 to 10 MeV), the absorption cross-section of all the absorbers become very low and ^{10}B is the only absorber material whose absorption cross-section is the highest (~2 barn); ^{10}B having a cross-section of 1 barn is very effective in the fast neutron range. The cross-section, σ, applies to a single nucleus and is called the microscopic cross-section. Since the target material contains "N" nuclei cm^{-3}, the quantity $N\sigma$ is equivalent to the cross-section of the material per cm^3 for a particular reaction [11]. This is called macroscopic cross-section and it is the quantity used in evaluating absorber materials and calculating their effects.

The macroscopic cross-section is $\Sigma = N\sigma\ (cm^{-1})$ (1.1)

It has the dimension of a reciprocal length. Its inverse, λ, is the mean free path with which a neutron would probably travel through material before undergoing a particular reaction. Macroscopic cross-sections are calculated as given below for:

Elements: $\Sigma = \frac{\rho N_\alpha}{A}$ (1.2)

Molecular compounds: $\Sigma = \frac{\rho N_\alpha}{M} (\sigma_1 \nu_1 + \sigma_2 \nu_2 + \ldots + \sigma_i \nu_i + \cdots)$ (1.3)

Mixtures: $\Sigma = N_1 \sigma_1 + N_2 \sigma_2 + \cdots + N_i \sigma_i + \cdots$ (1.4)

where, ρ is the density (g cc^{-1}), N_α is Avogadro's number, A is the atomic weight, M is the molecular weight, N_i is the nuclear density of atoms of the kind 'i' and ν_i and σ_i are the fraction of atoms of the kind 'i', and their microscopic cross-section, respectively, in the molecule or mixture.

1.6 Control system in FBTR

FBTR's control system consists of boron carbide enriched with 90 at.% ^{10}B as the control rod material [12-13]. B_4C compacts are stacked in a single SS316LN[7] pin which is vented and having sodium as the bonding material. Six B_4C control rods in the reactor core are held by grippers of individual drive mechanisms, which are in-line with the respective control rods and housed in control plug.

The functions of control rods and Control Rod Drive Mechanisms (CRDM) in FBTR are [13];

1. To start-up and to have controlled shut down of the reactor.
2. To control reactivity during normal operation of the reactor.
3. To scram the reactor on emergency conditions.
4. To have burn up compensations.

---

[7] *SS316LN contains chromium (16-18 wt.%), nickel (12-14 wt.%), molybdenum (2-3 wt.%) manganese (~2 wt.%), carbon (~0.08 wt.% maximum) and balance is iron.*

1.7 Control system of PFBR

PFBR's control system is designed a with defence-in-depth approach having redundancy, diversity and independence [14]**.** PFBR's control rod material consists of high-density compacts of B_4C enriched with 65 at.% ^{10}B isotope. The compacts of B_4C are stacked inside 20% cold worked D9 alloy[8] clad tube. The typical control rod subassembly is of vented type, with liquid sodium flowing at 823 K in the annular region during the normal operation of the reactor. PFBR has two independent fast acting diverse shut down systems [15-17]. The absorber rods of the first system are called control and safety rod (CSR). CSR and its drive mechanism are called CSRDM. The second system is called diverse safety rod (DSR) and the respective drive mechanism is called DSRDM. There are nine CSR and three DSR subassemblies in the reactor core and the positions of both CSR and DSR inside the core is shown schematically in Fig. 1.3. The radial shielding is provided by stainless steel (in 6 rows) and boron carbide subassemblies (in 3 rows).

The functions of CSRDM are to facilitate [14];

- Start-up and controlled shut down of the reactor and control of reactor power by raising and lowering of CSR.
- Shut down of the reactor at off-normal conditions by rapid insertion of CSR into the core (i.e., by scram action) under gravitational force.

The function of DSRDM is only to facilitate shut down of the reactor by scram action of DSR.

---

[8] *Alloy D9 contains chromium (13.5-14.5 wt.%), nickel (14.5-15.5 wt.%), molybdenum (2.0-2.5 wt.%), manganese (1.65-2.35 wt.%), carbon (0.035-0.05 wt.%) titanium (5-7.5C) and balance is iron.*

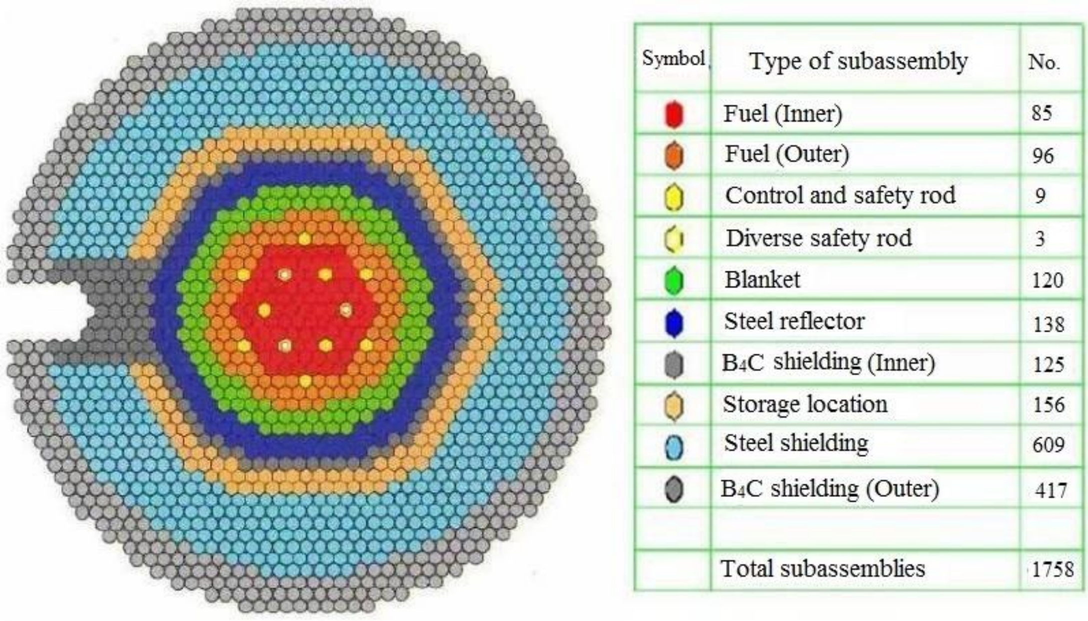

Symbol	Type of subassembly	No.
🔴	Fuel (Inner)	85
🟠	Fuel (Outer)	96
🟡	Control and safety rod	9
🟡	Diverse safety rod	3
🟢	Blanket	120
🔵	Steel reflector	138
⚫	B_4C shielding (Inner)	125
🟠	Storage location	156
🔵	Steel shielding	609
⚫	B_4C shielding (Outer)	417
	Total subassemblies	1758

Figure. 1.3. Position of CSR and DSR in PFBR core. Reproduced from Ref. [16]

1.8 Characteristics of neutron absorbers for fast reactors

For most of the control rod materials, the neutron absorption cross-sections are very low at high neutron energies. This makes the choice of control rod materials limited in the case of fast reactors. The performance requirements of neutron absorber materials are [18]:

- Neutron absorber should have the capability for capturing neutrons effectively to the degree required for reactivity control.
- A neutron absorber should have high neutron absorption cross-section. A minimum value of 100 barns for a thermal reactor and at least 1 barn for a fast reactor is essential for a material to act as a neutron absorber.
- It should have a high melting point so that it remains in solid phase at high temperatures.
- Good compatibility with the clad and coolant material: this reduces the chemical interaction with the clad and coolant.
- It should have good mechanical and physical properties.

- It should be economical to produce and fabricate.
- It should exhibit predictable irradiation behaviour and should not impose excessive lifetime or operational limitations on the control system.

The important neutron absorbers and their absorption cross-sections are given in Table 1.1 [18]. The choice of control rod material depends on the type of the reactor and the energy of the neutron to be absorbed. The combination of silver with 15 wt.% cadmium and 5 wt.% indium serves as control rod alloy over the spectrum of neutron energies present in pressurized light-water reactors. Hafnium is one of the promising absorbers for water moderated reactors because of its favourable neutronic, mechanical and physical properties. Hafnium has 6 isotopes which through (n, γ) capture reaction forms other hafnium isotopes. These isotopes are themselves neutron absorbers, which in turn extend the efficiency of the absorber. Hf is resistant to corrosion by water at high temperatures, can be readily fabricated, and has adequate mechanical strength. Cadmium has high neutron absorption cross-section in the thermal neutron range. Its use as a control rod material in fast reactors is limited due to its relatively low melting point (594 K) and lack of strength.

Table 1.1. Nuclear properties of elements used as absorbers

a	b	c	d	e	f	g
B	10.82	-	755 ± 2	104.00	0.54	^{7}Li
	10.00	0.198	3813		2.70	
Co	59.00	1.00	37.00 ± 1.5	3.37	-	^{60}Co
Ag	107.88	-	63 ± 1	3.63	-	^{108}Ag
	107.00	0.5135	31 ± 2	-	-	^{108}Cd
	109.00	0.4865	87 ± 7	-	-	^{110}Ag
	-	-	-	-	-	^{110}Cd
Cd	112.41	-	2450 ± 50	118.00	0.15	-
	113.00	0.1226	20000 ± 300	-		^{114}Cd
In	114.82	-	196 ± 5	7.30	-	^{114}In
	113.00	0.0423	58 ± 13	-	-	^{114}Sn
	115.00	0.9577	207 ± 21	-	-	^{116}In
	-	-	-	-	-	^{116}Sn
Sm	150.35	-	5600 ± 200	166.00	-	^{148}Sm
	147.00	0.1507	87 ± 60	-	-	^{150}Sm
	149.00	0.1384	40800 ± 900	-	-	^{153}Sm
	152.00	0.2363	224 ± 7	-	-	^{153}Eu
Eu	152.00	-	4300 ± 100	92.50	-	^{142}Eu
	151.00	0.4777	7700 ± 80	-	-	^{154}Eu
	153.00	0.5223	450 ± 20	-	-	^{155}Eu
	154.00	-	1500 ± 100	-	-	^{156}Gd
Gd	157.26	-	46000 ± 2000	1390.00	-	^{156}Gd
	155.00	0.1473	61000 ± 5000	-	-	^{158}Gd
	157.00	0.1568	240000 ±	-	-	
	-	-	12000	-	-	
Dy	162.51	-	950 ± 50	35.00	-	^{165}Gd
	164.00	0.2818	2600 ± 300	-	-	^{165}Ho
Hf	178.58	-	105 ± 5	4.81	-	^{175}Hf

174.00	0.0018	1500 ± 1000	-	-	^{177}Hf
176.00	0.0515	15 ± 15	-	-	^{178}Hf
177.00	0.1839	380 ± 30	-	-	^{179}Hf
178.00	0.2708	75 ± 10	-	-	^{180}Hf
179.00	0.1378	65 ± 15	-	-	^{181}Hf
180.00	0.3544	14 ± 5	-	-	^{181}Ta

a) element, b) atomic mass, c) atom fraction (isotopic abundance), d) microscopic cross-section, thermal neutrons (barns), e) macroscopic cross-section (cm^{-1}), f) microscopic cross-section, fast neutrons (barns), g) nuclide produced by neutron absorption.

1.9 Why boron is important control rod material for fast reactors

Due to attractive nuclear properties, boron and its compounds are extensively used as control rod materials in most types of the nuclear reactors [11]. Boron has two principal isotopes, ^{10}B and ^{11}B. Natural boron contains 19.8 at.% ^{10}B and the rest is ^{11}B. Both of them are chemically identical, but their nuclear characteristics are entirely different. The effectiveness of boron as a neutron absorber in the fast neutron region is due to the high absorption cross-section of ^{10}B isotope. The neutron-absorption cross-section is sufficiently high for low energy neutrons, thus making it suitable for use in thermal reactors. At higher energies, the cross-section of most other isotopes becomes very small, however for ^{10}B the cross-section decreases monotonically with neutron energy [11]. Absolute values across the entire energy spectrum are of sufficient magnitude to make it very effective in the intermediate and fast neutron spectrum. Fig. 1.4a and Fig. 1.4b shows the cross-section of ^{10}B in the low and the high energy neutron range respectively.

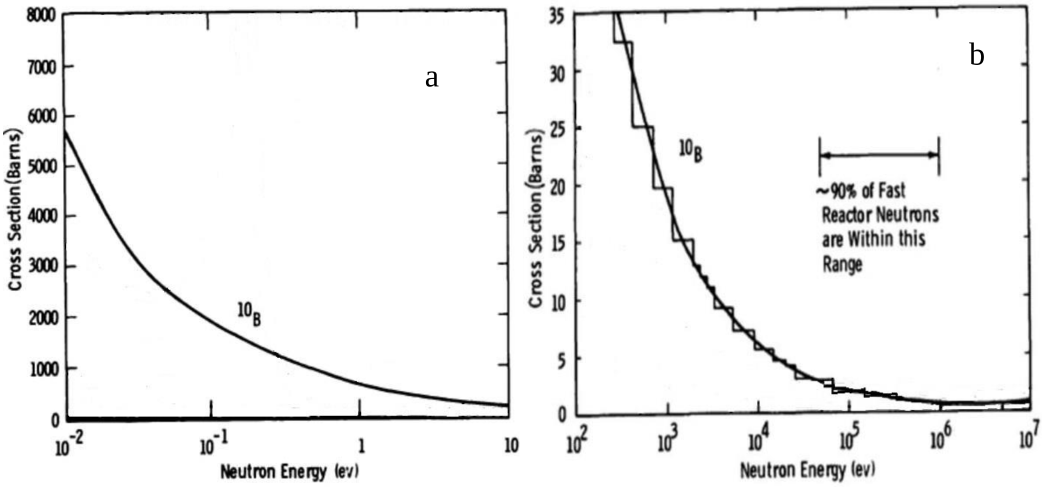

Figure 1.4. Nuclear cross-sections: a) at low neutron energies (thermal reactors), b) at high neutron energies (fast reactors) [11]

In addition to high absorption cross-section, boron has an additional advantage in terms of the irradiation point of view. The neutron absorption products of boron are stable, non radioactive isotopes. The neutron absorption reaction can be represented as:

$$^{10}_{5}B + \, ^{1}_{0}n \rightarrow \, ^{7}_{3}Li + \, ^{4}_{2}He + 2.6\,MeV \tag{1.5}$$

The reaction products do not emit any nuclear radiation. Hence, the decay heating problems during reactor shutdowns and transfer of depleted control rods are minimized. Another product generated by the absorption of neutron by ^{10}B is tritium ($^{3}_{1}H$) by the following reaction.

$$^{10}_{5}B + \, ^{1}_{0}n \rightarrow \, ^{3}_{1}H + 2\, ^{4}_{2}He \tag{1.6}$$

The cross-section of this reaction exists only above about 1MeV neutron energy and has a spectral average value of about 0.01b in fast neutron spectra.

Even though, ^{10}B has excellent neutron absorption cross-section in the fast region, the physicochemical properties of the element do not favour the use of elemental boron as such as a control rod material. Boron and compounds of boron have been studied extensively for control rod application in thermal and fast reactors

[11]. Among the compounds of boron, boron carbide is the most effective material for use in fast reactors because of its favourable physicochemical properties. The combination of outstanding nuclear properties, favourable physicochemical properties and predictable irradiation performance has made boron carbide as the principal control rod and shielding material in fast reactors.

PART I

Part I deals with the studies carried out on the synthesis of nanocrystalline boron carbide using a precursor method. It also deals with the studies on the sintering of the nanocrystalline boron carbide using hot pressing and spark plasma sintering techniques.

1.10 The B-C phase diagram

A number of phase diagrams were proposed for the B-C system [19-22]. Ridgway (1934) was the first to construct the approximate phase diagram on the basis of X-ray data. The phase diagram of the B-C system was studied by Ormont (1950), and Meerson and Samsonov (1953). Among them, Elliot (1970) and Kieffer (1971) suggested a wide homogeneity range for B_4C (9 to 20 at.% C) [19-20]. A large number of phases have been reported in the B-C system: B_6C, B_2C_2, BC, B_3C, B_7C, $B_{12}C$, $B_{50}C_2$, $B_{12}C_3$ and $B_{13}C_2$. The B-C phase diagram determined by Beauvy [22] is shown in Fig. 1.5. A peritectic point is shown as P in Fig. 1.5 has been reported for boron-rich compounds (melting point of 2348 K for a peritectic composition of 0.1 to 0.2 at.% carbon or 0.37 to 1 at.% carbon). Boron does not dissolve more than 21.6 at.% carbon at room temperature. A eutectic with 24.3 at.% carbon exists at high temperatures. Single phase boron carbide exists in the composition range of 8.8 to 20 at.% carbon. This is possible because of the substitution of carbon atoms within the icosahedra and the inter-icosahedral chains. The most widely accepted composition is B_4C.

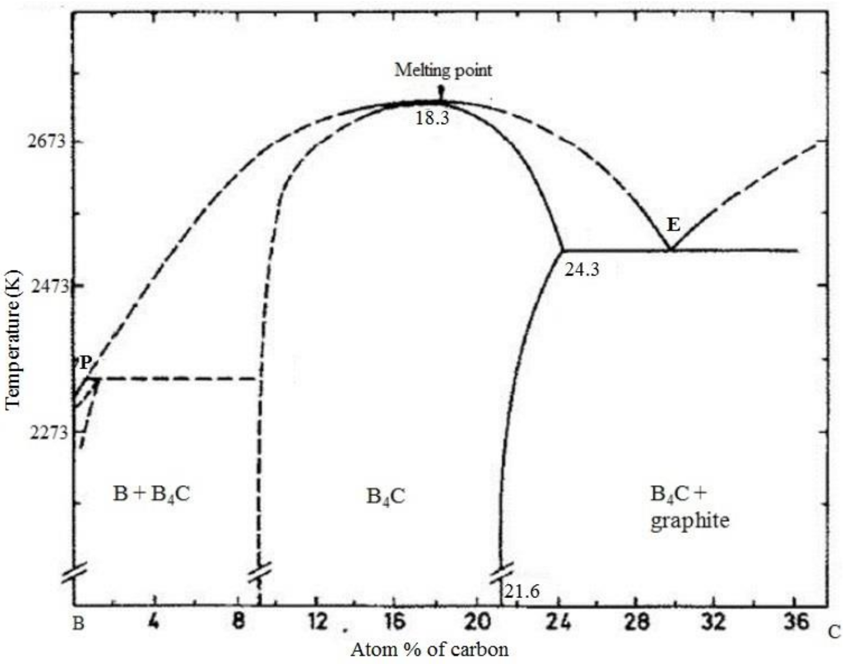

Figure 1.5. B-C phase diagram [22]

1.11 Boron carbide (B_4C)

Muhlhauser (1894), Moissan (1899) and Podszus (1933) were described the first attempts to prepare compounds of boron with carbon. Based on the chemical analysis, the products obtained were attributed to compositions of BC, B_2C_2, B_3C, B_4C and B_6C [19]. A boron carbide compound was first discovered in 1858, then Joly in 1883 and Moissan in 1894 prepared the compound and identified as B_3C and B_6C respectively. The stoichiometric formula, B_4C, was assigned in 1934 [20]. The characteristics and properties of B_4C are summarized in Table 1.2 [23]. Boron carbide, the black diamond, is the third hardest material after diamond and cubic boron nitride. It finds extensive applications in many industries owing to its fascinating properties such as high hardness, low density, high melting point, high elastic modulus, chemical inertness, excellent thermoelectric properties etc.

Table 1.2. Properties of B_4C

Property (Unit)	Value
Composition	$(B_{11}C)$ (CBC)
Molecular weight ($gmol^{-1}$)	55.26
Color	black (pure crystal is transparent and colorless)
X-ray density (gcm^{-3})	2.52
Melting point (K)	~2673
Specific heat (J $(molK)^{-1}$):	50.88
Heat of formation ($-\Delta H$) (kJ $(molK)^{-1}$ at 298.15 K)	57.8 ± 11.3
Thermal conductivity (W $(m°C)^{-1}$)	30
Thermal expansion ($10^{-6}(°C)^{-1}$)	4.3
Electrical resistivity (Ωcm):	0.1-10
Seebeck coefficient ($\mu V\ K^{-1}$):	200-300 @ 1250
Vickers hardness (GPa)	27.4- 34.3
Modulus of elasticity (GPa)	290-450
Shear modulus (GPa)	165-200
Bulk modulus (GPa)	190-250
Poisson’s ratio	0.18
Flexural strength (MPa)	323-430
Compressive strength (MPa)	2750
Oxidation resistance	in air up to 873 K
Absorption cross-section for thermal neutrons (barn)	755

1.12 Crystal structure of B_4C

Basic structural element for boron is icosahedron. Icosahedron is a polyhedron having twenty triangular faces, twelve equivalent vertices and I_{2h} symmetry, forming a cage of twelve atoms. Boron crystal is formed by combining these icosahedra in a rhombohedral configuration. Boron carbide can be described as a slightly distorted boron crystal structure in which the boron icosahedra are linked directly and also by a chain of three atoms located on the principal body diagonal [24]. The crystal structure of B_4C [24] is shown in Fig. 1.6. It consists of 12-atom icosahedra and linear 3-atom chains in a rhombohedral unit. The unit cell contains 15 atoms, i.e., one icosahedron and one chain [24]. Two crystallographically equivalent sites exist in the icosahedron-polar sites and equatorial sites. The six atoms which are at the top and bottom triangular faces of the icosahedron and directly linked to the atoms in the neighbouring icosahedra by covalent bonds constitute the polar sites (as shown in Fig. 1.6). The other six vertices of the icosahedron form a puckered hexagon and these symmetrically equivalent sites are called equatorial sites (as shown in Fig. 1.6). Each one of the six equatorial atoms is linked by a covalent bond to an atom at the end of a chain. The bond between the boron atoms in the icosahedra and between the carbon atoms and the boron atoms are covalent. Most of the icosahedra have a $B_{11}C$ structure with the carbon atom placed in a polar site [24]. However, the locations of the carbon atoms are not ordered within different icosahedra compared to one another. The linear 3-atom chains can be C-B-C, C-B-B or B-B-B. This depends on the variation in carbon concentration. B_4C (20 at.% C) structure consists of $B_{11}C$ icosahedra and C-B-C chains. As the composition becomes rich in boron, one of the carbon atoms from the C-B-C chain is replaced by boron. Near $B_{13}C_2$ composition, the structure consists of $B_{11}C$ icosahedra and C-B-B chains.

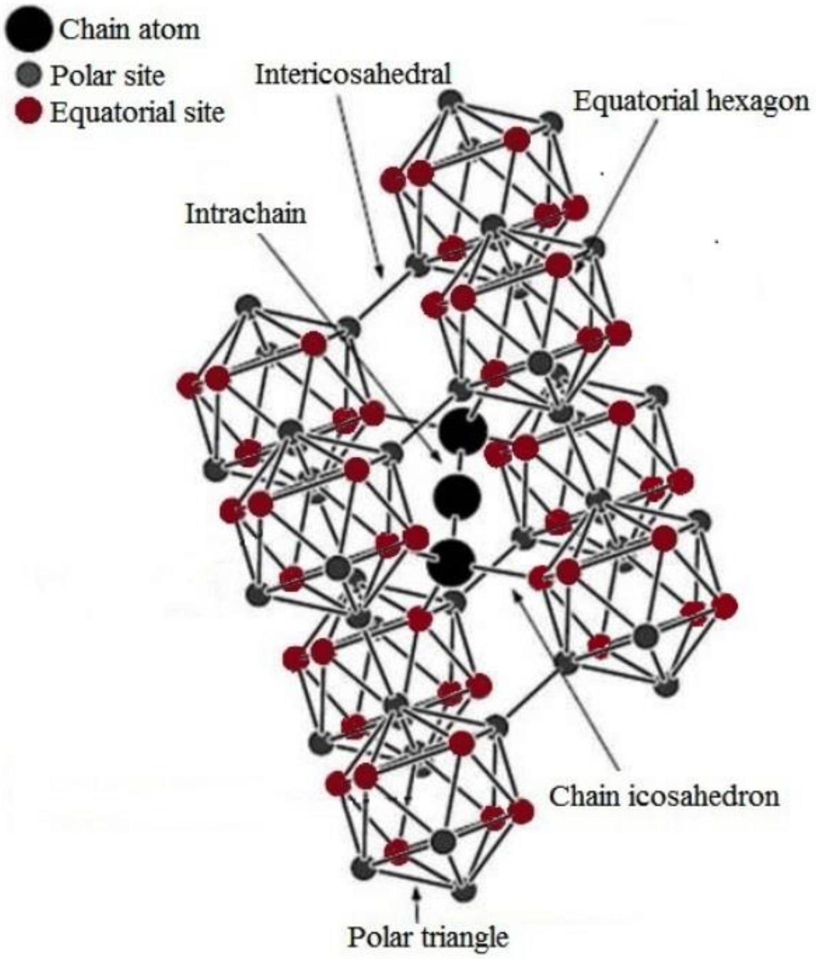

Figure 1.6. Crystal structure of B_4C [24]

1.13 Synthesis of B_4C

The methods of synthesis of B_4C in powder form or chunks are:

a. Carbothermic reduction

b. Magnesiothermic reduction

c. Synthesis from elements

d. Synthesis from precursors

1.13.1 Carbothermic reduction

Boron carbide is commercially produced by the carbothermic reduction of boric oxide or boric acid. The overall carbothermic reduction using H_3BO_3/B_2O_3 can be represented as shown below [25];

$$2B_2O_3(l,g) + 7C(s) \rightarrow B_4C(s) + 6CO(g) \tag{1.7}$$

$$4H_3BO_3(s) + 7C(s) \rightarrow B_4C(s) + 6CO(g) + 6H_2O(g) \tag{1.8}$$

This reaction (1.8) proceeds in the following three steps;

$$4H_3BO_3 \rightarrow 2B_2O_3 + 6H_2O \tag{1.9}$$

$$B_2O_3 + 3CO \rightarrow 2B + 3CO_2 \tag{1.10}$$

$$4B + C \rightarrow B_4C \tag{1.11}$$

Boric acid is converted to boric oxide by releasing water upon heating. The reduction of boric oxide with carbon monoxide (Eq. 1.10) is feasible above 1673 K. The furnace temperature is usually maintained at temperatures greater than 2273 K to enhance the rate of overall reaction. The process is highly endothermic and requires ~16800 kJmol^{-1}. The carbothermic reduction can be carried out in three types of electric heating furnaces, namely, tubular, electric arc or Acheson type (resistance heating with graphite rod). Alizadeh et al. [26] have synthesized B_4C using boric acid as the boron source and activated carbon or petroleum coke as the carbon source by carbothermic reduction process. B_4C formed only when the temperature was higher than 1673 K. The B_4C formed from H_3BO_3 and activated carbon at 1743 K was found to contain a mixture of B_4C and unreacted carbon[9]. The authors have reported 76.8 wt.% of boron and 0.8 wt.% of free carbon in the product. Here, the weight ratio of H_3BO_3/C was 3.3 compared to the stoichiometric weight ratio of 2.94. This indicated that excess boric acid in the reactant mixture decreased the free carbon content in the product. Addition of NaCl (1.5 wt.%) to the reactants helped to improve the boron content (77.1 wt.%) and reduced the free carbon content to 0.62 wt.%. These authors

---

[9] *The unreacted carbon impurity phase is referred to as 'free carbon' in this thesis. The carbon in the boron carbide is referred to as the 'bound carbon'. The bound carbon and free carbon together is referred to as 'total carbon' in the thesis.*

have reported that the addition of NaCl resulted in the decrease of unreacted raw material content and the increase of B_4C content in the product. When these authors have used petroleum coke (H_3BO_3 to C weight ratio = 3.5) instead of activated carbon, the same experimental conditions resulted in boron carbide with 76.5 wt.% boron and 1 wt.% free carbon. Jung et al. [27] have synthesized B_4C by carbothermic reduction of B_2O_3 and carbon. The reactants were mixed for 24 h and dried at 333 K for 24 h prior to carbothermic reduction. These authors have reported the formation of pure B_4C without carbon impurity phase when ($2B_2O_3 + 4C$) was used instead of stoichiometric reactants ($2B_2O_3 + 7C$) at 2073 K (20 min). Even though pure B_4C is formed by carbothermic reduction, it is energy intensive and time-consuming. Kobayashi et al. [28] have used B_4C seed grains and studied the effect of seed grains on the carbothermic reduction of B_2O_3 and carbon black and reported that the seed grains helped to improve the yield of boron carbide. These authors have also studied the effect of heat-treatment temperature and starting composition on the morphology of boron carbide particles synthesized by carbothermic reduction [29] using B_2O_3 and carbon black. The authors have reported spherical shapes for the B_4C particles synthesized at 1723 K. At 1823 K, the particles were large with skeletal shape and the particle sizes were found to increase with an increase in B_2O_3 content in the starting mixture. Beyond 1923 K, B_4C particles were dendrite-like with aggregation of small primary particles. Herth et al. [30] have synthesized nanocrystalline B_4C by carbothermic reduction of B_2O_3 and carbon black at 1623 K with excess B_2O_3 (100% excess) in the reaction mixture than that required for the stoichiometric reaction. These authors have reported an average particle size of 260 nm for the boron carbide powder synthesized by this method.

Many researchers have investigated the kinetics of carbothermic reduction, influence of process parameters on carbothermic reduction and conversion efficiency of carbothermic reduction for the synthesis of boron carbide. Rao et al. [31, 32] have designed a device for the measurement of core temperature for the synthesis of boron carbide by carbothermic reduction. Tumanov [33] has synthesized boron carbide by inductive heating of boron oxide and carbon black. Goller et al. [34] have produced boron carbide on a pilot plant scale using boric acid and carbon black. With the addition of 1.5 wt.% sodium chloride, these authors have reported an increase in the carbothermic reduction efficiency. Alizadeh et al. [35] have used boric oxide and petroleum coke or activated carbon for the synthesis of boron carbide by carbothermic reduction. These authors have found that the optimum weight ratio of boric oxide to the carbon bearing material to get boron carbide without free carbon was 1.8 for petroleum coke and 1.6 for activated carbon. The boron carbide product formed at 1743 K was found to contain 0.75 wt.% free carbon in the case of petroleum coke and 0.65 wt.% in the case of activated carbon. Gao et al. [36] have studied the process factors that influence the free carbon content in the product synthesized by rapid carbothermic reduction using boric acid as the boron source and carbon lamp black and Vulcan XC-72 (activated carbon) as the carbon source. These authors have reported that the dominant factors affecting the free carbon content in the final product were the reaction temperature, precursor (B_2O_3 and C) homogeneity, the particle size of the reactants and excess boron reactant. Gunnewiek et al. [37] have synthesized B_4C by employing microwave energy, using boric acid and carbon black as the reactants by carbothermic reduction. The microwave-assisted carbothermic reduction resulted in equiaxed boron carbide nanoparticles of ~50 nm along with elongated particles.

Even though carbothermic reduction is used for the commercial production of boron carbide due to the availability of cheap raw materials and simple equipment, the product obtained is often coarse-grained, and it is also an energy-intensive process. Due to the loss of boron during carbothermic reduction, this method is not suitable for the synthesis of boron carbide enriched with ^{10}B isotope for nuclear reactor applications.

1.13.2 Magnesiothermic reduction

The production of boron carbide by magnesiothermic reduction of boric oxide in presence of carbon is given below [25];

$$2\,B_2O_3 + 6\,Mg + C \rightarrow B_4C + 6\,MgO \tag{1.12}$$

This reaction takes place in two steps, equations (1.13) and (1.14), respectively.

$$2\,B_2O_3 + 6\,Mg \rightarrow 4\,B + 6\,MgO \tag{1.13}$$

$$4\,B + C \rightarrow B_4C \tag{1.14}$$

This reaction is exothermic.

Farzaneh et al. [38] have synthesized nanosized boron carbide by magnesiothermic reduction. These authors have reported that the use of mesoporous carbon as a carbon source in magnesiothermic reduction resulted in the formation of B_4C with a specific surface area of 60 m^2g^{-1} at 1023 K. Mohanty et al. [39] have investigated the influence of charge input mole ratio (B_2O_3:Mg:C), protective argon gas pressure and high compaction load on B_4C phase formation pattern and have found that a combination of 620 MPa compaction load, 10.2 MPa argon pressure and a mole ratio of (2:7.8:1.22) with optimized mineral acid leaching resulted in the formation of boron-rich boron carbide phases, $B_{13}C_2$, $B_{41.11}C_{4.45}$, B_8C, $B_{50}C_2$ along with $B_{12}C_3$ (B_4C) and elemental boron. Alkan et al. [40] have synthesized B_4C using B_2O_3, magnesium and carbon black by Self-Propagating High-Temperature Synthesis

(SHS) process followed by acid leaching. These authors have reported that the acid leaching helped to remove the by-products formed during magnesiothermic reduction and found that the amount of B_4C (14.8 g) formed was highest with initial molar ratios of B_2O_3:C:Mg as 1.0:0.8:3.0. Asgarian et al. [41] have investigated the effect of different sources of porous carbon on the synthesis of nanostructured B_4C by magnesiothermic reduction. These authors have found that the magnesiothermic reduction was not complete and carbon content of more than the stoichiometric amount was required for the completion of reduction. Singh et al. [42] have synthesized B_4C by using boric acid, activated magnesium and acetone. The average particle size was found to be ~12 nm.

From the literature, it is found that the major drawback of magnesiothermic reduction is the low yield of B_4C. The product will always be contaminated with magnesium oxide and magnesium borates or a mixture of higher carbides of boron, which necessitates the purification of the products synthesized by this route.

1.13.3 Synthesis from elements

The commercial method of carbothermic reduction is uneconomical for the production of B_4C enriched with ^{10}B isotope, due to loss of boron and boron held up in the furnace. The process results in lower yield due to significant loss of boron as oxides of boron during carbothermic reduction and subsequent process steps. The high vapour pressure of oxides of boron and high-temperature in the carbothermic reduction leads to the loss of boron. Hence, synthesis from elements is used in specialized applications such as the production of B_4C enriched with ^{10}B isotope for nuclear reactor applications [25]. Nuclear grade boron carbide control rod material for PFBR is produced by this method. The synthesis mainly consists of two steps:

a) production of high purity elemental boron and b) the synthesis of boron carbide from the elemental boron and carbon.

The high purity elemental boron is produced by a high-temperature (1073 K) molten salt electrowinning process [43-46]. This process involves the electrodeposition of boron from a melt (electrolyte) comprising of KCl (70 wt.%), KF (12 wt.%) and KBF_4 (18 wt.%) on a mild steel cathode [45]. The graphite crucible which is the container for electrolyte is the anode. The KBF_4 containing ^{10}B isotope is obtained by dissolving boric acid ($H_3{}^{10}BO_3$) in hydrofluoric acid, followed by precipitation using KOH [45]. Boron in boric acid is isotopically enriched in ^{10}B isotope by ion exchange method. Further, the elements, boron and carbon, are thoroughly mixed to form a uniform powder mixture. This mixture is then compacted and reacted at high temperatures (greater than 1773 K) under vacuum or inert atmosphere. The product thus obtained is then crushed and ground to obtain fine B_4C. The slow diffusion of elemental boron and carbon through B_4C layer formed during the course of reaction necessitates higher temperatures and longer duration for the complete conversion of the elements to B_4C [25]. The use of high purity boron powder in this method reduces the loss of boron as the volatile oxides of boron. Even though the control rod material for PFBR is produced by this method, it has certain disadvantages. The number of process steps involved in the production of high purity elemental boron is large. The method is not environmentally friendly due to the generation of toxic gases. Also, a huge amount of solid waste is generated during the production of high purity elemental boron. Hence, the method of production of boron carbide control rod material is energy and cost intensive.

Chang et al. [47] have investigated the production of B_4C nanoparticles by heating a mixture of amorphous carbon and boron at 1823 K using a conventional high-temperature furnace. The B_4C formed was found to be free of impurity phases and the average particle size was ~200 nm. The particle size of B_4C formed was found to depend on the particle sizes of the reactants. Sonber et al. [48] have synthesized B_4C using boron powder and petroleum coke at 2123 K by induction heating. These authors have reported that a higher amount of boron in the reactants resulted in the formation of the B_8C phase; however, this was not helpful in eliminating the free carbon content. Tamburini et al. [49] have synthesized B_4C using boron and carbon by spark plasma synthesis. These authors have found that the formation of B_4C at 1273 K and was completed at 1373 K. Ramos et al. [50] have synthesized boron carbide from the elements using high energy ball milling. The composition of the reactants was B-10 at.% C and B-18 at.% C powders and reported the formation of B_4C at 1473 K.

1.13.4 Precursor method

Recently, the precursor method is being developed as an alternative to the high-temperature commercial method of production of B_4C by using carbothermic reduction. In the precursor method, any boron-containing compounds such as boric acid/boric oxide/sodium borate and carbon-containing compounds such as citric acid/glycine/sucrose/polyvinyl alcohol can be taken as the boron and carbon source respectively. The heat-treatment of a mixture of suitable boron source and carbon source leads to the formation of a fine homogeneous dispersion of B_2O_3 and carbon, depending on the starting materials and the heat-treatment temperature. Further heat-treatment of the mixture of B_2O_3 and carbon thus obtained leads to the formation of boron carbide at a relatively lower temperature. Researchers have used carbon sources such as cellulose and glucose [51, 52], glycerine [53, 54], phenolic resin [55], citric acid [56-58], mannitol [59], poly(vinyl alcohol) [60-64], and sucrose [65-72].

Rafi-ud-din et al. [51] have studied the effect of structural homogeneity of the precursor on the low-temperature synthesis of boron carbide using boric acid as the boron source, cellulose as the carbon source and ethylene glycol as the solvent. The formation of crystalline boron carbide was completed at 1473 K. Maqbool et al. [52] have used boric acid and three different carbon sources such as cellulose, glucose and starch and studied the effect of different carbon sources on the synthesis and morphology of boron carbide. Ethylene glycol was the solvent used in the study. Among the three sources, the cellulose precursor resulted in the formation of carbon fibers and the dispersion of B_2O_3 into fibrous-carbon was finer as compared to that in the other precursors. The formation of B_4C commenced at 1373 K in the case of cellulose derived precursor compared to other precursors and this was 150 to 250 K lower as compared to glucose and starch derived precursors. The formation of B_4C was completed at 1473 K in the case of cellulose precursor. Tahara et al. [53] have reported the effect of the addition of tartaric acid on the synthesis of boron carbide from the boric acid-glycerin condensed product. These authors have studied the change in the precursor structure with the addition of tartaric acid and reported that the addition of 25 mol.% tartaric acid led to a homogeneous and finer dispersion of B_2O_3 into C than that without tartaric acid. The formation of crystalline B_4C was reported at 1523 K within a shorter duration of heating when 25 mol.% tartaric acid was used. Boron and free carbon contents were not quantified in all the work mentioned above. Kakiage et al. [54] have also used glycerin as the carbon source and boric acid as the boron source. These authors have reported that the formation of boron carbide commenced at 1423 K and was completed at 1523 K. Corradetti et al. [55] have used two different carbon sources, citric acid and phenolic resin for the synthesis of B_4C and used excess H_3BO_3 in order to compensate for the loss of boron during heat-treatment. The free carbon content in the product was found to be 9.1 wt.% even with excess H_3BO_3. Rafi-ud-din et al. [56] in their later work have studied the effect of the addition of ethylene glycol on the synthesis of boron carbide from boric acid and citric acid, and have reported a free carbon content of 4 wt.% in the synthesized product with the addition of ethylene glycol. The formation of boron carbide was reported to commence at 1373 K. However, crystalline B_4C was formed only at 1623 K. Khanra [57] has synthesized boron carbide using boric acid-citric acid gel precursor and reported a free carbon content of 9.8 wt.% in the product even at 1873 K. Sinha et al. [58] have synthesized B_4C using boric acid-citric acid gel precursor at 1973 K and have found 11.3 wt.% free carbon in the final product. Kakiage et al. [59] have also synthesized crystalline B_4C powder using a condensed boric acid-mannitol product. These authors have reported a lower free carbon in the boron carbide synthesized at 1523 K from a condensed product (thermally decomposed at 673 K). However, these authors have not quantified the amount of free carbon content in the product. Studies [60-64] have been reported the use of poly(vinyl alcohol) as the carbon source for the synthesis of boron carbide. Sucrose was used as the carbon source for the synthesis of B_4C in many studies [65-72]. Pilladi et al. [65] have used boric oxide-sucrose gel precursor for the synthesis of boron carbide at 1773 K and reported a free carbon content of 3.5 wt.% in the product obtained. These authors have also reported the synthesis of boron carbide using molten sucrose and boric acid [68] and found the product to contain free carbon content of 6 wt.% even at 1873 K for 3 h. Foroughi and Cheng [66] have used boric acid and sucrose for the synthesis of B_4C. These authors have observed significant non-uniformity in the morphology of the product synthesized at different temperatures with a heating rate of 10 K min^{-1} and it varied from large micron-sized polyhedral particles to nanowires, regardless of the uniformity of the starting mixture. Zakharova et al. [67] have used H_3BO_3 as the boron source and four different carbon sources viz. sucrose, potato starch, phenol-formaldehyde resin and carbon black for the synthesis of B_4C. These authors have reported a 95% yield in B_4C when sucrose was used with the addition of excess boric acid. Foroughi and Cheng [69] have also studied the effect of processing conditions such as temperature, time and heating rate, atmosphere, B_2O_3 to C molar ratio, precursor type and adsorbed moisture in the pyrolyzed powder on the morphology of B_4C, synthesized using H_3BO_3 and sucrose/polyvinyl alcohol using precursor method. These authors have reported that rapid heating rate and high temperature with a shorter duration of heating resulted in uniform submicron sized particles of B_4C. Avciata et al. [70] have synthesized B_4C from a sugar-based precursor. These authors have used sulfuric acid dehydration of sugar to synthesize the precursor and reported the formation of B_4C in the temperature range of 1673 to 1873 K. Watts et al. [71] have synthesized B_4C powder with uniform particle size and a high yield using H_3BO_3-sucrose precursor. These authors have found that the exposure of precursor powder to the humid atmosphere resulted in a significant change in the morphology of B_4C due to the absorption of water. This led to the decrease in the contact area between boron and carbon components and a lower yield of B_4C with the increase in the free carbon impurity. A systematic study was lacking with B_2O_3 or H_3BO_3 as the boron source and sucrose as the carbon source.

In all the above studies [51-71], the starting materials for the synthesis of precursor were taken as per the stoichiometric Eq. (1.7) with carbon to B_2O_3 mole ratio (CBMR) of 3.5. Pilladi [73] has computed a stability diagram for the B-O-C system using the thermochemical software ‘FactSage 6.2′ and reported that the carbothermic reduction of boric oxide was possible at temperatures greater than 1673 K and CBMR values in the range of 0.69 to 3.38 at 0.098 bar pressure. The carbothermic reduction in the temperature range of 1830 to 2743 K would result in B_4C and free carbon phases if the CBMR was ≥3.38. The calculation also showed that the carbothermic reduction would result in a biphasic mixture of B_4C and carbon when CBMR was equal to 3.5 irrespective of the temperature of heating. The presence of free carbon could be reduced by taking reactants with CBMR between 3.38 and 3.5.

In the present study, the formation and processing of the precursor with CBMR 3.38 was carried out systematically using B_2O_3 and sucrose with the objective to minimize the free carbon content in the final product. The temperature and time for the synthesis of boron carbide were optimized. The optimized results obtained with CBMR equal to 3.38 were compared with those obtained with the stoichiometric reactants, i.e. CBMR equal to 3.5.

In the precursor method, reactants are mixed in solid state; the mixture tends to be inhomogeneous. This often leads to a product mixture of B_4C and a significant amount of free carbon [51-54, 56, 59, 62, 63], necessitating a suitable modification in the process. The important factors influencing the presence of free carbon in the product prepared by precursor method are the homogeneity of the mixture of reactants such as boron and carbon-bearing species in the precursor, temperature, particle size of the components in the precursor and heating rate [36]. Improving the homogeneity of the components in the precursor helps to reduce the free carbon content in the final product significantly.

1.14 Improving the homogeneity of the reactants in the precursor by the method of freeze-drying and microwave-assisted heating of the reactants

In general, homogeneity of a mixture of reactant components can be improved by mixing them in a suitable solvent. Roth and Vanderah [74] and Windisch et al. [75] have indicated that wet grinding with acetone or alcohol medium improves the degree of homogeneity of the reactants. After wet mixing, the solvent needs to be removed. Rasmussen et al. [76] have tried different drying techniques such as drying in an oven, vacuum drying and freeze-drying in order to study the sinterability of hydroxide-derived yttria powders. They have found that the oxide obtained from freeze-dried powders had a higher specific surface area and better sinterability than the oven-dried precursors.

1.14.1 Freeze-drying

The basic principle of freeze-drying is sublimation i.e., the solid directly converts into gas. Freeze-drying is a process in which the solvent or the suspension medium is crystallized at low-temperatures and thereafter the solvent is removed by sublimation [77-79]. Water is the solvent generally used in freeze-drying. The freeze-drying mainly consists of three stages- freezing, primary drying and secondary drying. In the first stage, the material is frozen by placing it in a freeze-drying flask or shell freezer and then cooled by mechanical refrigeration or dry ice or liquid nitrogen. The material is cooled below its eutectic point which is the lowest temperature at which the solid and liquid phases co-exists. This ensures the sublimation in subsequent stages of freeze-drying. In the primary drying stage, the chamber is evacuated until the pressure is lower than the vapour pressure of the solvent. Secondary drying stage mainly helps to remove solvent molecules remaining after primary drying stage. The freeze-dried powders show improved sinterability and less agglomeration [80]. The ceramics prepared using water based slurry and freeze-drying have certain advantages such as less shrinkage due to sintering, widely controllable porosities and relatively good mechanical properties [81].

Freeze-drying is employed in the synthesis of a wide variety of materials in ceramic industry. Roehrig and Wright [82] have used freeze-drying to synthesize ultrafine tungsten carbide powder. These authors have used a colloidal suspension of graphite and ammoniacal tungstic acid solution and employed the freeze-drying technique to remove the solvent. This, they claim, resulted in an intimate mixing of the starting materials and formation of ultra-fine particles of tungsten carbide. Fukasawa et al. [81] have prepared porous ceramics with unique microstructure from water-based slurry and have used freeze-drying to remove water. Sofie and Dogan [83] have also used freeze casting method for the preparation of alumina parts by pressureless slip moulding using aqueous slurries. These authors have demonstrated the feasibility of fabricating complex-shapes with aqueous alumina slurries of high solid loading using freeze-drying method. Ding et al. [84] have used gel freeze-drying to synthesize porous mullite ceramics with an open porosity up to 92.9%. Fukasawa et al. [85] have also successfully synthesized porous silicon nitride with unidirectionally aligned channels using the freeze-drying process. The freeze-dried material upon heat-treatment resulted in porosity greater than 50% which makes the material suitable for various applications such as separation filter, support materials for catalysts and absorbents. Pérez-Coll et al. [86] have synthesized gadolinia doped ceria and samaria doped ceria from freeze-dried precursor powders. The reactants were dissolved in distilled water and were frozen using liquid nitrogen. Water was removed by sublimation in a freeze dryer to obtain a homogeneous nanocrystalline precursor. Zhao et al. [87] have used the freeze-drying method to synthesize mesoporous titania powder. Wang et al. [88] have used freeze-drying to remove water in the preparation of clay aerogels. The clay aerogels synthesized using the freeze-drying method exhibited better mechanical compressive properties as compared to that of extruded or injection moulded samples. Farhan et al. [89] have used freeze-drying to produce multi-walled carbon nanotube aerogel inside the pores of open cell carbon foam. Luan et al. [80] have studied the effect of different drying methods on the preparation of nanoscale barium titanate. These authors have used freeze-drying, azeotropic distillation and oven drying of the barium titanate synthesized using precipitation. The freeze-dried powders showed improved sinterability and less powder aggregation as compared to the powders obtained using other drying methods employed in their study. Drying of the gel by heating can lead to cracks, shrinkage and breakup of the network structure due to thermal stress and poor strength of gel network. Freeze-drying is an efficient method to remove water from water-based gels to obtain porous crack-free skeletons. The powder obtained by the freeze-drying method shows particles with small size, regular shape, uniform distribution, large specific surface area and less agglomeration as compared to the powders obtained by ball-milling, vacuum drying and heating / drying methods [87].

In the present study, the B_2O_3 and sucrose were made into a slurry in media such as water or ethanol and freeze-dried. The precursor for the synthesis of boron carbide was prepared by heat-treatment of this dried product.

The homogeneity can also be improved if the components are mixed on a molecular scale, say by complexation. Mannitol forms a stable 2:1 complex with boric acid via B-O-C bonds. The complex formed can be represented as shown below;

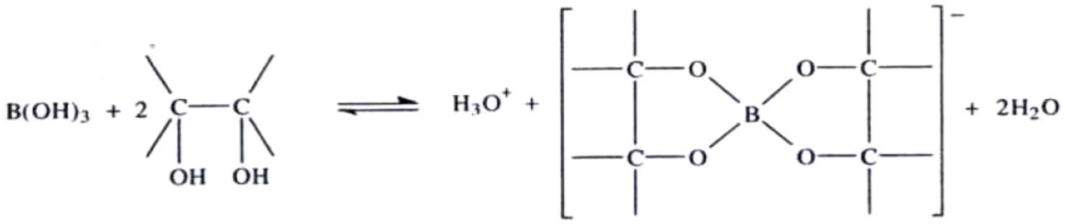

Synthesis of B_4C using mannitol as the carbon source employing the precursor method is limited [59]. Kakiage et al. [59] have prepared a condensed product by the dehydration condensation of H_3BO_3 and mannitol. The condensed product thus obtained was thermally decomposed in air at different temperatures. Further heat-treatment of the product under flowing argon resulted in the formation of B_4C. This they claim resulted in the formation of B_4C with less free carbon and occurs at a lower synthesis temperature.

The mannitol-boric acid condensed product can be prepared by heating the solution containing these using either a hot-plate or microwave oven. Microwave-assisted heating is different from conventional hot-plate heating. Microwave-assisted heating was used for the preparation of condensed product in the present study because of the uniform heating of the microwave as compared to the hot-plate.

1.14.2 Microwave-assisted synthesis of ceramics

Microwaves are electromagnetic radiation with a wavelength ranging from 1 mm to 1 m with a frequency of 300 GHz to 300 MHz respectively [90-92]. The generally used frequency of microwave for industrial and scientific applications is 2.45 GHz. Microwave energy is delivered directly to materials when the electromagnetic field of the microwave radiation interacts with the material as compared to conventional heating where the energy is transferred to the material by conduction, convection and radiation of heat from the surface of the material. Ultimately, the dielectric properties of the material will decide the effect of the electromagnetic field on the material. The interaction of microwave with the molecular dipoles results in rotation of dipoles and due to this rotation the heat energy will be dissipated. At microwave frequencies, the dipole polarization is the most important mechanism for energy transfer at the molecular level. The main heating mechanisms are dielectric loss and conduction loss [92]. The dielectric loss is effective in dielectric insulator materials such as water, ceramics, etc., in which dipoles are generated on exposure to the external electric field. The oscillating electric field creates agitation of molecular dipoles. Inertial, elastic, frictional and molecular interaction forces resist these changes in the orientation of molecules. As a result, molecular kinetic energy increases and results in volumetric heating. In addition, the increase in the kinetic energy of all the dipoles causes an increase in the temperature of materials within a shorter time. The conduction mechanism is significant in microwave processing of pure metals, metallic based materials and semiconductors [92]. The free electron in these materials moves in the direction of the electric field with a certain velocity. The high conductivities of these materials attenuate the field rapidly and as a result, a large current is induced. Hence an induced magnetic field is generated in the opposite direction of external magnetic field within the material. The induced magnetic field creates a force on moving electrons and as a result of this the path of the electron is reversed. Thus, a kinetic energy is imparted on electrons and its movement is restricted by the inertial, elastic, frictional and molecular interaction forces. This phenomenon is rapidly repeated by the oscillating electric field which generates uniform volumetric heating inside the material. The advantages of microwave heating compared to conventional heating are very rapid heating with high heating rates, time and energy saving and reduced processing time.

In this study, two complexes were prepared by using mannitol and boric acid with different carbon to B_2O_3 mole ratio; a) CBMR of 3.38 (C/B wt.% ratio = 1.87) and b) CBMR of 6 (excess carbon, C/B wt.% ratio = 3.33). Higher CBMR was chosen in order to see the effect of thermal decomposition on the removal of excess carbon than that required for stoichiometric reaction (CBMR = 3.5) as per Eq. (1.7). The mannitol-boric acid condensed product was prepared by microwave-assisted heating of the solution containing mannitol and boric acid.

1.15 Effect of 'free carbon' as an impurity phase in B_4C for nuclear reactor applications

As discussed in Section 1.7, the B_4C control rod material for PFBR is stacked inside 20% cold worked alloy D9 stainless steel clad tube. Chandran et al. [93] have studied the chemical compatibility of alloy D9 with B_4C control rod material (B = 76.1 wt.%, C = 19.8 wt.%) in the presence of liquid sodium. These authors have reported that the chemical interaction of D9-B_4C-Na resulted in the increase in carbon content of clad tube (~150 µm penetration depth after 5000 h of equilibration at 973 K). The maximum clad wastage reported by these authors was <15% of the clad thickness (D9 clad tube thickness in PFBR is 1.15 mm). However, 25% of clad wastage is acceptable for control rod applications [94]. Hence the nuclear grade B_4C control rod material is compatible with the clad material under normal operating conditions of the reactor. Nuclear grade B_4C control rod material for PFBR is produced from high purity elemental boron and carbon [25]. The method of production of boron carbide control rod material generates a huge volume of solid waste and toxic gases and also is energy and cost-intensive process as explained in Section 1.13.3. Consequently, cost and energy efficient methods of production of boron carbide need to be developed. Alternative to the high-temperature method of production of boron carbide, low-temperature methods based on precursors often end up with boron carbide-containing a significant amount of free carbon as the impurity phase. Considering the solubility of carbon in liquid sodium (30 ppm) at 823 K [95], the free carbon present as an impurity phase in the B_4C can diffuse through liquid sodium. This transfer of free carbon impurity from the B_4C to the cladding and diffusion of carbon in the clad matrix is accompanied by the carbide precipitation in the clad (carburization of clad). The precipitated carbide, $(Fe, Cr)_{23}C_6$ is a brittle phase and the cladding becomes too brittle for use when the carbon content exceeds 0.6 wt.%. The carbon can also get transported to the entire reactor core through the flowing liquid sodium. This leads to the carburization of structural materials. The clad carburization of the fuel pin clad leads to clad breach and the mixing of nuclear fuel with the liquid sodium coolant. This results in the transport of radioactivity in the reactor core. In order to minimize carburization of clad and structural materials in the nuclear reactor core, the free carbon impurity in the boron carbide should be low.

1.16 Sintering of nanocrystalline B_4C

Sintering is a thermal treatment for bonding particles into a coherent, predominantly solid structure via mass transport events that often occurs on atomic scale which leads to improved strength and lower system energy [96]. Sintering proceeds by evaporation-condensation, surface diffusion, grain boundary diffusion, volume diffusion, and plastic deformation or creep [97]. Only grain boundary diffusion, volume diffusion and plastic deformation/creep lead to densification. The other processes lead to microstructural coarsening. Lowering the surface energy of the particles is the driving force for sintering. The higher driving force for sintering is achieved by reducing the particle size and thereby increasing the surface area. Nanoceramics have their own sintering characteristics. Agglomeration, presence/formation of amorphous and/or metastable phases, sintering temperature and particle size distribution influences the sintering of nanoceramics. The huge specific surface area of ceramic nanoparticles is associated with high surface energy that often leads to agglomeration which results in poor densification. The low-temperature synthesis of nanoparticles or the synthesis from non-equilibrium processes produces nanoparticles at metastable states or consisting of polymorphic mixtures, precursors or amorphous phases of the desired material. This may result in poor densification due to the porosity associated with volume change during the decomposition or phase transformation of these materials. For many nanoparticles, the onset of sintering temperature is in the range of $0.2T_m$ to $0.3T_m$ (T_m is the melting point in Kelvin) compared to micron-sized systems, for which the onset of sintering temperature is $0.5T_m$ to $0.8T_m$ [97].

Consolidation of B_4C is difficult due to the high melting point, low self-diffusion coefficient and presence of covalent bonding [25]. It is estimated that the fraction of the covalent bond in B_4C is greater than 90% [98]. Low self-diffusion and a high ratio of grain boundary to surface energy lead to poor grain boundary and volume diffusion which are the mechanisms for densification. The grain boundary and volume diffusion become effective only at temperatures greater than 2273 K. At temperatures lower than 2273 K, surface diffusion and evaporation-condensation mechanisms occur which result in mass transfer without densification. Higher sintering temperature results in exaggerated grain growth leading to poor mechanical properties. Densification of B_4C with limited grain growth and without losing mechanical properties can be achieved by using a suitable sintering aid and/or by applying external pressure. Selection of the sintering method mainly depends on the end use of the product.

In the present study, consolidation of nanocrystalline boron carbide was carried out using pressure-assisted sintering as the rate of densification is very slow in conventional sintering. Pressure-assisted sintering can accelerate nanoceramic densification by providing an external driving force for sintering. As a result, near theoretical densification is achieved at lower sintering temperatures and at shorter sintering durations. Sintering methods used in this work were hot pressing and Spark Plasma Sintering (SPS).

1.16.1 Hot pressing

Hot pressing is a non-conventional sintering method. It generally involves heating a powder compact with simultaneous application of pressure [99, 100]. The powder compacts are heated externally using graphite heating-element and the pressure is applied hydraulically. Heating mainly occurs as a result of conduction from external surface of the container to the powder. As a result, heating rates will be low. Hot pressing is the most common method for fabricating dense B_4C [25]. Without sintering additives, at temperatures greater than 2373 K, with an applied load of ≥30 MPa, B_4C can be densified to 100% theoretical density (TD) by hot pressing. Densification by hot pressing mainly occurs by three mechanisms [25];

i. Particle rearrangement: In this stage, the total and open porosities decrease and closed porosities remain constant (T = 2073 to 2223 K).

ii. Plastic flow: In this stage, the closing of open porosities happens without affecting the closed porosity (T = 2223 to 2373 K).

iii. Volume diffusion and pore elimination (T = 2373 to 2473 K).

Density, porosity and microstructure of the hot pressed B_4C depends on the hot pressing parameters-temperature, pressure, time and heating/cooling rate.

Reviews on the hot pressing of B_4C with and without additives are reported [20, 25]. Kalandadze et al. [101] have used hot pressing to sinter B_4C powder compacts in the temperature range of 2173 to 2373 K and pressures 20 to 40 MPa in boron nitride lined graphite moulds using resistance heating and induction heating. Microstructure of the sintered B_4C powder compacts revealed homogeneous (almost similar size) and inhomogeneous (various sizes) grains, which were due to a mixture of monodisperse and polydisperse particles in the powder. Du et al. [102] have investigated densification and grain growth kinetics of B_4C as a function of various parameters such as sintering temperature, sintering pressure and dwell time during hot pressing. These authors have reported that plastic deformation of particles dominated during initial stage of sintering and the grain boundary diffusion dominated in the final stage of sintering. Angers and Beauvy [103] have hot pressed seven different B_4C powders (from different manufacturers) in the temperature range 1775 to 2575 K at pressures from 20.7 to 68.9 MPa and with varying dwell times. These authors have studied the influence of temperature, pressure, time and heating/cooling rate on densification and microstructure of these powders and have reported that temperatures greater than 2400 K were required to sinter B_4C to 100% theoretical density (TD). Chen [104] has carried out microstructural characterization using TEM on commercially available hot-pressed B_4C (2 samples, one with purity 98.5% and other with purity 99.5%, the density of both samples >98.5% of TD). These authors have reported the presence of secondary phases, sub-micrometer triple-junction phases (rhombohedral Fe_2B_{103}, orthorhombic Ti_3B_4) and nano-scale intra-granular precipitates (AlN, $Mo_2(C, B)$ and graphite) in the hot-pressed B_4C. Zhang et al. [105] have studied the effect of pressures (30 MPa to 110 MPa) on the densification behaviour, microstructure and mechanical properties of B_4C sintered by hot pressing. These authors have reported a density between 98.49 and 99.76% of TD and plastic deformation as the main densification mechanism under high pressure. These authors have also carried out a comparative study on the densification, microstructure and mechanical properties of B_4C sintered using hot pressing and spark plasma sintering [106]. These authors have reported a homogeneous microstructure with a density of 91% (TD) for the B_4C obtained at 2173 K under a pressure of 40 MPa for 60 min. Dole et al. [107] have carried out sintering of B_4C by hot pressing at 2373 K under 40 MPa pressure and reported a density of 95% (TD) for the sintered B_4C. Kuzenkova et al. [108] have studied the kinetics of recrystallization in sintered and hot pressed B_4C and reported that in hot pressed B_4C, grain growth was rapid at temperatures greater than 2373 K (30 to 40 min). Roszeitis et al. [109] have carried out reactive sintering of boron and carbon with various compositions of carbon (9.1, 11.1, 13.3 and 18.8 at.%) at 2323 K using hot pressing to obtain dense B_4C. These authors observed that the density of B_4C with these various carbon components were greater than 99% (TD).

In most of the studies reported in the literature, researchers have used commercially available B_4C powder prepared by either carbothermic reduction or elemental synthesis to study the densification behaviour. In the present study, nc-B_4C synthesized using the B_2O_3-sucrose precursor method was used for the sintering studies. Boron carbide powder synthesized by carbothermic reduction at high-temperature (commercially available powder) was also used for comparison of the densification using hot pressing. Even though hot pressing results in dense B_4C, the entire process is time-consuming. The longer duration of heating at the desired temperature may result in microstructural coarsening.

1.16.2 Spark plasma sintering (SPS) technique

SPS is an advanced sintering technique at a lower temperature with a shorter duration of heating for the consolidation of powders, especially those in the nano range [25]. The materials to be sintered are placed in a graphite die and plunger assembly. The driving force for sintering is provided by the application of high current through the sample with simultaneous application of pressure. In a conducting material, the current passes directly through the sample and heats it rapidly, whereas the non- conducting samples are usually heated by the heat conduction from the die walls [110-113]. The main advantage of the SPS over conventional pressure-less furnace sintering and hot pressing is the possibility of short densification time, lower sintering temperature and production of fully dense materials with limited grain growth.

In the SPS process, ON-OFF DC pulse voltage and current from a special pulse generator are applied to the powder particles. This ON-OFF DC pulse energizing method generates, spark plasma, spark impact pressure, Joule heating and an electrical field diffusion effect. The pulsed current flow through the powder particles are shown schematically in Fig. 1.7. The passage of electric current through the particles results in Joule heating which leads to welding of the particle under mechanical pressure.

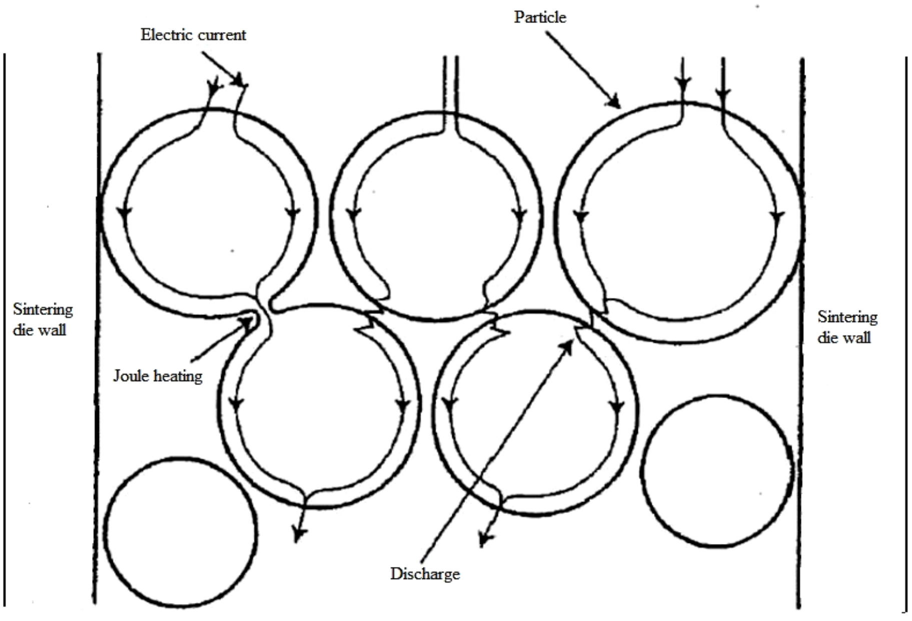

Figure 1.7. Pulsed current flow through powder particles [110]

Recently, SPS has been used for the densification of B_4C without sintering additives by many researchers [114-133] as it is advantageous over the conventional methods. Hayun et al. [114] have studied the static mechanical properties and dynamic compressive behaviour of SPS consolidated B_4C powder. These authors have reported that the hardness, Young's modulus, fracture toughness, flexural strength and Hugoniot elastic limit were better than the hot-pressed B_4C. These authors have also carried out the microstructural characterization of B_4C sintered using SPS in the temperature range 2073 to 2473 K under pressure of 32 to 51 MPa [115]. These authors have found abnormal grain growth for the samples sintered at 2473 K with a heating rate in the range of 50 to 400 K min^{-1} and homogeneous finely equiaxed grains with a heating rate of 600 K min^{-1}. Cengiz et al. [116] have fabricated B_4C ceramics using SPS in the temperature range of 1973 to 2073 K for 5 min under an applied pressure of 50 MPa and reported a density greater than 97% (TD). Moshtaghioun et al. [117] have studied the effect of spark plasma sintering parameters on microstructure and room-temperature hardness and toughness of fine-grained B_4C. B_4C with 100% TD was obtained at 1973 K (3 min) with mean grain size equal to ~0.69 µm. These authors have also carried out a detailed study to elucidate the role of temperature, time and heating ramp on the densification of B_4C [118]. The grain size reported was 370 nm and the density was ~98.5% (TD) for the B_4C sintered at 1973 K (3 min). Badica et al. [119] have used high pressure (300 MPa) and low temperature (1873 K) to obtain dense B_4C (>95% TD) using SPS. This they claim resulted in improved fracture toughness and dynamic toughness when compared to the sample sintered at 2373 K under a pressure of 50 MPa. Li et al. [120] have studied the influence of sintering temperature, heating rate and holding time on the densification and microstructure of B_4C using SPS in the temperature range of

1673 to 1873 K. The optimum sintering temperature reported by them was 1873 K and this resulted in a density of ~98.33% (TD). Densification behaviour of B_4C powder in the temperature range of 1373 to 2073 K was studied using SPS by Sairam et al. [121]. These authors have reported hardness, fracture toughness and elastic modulus of B_4C with 100% TD as 37.2 GPa, 2.8 $MPam^{1/2}$ and 570 GPa respectively. Moshtaghioun et al. [122] have also studied nanograin retention of commercially available B_4C powder using SPS. In this work, these authors have suggested a two-step sintering for B_4C which would have resulted in nanograin retention in the sintered samples. These authors have also studied the room temperature fracture toughness and hardness of B_4C ceramics with grain sizes ranging from 120 nm to 17 µm [124]. Moshtaghioun et al. [126] have also studied the effect of methylation-induced purification of B_4C powder and its densification using SPS. It was reported that the purified powders showed better densification as compared to the raw powder. Ji et al. [123] have proposed plastic deformation as the dominant densification mechanism during the SPS of B_4C. Chaim [125] has also proposed that plastic deformation and viscous particle sliding are the main deformation mechanisms during the densification of ceramic particles by SPS. Belon et al. [127] have studied the room-temperature mechanical properties (Vickers hardness and fracture toughness) and high-temperature (up to 1873 K) bending tests (elastic modulus and flexural strength) on B_4C sintered at 1923 K using SPS. These authors did not observe any brittle-to-plastic transition up to 1873 K. Thermodynamic modelling and investigation of the effect of oxygen on the sintering of B_4C was studied by Asadikiya et al. [128]. These authors have reported a density of 88% (TD) at 2073 K (20 min) for the as-received commercial powder (Grade HD 15, d (50) particle size: 0.6 to 0.9 mm, oxygen content: up to 1.8 wt.%, H. C. Starck, Germany). When the methanol-washed powder was used, a density of 92% (TD) was obtained. Methanol washing helped to remove the B_2O_3 and thereby improved the density of the sintered compacts. These authors have also studied the effect of sintering parameters such as temperature, heating rate and holding time on the hardness of spark plasma sintered B_4C [129]. Moskovskikh et al. [130] have fabricated bulk B_4C ceramics from boron and carbon mixtures using reactive spark plasma sintering. The porosity in the compacts was found to be <2% and the compacts had fine grains (3 µm). Ortiz et al. [131] have carried out the spark plasma sintering on the B_4C obtained by high energy ball milling in dry and wet conditions (methanol). These authors recommended dry shaker milling to obtain B_4C with better sinterability. Toksoy et al. [132] have used submicrometer B_4C synthesized using rapid carbothermic reduction for the spark plasma sintering and reported that higher density (<99%, TD) was achieved with a shorter duration (5 min) as compared to the commercial powder (20 min). Microstructural evolution and densification mechanisms during the SPS of B_4C in the temperature range of 1973 to 2373 K were studied by Zhang et al. [133]. These authors have proposed a creep deformation model as the controlling mechanism during densification of B_4C using SPS in the temperature range of 1973 to 2373 K under a pressure of 40 MPa.

In most of these studies, researchers have used commercially available B_4C powder synthesized mostly by carbothermic reduction to study the densification behaviour using SPS. The present study explores the possibility of using advanced sintering technique (SPS) for the densification of nanocrystalline sinteractive boron carbide synthesized using a low-temperature method (B_2O_3-sucrose precursor method). Boron carbide powder prepared by a high-temperature carbothermic reduction (commercially available powder) is also used for comparison of the densification using SPS.

PART II

Part II of the thesis presents the studies on the synthesis of Yttria-Stabilized Zirconia (YSZ) and the measurement of its conductivity.

1.17 YSZ

Zirconia (ZrO_2) exists in three polymorphic forms: monoclinic, tetragonal and cubic. At room temperature, the monoclinic phase is the stable phase and it transforms to tetragonal and to cubic phase at 1443 and 2643 K, respectively [134, 135]. The cubic phase is stable up to the melting point of zirconia, 2953 K. The tetragonal phase is metastable and it transforms into the monoclinic phase under stress. All these phase transformations are martensitic in nature. The cubic phase of zirconia can be stabilized at room temperature by incorporating metal ions such as Y^{3+}, Ca^{2+}, Th^{4+}, Ce^{3+} and Mg^{2+}. This avoids the destructive cubic-tetragonal-monoclinic phase transformation. Charge compensation for cations of lower charge is achieved by creating vacant sites at the anion sublattice. This can be represented as,

$$Y_2O_3 \rightarrow 2Y'_{Zr} + 3O_O^x + \ddot{V_O} \tag{1.15}$$

where, Y'_{Zr} represents the yttrium ions on regular cationic sites (instead of Zr) with a relative charge of -1, O_O^x is the oxygen ions on regular sites and $\ddot{V_O}$ is the double positively charged oxygen vacancies. Two dopant Y ions are needed to introduce a single oxygen vacancy.

YSZ is one of the most important oxide ion conducting ceramics. It has been used extensively in the field of solid oxide fuel cells, catalysts, oxygen gas sensors and oxygen pumps. The system ZrO_2-Y_2O_3 has been studied extensively [136-142].

1.18 Synthesis of YSZ

YSZ has been prepared by using different methods such as hydrothermal methods [143, 144], homogeneous precipitation [145, 146], sol-gel method [147-149], plasma spray synthesis [150, 151], organic precursor route [150], reverse micro-emulsion route [153] and combustion synthesis [154-163], apart from the conventional solid state reaction [164]. Each method has its own advantages and disadvantages. The preparation condition plays a crucial role in the properties of the synthesized powders. For example, in the co-precipitation method, the process parameters such as the type of the precipitating agent, the sequence of addition, the rate of addition etc. have to be optimized to get powders of the required quality [145]. Hydrothermal method also involves an initial co-precipitation. The precipitate formed needs to be heat-treated at high-temperatures to obtain crystallinity [143]. In the sol-gel method, process parameters such as the concentration of metallic precursor in the sol, organic compounds, additives etc. will influence the product quality [147-149]. Even though the reaction time is shorter and controllable in the plasma spray techniques, the properties of the sprayed YSZ powder can be affected by many parameters such as solution concentration, feeding rate, plasma power, composition of the plasma gas, solvents and precursors, size of the atomization nozzle, air or water quenching, post-treatment etc. [147]. The technique is cost-intensive. In reverse microemulsion method, the parameters such as molar ratio of water to surfactant, the type of ions, electrolyte concentration in the aqueous phase and the co-surfactant used will affect the size and shape of reverse micelles. The density of the compacts achieved is lesser compared to those obtained using other techniques [153]. The conventional solid-state reaction usually leads to a coarser inhomogeneous product, which necessitates high temperature for sintering [164]. Most of the techniques require a long processing time.

1.19 Combustion synthesis

Combustion synthesis is used for the synthesis of a wide variety of industrially useful materials because it is an effective and low cost method. Solution combustion synthesis is based on a redox system of solutions, that upon heating to moderate temperatures, results in strongly exothermic reaction which supplies the energy required for the product formation [165]. The combustion synthesis reaction is influenced by the type of fuel and the fuel-to-oxidizer ratio. The addition of fuel helps to reduce the decomposition temperature of the metal nitrates. Hence, the selection of fuel is critical in deciding the exothermicity of the redox reaction between the fuel and metal nitrate [166]. Depending on the exothermicity of the reaction, combustion can be smoldering, flaming or explosive.

Important criteria for an ideal fuel are:

- It should be preferably water soluble.
- It should have low ignition temperature (<773 K).
- It should be compatible with metal nitrates, implies that the combustion reaction should not lead to explosion.
- Evolve large amounts of gases that are of low molecular weight and harmless during combustion.
- It should not result in other by-products.
- It should be readily available or easy to prepare.

The precursor solution for the combustion synthesis generally contains metal nitrates which simultaneously acts as a metal source and oxidizing agent (referred to as ‘oxidant’ in this thesis). An organic fuel acts as a reducing agent. Thus the combustion synthesis involves a self-sustained reaction containing a metal nitrate and an organic fuel. In a combustion synthesis, the initial reaction media is in solution form, which allows molecular level mixing of the reactants that result in a homogeneous product. The evolution of a huge amount of gases such as CO_2, NO_x, and H_2O results in fine porous powder, which is amenable for further processing.

Combustion synthesis is used for the synthesis of a wide variety of industrially useful materials [167-171]. Ringuede´ et al. [154] have used combustion synthesis to obtain alternate cermet material for solid oxide fuel cell anodes using urea as the fuel. Juarez et al. [155] have synthesized nanocrystalline tetragonal ZrO_2-2.8 mol.% Y_2O_3 by combustion synthesis using citric acid as the fuel. Wang et al. [156] have used the glycine-nitrate process for the synthesis of 8 mol.% YSZ. These authors have reported that with the increase in the amount of glycine, the crystallite size increased and the specific surface area decreased. The density of the compacts were reported to be ~90% TD. Silva et al. [157] have studied the effect of the type of fuel for the synthesis of 8 mol.% YSZ with urea and glycine as fuels. The specific surface area of powders obtained using urea as fuel was reported to be lower than that obtained using glycine as fuel. When the fuel to metal nitrates mole ratio was 1, the densities of the compacts sintered at 1873 K were ~97.5 and ~79.4% of TD for glycine and urea as fuels respectively. When the fuel to metal nitrates ratio was changed (2:1), the density of compacts prepared from powders obtained using glycine as fuel was ~94.3% whereas it was only ~83.9% TD for the compacts prepared from powders obtained using urea as the fuel, indicating the importance of the composition of the combustion mixture. Singh et al. [158] have studied the effect of citric acid on the synthesis of nanocrystalline YSZ powders by citrate-nitrate solution combustion synthesis using both hot-plate as well as a microwave oven. The particle size of the powders prepared using microwave heating was lower compared to that obtained using hot-plate heating. Shukla et al. [159] have used the combustion method for the synthesis of yttria and calcia stabilized zirconia using carbohydrazide as the fuel. He et al. [160] have synthesized nanocrystalline 8 mol.% yttria-stabilized zirconia powder using glycine-nitrate process. These authors have studied the effect of metal to glycine molar ratio and heat-treatment conditions on the synthesis, sintering and properties of the synthesized powders. Yang et al. [161] have used the nitrate-citrate combustion method to obtain nanocrystalline yttria-stabilized zirconia powder. Kaus et al. [162] have synthesized nanocrystalline 8 mol.% yttria-stabilized zirconia using smoldering combustion synthesis with glycine as the fuel. Biswas et al. [163] have studied the synthesis of yttria-stabilized zirconia by varying the yttria content by combustion method using urea as the fuel. The reaction between the fuel and the oxidizer would result in some residual carbon that can affect the performance of YSZ as a solid electrolyte.

Combustion synthesis of materials using microwave energy is a novel method for the synthesis of nanocrystalline materials [172-175]. YSZ was synthesized by employing microwave-assisted heating [144, 157, 176, 177]. Pakharukova et al. [176] have exploited microwave energy for drying co-precipitated yttrium and zirconium hydroxides. Combemale et al. [177] have used microwave flash synthesis for the preparation of YSZ and the powders thus obtained had high specific surface area, 228 m^2g^{-1}.

The ionic conductivity of stabilized zirconia depends on the type of dopant, dopant concentration and phase assemblage [134]. The amount of dopant required to fully stabilize the cubic phase of ZrO_2 is 8 to 12 mol.% yttria [134, 142]. Badwal [134] has reported that at 1273 K, the maximum conductivity is observed for the 8 mol.% composition, below and above which the conductivity decreases. This corresponds to the optimum amount of dopant required to fully stabilize the fluorite phase with maximum ionic conductivity. Even though data on the conductivity of YSZ are abundant, most of the data are for YSZ samples that are not completely characterized. The objective of the present study is to synthesize and characterize nanocrystalline 8 mol.% YSZ by microwave-assisted gel-combustion synthesis using citric acid/glycine/urea as the combustion fuels. The effect of nature of the fuels on the gel-combustion process and the physicochemical properties of the powders were studied. The performance of YSZ prepared as a solid electrolyte was also examined by measuring its ionic conductivity at different temperatures. Studies were also carried out to synthesize YSZ using hot-plate heating in order to compare the physical properties of the powders obtained using both microwave as well as hot-plate heating modes.

1.20 Scope and objectives of the present work

This thesis mainly deals with the research and development related to the synthesis and sintering of nanocrystalline boron carbide and yttria-stabilized zirconia. The present study aims at developing novel methods for the synthesis of sinteractive B_4C and YSZ powders suitable for fabricating high-density compacts at a relatively low sintering temperature, since the conventional methods use very high temperatures which are energy and cost intensive.

Commercial method of production of boron carbide is by the carbothermic reduction of H_3BO_3/B_2O_3. The boron carbide synthesized by this method is coarse-grained and very high temperatures are required to obtain high-density compacts. The commercial method of carbothermic reduction is uneconomical for the production of B_4C enriched with ^{10}B isotope due to significant loss of boron as oxides of boron at high temperatures involved in the reduction process and boron held up in the furnace during the reduction and subsequent processing steps. Even though, the boron carbide enriched with ^{10}B isotope is from the high purity elemental boron and carbon, the method of production of high purity elemental boron makes this process uneconomical as explained in Section 1.13.3. Hence, the present study explores the possibility of developing methods for synthesizing sinteractive nanocrystalline boron carbide powders and sinter the compacts of these powder to high densities at relatively low-temperatures using advanced sintering techniques, in order to reduce the cost and energy of production of these materials.

Precursor method is being developed for the synthesis of boron carbide at relatively low temperatures as an alternative to the high-temperature methods. Precursor method uses any boron containing compound such as boric acid, boric oxide, sodium borate etc as the boron source. Citric acid, sucrose, glycine, mannitol etc can be used as the carbon source. Hence, in the present study, the precursor for the synthesis of boron carbide was prepared using boric oxide and sucrose. A homogeneous mixture of these reactants was heat-treated at various temperatures for identifying optimum temperature for the preparation of precursor. The homogeneous mixture of boric oxide and sucrose on heat-treatment prepares the precursor, which is a mixture of boric oxide and carbon. The boric oxide and carbon thus formed was the precursor for the synthesis of boron carbide. The boron carbide was synthesized by the heat-treatment of the precursor.

In the precursor method, the reactants are mixed in solid state; the mixture tends to be inhomogeneous and often results in a product with a significant amount of free carbon as the impurity phase. It is one of the objectives of the present study to develop a low-temperature method for the synthesis of boron carbide with a minimum amount of free carbon as the impurity phase. This necessitates a suitable modification in the precursor preparation process.

The important factors influencing the presence of free carbon in the final product obtained by the precursor method are the homogeneity of the reactants such as B_2O_3 or H_3BO_3 and carbon components in the precursor, temperature, particle size of the components in the precursor and heating rate. Improving the homogeneity of the reactants in the precursor helps to reduce the free carbon impurity. Homogeneity of the components in the precursor can be improved by mixing them in a suitable medium/solvent and removing the solvent or medium by suitable methods. In the present study, the boric oxide and sucrose were made into a slurry in medium such as water or ethanol and freeze-dried to remove the slurry medium. The precursor for the synthesis of boron carbide was prepared using this dried product.

The homogeneity of the reactants can also be improved if the components are mixed on a molecular scale, say by complexation. Mannitol has excellent complexation capacity with boric acid and forms B-O-C bonds thereby improving the dispersion of boron and carbon. Hence, in the present study, the precursor was also prepared by taking H_3BO_3 as the boron source and mannitol as the carbon source. The mannitol-boric acid condensed product was prepared by heating the solution containing mannitol-boric acid using a microwave oven. The precursor was prepared by the thermal decomposition of this condensed product.

The sintering of boron carbide ceramic compacts is generally influenced by the powder characteristics such as surface area, particle size distribution, free carbon content etc. The present study has been carried out to optimize process parameters to obtain nanocrystalline boron carbide with desired powder characteristics for sintering at relatively low temperatures using advanced sintering techniques. Novel and energy efficient methods of sintering of nanocrystalline boron carbide were developed employing advanced sintering techniques, namely, spark plasma sintering and hot pressing.

Yttria-stabilized zirconia is used as an oxide ion conducting solid electrolyte. Preparation conditions play a crucial role in the properties of the synthesized powder. The method of preparation includes hydrothermal synthesis, co-precipitation, sol-gel method, plasma spray synthesis, combustion method etc. Most of the techniques require a long processing time. Among the various methods, combustion synthesis is an effective and low cost method for the synthesis of nanocrystalline materials. A new method based on microwave-assisted combustion synthesis was also developed to synthesize sinteractive nanocrystalline yttria-stabilized zirconia in the present study.

Chapter 2

Experimental

The experimental methods involved in the present study are discussed in this chapter. The details of various materials and chemicals used in this study are provided. The chapter also describes various preparation methods adopted and the sintering techniques used in the present study. The analytical methods adopted for the quantitative estimation of boron, total carbon and free carbon content in the nanocrystalline boron carbide are also detailed. Detailed description on X-ray diffraction, scanning electron microscopy, transmission electron microscopy, particle size distribution, specific surface area, Raman spectroscopy, and electrical conductivity measurements are also provided in this chapter.

2.1 Chemicals

Boric oxide (99.98%, M/s. Sigma Aldrich, USA) as the boron source and sucrose (99.98%, M/s. Thermo Fischer Scientific India Pvt. Ltd., India) as the carbon source were used for the preparation of precursor for the synthesis of B_4C. Millipore water and ethanol (AR grade, M/s. Merck KGaA, USA) were used as media for the mixing of the reactants for freeze-drying experiments. For the preparation of precursor using the microwave-assisted method, boric acid (99.5%, M/s. SD Fine-Chemicals Ltd., India) was used as the boron source and mannitol (99.5%, M/s. Chemspure, India) as the carbon source.

Potassium hydroxide (AR grade, M/s. Merck Life Science Pvt. Ltd., India), Na_2CO_3 (AR grade, M/s. Chemspure, India), D-mannitol (AR grade, M/s. Chemspure, India), p-nitrophenol (AR grade, M/s. Hi-Pure fine chemicals, India), phenolphthalein (M/s. Merck, India) and hydrochloric acid (AR grade, M/s. Hi-Pure, India) were used for the estimation of boron. Potassium hydrogen phthalate (KHP)

(AR grade, M/s. Merck, India) and $Ba(OH)_2$ (98%, M/s. Sarabhai M Chemicals Pvt. Ltd., India) were used for the determination of free carbon content.

Zirconyl nitrate monohydrate ($ZrO\,(NO_3)_2{\cdot}H_2O$, M/s. Lobachemie, India) and yttrium nitrate hexa hydrate ($Y(NO_3)_3{\cdot}6H_2O$, 99.99%, M/s. Chempure, India) were used as the precursors for the combustion synthesis of YSZ. Citric acid (99%) and glycine (99%) both from M/s. Chempure, India and urea (99.5%) from M/s. Hi-Pure, India were used as the fuels for experiments involving combustion synthesis of YSZ. All the chemicals were used as such without further processing.

2.2 Materials

2.2.1 Experimental assembly for the preparation of precursors for the synthesis of boron carbide

A schematic of the vessel used for the preparation of precursor is shown in Fig. 2.1. The vessel is made up of stainless steel and consists of the main vessel and an inner reaction vessel. The main vessel is provided with gas inlet and outlet. It also contains a lid sealed with O-ring. Water inlet and outlet are provided at the top of the main vessel for cooling in order to protect the O-ring. B_2O_3 and sucrose were taken in the inner stainless steel vessel and closed with a stainless steel lid having a pinhole and placed in the main vessel. The pinhole helps to reduce the pressure developed due to the generation of gaseous products in the inner reaction vessel. The vessel was heated in a vertical furnace supplied by M/s. Technico, India (Serial number 2651, 4000 W).

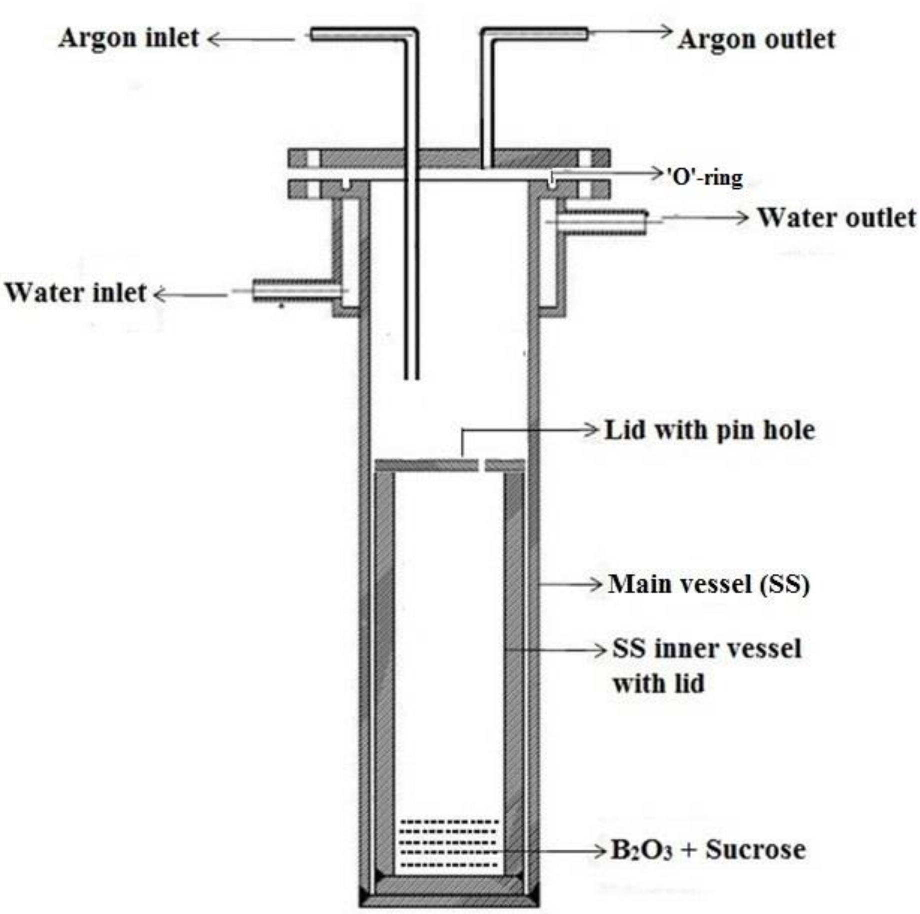

Figure 2.1. Schematic of the reaction vessel used for the preparation of the precursor

2.2.2 Furnace for the synthesis of nanocrystalline boron carbide (nc-B_4C) by the precursor method

A schematic representation of the furnace used for the studies on the synthesis of boron carbide is shown in Fig. 2.2. The furnace is made in-house. A photograph of the furnace is given in Fig. 2.3. One-end-closed high-density graphite tube (length: 120 mm, diameter: 11 × 9 mm, M/s. Pure components Pvt. Ltd, India) was used as the sample holder as well as the heating element. A photograph of the graphite tube along with the lid is shown in Fig. 2.4. The open end of the graphite tube was closed with a graphite lid. Both the ends of the graphite tube were firmly connected to copper electrodes using high-tension spring and screw arrangement as shown in Fig. 2.2. The graphite tube was enclosed in an alumina tube (diameter: 30 mm, length: 80 mm) which was wrapped with a thermal insulator. The thickness of the thermal insulator was also 30 mm. The insulator, alumina tube and graphite tube were further enclosed in a stainless steel sheath. Water circulation was provided to the outer surface of the stainless steel sheath using copper coils. Current was supplied to the graphite tube through water-cooled copper connectors. The temperature of the reaction is measured using a C-type (tugsten (W)-26% rhenium (Re) and W-3%Re) thermocouple. The thermocouple was provided from the top of the stainless steel sheath and was placed at the centre of graphite tube touching the sample compact so that the exact temperature of the sample is measured. Thermal shielding was provided at both ends of the alumina tube using tungsten sheets. The entire set up was fixed inside a transparent polycarbonate vessel in order to monitor the course of the reaction. The vessel was evacuated using a rotary pump (M/s. Edwards, Model: RV8). A variable power supply (12 V, 300 A) was used for heating the graphite heating element.

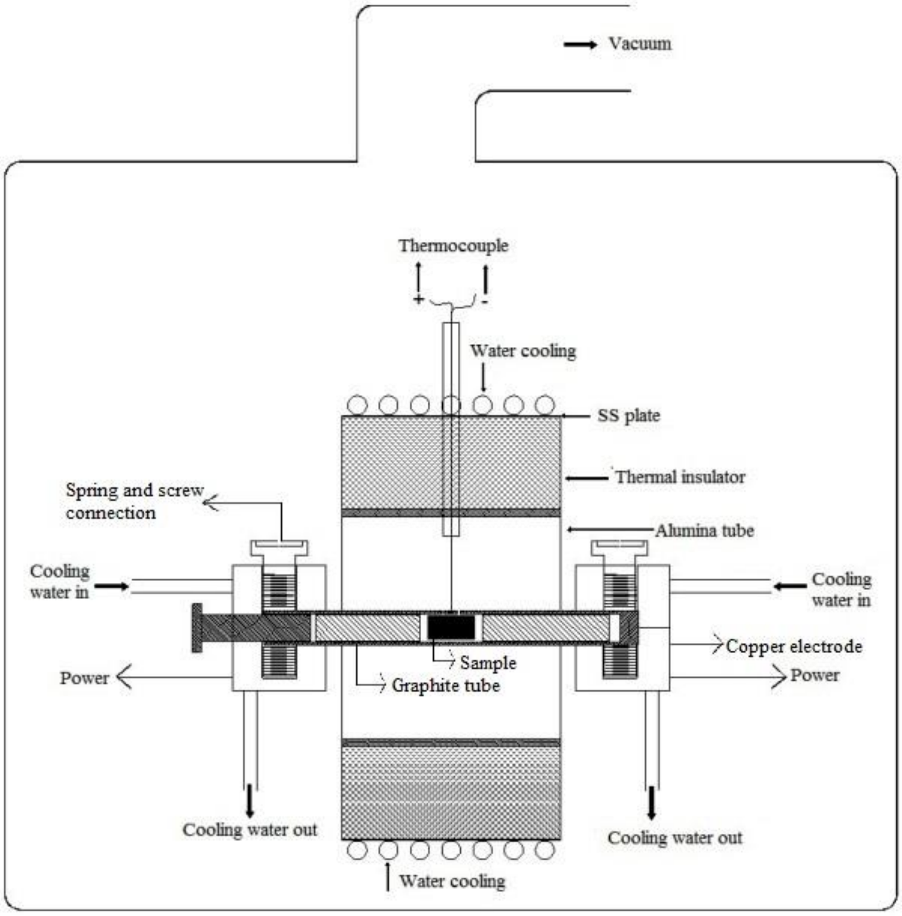

Figure 2.2. Schematic of the furnace used for the synthesis of nc-B_4C

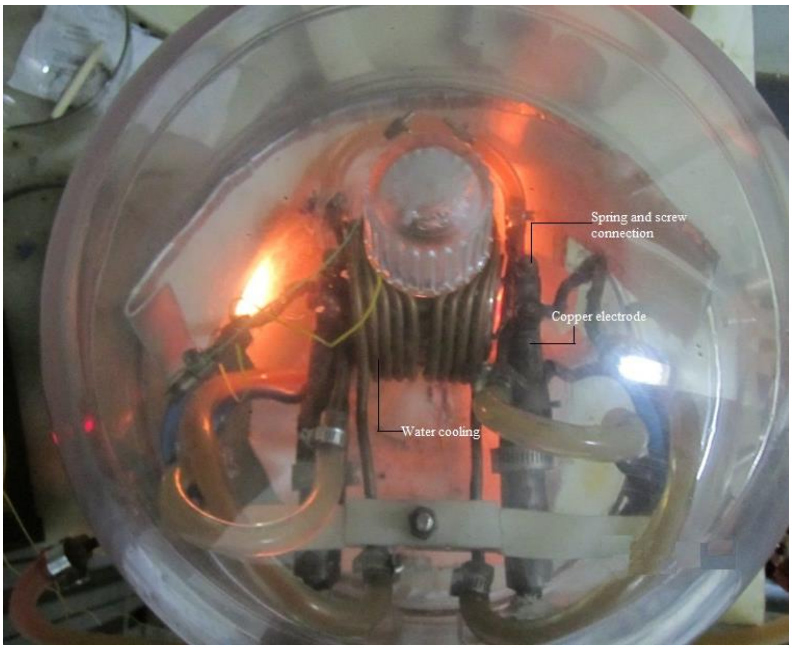

Figure 2.3. Photograph of the furnace used for the synthesis of nc-B_4C

Figure 2.4. Photograph of the graphite tube with lid

2.2.3 Design of the furnace made in-house for the bulk synthesis of nc-B_4C for sintering studies

The use of the furnace described in Section 2.2.2 is limited for the small-scale synthesis (~300 mg) of B_4C. In order to synthesize larger quantities of boron carbide powder (~8 g) for sintering studies a new furnace was designed and made in-house, which can be operated at higher temperatures with very high heating rates. The capacity of this furnace is ~8 g. A schematic of the furnace used for the bulk synthesis of nc-B_4C using the precursor method is shown in Fig. 2.5. It is a resistance heating furnace with graphite as the heating element. The photograph of the graphite heating element is given in Fig. 2.6. The heating element is a split type with a split width of 1 mm. The height of the graphite heating element is 120 mm with an internal diameter of 46 mm. The thickness of the top portion is 8 mm and the thickness of the bottom cylindrical part is 1.5 mm. The graphite used for the fabrication of heating element is grade-PC348GTO and its specifications are given in Table 2.1. The heating element was procured from M/s. Pure Components Pvt. Ltd, India. A photograph of the graphite vessel used for the synthesis of nc-B_4C is given in Fig. 2.7. A graphite lid with pinholes was used to close the graphite vessel, to vent out the gases formed during the reaction**.** A water-cooled cylindrical aluminium alloy (diameter: 150 mm, height: 230 mm) with stainless steel end flange was used for housing the electrodes and heating assembly. The graphite heating element was connected to the copper electrode as shown in Fig. 2.5. The copper block was provided with water cooling. A resistance temperature detector (RTD) with a pre-set temperature (333 K) was connected to the copper block. The entire body of the furnace was water cooled. Power to the furnace was drawn from an oil cooled transformer with high current (input: 440 V, output: 22 V, 1000 A). The transformer was connected to the copper electrode using a bus bar. The input to the transformer was controlled using a 16 kVA rheostat and a temperature controller. The furnace was evacuated using a rotary pump (Make: M/s. Edwards, Model E2M80). The temperature was measured using a C-type (W-26% Re and W-3% Re) thermocouple as shown in the schematic of the furnace. A uniform temperature zone of 60 to 70 mm was obtained from the bottom of the heating element.

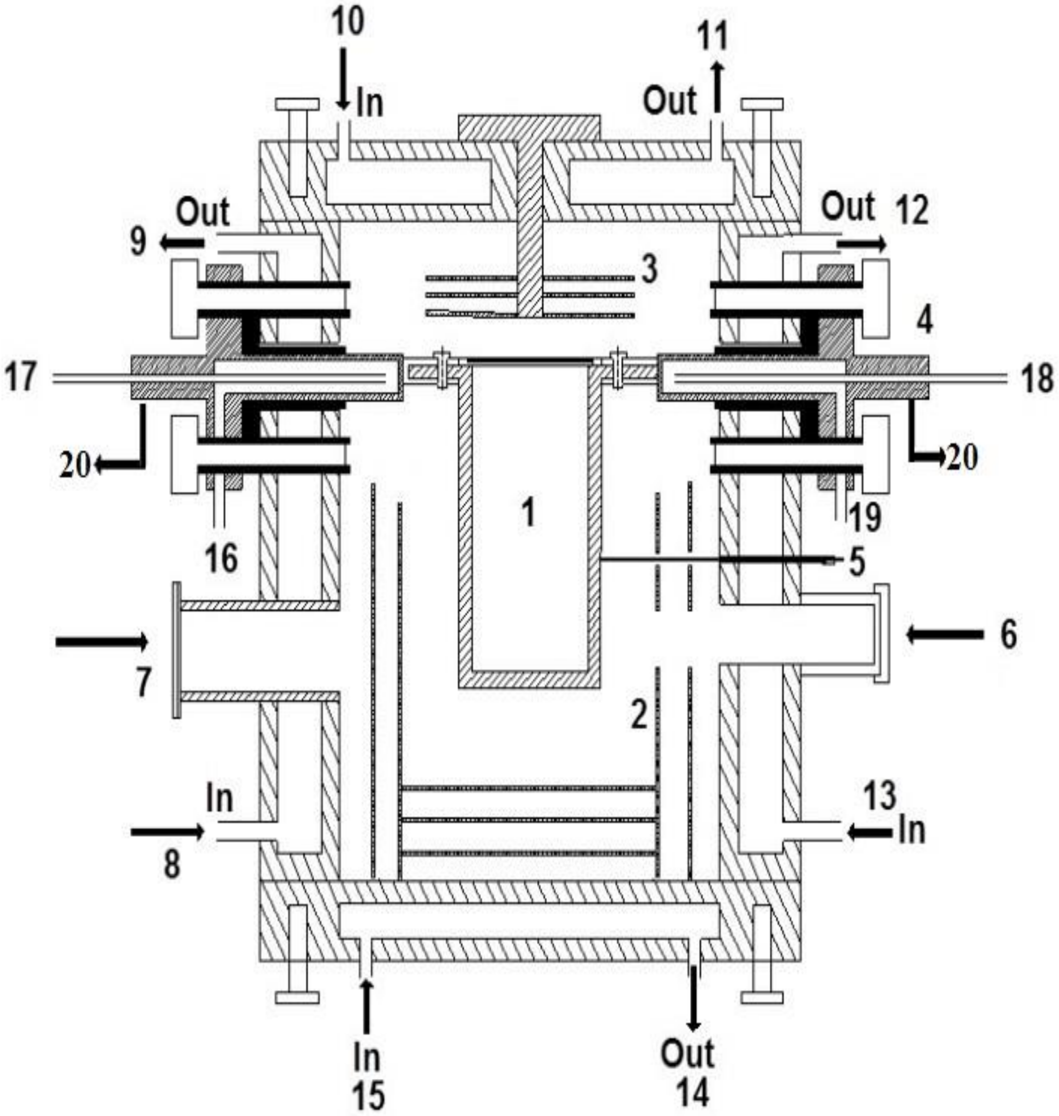

1	Graphite heating element
2, 3	Thermal insulator
4	Electrical connection
5	Thermocouple
6	Optical window for temperature measurement
7	Port for connecting a vacuum pump
8,10,13,15,17,18	Water inlet
9,11,12,14,16,19	Water outlet
20	Copper electrode

Figure 2.5. Schematic of the furnace used for the bulk synthesis of nc-B_4C

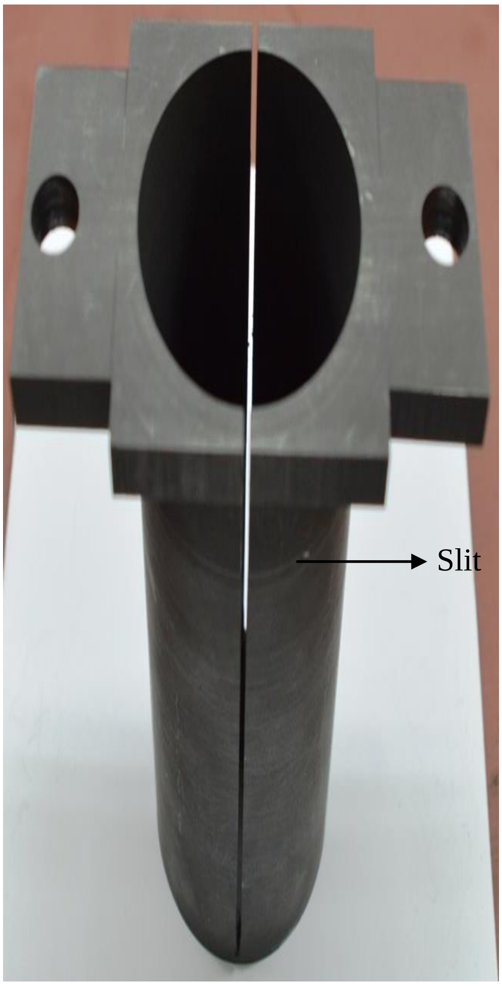

Figure 2.6. Photograph of the graphite heating element used for the bulk synthesis of nc-B_4C

Table 2.1. Specifications of the graphite heating element

Property	Value
Specific gravity / Density (g cc^{-1})	1.92
Specific resistance (μ Ω m)	10
Young’s modulus (GPa)	12.3
Flexural strength (MPa)	63.7
Shore hardness	68
Co-efficient of thermal expansion (x 10^{-6} $(°C)^{-1}$)	5.5
Thermal conductivity ($W(mK)^{-1}$)	128

Figure 2.7. Photograph of the graphite vessel with graphite lid used for the bulk synthesis of nc-B_4C

2.3 Synthesis of nc-B_4C by the precursor method

2.3.1 Synthesis of nc-B_4C using B_2O_3-sucrose precursor

2.3.1.1 Preparation of B_2O_3-sucrose precursor

A homogeneous mixture of the reactants, B_2O_3 and sucrose with a C/B wt.% ratio of 1.87 (carbon to B_2O_3 mole ratio, CBMR of 3.38) was taken and heated sequentially at 463 K for 2 h and at 573 K for 2 h under flowing argon gas in a vertical furnace (M/s. Technico, India). In order to optimize the precursor preparation temperature, i.e., the second temperature in the heating cycle, the experiments were repeated at 673, 773, 873, 973 and 1073 K. The optimized temperature for the preparation of precursor was found to be 873 K. Hence, the experiment was also carried out at 873 K by using B_2O_3 and sucrose with a C/B wt.% ratio of 1.94 (CBMR of 3.5).

2.3.1.2 Processing of the precursor obtained from B_2O_3-sucrose

The precursor obtained at each temperature was ground for 3 h into a fine powder using a planetary ball mill (M/s. Fritsch, Germany). All the samples after ball milling were stored under vacuum in a desiccator. The fine powders obtained were compacted into pellets of 8 mm diameter and 12 mm thickness by applying a pressure of 100 MPa using an uniaxial pellet press (M/s. Kimaya engineers, India). The compaction did not require lubricant or binder. The compacts thus prepared were heat-treated at different temperatures ranging from 1273 to 1873 K for 10 to 240 min under a vacuum of 20 Pa. The duration of heating depends on the temperature- for lower temperatures, longer durations were used. The scheme of the synthesis is shown in Fig. 2.8. The details of the samples and experimental conditions are given in Table 2.2.

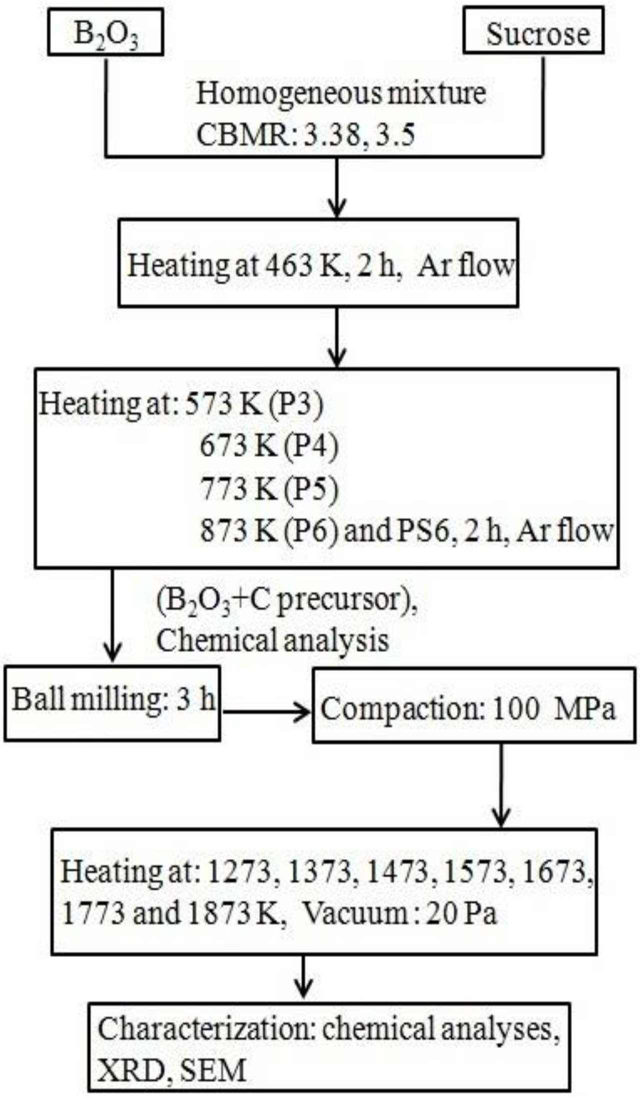

Figure 2.8. Scheme of the synthesis of nc-B_4C using B_2O_3-sucrose gel precursor

Table 2.2. Sample designation of the precursors and the products obtained from B_2O_3 and sucrose

Sample designation	Temperature (K)	Duration of heating (min)	Remarks
P3	^{a}573	120	Precursor, CBMR 3.38
P4	^{a}673	120	Precursor, CBMR 3.38
P5	^{a}773	120	Precursor, CBMR 3.38
P6	^{a}873	120	Precursor, CBMR 3.38
PS6	^{a}873	120	Precursor, CBMR 3.5
P4BC16, P5BC16, P6BC16, PS6BC16	^{b}1873	10	Products from the precursors
P4BC15, P5BC15, P6BC15, PS6BC15	^{b}1773	30	Products from the precursors
P5BC14, P6BC14, PS6BC14	^{b}1673	60	Products from the precursors
P5BC13, P6BC13, PS6BC13	^{b}1573	120	Products from the precursors
P5BC12, P6BC12, PS6BC12	^{b}1473	180	Products from the precursors
P4BC10, P5BC10, P6BC10, PS6BC10	^{b}1273	240	Products from the precursors

P- precursor, 3,4 etc.- temperature in degree Celcius (3-300, 4-400 etc.), BC-boron carbide, P4BC16-precursor prepared at 400 °C, boron carbide synthesized at 1600 °C, ^{a}precursor preparation temperature and ^{b}precursor processing temperature

2.3.2 Improving the homogeneity of the precursor by the method of freeze-drying

2.3.2.1 Preparation of B_2O_3-sucrose precursor by freeze-drying

The precursor for the synthesis of boron carbide was prepared from B_2O_3 and sucrose using water or ethanol as the slurry medium.

2.3.2.1.1 Water as the medium of mixing

A mixture of B_2O_3 and sucrose with C/B wt.% ratio of 1.87 (CBMR equal to 3.38) was taken and made into a slurry in minimum quantity of water (~12 mL for

~25 g). This slurry was refrigerated overnight in a refrigerator [M/s. Hitachi, India]. The frozen slurry was freeze-dried in a TFD series freeze dryer (M/s. IlshinBioBase, South Korea) at 198 K and at 5×10^{-3} mbar pressure for about 20 h. This dried powder was heated at 463 K for 2 h under flowing argon. This was subsequently heated at 873 K under flowing argon. The precursor thus obtained was designated as PW.

2.3.2.1.2 Ethanol as the medium of mixing

A mixture of the B_2O_3 and sucrose with C/B wt.% ratio of 1.87 (CBMR equal to 3.38) was taken and made into a slurry in minimum quantity of ethanol (~13 mL for ~25 g). The container along with the slurry was placed in liquid nitrogen for the solidification of slurry. The frozen mixture was freeze-dried at 198 K and at 5×10^{-3} mbar pressure for about 10 h. This dried powder was heated as described in Section 2.3.2.1.1. The precursor thus obtained was designated as PE.

2.3.2.2 Processing of the precursors, PW and PE

The precursors, PW and PE, were ground into fine powder using a planetary ball mill (M/s. Fritsch, Germany) for 3 h. The samples were stored under vacuum in a desiccator. The fine powders obtained were compacted into pellets of 8 mm diameter and 12 mm thickness by applying a pressure of 100 MPa using an uniaxial pellet press. All the compacts were made without using any binder. The compacts made using PW were heated at temperatures ranging from 1273 to 1873 K for different durations ranging from 10 to 240 min under vacuum. The duration depended on the temperature-higher the temperature, shorter is the duration. Similarly, the compacts made using PE were heat-treated at 1573 to 1873 K for 10 to 120 min. The compact prepared from PE was also heat-treated at 1273 K for 240 min to explore the minimum temperature required for the formation of B_4C.

The photograph of the freeze drier used in the study is shown in Fig 2.9. The details of the samples synthesized are given in Table 2.3. The scheme of the synthesis of boron carbide is shown in Fig. 2.10.

Table 2.3. Sample designation of the products obtained by the heat-treatment of B_2O_3-sucrose precursor prepared by freeze-drying

Sample	Temperature (K)	[a]Duration of heating (min)
PW16, PE16	1873	10
PW15, PE15	1773	30
PW14, PE14	1673	60
PW13, PE13	1573	120
PW12	1473	180
PW10, PE10	1273	240

PW-precursor water, PE-precursor ethanol, 16, 15 etc. is the precursor processing temperature in degree Celcius (16-1600 °C, 15-1500 °C etc.) and [a]precursor processing time

Figure 2.9. Photograph of the freeze dryer used in the study

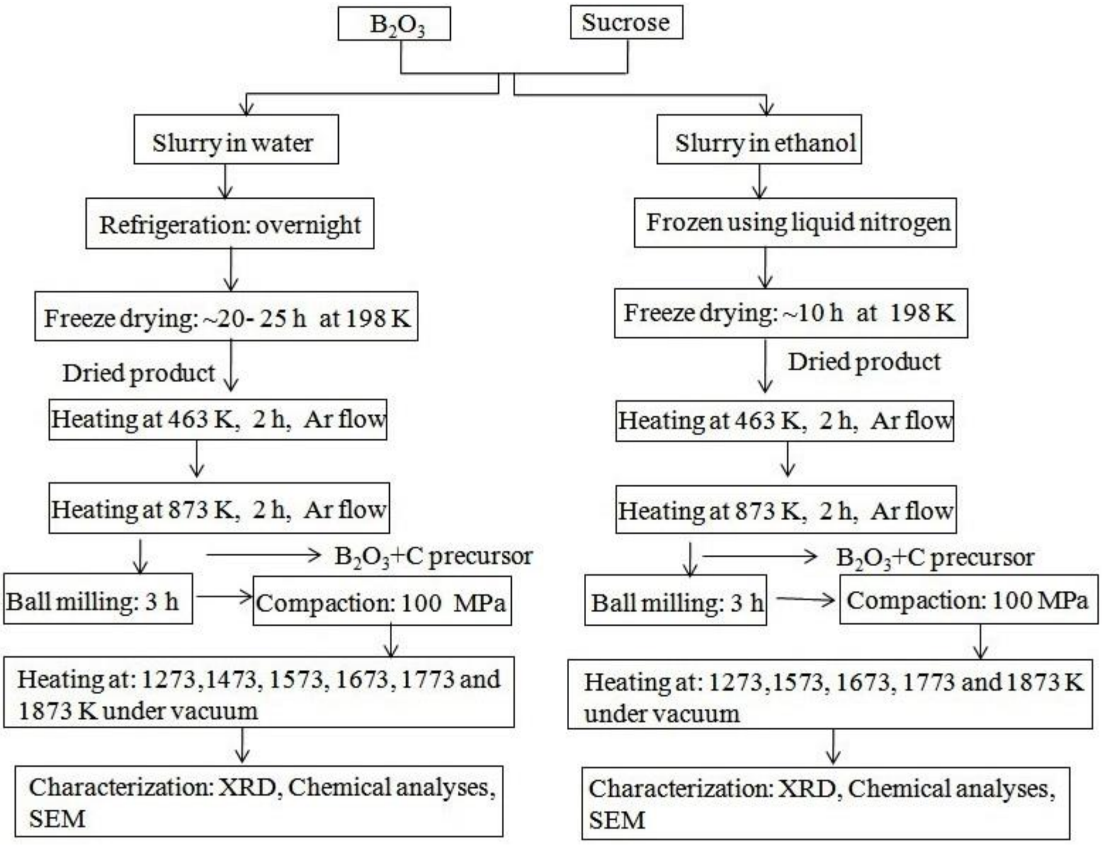

Figure 2.10. Scheme of the synthesis of nc-B_4C using the precursor prepared by freeze-drying

2.3.3 Microwave-assisted preparation of the precursor for the synthesis of nc-B_4C

2.3.3.1 Preparation of the precursor using H_3BO_3 and mannitol

Boric acid was used as the source of boron and mannitol was used as the source of carbon. Boric acid and mannitol were taken with a C/B wt.% ratio of 1.87 (CBMR of 3.38). Boric acid was dissolved in hot water and a saturated aqueous solution of mannitol was added under constant stirring. This solution was heated in a microwave oven (Make: LG, Model MC-8087ABR, LG Electronics India Pvt. Ltd., India) for ~25 min. The condensed product obtained by the microwave heating was ground into powder using pulveriser (M/s. Fritsch analysette 3, Germany). The powder obtained was heated in air at 673, 773 and 873 K for 2 h. The boric acid-mannitol solution was also prepared by keeping the C/B wt.% ratio of 3.33 (CBMR equal to 6) and the same procedure as described above was used for the preparation of precursor.

2.3.3.2 Processing of the precursor obtained from H_3BO_3 and mannitol

The precursors obtained at all the temperatures were ground for 3 h into a fine powder using planetary ball mill (M/s. Fritsch, Germany). All the samples after ball milling were stored under vacuum in a desiccator. The fine powders were compacted into pellets of 8 mm diameter and 12 mm thickness by applying a pressure of 100 MPa using an uniaxial pellet press (M/s. Kimaya engineers, India). All the compacts were made without using any binder or lubricant. The compacts thus prepared were heat-treated at different temperatures ranging from 1273 to 1873 K for 10 to 240 min, for higher temperatures shorter duration of heating was used, under a vacuum of 20 Pa. The scheme for the synthesis is shown in Fig. 2.11. The details of the samples and experimental conditions are given in Table 2.4.

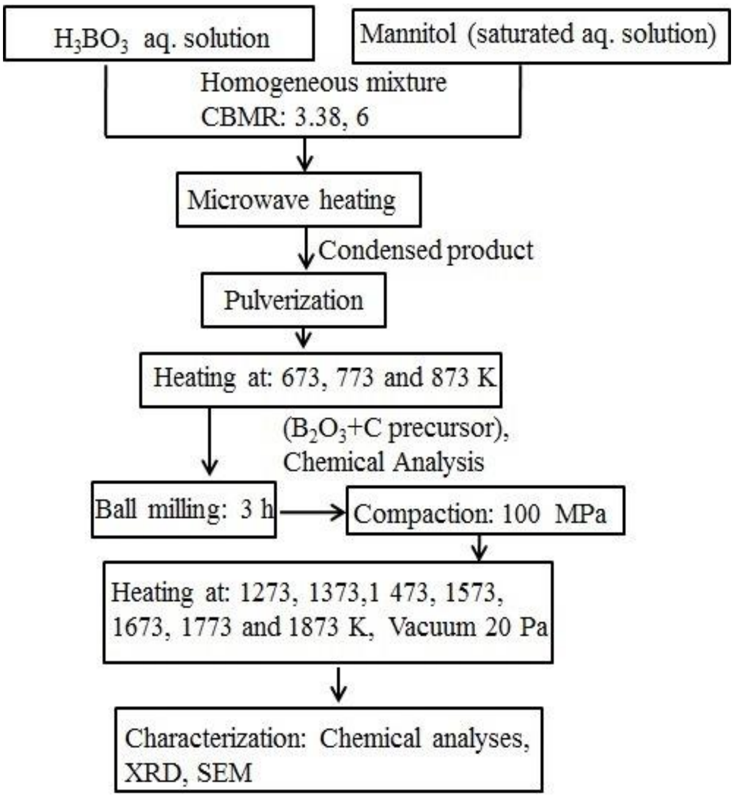

Figure 2.11. Scheme of the microwave-assisted preparation of the precursor and its processing

Table 2.4. Sample designation of the precursors prepared from the thermally decomposed condensed product of mannitol-H_3BO_3 and the products obtained by heat-treatment of the precursors

Sample designation	Temp. (K)	Duration of heating (min)	Remarks
MW1P	[a]673	120	Precursor, CBMR 3.38
MW2P	[a]773	120	Precursor, CBMR 3.38
MW3P	[a]873	120	Precursor, CBMR 3.38
MW4P	[a]673	120	Precursor, CBMR 6
MW5P	[a]773	120	Precursor, CBMR 6
MW6P	[a]873	120	Precursor, CBMR 6
MW1P16, MW2P16, MW3P16, MW4P16, MW5P16, MW6P16	[b]1873	10	Products from the precursors
MW1P15, MW2P15, MW3P15, MW4P15, MW5P15, MW6P15	[b]1773	30	Products from the precursors
MW1P14, MW2P14, MW3P14, MW4P14, MW5P14, MW6P14	[b]1673	60	Products from the precursors
MW1P13, MW2P13, MW3P13, MW4P13, MW5P13, MW6P13	[b]1573	120	Products from the precursors
MW1P12, MW2P12, MW3P12, MW4P12, MW5P12, MW6P12	[b]1473	180	Products from the precursors
MW1P10, MW2P10, MW3P10, MW4P10, MW5P10, MW6P10	[b]1273	240	Products from the precursors

MW1P-Microwave precursor (1- CBMR 3.38), MW2P (2- CBMR 3.38), MW3P (3- CBMR 3.38), MW4P (4-CBMR 6), MW5P (5-CBMR 6), MW6P (6-CBMR 6), MW1P16 –MW1P heat-treated at 1600 °C (16, 15 etc is the temperature in degree Celcius-1600, 1500 °C etc.), [a]thermal decomposition temperature of the condensed product and [b]precursor processing temperature

2.4 Spark plasma sintering of nc-B_4C synthesized by the precursor method

nc-B_4C synthesized by the precursor method was sintered by SPS technique. The nc-B_4C was characterized for phase purity, boron, total carbon and free carbon content, specific surface area and particle size distribution prior to SPS. The presence of B_2O_3 is detrimental for the densification of B_4C to near theoretical density [129]. It was reported that [126] methanol washing helps to remove the B_2O_3 and thereby improves the densification. The nc-B_4C synthesized in the present study was subjected to methanol washing and subsequent drying in an oven at 343 K prior to sintering. The dried samples were also characterized for their chemical composition. SPS was carried out in Dr. Sinter 1050 apparatus (M/s. Sumitomo Coal Mining Co. Ltd., Japan) using a graphite die and plunger with 20 mm internal diameter and graphite die wall thickness of 15 mm. The inner side of the graphite die and plunger was covered with a graphite foil of thickness 0.2 mm. The graphite foil helps in the easy removal of sintered compacts and also prevents the direct interaction of material with the die wall. The samples were sintered at 1873, 1973 and 2073 K (± 20 K) with a heating rate of 100 K min^{-1} for 5 min at the desired temperature with a pulse on-off ratio of 12:2. Temperatures were continuously recorded using a radiation pyrometer focused on the graphite die wall. 4 g of the sample was taken for each run and an initial pressure of 50 MPa was applied in each run. The B_4C samples were designated as nc-B_4C16, nc-B_4C17 and nc-B_4C18 which were sintered at 1873, 1973 and 2073 K respectively. Here ‘nc’ stands for nanocrystalline, B_4C is boron carbide and 16, 17, 18 corresponds to temperatures in degree Celsius (16 = 1600, 17 = 1700 and 18 = 1800). A commercial boron carbide sample procured from M/s. Sigma Aldrich (designated as c-B_4C) was also washed with methanol and characterized similar to that of nc-B_4C. The SPS of c-B_4C was carried out at 1973 K with the conditions of sintering the same as that of nc-B_4C. This sintered compact was designated as c-B_4C17, where c = commercial. A schematic of the SPS system used in the present study is shown in Fig. 2.12.

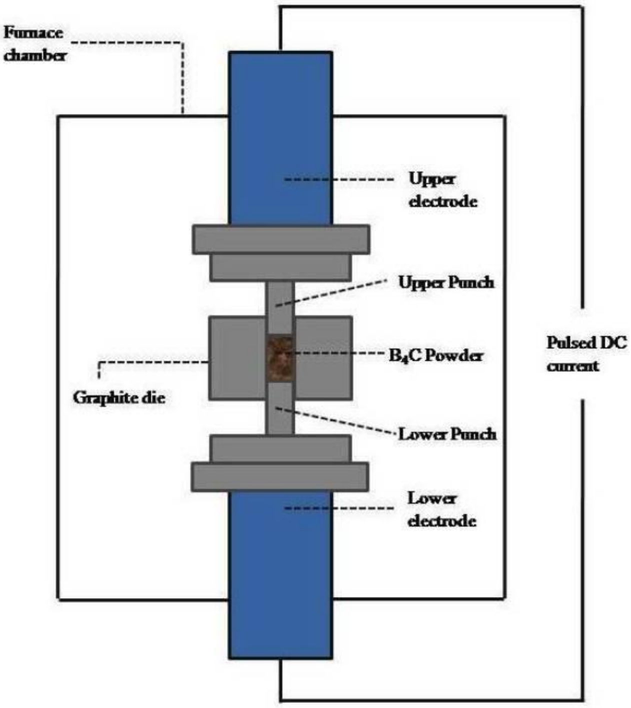

Figure 2.12. Schematic of the SPS equipment

2.5 Sintering of nc-B_4C by hot pressing technique

The nc-B_4C powder prepared by the precursor method and c-B_4C powder was washed with methanol for removing unreacted B_2O_3 and dried in an oven. The nc-B_4C and c-B_4C were characterized for phase purity, chemical composition, specific surface area and particle size distribution before and after methanol washing prior to hot pressing. The hot pressing was carried out by filling the powder in a graphite die that withstands temperatures up to about 2573 K under pressures of up to 35 MPa. The internal diameter of the graphite die is 60 mm. The inner side of the graphite die and plunger was covered with graphite foil (0.2 mm thickness) before filling the powder into it. Sintering of both nc-B_4C and c-B_4C were carried out at 1973 and 2073 K (±15 K) for 60 min at each temperature using a hot press (M/s. Hind Hi Vacuum Pvt. Ltd., India). The actual temperature of the hot press was measured by a two colour optical pyrometer. The heating rate up to 1273 K was 400 K h^{-1} and above this temperature it was around 200 K h^{-1}. After completion of the holding period, the load was released slowly and cooled down to room temperature in vacuum. A schematic of the hot pressing equipment is shown in Fig. 2.13.

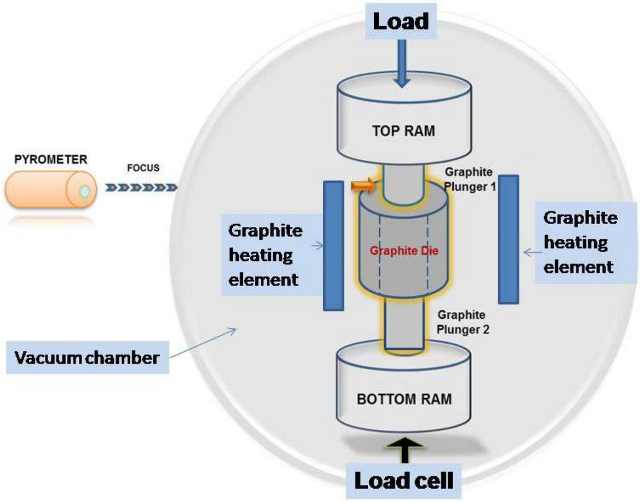

Figure 2.13. Schematic of the hot pressing equipment

2.6 Synthesis of nanocrystalline yttria-stabilized zirconia (nc-YSZ) by microwave-assisted combustion synthesis

Required quantities of starting materials (as given in Table 2.5) were taken so as to obtain a final product of the composition, $(Y_{0.08}Zr_{0.92})O_2$. The nitrates and one of the three fuels (1:1 mol ratio) were dissolved in distilled water and mixed to get a homogeneous solution. The solution was transferred to a combustion bowl and heated using either a microwave oven (Model No: LG MC-8091HLQ, 2.45 GHz, supplied by M/s. Apollo electronics, India) or a hot-plate. The combustion bowl with the reaction mixture was placed inside the microwave oven. Once the gel is formed, heating was continued nonstop. A similar procedure was used for the hot-plate heating. No attempt was made to measure the temperature of the gel inside the microwave oven. The resultant product (‘as-prepared’) was calcined under flowing oxygen (flow rate: 5 mL min^{-1}) at 1073 K for 4 h to remove all the volatiles and residual carbonaceous material. The calcined powders were uniaxially pressed (without the addition of binders and lubricants) into pellets of 10 mm diameter and 2 mm thickness by applying a pressure of 200 MPa. These green pellets were sintered at 1873 K (M/s. Carbolite Ltd., UK) for 4 h with a heating and cooling rate of 5 K min^{-1} in air. The samples were designated based on the method of preparation and the fuels used and are given in Table 2.6.

Table 2.5. The quantities of the reactants (oxidants) and fuels taken for experiments

No.	Yttrium nitrate hexahydrate (g)	Zirconyl nitrate monohydrate (g)	Fuel (g)
1	2.5113	17.3802	citric acid:35.7118
2	2.5065	17.3814	glycine:12.7569
3	2.5037	17.3815	urea:10.2058

Table 2.6. Sample designation and experimental conditions of calcination and sintering of 'as-prepared' YSZ powders

No.	Sample name	Calcination		Sintering	
		Temp. (K)	Time (h)	Temp. (K)	Time (h)
1	ZACM	1073	4	1873	4
2	ZASM	1073	4	1873	4
3	ZACH	1073	4	1873	4
4	ZASH	1073	4	1873	4
5	ZGCM	1073	4	1873	4
6	ZGSM	1073	4	1873	4
7	ZGCH	1073	4	1873	4
8	ZGSH	1073	4	1873	4
9	ZUCM	1073	4	1873	4
10	ZUSM	1073	4	1873	4
11	ZUCH	1073	4	1873	4
12	ZUSH	1073	4	1873	4

Z-8 mol.% YSZ, A-citric acid, G-glycine, U-urea, H-hot-plate heating, M-microwave heating, S-sintered, C-calcined, (ZACAPM, ZACAPH, ZGAPM, ZGAPH, ZUAPM and ZUAPH are 'as-prepared' powders, AP-'as-prepared')

2.7 Characterization techniques

2.7.1 Estimation of boron

Principle: The boron content in the boron carbide samples synthesized in this study was determined using the sodium carbonate fusion method [178]. Borax is produced as a result of the fusion of boron carbide and sodium carbonate. The reaction between borax and hydrochloric acid liberates boric acid. The excess HCl is neutralized to pH7 using aq.KOH and p-nitrophenol as indicator. Boric acid, $B(OH)_3$, is a very weak monobasic acid and acts exclusively by hydroxyl ion acceptance rather than proton donation [179].

$$B(OH)_3 + 2H_2O \leftrightarrow H_3O^+ + B(OH)^{4-} \qquad pK_a = 9.5 \tag{2.1}$$

The acidity of boric acid can be enhanced by chelation with polyhydric alcohols such as mannitol, glycerol, etc. After the addition of solid mannitol, the pK_a of the above reaction drops to 5.5, indicating an increase in the acid equilibration constant by a factor of 10^4. The mannitol-boric acid complex is estimated by NaOH/KOH using phenolphthalein as the indicator [180, 181].

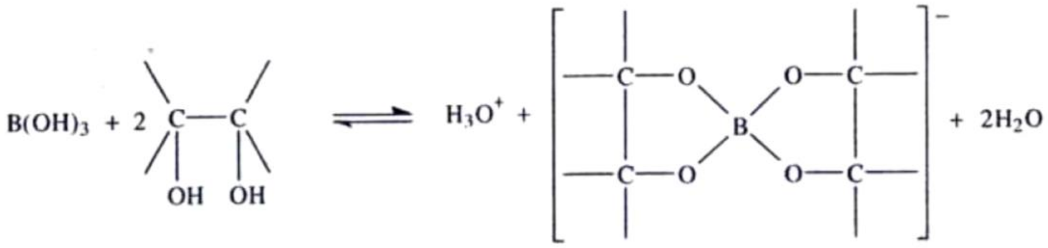

Procedure: 1.5 g of finely ground Na_2CO_3 was pressed into a platinum crucible and a small cavity was made at the center. An intimate mixture of 0.5 g of Na_2CO_3 and pre-weighed B_4C was added and a further 1.5 g of Na_2CO_3 was spread over the mixture to cover it completely. The crucible along with the sample was placed in a muffle furnace and heated to 873 K in 1 h and to 1023 K in 1 h and then to 1173 K in 1 h 30 min and held at this temperature for 30 min. The heating profile is given in Fig. 2.14. The melt was cooled and was transferred into a Teflon beaker and dissolved in 1:3

HCl solution and further diluted with distilled water. The beaker was heated gently to remove any traces of dissolved CO_2. The solution was made up to 100 mL and 20 mL aliquot of this solution was taken for titration. Then 5 drops of p-nitrophenol was added and titrated with the drop wise addition of 0.5 N aq. KOH solution till the colourless solution turned to yellow colour. Then 2.5 g of mannitol and a drop of phenolphthalein were added and the solution was titrated against standard 0.1 N aq. KOH solution.

The percentage of boron was calculated using the following formula.

$$\% \text{ B} = (10.81 \times [\text{KOH}] \times V_{\text{KOH}})/\text{weight of the sample (mg)} \qquad (2.2)$$

(Factor 10.81 = (isotopic abundance x atomic weight) of ^{10}B + (isotopic abundance x atomic weight) of ^{11}B), [KOH] is the concentration of aq. KOH and V_{KOH} is the volume of aq. KOH consumed.

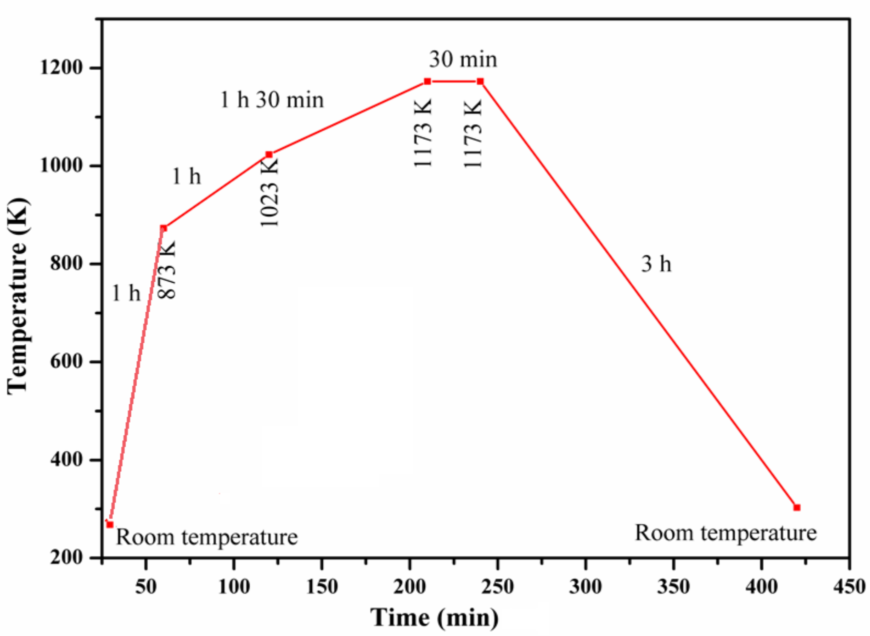

Figure 2.14. Heating profile for the sodium carbonate fusion

2.7.2 Estimation of total carbon

The total carbon content in the precursor, boron carbide and YSZ samples were determined by using a carbon determinator (M/s. Eltra CS 800, Germany).

Principle: The estimation of carbon is based on the combustion of carbon present in the sample to CO_2 which after purification is detected by the IR detector. A known amount of sample is subjected to combustion in a ceramic crucible with tungsten as the accelerator in flowing oxygen by induction heating. The gases evolved are carried by oxygen through moisture trap and hot copper oxide. Hot copper oxide converts trace amount of CO formed to CO_2. The purified CO_2 is detected by IR detector at 2700 or 4300 nm wavelength.

Procedure: The ceramic crucibles used as the sample container were fired at 1073 K to avoid any carbon contamination to the sample and to reduce the blank value. The calibration was carried out using ferrochromium (NBS standard) for which the carbon content was known accurately. A mixture of ~25 mg of the sample, 1.5 g of tungsten accelerator and 0.5 g of pure iron accelerator (M/s. Eltra, Germany) were used for the estimation. An average of three analyses is reported as the % C by weight in the boron carbide samples.

2.7.3 Estimation of free carbon

Free carbon present in the samples was estimated by wet chemical analysis [182].

Principle: The determination of free carbon is based on the selective oxidation of free carbon present in the sample to CO_2 using a chromic-sulphuric acid mixture. The boron carbide phase remains unreacted during the oxidation.

$$C_{free} + H_2CrO_4 \rightarrow Cr_2O_3 + CO_2 \tag{2.3}$$

The carbon dioxide thus formed is collected into a known excess of an aqueous solution of barium hydroxide as barium carbonate precipitate.

$$CO_2 + Ba(OH)_2 \rightarrow BaCO_3 + H_2O \tag{2.4}$$

Excess barium hydroxide was then determined titrimetrically using standard potassium hydrogen phthalate (KHP) as the titrant and phenolphthalein as indicator. Schematic of the experimental assembly used for the estimation of free carbon is shown in Fig. 2.15.

Procedure: The weighed sample was taken in a round bottom (RB) flask and the flask along with the sample was flushed using argon gas to remove any CO_2. After 10 min, a known excess of aqueous barium hydroxide was added into the burette and chromic acid was added into the RB flask and the reaction was allowed to occur for 30 min. The chromic acid oxidizes the free carbon alone to CO_2 and the CO_2 thus evolved was carried by argon gas through a distilled water bubbler into a known excess of barium hydroxide solution. The barium carbonate was thus precipitated. The excess barium hydroxide solution was titrated against standard KHP solution using phenolphthalein as indicator.

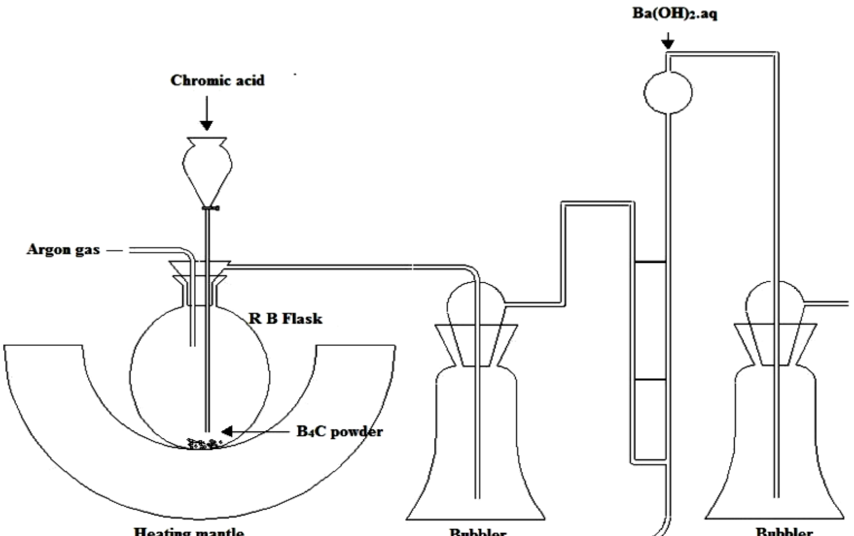

Figure 2.15. Schematic of the experimental assembly for the estimation of free carbon

2.7.4 X-ray diffraction (XRD) analysis of the powders

X-ray diffraction is a very useful technique in the field of characterization of crystalline materials [183, 184]. X-ray diffraction is based on the diffraction of the characteristic X-ray beam on crystalline solids. The crystalline solid consists of a regular repetitive array of atoms/ions with inter-planar spacing comparable to the wavelength of X-rays. Hence, when an X-ray beam impinges on a crystalline solid, diffraction occurs. The characteristic X-rays are used for the experiments and they are produced when a fast moving electron strikes the metal targets. If kinetic energy of incoming electron is sufficient enough to knock out the K-shell electron from the metal target, a vacancy is created in the K-shell. This vacancy is filled by an outer shell electron with the emission of radiation with a definite wavelength. When the vacancy in the K-shell is filled up by electrons from the L-shell, characteristic K_α lines are formed and when it is filled up by electrons from the M-shell, characteristic K_β lines are formed. The K_α lines are generally used for XRD. The commonly used metal target is copper, whose characteristic wavelength for K_α radiation is 1.5418 Å. Cr (K_α = 2.29 Å), Fe (K_α = 1.94 Å), Co (K_α = 1.79 Å), and Mo (K_α = 0.71 Å) are the other metal targets used in X-ray generating tubes.

When the geometry of the incident X-ray beam falling on the crystal satisfies the Bragg equation (Eq.2.5), constructive interference occurs [183, 184].

$$n\lambda = 2d\ Sin\theta \qquad (2.5)$$

where n is the order of diffraction, λ is the wavelength of the incident X-ray beam, d is the inter-planar spacing and θ is the angle of incidence.

X-ray diffraction analyses of all boron carbide samples synthesized by different methods were carried out as explained below.

Phase identification of the precursor and the product obtained after heat-treatment was carried out using powder X-ray diffractometer (M/s. GNR, Italy) using filtered Cu K_α radiation (λ = 1.5418 Å). The data were collected in the range of 20 to 80° with a step size of 0.02° (2θ). The XRD of all the samples were recorded by uniformly spreading almost the same quantity of sample on a zero background sample holder (diameter: 25 mm, depth: ~0.5 mm). The phase analyses of the products were carried out by comparing their XRD patterns with standard patterns in the International Centre for Diffraction Data (ICDD) database. The XRD pattern of the carbon after the removal of B_2O_3 from the precursor was also recorded.

XRD of the nc-B_4C synthesized for SPS and hot pressing was recorded before and after methanol washing with a slow scan.

Phase identification of YSZ samples was carried out using powder X-ray diffraction with X-ray diffractometer (M/s. PANalytical X'pert PRO, The Netherlands) using filtered Cu K_α (λ = 1.5418 Å) radiation and the data were collected in the scanning range of 20 to 80°. The crystal structures of the products were identified by comparing their XRD patterns with the standard patterns in the ICDD database file. The average X-ray crystallite sizes (XCS) were calculated using the Scherrer formula [183]. The standard silicon powder (NIST No. 640) was used as the reference to get the instrumental broadening.

The details of the samples analyzed by XRD is given in Table 2.7.

Table 2.7. Details of the samples analyzed by XRD

No.	Sample	Description	Analyzed form
1	P3, P4, P5, P6, PS6, PW, PE, MW1, MW2, MW3, MW4, MW5,MW6	Precursors for the synthesis of boron carbide	Powder
2	P4BC16, P4BC15, P4BC10, P5BC16, P5BC15, P5BC14, P5BC13, P5BC12, P5BC10, P6BC16, P6BC15, P6BC14, P6BC13, P6BC12, P6BC10, PS6BC16, PS6BC15, PS6BC14, PS6BC13,PS6BC12, PS6BC10,	Boron carbide powder prepared from various precursors	Powder

	PW16, PW15, PW14, PW13, PW12, PW10, PE16, PE15, PE14, PE13, PE10, MW1P16, MW1P15, MW1P14, MW1P13, MW1P12, MW1P10, MW2P16, MW2P15, MW2P14, MW2P13, MW2P12, MW2P10, MW3P16, MW3P15, MW3P14, MW3P13, MW3P12, MW3P10, MW4P16, MW4P15, MW4P14, MW4P13, MW4P12, MW4P10, MW5P16, MW5P15, MW5P14, MW5P13, MW5P12, MW5P10, MW6P16, MW6P15, MW6P14, MW6P13, MW6P12, MW6P10		
3	nc-B_4C16, nc-B_4C17, c-B_4C17,	SPS^{ed} compacts	Compact
4	nc-B_4CH18, c-B_4CH18	Hot pressed compacts	Compact
5	ZAAPM, ZAAPH, ZGAPM, ZGAPH, ZUAPM, ZUAPH, ZACM, ZACH, ZGCM, ZGCH, ZUCM, ZUCH, ZASM, ZASH, ZGSM, ZGSH, ZUSM, ZUSH	‘as-prepared’, calcined and sintered samples of YSZ	Powder

2.7.5 Determination of the size distribution of particles in nc-B_4C powders synthesized for sintering studies and YSZ powders

Dynamic light scattering method (DLS): Particle size and size distribution of the particles in powders can be determined by measuring the random changes in the intensity of light scattered from a suspension or solution [185, 186]. The DLS measures the Brownian motion of the particles in the suspension medium and correlates it with size of the particles.

A particle size analyzer (Mastersizer, M/s. Malvern, Worcestershire, UK) was used to measure the size distribution of particles. An appropriate quantity of sample was dispersed into the holder containing millipore water with stirring and passed through the measurement area of the optical bench, where a laser beam illuminates the particles. A series of detectors located at different angles measure the counts. The small particles will scatter light at large angles and large particles will scatter light at small angles.

2.7.6 Measurement of the Specific Surface Area (SSA) *of nc-B$_4$C synthesized for sintering studies and YSZ powder*

Brunauer-Emmett-Teller (BET) method [187, 188]: BET theory enables to calculate the number of molecules required to form a monolayer. The surface area is the product of the number of molecules in a completed monolayer and the effective cross-sectional area of an adsorbate molecule.

BET equation is used to compute the amount of adsorbate required to form a monolayer and is given by

$$\frac{\frac{P}{P^{\circ}}}{V\,(1-\frac{P}{P^{\circ}})} = \frac{1}{V_m C} + \frac{C-1}{V_m C}\,(\frac{P}{P^{\circ}}) \qquad (2.6)$$

where, P = partial pressure of adsorbate gas in equilibrium with the surface at 77 K

P° = the saturation equilibrium vapour pressure of the adsorbate at a given relative pressure $\frac{P}{P^{\circ}}$

V_m = volume of gas adsorbed on a monolayer.

C = a constant which is a function of the adsorbate-adsorbent interaction energy

The determination of surface area from the BET theory is straight forward. A plot of $\frac{1}{V_m[\left(\frac{P^{\circ}}{P}\right)-1]}$ Vs $\frac{P}{P^{\circ}}$ will yield a straight line in the range of $0.05 \leq \frac{P}{P^{\circ}} \leq 0.35$.

From the slope and intercept, weight adsorbed on a monolayer can be calculated.

$$\text{Slope} = \frac{C-1}{V_m C} \quad (2.7)$$

$$\text{Intercept} = \frac{1}{V_m C} \quad (2.8)$$

(Slope + Intercept) gives V_m, $V_m = \frac{1}{Slope+Intercept}$ (2.9)

Substituting the value of V_m in Eq. (2.10) gives the value of specific surface area.

$$\text{Specific surface area} = \frac{V_m N_A\, A}{2400 * m} \quad (2.10)$$

where A is the cross-sectional area of one adsorbate molecule (For N_2, A = 0.162 nm^2), m is the weight of the sample, N_A is the Avogadro number, V_m is the volume of gas adsorbed on a monolayer. The specific surface area can be obtained by dividing the sample weight.

The specific surface area of all the nc-B_4C powders synthesized for sintering studies was determined by using Thermo Scientific Surfer gas adsorption porosimeter (M/s. Thermo Fisher Scientific S.p.A, Italy). The powders were heated (degassed) at 393 K for 2 h to remove surface adsorbed moisture and gases and were subsequently evacuated at a pressure of 0.1 Pa for 5 h by using a rotary pump (M/s. Pfeiffer-Model Duo1.6, Germany). Then the weighing burette along with the sample was connected to the instrument. The weight of the sample was entered in the measurement software (Surfer acquisition version 1.7.0). The valves in the instrument were opened and evacuated. Liquid nitrogen was filled in the vessel, lifted up and covered the weighing burette. The weighing burette along with the sample was now immersed in the liquid nitrogen. The entire set up was again evacuated. Now nitrogen gas was injected into the burette with a pre-determined pressure (40 torr). When the equilibrium was reached, the volume of the adsorbed gas as a function of pressure was recorded. This procedure was repeated to until 760 torr in steps of 40 torr. The plot obtained is adsorption isotherm. After this, desorption isotherm was obtained by releasing the pressure in steps of 150 torr and equilibrating with the sample in the burette. From the adsorption isotherm, a plot of $\frac{1}{V_m[\left(\frac{P^\circ}{P}\right)-1]}$ Vs $\frac{P}{P^\circ}$ yields a straight line. From this, SSA was calculated as explained above in BET theory. The calculation parameters used for BET was $\frac{P}{P^\circ}$ the initial value of 0.05 and the final value of 0.3.

The specific surface area of the calcined YSZ powders was measured using the BET method (MONOSORB, Model no: MS16, M/s. Quantachrome, USA) employing nitrogen gas adsorption-desorption measurement at 77 K. The powders were degassed at 393 K for 12 h in flowing argon prior to the measurement. The instrument was calibrated by injecting 1 mL of nitrogen gas. The corresponding surface area value was 2.84 m^2. The count rate in the instrument was adjusted to get the surface area value for nitrogen accurately. For measuring the surface area of the sample, the degassed sample with the sample cell was connected to the instrument. A mixture of helium and nitrogen (flow rate: 13.9 and 6.1 mL min^{-1}, respectively) gas was allowed to pass over the sample. The sample was cooled to liquid nitrogen temperature until the adsorption of nitrogen gas was complete. The adsorption was complete when the signal value showed zero. Later the sample was heated by using a hot air blower to carry out desorption and the corresponding signal was used to calculate the specific surface area.

2.7.7 Microstructural characterization

2.7.7.1 Scanning Electron Microscopy (SEM): Electron microscopy is a widely used method for studying the morphology of materials as it provides the observation and characterization of materials on the micrometer to nanometer scale.

In SEM, the surface of the material is scanned under an accelerated electron beam. This accelerated electron beam interacts with the material and results in secondary electrons, backscattered electrons, diffracted backscattered electrons, characteristic X-rays, visible light and heat [189, 190]. Secondary electrons and backscattered electrons are commonly used for imaging the sample. Secondary electrons are the most valuable for showing the morphology and topography of the sample. On the other hand, backscattered electrons are valuable in producing compositional contrast in multiphase samples. The electrons coming out of the material are collected by the corresponding detectors. The output signal from the detector is amplified and transferred to the display unit.

In addition to imaging, Energy Dispersive X-ray (EDX) analysis is also a useful tool for getting the chemical composition of the material. The essential components of an electron microscope are electron emission gun, electron lenses, sample stage, detectors for all signals of interest, display and data acquisition devices. A schematic of the SEM instrument is given in Fig. 2.16.

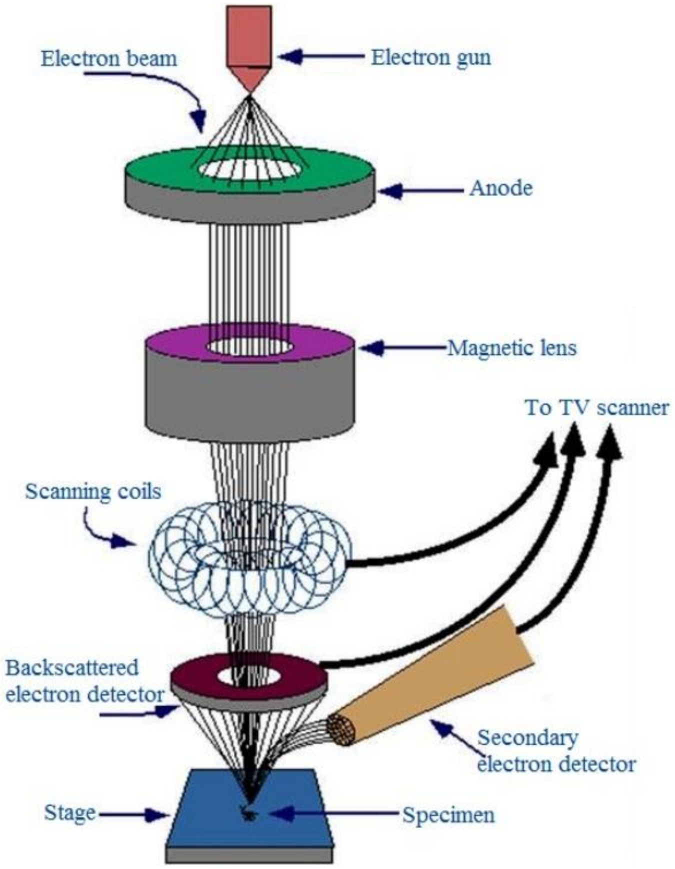

Figure 2.16. Schematic of the SEM instrument [190]

Morphologies of the boron carbide synthesized in this study and carbon obtained from the precursors were examined using the scanning electron microscope (M/s. FEI Helios Nanolab 600i Field Emission Scanning Electron Microscope, Netherlands). A few milligrams of the powder was dispersed on a carbon tape and gold coated prior to SEM analysis. The morphologies of the sample prepared at 1873 and 1773 K from B_2O_3-sucrose precursor and that obtained from freeze-dried precursors were examined. The morphology of the boron carbide synthesized at temperatures 1473 to 1873 K from microwave-assisted precursor prepared at 773 K using H_3BO_3-mannitol with CBMR 3.38 was also examined. In order to determine the morphology of the carbon formed by the decomposition of sucrose, precursor (CBMR: 3.38, T = 873 K) was washed with hot water, filtered and dried under an IR lamp to remove B_2O_3. The morphology of the precursor prepared at 873 K was also examined without removing B_2O_3 from the precursor. All the samples were coated with gold before taking SEM images.

The morphologies of the sintered compacts of YSZ were obtained using the scanning electron microscope (M/s. Philips model XL 30, The Netherlands). The sintered compacts were coated with gold to make it electrically conducting before taking the SEM images.

2.7.7.2 Transmission Electron Microscopy (TEM)

In TEM, an accelerated electron beam is allowed to pass through a very thin specimen [191, 192]. The major components of a transmission electron microscope are the illumination system composed of an electron gun and condenser lenses to produce a fine electron beam, an objective lens to produce the diffraction pattern and an initial magnified image of the specimen, a magnification system to produce the final image and a sample chamber. In the conventional mode (image mode), TEM is operated to form images by bright field, dark field or lattice image (phase) contrast. A bright field or dark field image is formed only when the diffracted beam is used for image formation. This is done with an objective aperture, which prevents the passage of all other beams to the detecting system. A phase contrast (lattice fringe) is formed by the interference of beams in the image plane of the objective lens. During the image-forming process, all the beams passing through the objective aperture are made to recombine such that their phases and amplitudes are preserved. A diffraction pattern is formed by the objective lens in the back focal plane of the objective lens. The first image is rotated 180° against the diffraction pattern. Then the diffraction pattern and the first image are magnified using intermediate and projector lenses. The pattern is formed by the diffraction of electrons from the whole area of the specimen which was illuminated by the beam. An aperture is inserted above the specimen in order to get the diffraction from the specific area of the specimen. It is called the Selected Area Electron Diffraction (SAED). Schematic of image and diffraction modes are shown in Fig. 2.17.

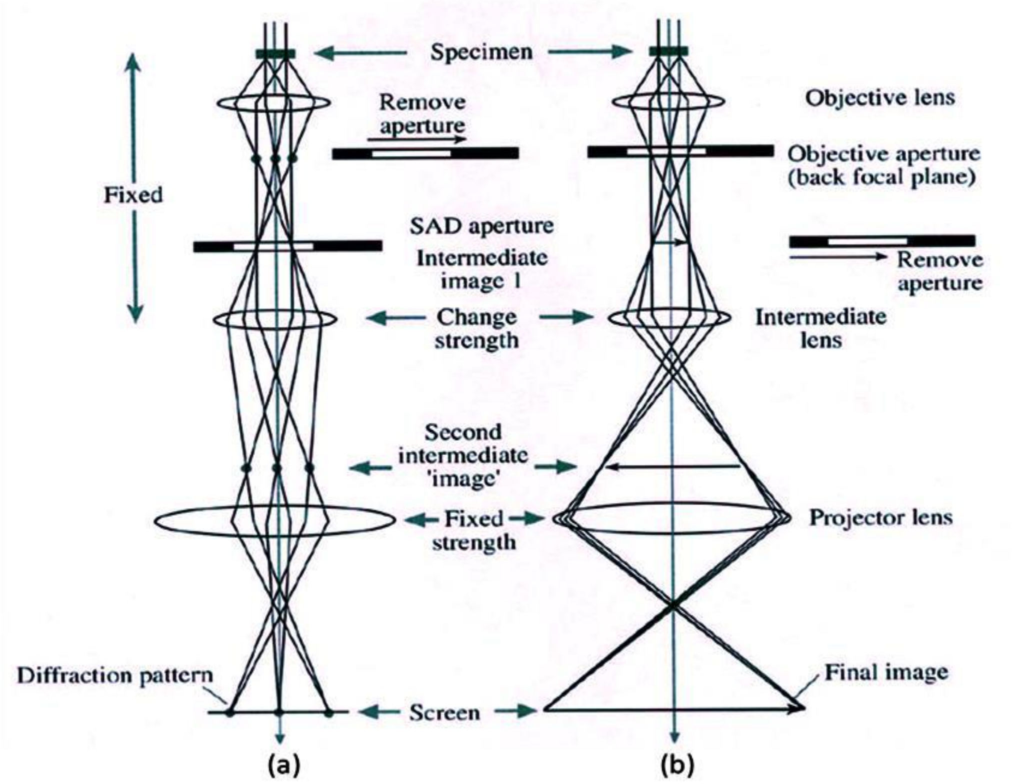

Figure 2.17. Schematic representation: (a) diffraction and (b) image modes in TEM

The powder morphology of the YSZ powders prepared using the microwave-assisted method was studied using the transmission electron microscope (M/s. Philips CM-200 operated at 200 kV). TEM images were obtained only for those samples prepared by using the microwave heating method. The samples for TEM were prepared by sonicating the powder suspended in methanol. A drop of the suspension was deposited on a holey carbon-coated Cu grid and dried overnight under IR lamp.

2.7.8 Spectroscopic analysis of the samples: Raman Spectroscopic analysis

Raman spectroscopy is based on the inelastic scattering of monochromatic light by matter [193, 194]. Raman spectra arise from the change in polarizability of the molecule as a result of the interaction of light with matter. The sample is illuminated with a monochromatic laser beam. The interaction of laser beam with the sample results in the scattering of light. The scattering occurs in all directions. When the frequency of the scattered light is equal to the frequency of the incident light, the scattering is known as Rayleigh scattering. Only a small portion of the scattered light has frequency different from that of the incident radiation and which constitutes Raman scattering. When the frequency of the incident light is higher than that of the scattered light, Stokes lines appear in the Raman spectrum. When it is lower than the scattered light, it results in anti-Stokes lines in the Raman spectrum. Stokes-shifted Raman bands are formed by the transitions from lower to higher energy vibrational levels and therefore, Stokes bands are more intense than anti-Stokes bands and hence are measured in conventional Raman spectroscopy.

Raman spectra (M/s. Renishaw-Invia, Germany) of the calcined and sintered YSZ samples prepared by microwave-assisted combustion synthesis were recorded in order to ascertain the XRD results. The excitation source was 514.5 nm line of an argon laser at the power level of 40 mW.

2.7.9 Thermogravimetric analysis of mannitol and mannitol-boric acid complex

The thermogravimetric analysis was carried out for: a) Mannitol, b) the condensed product of mannitol-boric acid complex-MBC 3.38 (CBMR 3.38, C/B wt.% ratio 1.87) and c) the condensed product of mannitol-boric acid complex-MBC 6 (CBMR 6, C/B wt.% ratio 3.33) using a TGA/SDTA851e thermogravimetric analyzer supplied by M/s. Mettler Toledo, Switzerland. Heating scans were carried out up to 973 K for the condensed products and up to 773 K for mannitol with a heating rate of 5 K min^{-1} in air.

2.7.10 Microhardness of sintered B_4C compacts

The hardness of the sintered compacts was measured by microhardness machine under an applied load of 9.81 N for 15 s (M/s. Omni Tech Microhardness tester, Model S. Auto-II). The resulting indentation diagonals were measured to obtain the Vickers hardness number [195]. The instrument was calibrated using a calibration standard (HV1 720) prior to the hardness measurement of the sample.

2.7.11 Ionic conductivity of YSZ: Impedance analysis

Ionic conductivity of the sintered YSZ compacts was determined using ac-impedance measurement.

Impedance spectroscopy [196-198]: Impedance spectroscopy is a powerful tool for characterizing many of the electrical properties of materials and their interfaces with electronically conducting electrodes. It is a perturbation technique in which the system is perturbed by applying a small amplitude sinusoidal ac voltage as a function of frequency and measuring the response of the system. The response of a system to small sinusoidally varying ac voltage is measured as a function of frequencies. The locus of impedance as a function of angular frequency is called the impedance spectrum. In conductivity measurement a small voltage is applied and the resulting current across the sample is measured. The applied potential and the resulting current are given by

$$E = E_0 \, \mathrm{Sin}(\omega t) \tag{2.11}$$

$$I = I_0 \, \mathrm{Sin}(\omega t + \varphi) \tag{2.12}$$

where φ is the phase difference. The output current has the same angular frequency ω but would differ in amplitude and phase from the voltage signal and this depends on the impedance offered for charge transport processes.

Impedance (Z) can be defined as the resistance to the flow of current and it can be obtained as the ratio of applied voltage to the resultant current.

$$Z = \frac{E}{I} = \frac{E_0 \text{ Sin}(\omega t)}{I_0 \text{ Sin}(\omega t+\varphi)} = Z_o \frac{\text{Sin}(\omega t)}{\text{Sin}(\omega t+\varphi)} \qquad (2.13)$$

By using Euler's relationship, it is possible to express impedance as a complex function. ie,

$$E = E_o \exp(j\omega t) \qquad (2.14)$$

$$I = I_o \exp j(\omega t - \varphi) \qquad (2.15)$$

The impedance can be represented as,

$$Z(\omega) = \frac{E_o \exp(j\omega t)}{I_o \exp j(\omega t - \varphi)}$$

$$= Z_0 \exp(j\varphi) = Z_0 (\cos\varphi + j\, sin\varphi) = Z_0\, cos\varphi + jZ_0\, sin\varphi = Z' + jZ'' \qquad (2.16)$$

where, $Z' = Z_0\, cos\varphi$, $Z'' = Z_0\, sin\varphi$ and $j = \sqrt{-1}$. Z' is the real part of impedance and Z'' is the imaginary part of the impedance.

The phase difference, $\varphi = tan^{-1} \frac{Z''}{Z'}$ (2.17)

The impedance of a pure resistor, capacitor and inductor respectively are,

$$Z = R \qquad (2.18)$$

$$Z = \frac{1}{j\omega C} \qquad (2.19)$$

$$Z = j\omega L \qquad (2.20)$$

where, R is the resistance of the resistor, C the capacitance of the capacitor and L is the inductance of the inductor. The current through a capacitor is referred imaginary and it leads the voltage by 90° i.e. a phase difference of 90° exists between the applied sinusoidal voltage and the resulting current.

Impedance data can be analyzed by plotting the imaginary part (Z") against the real part (Z'). When the data is plotted on a linear scale, it takes in the form of semicircles. The plot is known as the Nyquist plot.

When an ac voltage is applied, charge transfer across the sample occurs. This charge transfer consists of various processes at the electrode-electrolyte interface and in the bulk of the sample. Processes at the electrode-sample interface could involve adsorption, diffusion and dissociation of adsorbed species and charge transfer to or from the electrode. Charge transport across the bulk of a polycrystalline sample can be a combination of transport through grains and grain boundaries. The charge transport process individually would have different time constants and they would get separated in the frequency domain during measurement. The measured impedance can be correlated to various elementary processes occurring in the material which can be understood from the equivalent electrical circuits. The equivalent electrical circuit of a ceramic electrolyte, consisting of a series combination of resistors (R) and capacitors (C) connected in parallel as shown in Fig. 2.18, and the corresponding impedance spectrum is shown in Fig. 2.19. The frequency windows of various processes are given in Fig. 2.20.

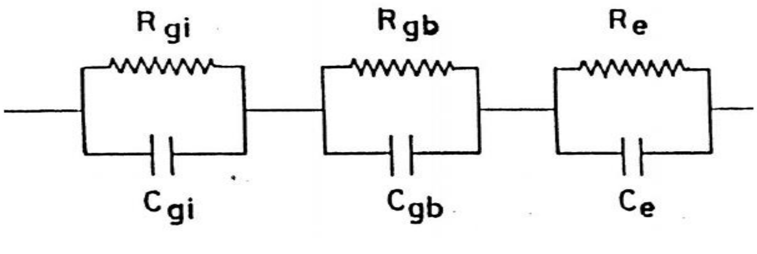

Figure 2.18. Equivalent electrical circuit of a ceramic electrolyte, consisting of a series combination of parallely connected resistors (R) and capacitors (C)

(C_{gi}, C_{gb} and C_e are the capacitances and R_{gi}, R_{gb} and R_e are the resistances corresponding to the grain, grain boundary and electrode-electrolyte interface)

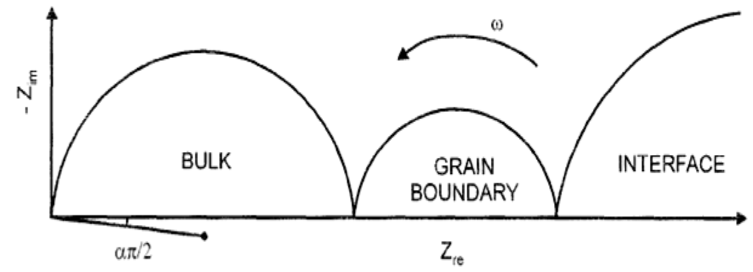

Figure 2.19. Impedance spectrum of a solid ionic conductor

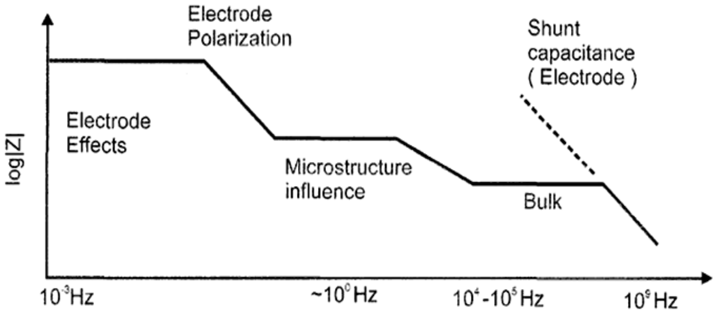

Figure 2.20. Frequency windows of various elementary processes

Procedure: The YSZ compacts used in the conductivity measurements were of ~8 mm diameter and ~2 mm thickness. Both sides of the pellets were gold coated using a DC-magnetron sputtering unit before the conductivity measurements. The schematic of the cell used for the measurement of ionic conductivity is shown in Fig. 2.21. Impedance data were obtained by applying an ac amplitude of 100 mV in the frequency range 10 Hz to 1 MHz using a frequency response analyzer (model number SI 1260, M/s. Schlumberger, UK) with an electrochemical interface (model number 1287, Solartron, M/s. Schlumberger, UK). The data were recorded in the temperature range of 623 to 1073 K (Tubular furnace, M/s. Technico, India) in air at 50 K intervals. Samples were equilibrated at each temperature for ~60 min prior to each set of the measurements. The impedance data obtained at each temperature were fitted by Zview® software. The bulk resistance of the material was obtained by fitting a semicircle to the experimentally obtained Nyquist plot. The ionic conductivity, σ, was calculated using the following expression:

$$\sigma = \frac{t}{RA} \tag{2.21}$$

where t is the thickness of the sample, A is the electrode area and R is the resistance as determined by the impedance spectroscopy. Arrhenius plot for conductivity was then obtained by plotting log σ as a function of 1/T. Activation energy was calculated from the slope of the straight line.

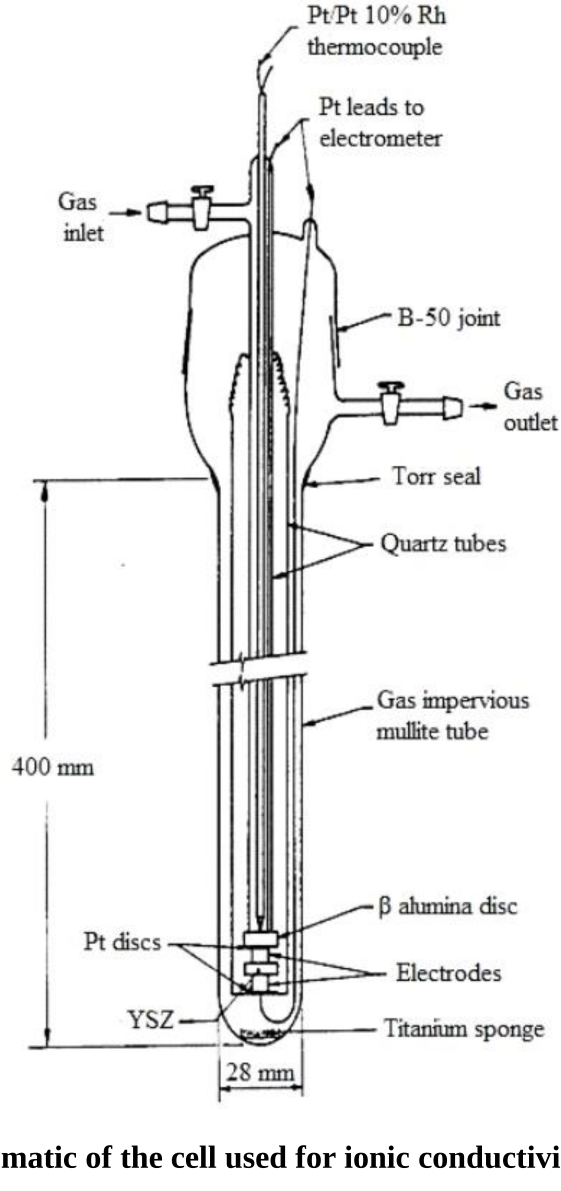

Figure 2.21. Schematic of the cell used for ionic conductivity measurement.

Chapter 3

Studies on the synthesis of nc-B_4C by precursor method

*This chapter presents the results of the studies carried out to synthesize nc-B_4C employing the precursor method***.** *Boric oxide was used as the boron source and sucrose was used as the carbon source for the preparation of the precursor. The process parameters were optimized to obtain pure nc-B_4C with a minimum amount of free carbon impurity. The amount of free carbon in the product mixture of B_4C and free carbon is taken as a measure of homogeneity of the reactants in the precursor. The amount of free carbon in the product synthesized by the precursor method mainly depends on the homogeneity of the reactant mixture in the precursor, temperature and rate of the reaction. Hence, different methods were adopted to improve the homogeneity of the reactant mixture in the precursor in order to reduce the free carbon content in the product. Two different methods were adopted to prepare the precursor to study the influence of the homogeneity of the reactant mixture in the precursor on the free carbon content in the product: a) mixing of boric oxide-sucrose in a dispersion medium to form a slurry and removal of the dispersion medium by freeze-drying followed by heat-treatment of the freeze-dried powder and b) preparation of a condensed product by microwave-assisted heating of a solution containing mannitol and boric acid. The condensed product was thermally decomposed to obtain the precursor. The precursors thus obtained were used for the synthesis of B_4C. The precursors and the products were characterized for phase purity, chemical composition and morphology.*

3.1 Synthesis of nc-B_4C by using B_2O_3-sucrose precursor method

The method of preparation of precursor is explained in Section 2.3.1.1 of Chapter 2 and the processing of the precursor is explained in Section 2.3.1.2 of the same chapter. The sample designation is also given in Table 2.1 of Chapter 2.

3.1.1 B_2O_3-sucrose precursor

The heating of the mixture of B_2O_3 and sucrose at 463 K led to melting of sucrose and dispersion of B_2O_3 particles in molten sucrose. This molten sucrose-B_2O_3 mixture was further heated at various temperatures to ensure the decomposition of sucrose as well as a uniform dispersion of B_2O_3. The precursor prepared at all the temperatures, except at 573 K, was porous and black in colour. The precursor formed at 573 K was black in colour with a brown tinge and this may be due to the incomplete decomposition of sucrose at this temperature [199] in the presence of B_2O_3. A typical photograph of the precursor prepared at 773 K is shown in Fig. 3.1. With the increase in the precursor preparation temperature, the voluminous nature of the precursor was found to decrease. The precursors obtained at 973 and 1073 K were less voluminous as compared to those obtained at lower temperatures. This may be due to the escape of gaseous components during the heating and crumbling of the pore structure.

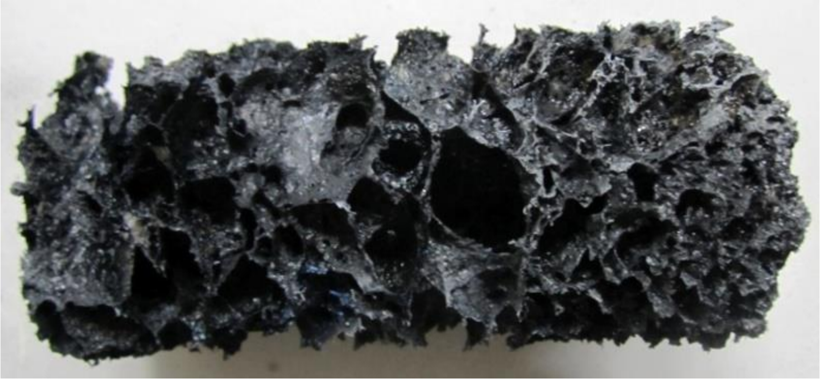

Figure 3.1. Photograph of the precursor formed from B_2O_3 and sucrose at 773 K

3.1.2 XRD analysis of the precursor obtained from B_2O_3 and sucrose

Typical XRD patterns of the precursors P3, P4, P5, P6 and PS6 are shown in Fig. 3.2. The XRD patterns of the precursors matched with the pattern corresponding to ICDD file number 00-006-0297. The XRD patterns indicated the presence of only cubic B_2O_3. The features corresponding to that of the carbon in the XRD patterns of the precursors were absent. This shows that the carbon formed by the decomposition of sucrose is either predominantly amorphous, or it is a very fine crystalline powder. This was further confirmed by recording the XRD pattern of the carbonaceous material after the removal of B_2O_3 from the precursor, and it is shown in Fig. 3.3.

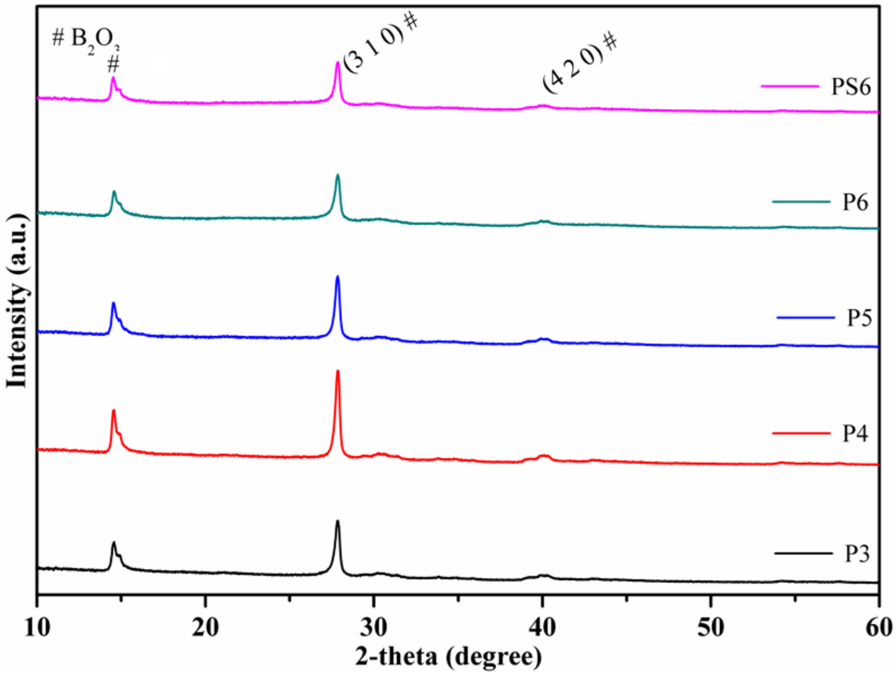

Figure 3.2. XRD patterns of the precursors: P3, P4, P5, P6 and PS6

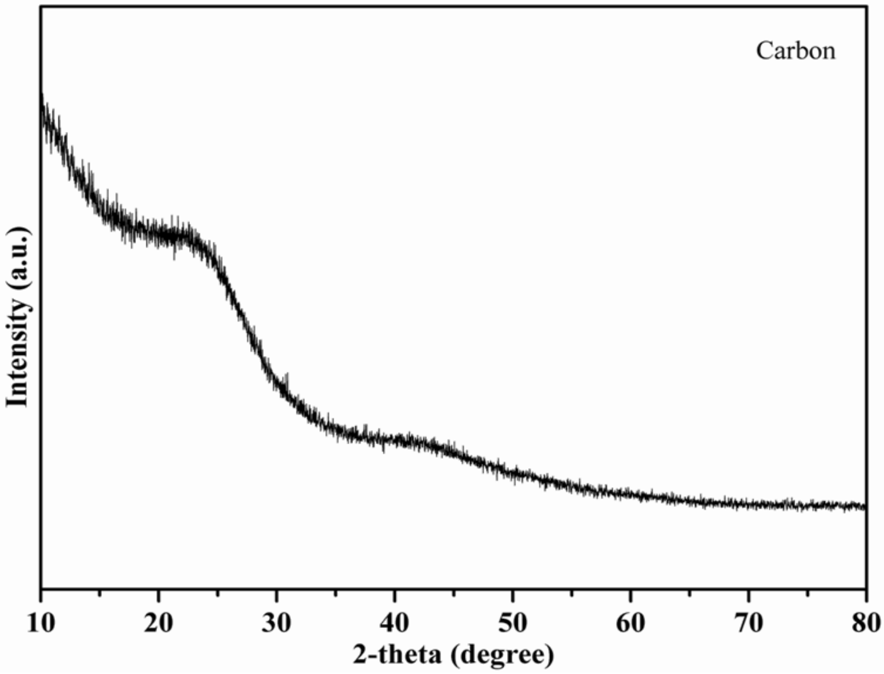

Figure 3.3. XRD pattern of the carbonaceous material after the removal of B_2O_3 from P6

B_2O_3 melts at 723 K [200]. Sucrose melts at 459 K [199] and decomposes upon further heating to give carbon. Perhaps this could have resulted in a more homogeneous distribution of the molten boric oxide and carbon leading to the formation of a more uniform precursor as mentioned in Ref. [36]. The boric oxide dispersed in carbon network is the precursor for the synthesis of boron carbide.

The possible chemical reactions for the formation of boron carbide from B_2O_3 and sucrose are given as:

$$C_{12}H_{22}O_{11} \rightarrow 12\,C + 11\,H_2O \tag{3.1}$$

$$2\,B_2O_3 + 7\,C \rightarrow B_4C + 6\,CO \tag{3.2}$$

3.1.3 XRD analysis of the products obtained by the heat-treatment of precursors obtained from B_2O_3 and sucrose

The boron carbide synthesized from these precursors at all the temperatures was grey in colour. However, the B_4C formed at lower temperatures was black in colour, perhaps due to the presence of a significant amount of unreacted carbon.

The XRD patterns of all the samples were recorded by uniformly spreading almost the same quantity of sample on a zero background sample holder (diameter: 25 mm, depth: ~0.5 mm). The XRD patterns of the products obtained after heat-treatment of the precursors matched with the ICDD database file number 00-035-0798. The XRD patterns of the products obtained from the precursors, P4, P5, P6 and PS6 are shown in Figs. 3.4 to 3.7, respectively. XRD patterns indicated that the formation of B_4C occurs at all the temperatures (1273 to 1873 K), regardless of the precursor preparation temperature. Fig. 3.4 shows typical XRD patterns of the product obtained from the precursor P4 after heat-treatment at 1273, 1773 and 1873 K. Peaks pertaining to B_2O_3 were present in the XRD patterns of the products even at 1773 and 1873 K, indicating an incomplete reaction. The peaks pertaining to B_2O_3 were not discernible in the XRD pattern of the product formed at 1273 K due to the broad peak in the 2θ range of 20 to 30°. The product formed by heating the precursor P5 is shown in Fig. 3.5. At 1473 K, even heating for 3 h was not sufficient for the reaction to go to completion. Fig. 3.6 shows the XRD patterns of the products formed after the heat-treatment of the precursor P6 at different temperatures ranging from 1273 to 1873 K. Formation of B_4C was found to occur even at 1273 K irrespective of the precursor preparation temperature, whereas Jung et al. [27] have observed during carbothermic reduction the presence of B_4C peaks only in samples heated at temperatures above 1673 K. The XRD patterns of the products formed at different temperatures, 1273 to 1873 K, using a stoichiometric mixture of B_2O_3 and carbon ie., PS6, are shown in Fig. 3.7. The peak pertaining to carbon (ICDD file number 00-056-0159) was clearly seen in the boron carbide samples synthesized at 1273 K. The intensity of (021) peak in the XRD patterns of boron carbide prepared at 1873 and 1273 K from P4, P5, P6 and PS6 were plotted and is shown in Fig. 3.8. It can be seen that the intensity of boron carbide peak increases with temperature of preparation of the precursor. This is as expected. It is clear from the plot that the intensity of (021) peak of boron carbide appeared to vary linearly (qualitative) with the preparation temperature of the precursor. The intensity of (021) peak of boron carbide obtained from PS6 was lower than that obtained from P6. This can be explained by considering the fact that the carbothermic reduction of the reactants with CBMR equal to 3.5 (C/B wt.% ratio 1.94) results in a biphasic mixture of B_4C and C [73]. The maximum intensity was obtained for the boron carbide synthesized from precursor P6. This could be due to better homogeneity of the precursor formed at 873 K. The intensity of boron carbide peak showed a similar trend at both 1273 and 1873 K.

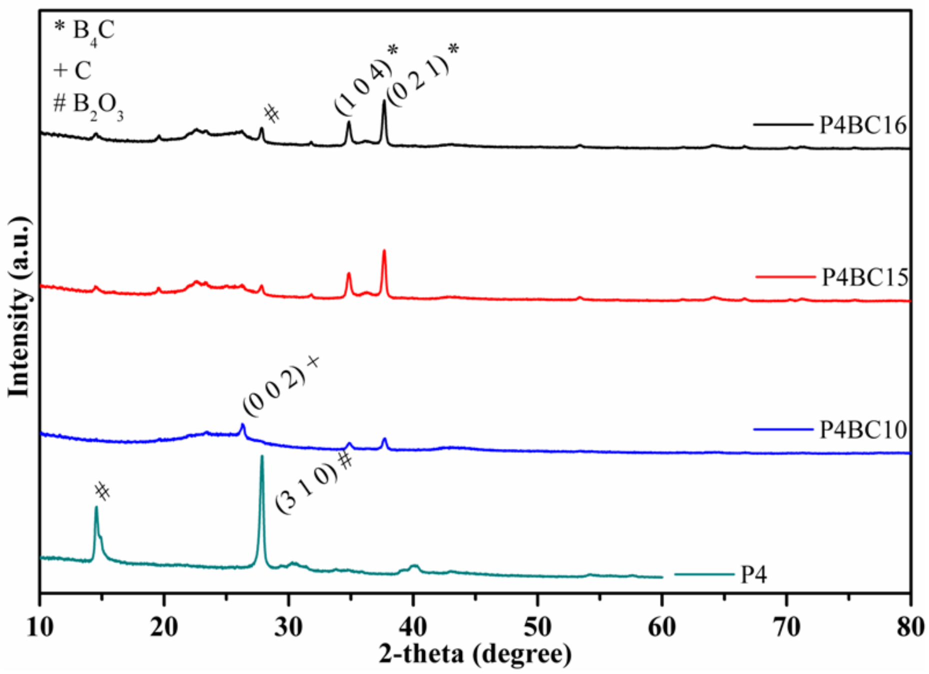

Figure 3.4. XRD patterns of the products obtained from the precursor P4

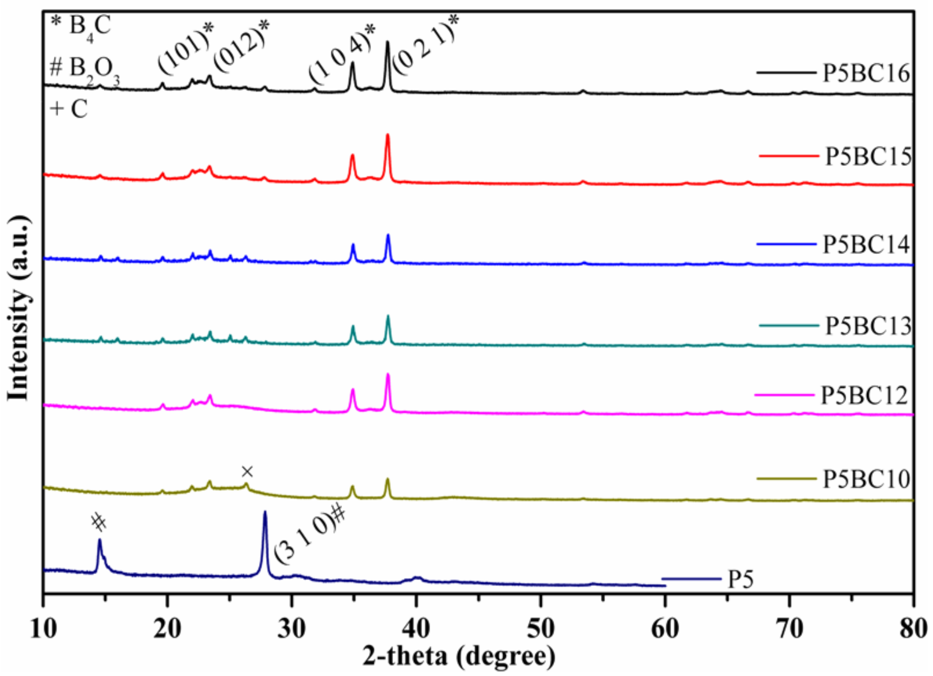

Figure 3.5. XRD patterns of the products obtained from the precursor P5

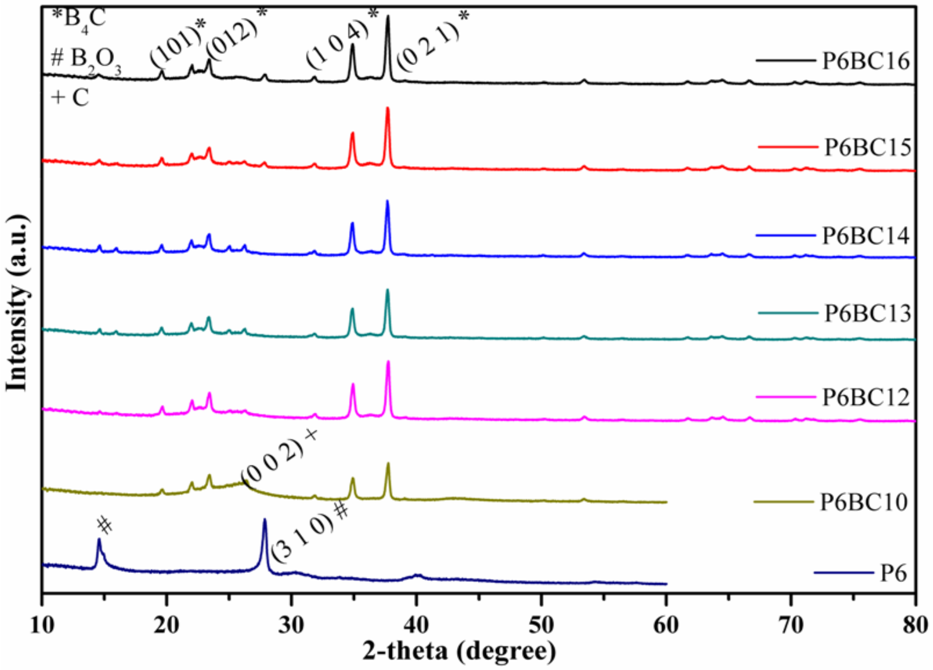

Figure 3.6. XRD patterns of the products obtained from the precursor P6

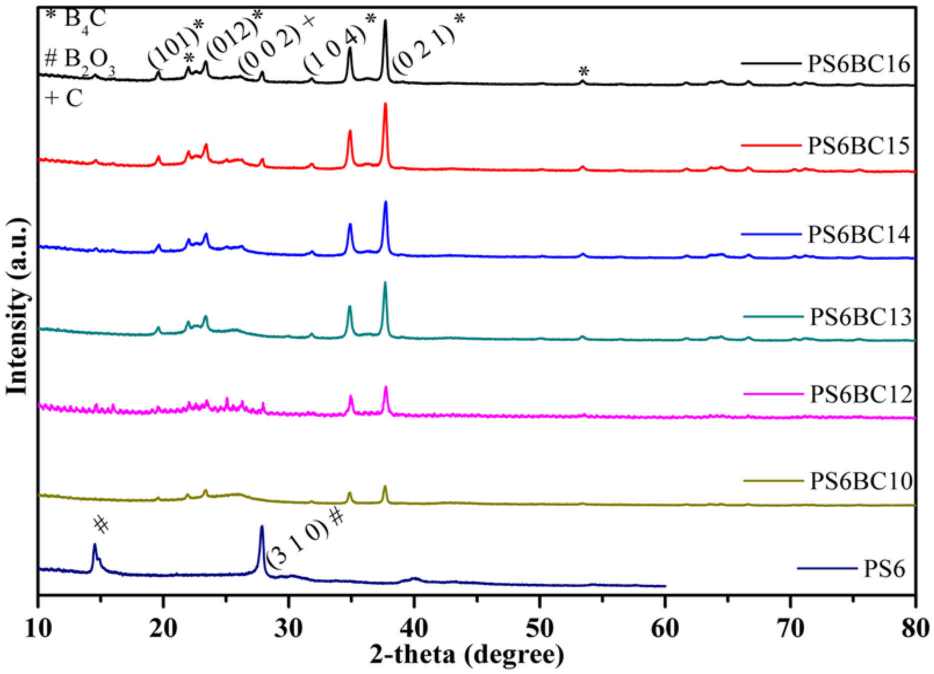

Figure 3.7. XRD patterns of the products obtained from the precursor PS6

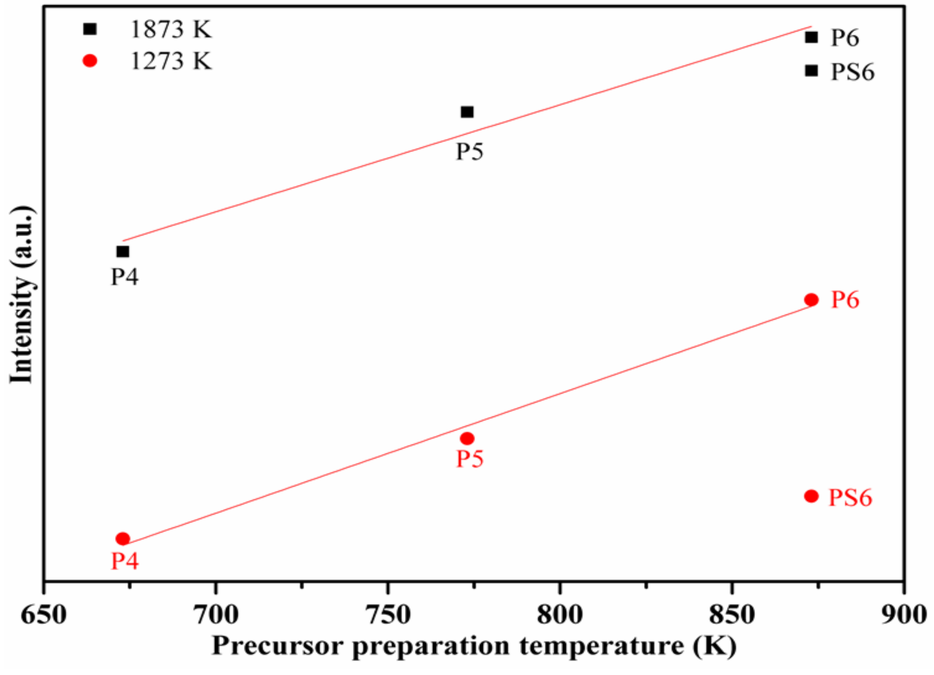

Figure 3.8. Intensity of (021) peak of B_4C synthesized at 1873 and 1273 K

The average X-ray crystallite sizes of B_4C obtained from precursors (P4, P5, P6 and PS6) were in the range of 30 to 35 nm irrespective of the temperature (1473 to 1873 K) and duration of heating (10 to 180 min). This could be due to longer heating schedule followed at lower temperatures and shorter heating schedule followed at higher temperatures. Rafi-ud-din et al. [51] have reported a crystallite size of 94 nm for B_4C synthesized at 1473 K using a precursor prepared from cellulose and boric acid. Pilladi et al. [65] have reported an average crystallite size of 60 nm for B_4C synthesized using boric oxide-sucrose precursor at 1773 K for 3 h. The average crystallite size reported in the present study was lower than that reported in the above mentioned works, perhaps due to the shorter duration of heating employed in the present study.

3.1.4 Results of chemical analyses of the precursors prepared by using B_2O_3-sucrose and the products obtained from these precursors

3.1.4.1 Results of chemical analyses of precursors prepared from B_2O_3 and sucrose

C/B wt.% ratio calculated for the precursor prepared by using B_2O_3 and sucrose with a CBMR equal to 3.38 is 1.87 and that with a CBMR equal to 3.5 is 1.94. The C/B wt.% ratios of the precursors obtained at each temperature (673 to 1073 K) were determined and are shown in Fig. 3.9. The experimentally determined C/B wt.% ratio of the precursor prepared at 873 K was close to the calculated ratio. It is observed that the C/B wt.% ratio of the precursors obtained at 973 and 1073 K deviated more from the calculated ratio. Though the C/B wt.% ratio of precursor obtained at 673 K was close to the calculated ratio, the experimental results indicated that there is inhomogeneity in the precursor obtained at this lower temperature also.

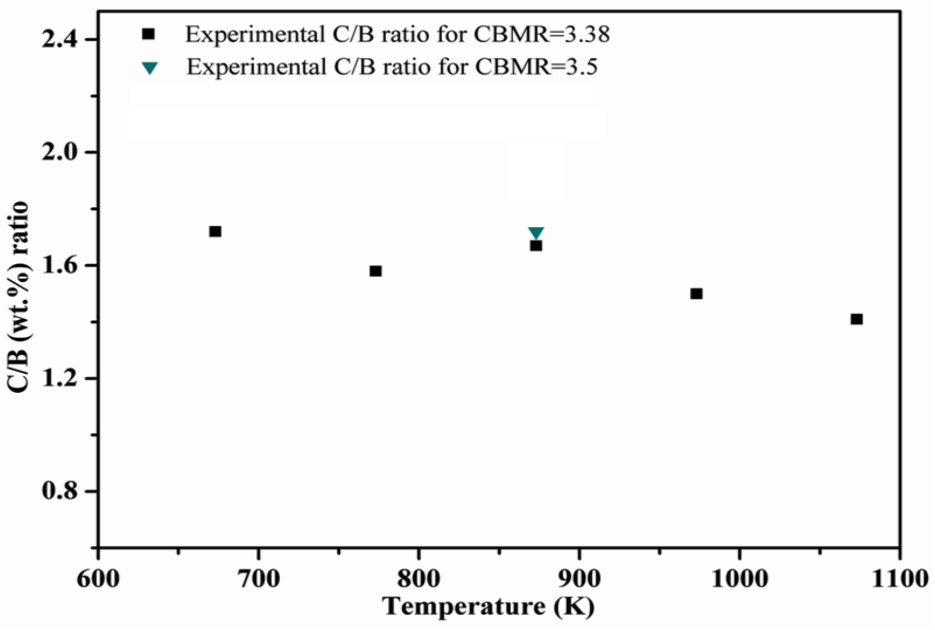

Figure 3.9. C/B wt.% ratio of the precursors obtained from B_2O_3 and sucrose

3.1.4.2 Results of chemical analyses of the products obtained by heat-treatment of the precursors prepared from B_2O_3 and sucrose

The results of chemical analyses of the B_4C products obtained from each precursor, P4, P5, P6 and PS6 are listed in Tables 3.1 to 3.4, respectively. The product obtained from P4 at 1873 K was found to contain boron content of 57.4 wt.% and total carbon content of 42.0 wt.%. The product obtained from P4 at 1773 K had 60.3 wt.% boron and 39.4 wt.% total carbon. This indicates that the reaction is incomplete, which is in agreement with the XRD results. The boron and total carbon content in the product obtained from P5 at 1873 K were 72.6 and 27.6 wt.%, respectively and that at 1773 K were 74.2 and 28.1 wt.%. The free carbon contents in these samples were found to be 6.4 and 6.9 wt.%, respectively. At 1873 K the product obtained from the precursor P6 showed boron and total carbon content of 76.6 and 25.4 wt.% respectively. The boron and total carbon content at 1773 K in P6 were 75.5 and 26.5 wt.% respectively. The free carbon content in these samples were 3.9 and 2.4 wt.% respectively at 1773 and 1873 K. The product obtained from PS6 showed

70.7 and 73.5 wt.% of boron at 1773 and 1873 K, respectively. The total carbon content at these temperatures were 29.8 and 27.6 wt.%, respectively. The free carbon contents were found to be 4.0 and 3.3 at 1773 and 1873 K, respectively in the product obtained from PS6. Even though, the peak pertaining to carbon is not prominent in the XRD patterns of the products obtained after heat-treatment of the precursors, the chemical analyses of the products indicated the presence of free carbon. The results of the chemical analyses of B_4C prepared by different methods reported in literature are given in Table 3.5. Gao et al. [36] have reported a free carbon content of 1.7 wt.% in the B_4C product synthesized at 2123 K even with 15 mol.% excess of H_3BO_3. When the authors increased the amount of H_3BO_3 to 80 mol.%, the free carbon content was found to be reduced to 0.38 wt.%. Corradetti et al. [55] have reported a free carbon content of 9.1 wt.% in the B_4C synthesized at 2173 K using a precursor prepared from H_3BO_3 and citric acid. Rafi-ud-din et al. [56] have reported a free carbon content of 4.0 wt.% for the B_4C product synthesized from the borate-citrate precursor with the addition of 20 wt.% ethylene glycol at 1623 K with 4 h heating. In the present study, the free carbon content in the B_4C product (from P6) was less than 4.0 wt.% even at 1673 K and with 1 h heating. The amount of free carbon in the B_4C product reported in the present study is comparable with that of Rafi-ud-din et al. [56] even though at the same temperature the duration of heating was 3 h less than that reported by these authors. This could be due to the better homogeneity of the precursor formed in the present study compared to that employed by Rafi-ud-din et al. [56].

Table 3.1. B, total C and free C in the products obtained from P4

Sample	Boron (wt.%)	Total C (wt.%)	XCS (nm)
P4BC16	57.4	42.0	34
P4BC15	60.3	39.4	32

Expanded uncertainty in B is ± 0.7 wt.% and total C is ±0.5 wt.% with 0.95 level of confidence.

Table 3.2. B, total C and free C in the products obtained from P5

Sample	Boron (wt.%)	Total C (wt.%)	Free C (wt.%)	XCS (nm)
P5BC16	72.6	27.6	6.4	33
P5BC15	74.2	28.1	6.9	30
P5BC14	72.4	28.1	9.0	23
P5BC13	69.6	27.9	9.6	22
P5BC12	65.5	31.1	6.6	32

Expanded uncertainty in B is ± 0.7 wt.%, total C is ± 0.5 wt.% and free C is ± 0.6 wt.% with 0.95 level of confidence.

Table 3.3. B, total C and free C in the products obtained from P6

Sample	Boron (wt.%)	Total C (wt.%)	Free C (wt.%)	XCS (nm)
P6BC16	76.6	25.4	2.4	32
P6BC15	75.5	26.5	3.9	32
P6BC14	75.2	27.1	3.5	34
P6BC13	74.8	27.6	4.7	34
P6BC12	69.9	30.0	6.4	34

Expanded uncertainty in B is ± 0.7 wt.%, total C is ± 0.5 wt.% and free C is ± 0.6 wt.% with 0.95 level of confidence.

Table 3.4. B, total C and free C in the products obtained from PS6

Sample	Boron (wt.%)	Total C (wt.%)	Free C (wt.%)	XCS (nm)
PS6BC16	73.5	27.6	3.3	33
PS6BC15	70.7	29.8	4.0	31
PS6BC14	70.7	29.4	7.7	29
PS6BC13	71.2	28.6	8.0	31
PS6BC12	63.6	33.0	10.3	

Expanded uncertainty in B is ± 0.7 wt.%, total C is ± 0.5 wt.% and free C is ± 0.6 wt.% with 0.95 level of confidence.

Table 3.5. Results of chemical analyses of B_4C reported in literature

Author	Reactants	[a]Conditions	[b]Temp. (K)	[c]Time (min)	B	C_T	C_f	[d]Method	Ref.
Alizadeh et al.	H_3BO_3-activated carbon	$H_3BO_3/C = 3.3$	1743	300	76.8	-	0.8	Carbothermic reduction	[26]
	H_3BO_3-petroleum coke	$H_3BO_3/C = 3.5$	1743	300	76.5	-	1	Carbothermic reduction	
Jung et al.	B_2O_3-carbon	$2B_2O_3 + xC$, 57% carbon content	2073	20	-	-	-	Carbothermic reduction	[27]
Kobayashi et al.	B_2O_3-carbon black	B_4C seed grains, B_2O_3/C wt. ratio = 1.66	1723-2023	180	-	-	-	Carbothermic reduction	[28]
Kobayashi et al.	B_2O_3-carbon black	B_2O_3/C wt. ratio = 1.66, 2.32, 3.86	1723-2023	180	-	-	-	Carbothermic reduction	[29]
Herth et al.	B_2O_3-carbon black	-	1573-1773	30	-	-	-	Carbothermic reduction	[30]
Tumanov et al.	B_2O_3-carbon black	-	2500	-	77.5	20.4	0.4	Carbothermic reduction	[33]
Goller et al.	H_3BO_3-petroleum coke	H_3BO_3/C ratio = 3.6.	2273	-	78.6	20.3	Nil	Carbothermic reduction	[34]
Gao et al.	H_3BO_3 - carbon	50 mol.% excess H_3BO_3	2123		-	-	0.36	Rapid carbothermic reduction	[36]
Sonber et al.	boron powder-petroleum coke	B\C = 4	2123	180	77.1	22.9		Synthesis from elements	[48]
Rafi-ud-din et al.	H_3BO_3-EG-cellulose	$C/B_2O_3 = 3.5$	1473	240	-	-	-	Precursor method	[51]
Maqbool et al.	H_3BO_3-starch/ cellulose/glucose/	$C/B_2O_3 = 3.5$	1323-1723	0-240	-	-	-	Precursor method	[52]

Tahara et al.	H_3BO_3-glycerine-tartaric acid	C/B_2O_3 = 3.30-3.44 0-50 mol.% TA	1523	0-300	-	-	-	Precursor method	[53]
Kakiage et al.	H_3BO_3-glycerine	C/B_2O_3 = 3.5	1523	300	-	-	-	Precursor method	[54]
Corradetti et al.	H_3BO_3-citric acid	H_3BO_3/C wt. Ratio = 3.7:1	1773	-	-	-	9.1	Precursor method	[55]
	H_3BO_3-phenolic resin		1773	-	-	-	21.2		
Rafi-ud-din et al.	H_3BO_3-citric acid-EG	EG = 0-50 mol%	1323-1673	0-240	-	-	4	Precursor method	[56]
Khanra et al.	H_3BO_3-citric acid	-	1873	-	-	-	9.8	Precursor method	[57]
Sinha et al.	H_3BO_3-citric acid	H_3BO_3/citric acid mole ratio 12/7	1723	120	68.8	30	11.1	Precursor method	[58]
Kakiage et al.	H_3BO_3-mannitol	C/B_2O_3 ratio = 3, 3.5, 6	1523	300	-	-	-	Precursor method	[59]
Mondal et al.	H_3BO_3-PVA	-	1073	180	-	-	-	Precursor method	[60]
Barros et al.	H_3BO_3-PVA	-	1273	60	-	-	-	Precursor method	[61]
Kakiage et al.	H_3BO_3-PVA	-	1473	300	-	-	-	Precursor method	[62]
Yanase et al.	H_3BO_3-PVA	-	1573	300	-	-	-	Precursor method	[63]
Kakiage et al.	H_3BO_3-PVA	-	1373	1200	-	-	-	Precursor method	[64]
Pilladi et al.	B_2O_3-sucrose	-	1173	180	75.8	23.4	3.5	Precursor method	[65]

Foroughi et al.	B_2O_3-sucrose	-	1523, 1623, 1723	20, 120, 1440	-	-	-	Precursor method	[66]
Zakharova et al.	H_3BO_3-sucrose/ potato starch/ carbon black/phenol-formaldehyde resin	30-100% excess H_3BO_3	1573-1823	60-180	-	-	-	Precursor method	[67]
Pilladi et al.	H_3BO_3-sucrose	-	1823	180	75.8	23.9	6	Precursor method	[68]
Foroughi et al.	H_3BO_3-sucrose/PVA	-	1423-2023	3-1440	-	-	-	Precursor method	[69]
Avciata et al.								Precursor method	[70]
Watts et al.	H_3BO_3-sucrose	-	1673	240	-	-	-	Precursor method	[71]
Vijay et al.	B_2O_3-sucrose	C/B_2O_3 mole ratio = 3.38	1873	10	76.57	25.39	2.42	Precursor method	[72]

B-boron content in wt.%, C_T-total carbon in wt.%, C_f- free carbon in wt.%, EG-ethylene glycol, PVA = poly(vinyl alcohol) and TA-tartaric acid, ^{a} reactant stoichiometry, ^{b}boron carbide synthesis temperature and ^{c}duration of heating, ^{d}method of synthesis

3.1.5 Morphology of the products obtained from the precursors prepared by using B_2O_3 and sucrose: SEM

The morphology of the precursor prepared at 873 K (P6) is shown in Fig. 3.10a. The microstructure is an aggregate of fine particles with no discernible morphology. Morphology of the carbon obtained after the removal of B_2O_3 from the precursor prepared at 873 K (P6) is shown in Fig. 3.10b. The microstructure looks like a three dimensional porous network perhaps due to the removal of B_2O_3. This is similar to the three-dimensional bicontinuous structure reported by Tahara et al. [53], but with a finer network of carbon in the present study. It is clear from the SEM image that the precursor is a homogeneous dispersion of B_2O_3 and carbon and this resulted in the increased contact area between the reactants. The uniform distribution of B_2O_3 in the carbon network provides more number of nucleation sites during heating. Fig. 3.11a and Fig. 3.11b shows typical morphologies of boron carbide obtained from P6 at 1773 and 1873 K respectively, whereas Fig. 3.11c and Fig. 3.11d shows the morphologies obtained from P5 at 1773 and 1873 K respectively. Two types of grains are observed in all the images, one with aggregates of fine equiaxed particles of size <0.2 μm and the other with larger equiaxed particles of size <2 μm. It is surmised that higher heating rate and temperature coupled with shorter processing times would have resulted in increased nucleation and the formation of many small crystallites from a uniform precursor [201]. Similar dual sizes were reported by Watts et al. [71] and the authors have reported that the loss of homogeneity of the precursor would have resulted in the formation of particles with dual sizes. These authors have studied the effect of moisture content on the morphology of boron carbide prepared using boric acid and sucrose. Presence of moisture in the precursor resulted in boron carbide with large rod-like particles and the precursor without moisture resulted in

B_4C with uniform particles as reported in the present study. Kobayashi et al. [29] and Weimer et al. [201] have reported that the morphology of B_4C powder synthesized by carbothermic reduction depended on heat-treatment temperature and the composition of the starting powder mixture. Zakharova et al. [67] have reported coarse needle-shaped morphology for the boron carbide synthesized using boric acid and sucrose with excess boric acid, whereas Pilladi et al. [68] have reported an irregular morphology for the boron carbide synthesized from boric acid and sucrose precursor. In the present study, boron carbide obtained showed equiaxed morphology irrespective of the precursor preparation temperature and processing temperature.

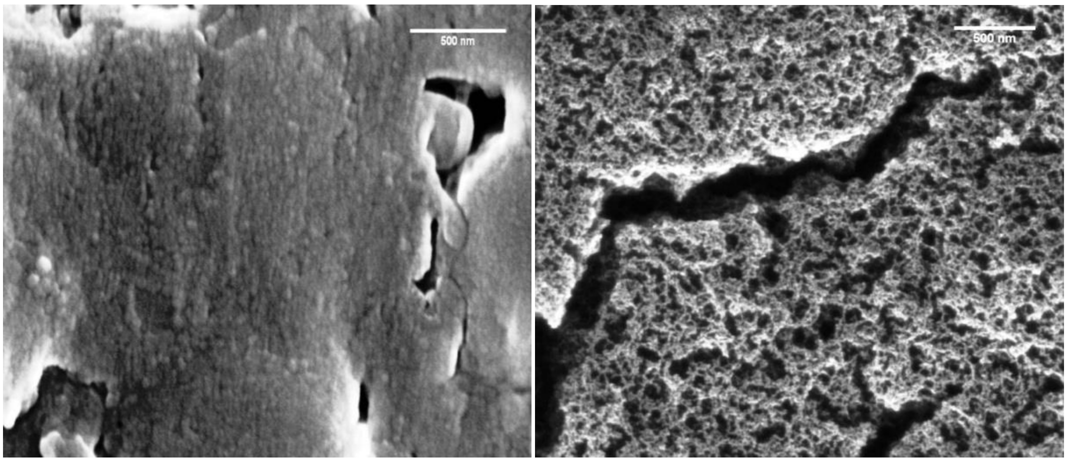

(a) (b)

Figure 3.10. SEM images: (a) precursor (P6) before removing B_2O_3, (b) C after removing B_2O_3 from the precursor (P6)

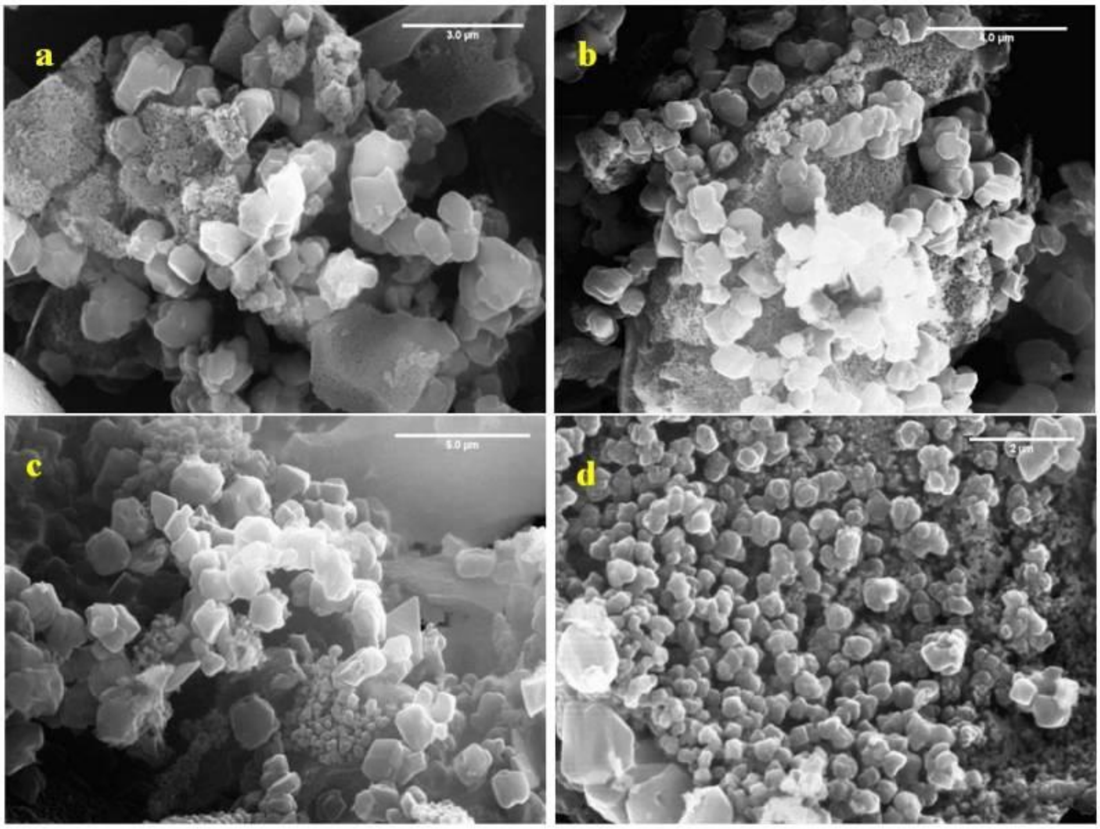

Figure 3.11. SEM images: a) P6BC16, b) P6BC15, c) P5BC16 and d) P5BC15

3.2 Improving the homogeneity of B_2O_3-sucrose precursor by freeze-drying

The preparation and processing of the precursors are respectively explained in Section 2.3.2.1 and 2.3.2.2 of Chapter 2. The sample designation is also given in Table 2.3 of Chapter 2.

3.2.1 B_2O_3-sucrose precursor by freeze-drying

The slurry of B_2O_3 and sucrose prepared using water became a white solid after freeze-drying. The precursor obtained after heat-treatment of this white solid powder was black, porous and hard. The slurry of B_2O_3 and sucrose prepared using ethanol turned into a white solid after freeze-drying. It was found that the inner chamber of the freeze-dryer was coated with a fine layer of white powder during freeze-drying of the slurry prepared using ethanol, which on chemical analysis was found to be B_2O_3. This loss of boric oxide was reflected in the increase in C/B wt.%

ratio of the PE. The C/B wt.% ratio obtained for PE was 2.41 compared to the initial value of 1.87. The C/B wt.% ratio of PW was 1.60 which is closer to the calculated C/B wt.% ratio in the precursor as compared to that of PE.

3.2.2 XRD analysis of the precursors obtained by freeze-drying and the products obtained from the precursors

The chemical reaction for the formation of boron carbide is represented by Eq. (3.2).

Fig. 3.12 shows typical XRD patterns of the precursor (PW) and the products obtained after the heat-treatment of PW. The XRD patterns of the precursor matched with the ICDD file number 00-006-0297. The XRD pattern of PW clearly showed the presence of cubic B_2O_3 and the absence of peaks pertaining to carbon. This indicates that the carbon is in predominantly an amorphous state or a very fine crystalline state. The XRD patterns of the product obtained after the heat-treatment of PW matched with the ICDD database file number 00-035-0798. The formation of B_4C was found to occur at all the temperatures from 1273 to 1873 K. B_2O_3 as an impurity phase was seen in the XRD patterns of the products obtained from PW at all temperatures (1273 to 1873 K), indicating that optimization of the duration of heating is necessary. The peak corresponding to carbon was present (a broad peak in the 2θ range 20 to 30°) in the product obtained at 1273 K from PW and is shown as the inset in Fig. 3.12. The presence of B_2O_3 and carbon could be either due to low reaction temperature or insufficient duration of heating or both for the reaction to go to completion.

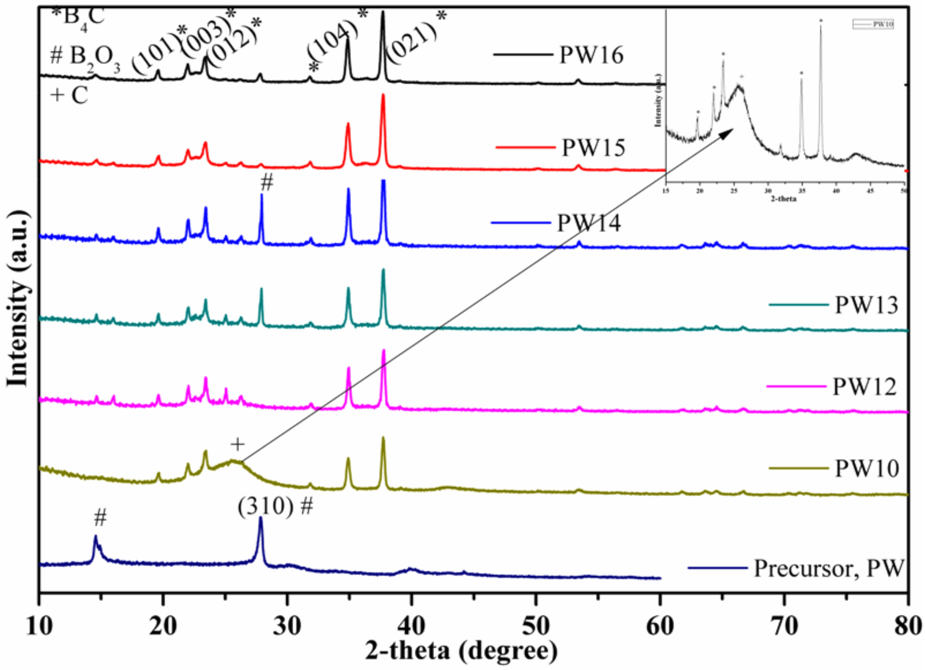

Figure 3.12. XRD patterns of the precursor (PW) and the products obtained from PW at 1273 to 1873 K. The figure shown as the inset is the zoomed portion of PW10

The XRD patterns of the precursor (PE) and the products formed after the heat-treatment of PE are shown in Fig. 3.13. B_4C formation was observed in all the cases (PE10 to PE16), however the reaction (3.2) did not go to completion even at 1873 K, perhaps due to the following reasons: i) the reaction time is too short or ii) inhomogeneity of the reaction mixture (B_2O_3 and carbon) or iii) both the above reasons. The inhomogeneity of the reactants could also be due to the loss of boric oxide at the freeze-drying stage itself as explained in Section 3.2.1. The inhomogeneity is exemplified by the presence of a broad peak in the 2θ range of 20 to 30° as seen in all the samples (shown as the inset of Fig. 3.13). The broadness of the XRD peak could be due to a very fine dispersion of carbon. Due to the broadness, the peaks corresponding to boron carbide in the range of 2θ (20 to 30°) were not well defined and B_2O_3 peaks were not discernible. However, the formation of B_4C commenced at 1273 K in the case of PW and PE. The average crystallite sizes of particles in all the samples calculated using the Scherrer formula were found to be ~30 nm. The lower temperature and the shorter duration of heat-treatment of precursors at higher temperatures resulted in nanocrystalline boron carbide.

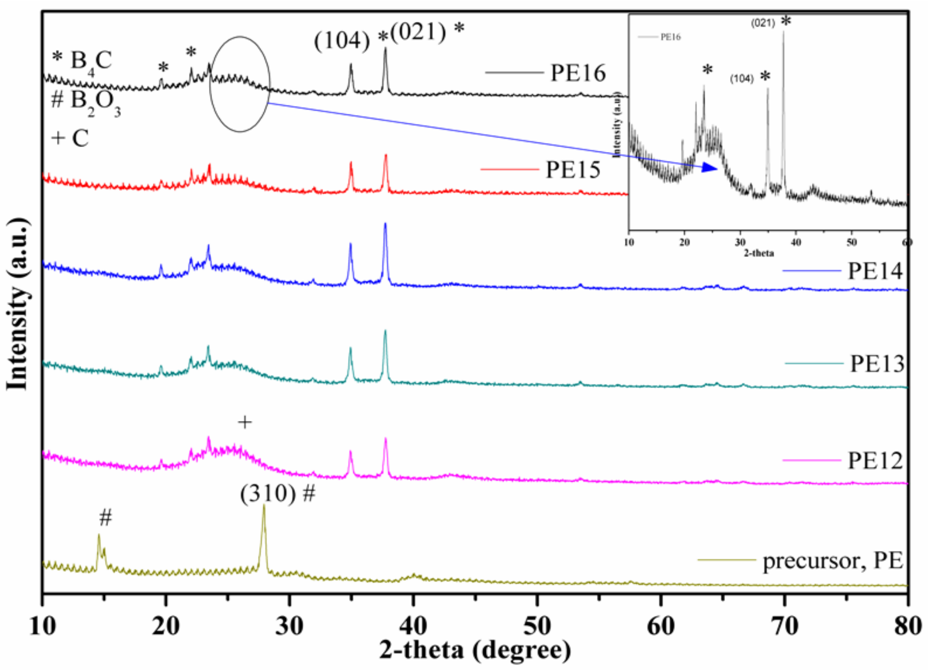

Figure 3.13. XRD patterns of the precursor (PE) and the products obtained from PE at 1273 to 1873 K. The figure shown as the inset is the zoomed portion of PE16

3.2.3 Results of chemical analyses of PW, PE and the products obtained from PW and PE

The results of chemical analyses of precursors (PW, PE) and the products obtained from these precursors are given in Tables 3.6 and 3.7 respectively. The boron, total carbon and free carbon content in the product obtained from PW at 1873 K were 80.2, 21.7 and 1.6 wt.%, respectively. The boron and total carbon content in the product obtained from PE at 1873 K were 53.6 and 47.7 wt.%, respectively. The presence of excess carbon indicated that formation of pure B_4C is not feasible. The boron, total carbon and free carbon content obtained from PW at 1773 K were 79.5, 22.1 and 1.8 wt.% respectively. The free carbon content in the product was lower than that reported by Pilladi et al. [65] using a B_2O_3-sucrose gel precursor even after heating for 3 h at 1773 K. In the present study, the free carbon content was reduced to 1.8 wt.% and the reaction was completed within half an hour at 1773 K. A highly homogeneous precursor with uniform dispersion of B_2O_3 in carbon-network resulted in the formation of B_4C at a lower temperature. On the other hand, the boron and total carbon content obtained from PE at 1773 K were 54.9 and 46.0 wt.% respectively. The results of chemical analyses of the products obtained from PE clearly indicated that the formation of B_4C was incomplete, which was supported by the XRD results.

Table 3.6. Results of chemical analyses of PW and the products obtained from PW

Sample	Boron (wt.%)	Total C (wt.%)	Free C (wt.%)	XCS (nm)
PW	19.4	30.8	-	-
PW16	80.2	21.7	1.6	28
PW15	79.5	22.1	1.8	25
PW14	78.5	23.2	3.1	32
PW13	76.3	24.0	4.1	31
PW12	74.1	27.5	8.5	31

Expanded uncertainty in B is ± 0.8 wt.%, total C is ± 0.5 wt.% and free C is ± 0.5 wt.% with 0.95 level of confidence.

Table 3.7. Results of chemical analyses of PE and the products obtained from PE

Sample	Boron (wt.%)	Total C (wt.%)	XCS (nm)
PE	15.6	37.6	-
PE16	53.6	47.7	31
PE15	54.9	46.0	33
PE14	57.0	41.6	30
PE13	54.6	40.9	29

Expanded uncertainty in B is ± 0.8 wt.% and total C is ± 0.5 wt% with 0.95 level of confidence.

3.2.4 Morphology of the products obtained from PW and PE at 1773 and 1873 K: SEM

The morphologies of the product obtained from PW at 1773 and 1873 K are shown in Fig. 3.14. Fig. 3.14a is the SEM image of PW15 and 3.14b is the SEM image of PW16. Grains of two sizes are seen at each temperature. The larger equiaxed particles are ~1 µm in size and the aggregation of fine particles of irregular morphology are <0.1 µm in size (as shown in the black circle). The morphology is similar to that reported in Section 3.1.4 (P6BC16) with a smaller particle size in the present study. The freeze-drying has improved the homogeneity of the reactants in the precursor (PW) and resulted in more nucleation sites for the formation of B_4C. Rafi-ud-din et al. [51] have observed that the homogeneity of the reactants in the precursor resulted in more nucleation sites for the formation of boron carbide. Pilladi et al. [65] have reported an irregular morphology for the boron carbide powder synthesized by boric oxide-sucrose gel precursor. Fig. 3.14c shows the magnified image of the fine aggregates in PW15. The fine aggregates have an irregular morphology. The smaller size could be due to the lower reaction temperatures, 1773 and 1873 K and shorter duration of heating (30 and 10 min, respectively) at each temperature.

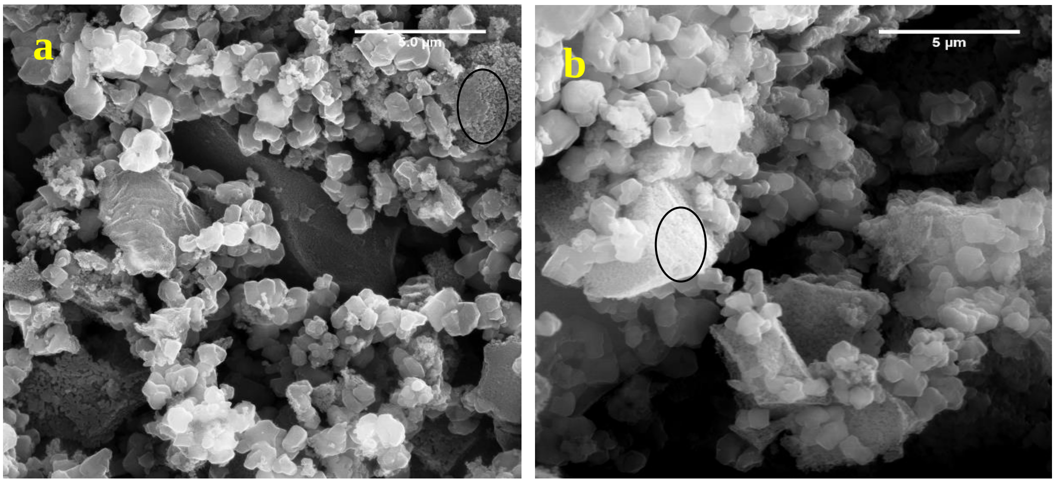

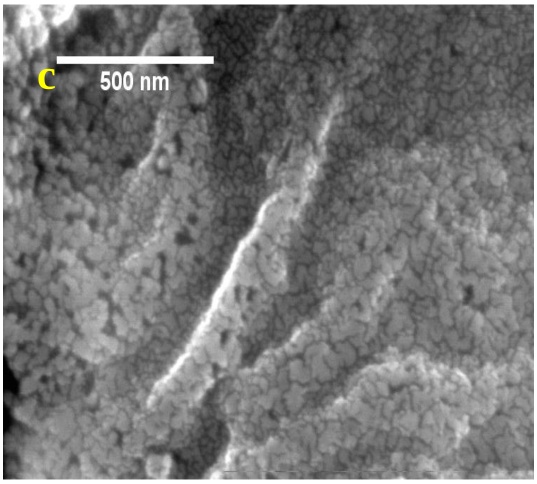

Figure 3.14. SEM images: a) PW15, b) PW16 and c) PW15

The morphologies of the products obtained from PE heat-treated at 1773 and 1873 K are shown in Fig. 3.15a and Fig. 3.15b, respectively. Two different morphologies are observed: one with uniform particles of equiaxed morphology (size ~1 µm) and the other with fine aggregates of a flaky morphology, size varying between 5 to 20 µm. Fig. 3.15c shows the magnified image of PE15. In the magnified image, it is seen that the particles are distributed all over the flaky matrix. It is surmised that the smaller particles distributed are the boron carbide particles and the flaky matrix is the unreacted precursor. At 1773 and 1873 K, it is seen that the unreacted precursor material is uniformly distributed with the boron carbide particles. This was further confirmed qualitatively by Energy Dispersive X-ray (EDX) Analysis of the distributed particle and the precursor matrix. The EDX spectrum of one of the grains (marked 1 in Fig. 3.15a) is shown in Fig. 3.16a and that of the flaky matrix (marked 2 in Fig. 3.15a) is shown in Fig. 3.16b. The peak corresponding to gold is clearly seen in both the images. The peak corresponding to gold is due to the gold coating of the powder samples. In Fig. 3.16a, the major peak is that of boron and the peak corresponding to oxygen is also present. In B_4C, the boron and carbon are in the atom ratio of 4:1 and the EDX spectrum showed the corresponding intensity ratios;

i.e., the major peak is that of boron and the carbon peak intensity is less as compared to that of boron as per the atomic ratio of B and C in boron carbide. In Fig. 3.16b also boron, carbon and oxygen peaks are seen. As per the stoichiometric reaction (3.2), boric oxide and carbon are present in the precursor matrix with the boron to carbon atom ratio of 4:7. The EDX spectrum of the precursor matrix also showed that the major peak is that of carbon. Hence, it is surmised from the peak heights of boron and carbon that the portion marked 2 corresponds to that of incompletely reacted precursor with carbon present as the major element. This shows that the formation of B_4C was incomplete at 1773 and 1873 K, perhaps due to the inhomogeneity of the precursor prepared using ethanol as the slurry medium. Hence, ethanol is not a suitable medium for the preparation of a homogeneous precursor.

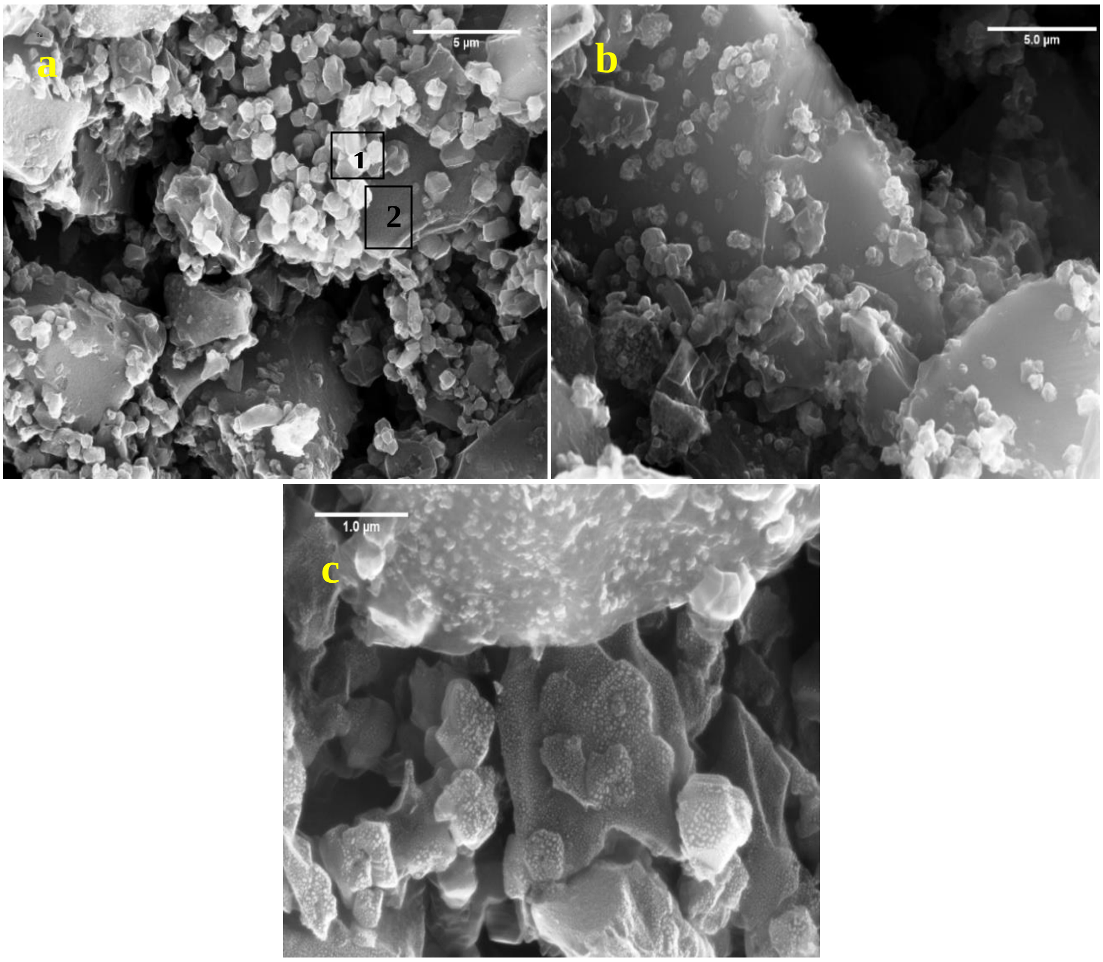

Figure 3.15. SEM images: a) PE15, b) PE16 and c) PE15

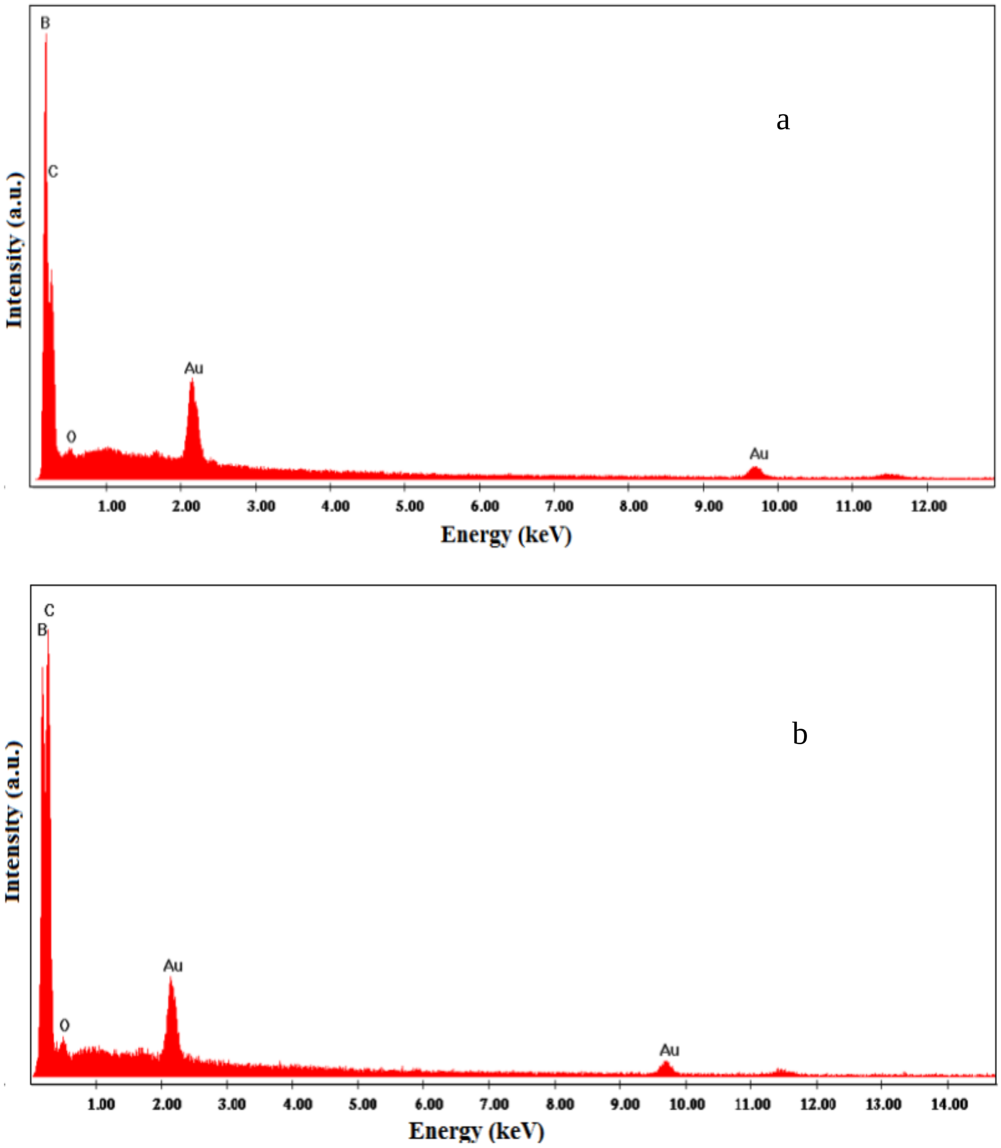

Figure 3.16. EDX spectrum: a) B_4C and b) the precursor matrix

3.3 Microwave-assisted preparation of the precursor by using H_3BO_3-mannitol for the synthesis of nc-B_4C

The preparation of precursor and its processing are respectively explained in Section 2.3.3.1 and 2.3.3.2 of Chapter 2. The sample designation is also given in Table 2.4 of Chapter 2.

3.3.1 H_3BO_3-mannitol precursor

The aqueous solution prepared using boric acid and mannitol was transparent. Microwave heating of this solution resulted in the evaporation of water and led to the formation of a gel. Further heating of this resulted in the formation of a glassy white and highly porous solid. A typical photograph of the condensed product obtained by microwave heating is shown in Fig. 3.17. The thermal decomposition of the powdered condensed product led to a black solid which was also porous. A typical photograph of the cross-section of the thermally decomposed product with a porous structure is shown in Fig. 3.18.

Figure 3.17. Photograph of the condensed product obtained by the microwave-assisted heating of the mannitol-boric acid solution

Figure 3.18. Photograph of the thermally decomposed product

3.3.2 XRD analysis of precursors obtained from H_3BO_3 and mannitol

The XRD patterns of all thermally decomposed products (MW1P to MW6P) are shown in Fig. 3.19. The XRD patterns of the thermally decomposed products matched with the ICDD database file number 00-006-0297. XRD patterns indicated the presence of cubic B_2O_3 and the peak pertaining to carbon was absent. This indicated that the carbon formed was predominantly amorphous.

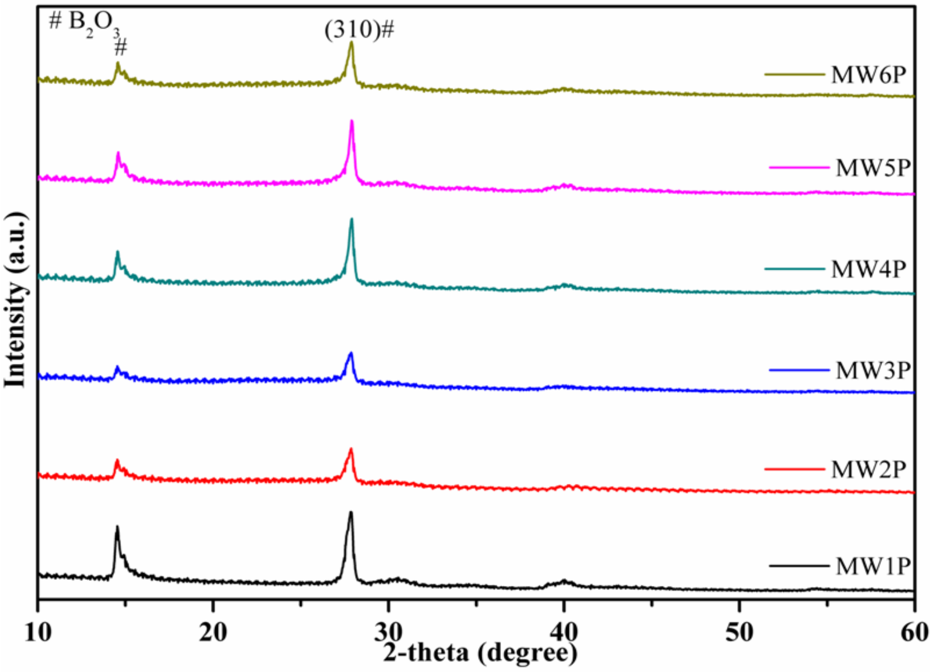

Figure 3.19. XRD patterns of the precursors: MW1P-MW6P

3.3.3 XRD analysis of the products obtained from the precursors (MW1P- MW6P)

The XRD patterns of the products obtained after heat-treatment of all precursors (MW1P to MW6P) at 1273 to 1873 K are given in Figs. 3.20 to 3.25. XRD patterns of all the products obtained from the precursors matched with the ICDD database file number 00-035-0798. Fig. 3.20 shows the XRD patterns of the products obtained from the precursor MW1P. B_4C formation was observed in all the cases (MW1P-10 to MW1P-16). B_2O_3 as an impurity phase was seen in the XRD patterns of MW1P-14 to MW1P-16. Peak pertaining to carbon was seen in the XRD patterns of MW1P-14 and MW1P-15. In all other patterns, the peak was not discernible, perhaps due to the broadness in the 2θ range of 20 to 30°. XRD patterns indicated that the formation of boron carbide commenced at 1273 K. Fig. 3.21 shows the XRD patterns of the products obtained by the heat-treatment of MW2P. The XRD pattern of MW2P-10 indicated that the formation of boron carbide was incomplete at 1273 K and B_2O_3 peak was the prominent peak in the XRD pattern. The peak pertaining to carbon (ICDD database file number 00-056-0159) was also clearly seen in the XRD pattern of MW2P-10, perhaps due to the improved crystallinity with an increase in the temperature. B_2O_3 peaks were also seen in the XRD patterns of MW2P-13, MW2P-15 and MW2P-16. XRD patterns of the products obtained by heat-treatment of the precursor, MW3P are shown in Fig. 3.22. B_2O_3 peaks were present in the XRD patterns of MW3P-15 and MW3P-16 and carbon peak was seen in the XRD patterns of all the samples. Fig. 3.23 shows the XRD patterns of the products obtained after the heat-treatment of MW4P. A broad peak in the 2θ range of 23 to 27° was clearly seen in all the patterns, from MW4P-10 to 16. A magnified image of the pattern in the 2θ range of 10 to 40° of MW4P-16 is given as inset in Fig. 3.23. Due to broadness, the peaks pertaining to carbon and that of B_2O_3 were not discernible. The formation of boron carbide was incomplete in the products obtained by heat-treatment of MW4P. This could be due to the excess carbon in the decomposed product formed from the reactants with CBMR 6 (C/B wt.% ratio 3.33). In addition, reaction temperature (673 K) might not have been sufficient to remove the excess carbon present in the precursor than that required for a stoichiometric reaction as per Eq. (3.2). The XRD patterns of the products formed as a result of the heat-treatment of MW5P are shown in Fig. 3.24. The peaks pertaining to B_2O_3 were seen in the XRD patterns of all the products, MW5P-10 to MW5P-16. Due to the broadness in the 2θ range of 20 to 27°, carbon peaks were not discernible. Fig. 3.25 shows the XRD patterns of the products formed from MW6P at 1273 to 1873 K. The presence of B_2O_3 as an impurity phase was seen in the XRD patterns of all the products, MW6P-

10 to MW6P-16. The peak pertaining to carbon was seen in all the patterns, except in MW6P-16. In all the XRD patterns, the peak pertaining to B_4C appears in samples heat-treated at temperature above 1273 K indicating the temperature of formation of B_4C is 1273 K, irrespective of the composition of the reactants. This temperature is 150 K less than that reported by Kakiage et al. [59]. These authors have reported that the formation of B_4C commenced at 1423 K using a similar condensed product. Perhaps, in the present study microwave-assisted heating resulted in the formation of more homogeneous precursor and that lowered the formation temperature of B_4C. The average X-ray crystallite sizes calculated for the products obtained from MW1P, MW2P, MW3P, MW5P and MW6P are given in Table 3.8. The average XCS was found to be <31 nm for all the samples.

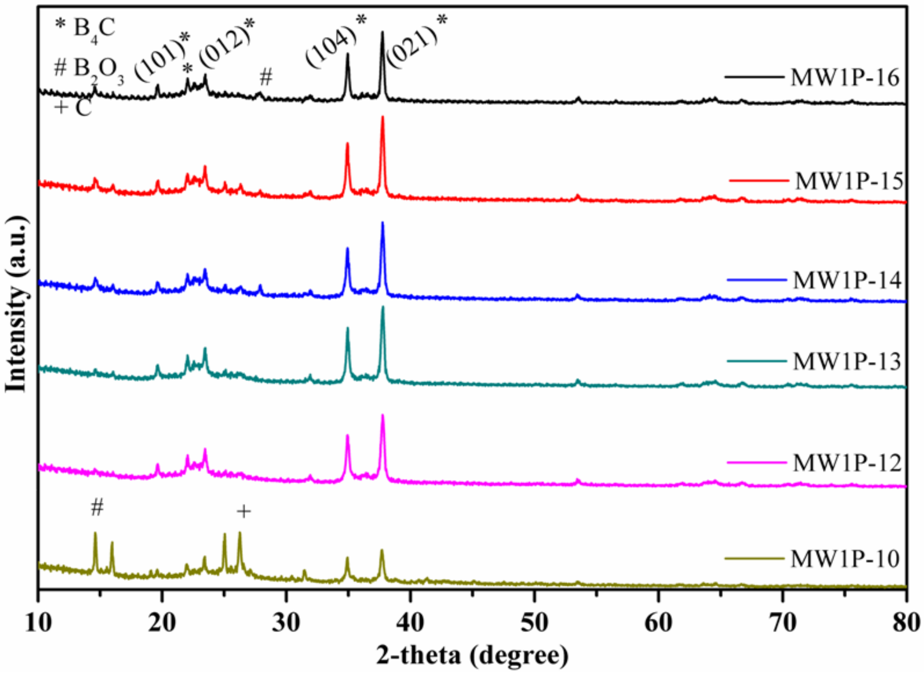

Figure 3.20. XRD patterns of the products obtained from MW1P at 1273-1873 K

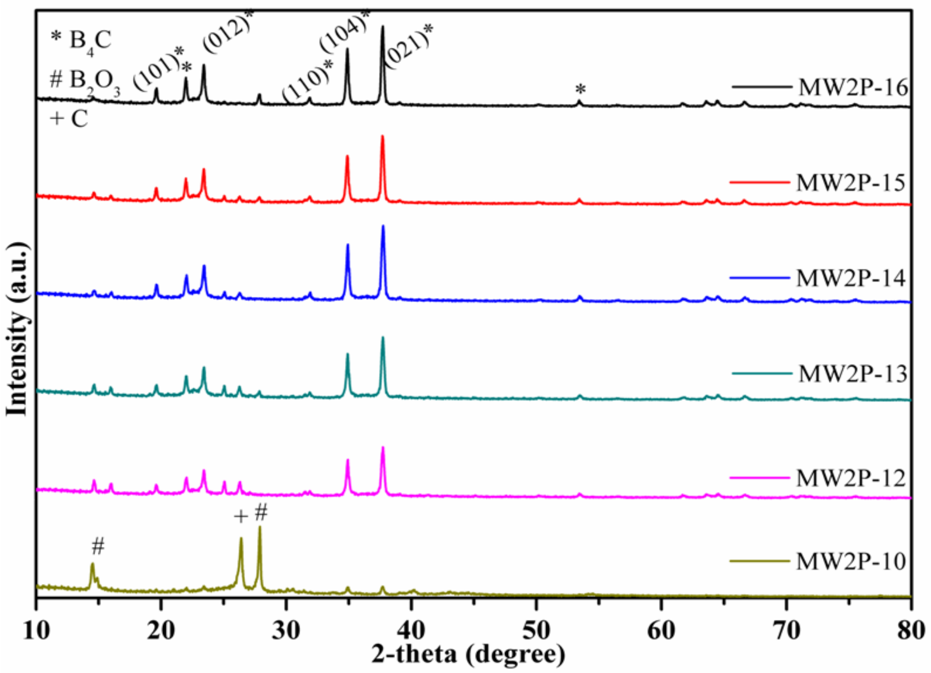

Figure 3.21. XRD patterns of the products obtained from MW2P at 1273-1873 K

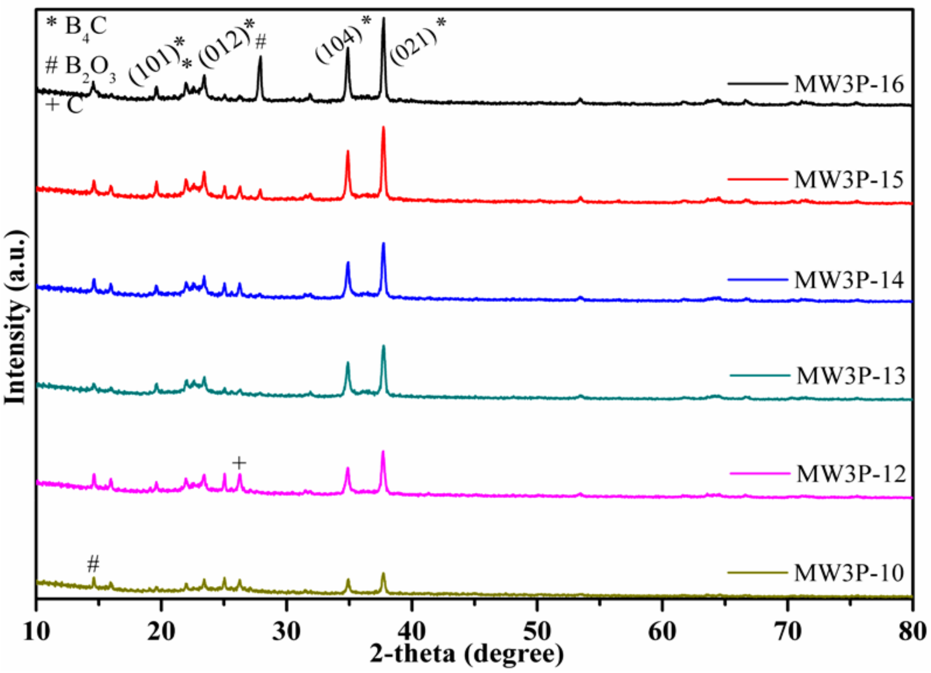

Figure 3.22. XRD patterns of the products obtained from MW3P at 1273-1873 K

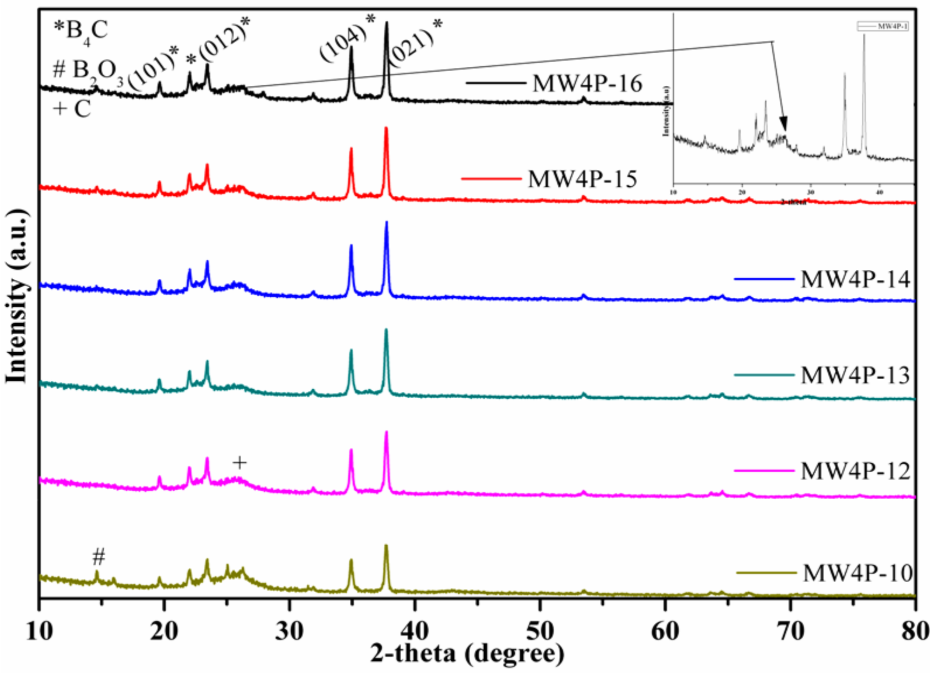

Figure 3.23. XRD patterns of the products obtained from MW4P at 1273-1873 K

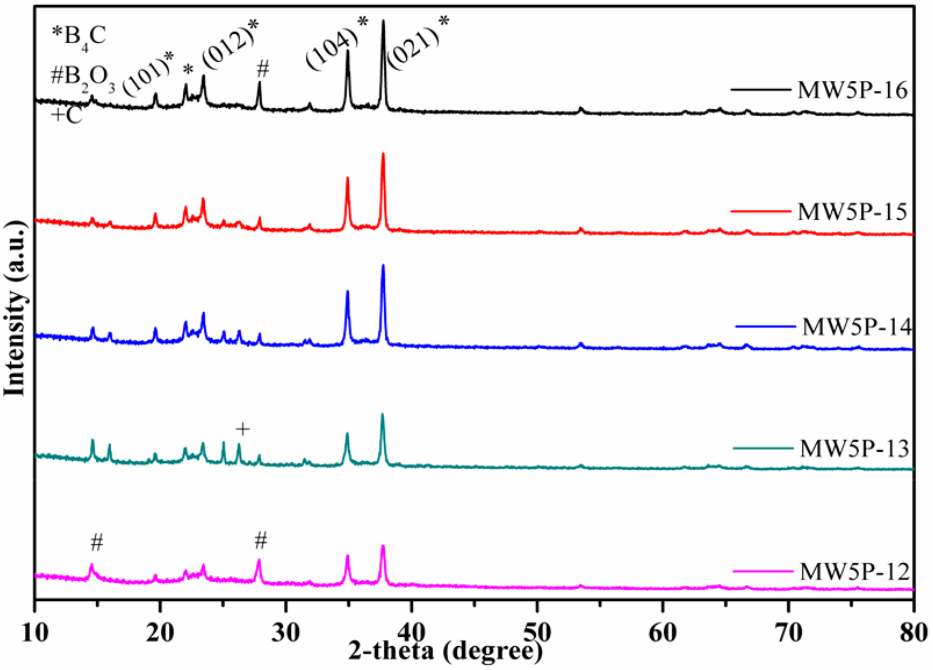

Figure 3.24. XRD patterns of the products obtained from MW5P at 1273-1873 K

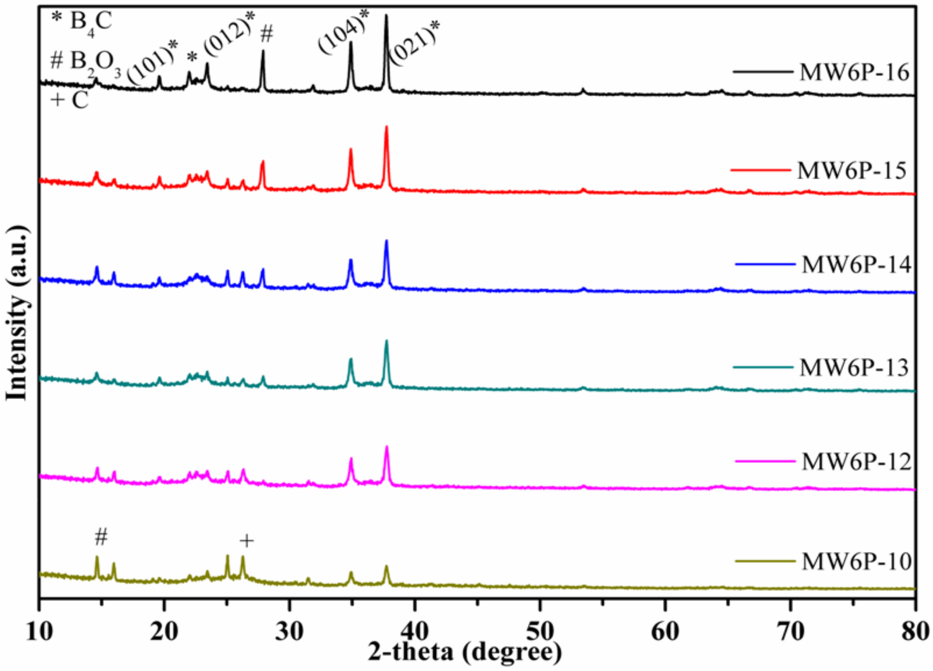

Figure 3.25. XRD patterns of the products obtained from MW6P at 1273-1873 K

Table 3.8. X-ray crystallite sizes of the B_4C synthesized from MW1P, MW2P, MW3P, MW5P and MW6P

Sample	XCS (nm)
MW1P-16	31
MW1P-15	30
MW1P-14	28
MW1P-13	29
MW1P-12	27
MW2P-16	34
MW2P-15	33
MW2P-14	31
MW2P-13	32
MW2P-12	31
MW3P-16	32
MW3P-15	32
MW3P-14	30
MW3P-13	28

MW3P-12	28
MW5P-16	31
MW5P-15	31
MW5P-14	30
MW5P-13	28
MW5P-12	27
MW6P-16	33
MW6P-15	30
MW6P-14	28
MW6P-13	28
MW6P-12	27

3.3.4 Results of TG analyses of mannitol and mannitol-boric acid complex

The results of the TG analyses are shown in Fig. 3.26. Significant decomposition of pure mannitol took place at 553 to 598 K and that of MBC 3.38 (mannitol-boric acid condensed product CBMR 3.38) at 643 to 673 K. The decomposition of MBC 6 was almost complete at 703 K. The condensed products showed similar decomposition behaviour. The decomposition temperature of the mannitol-boric acid complex was higher than that of pure mannitol. This clearly indicates that the complex formed by the mannitol and boric acid is stable than that of pure mannitol or boric acid. However, the decomposition temperature range of the complex is narrow. Based on these results, the thermal decomposition of the complex was carried out from 673 to 873 K. The complex formed by boric acid and mannitol can be represented by the following scheme;

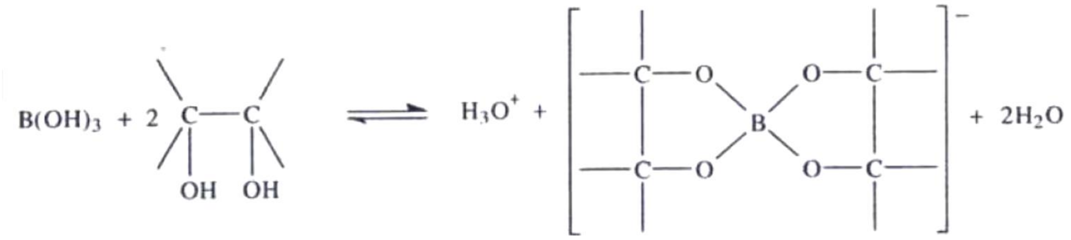

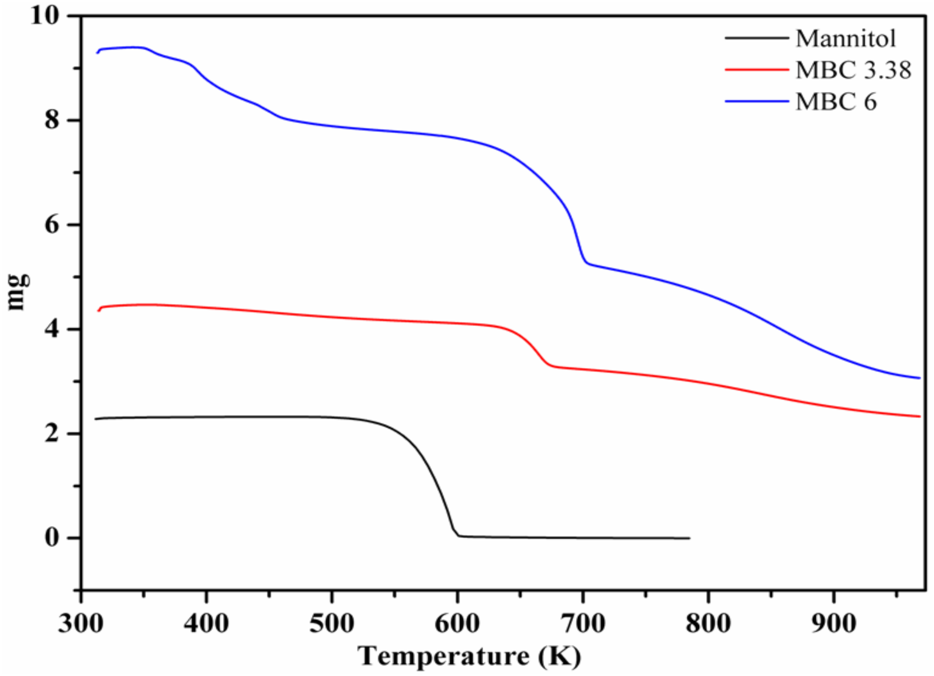

Figure 3.26. TG Plot of mannitol and the condensed product formed by boric acid and mannitol

3.3.5 Results of chemical analyses of the products obtained from MW1P to MW6P

The results of chemical analyses of the products obtained by the heat-treatment of precursors (MW1P, MW2P, MW3P, MW5P and MW6P) are given in Tables 3.9 to 3.13. The chemical analysis was not carried out for the products obtained from MW4P as the XRD patterns indicated the presence of a large amount of free carbon. This could be due to the low thermal decomposition temperature of 673 K. This temperature was insufficient to remove the excess carbon from the condensed product. The results of quantitative analyses for boron, total carbon and free carbon content in the products obtained by heat-treatment of MW1P are given in Table 3.9. The free carbon content in all the samples were found to be high, >3.5 wt.% except that of MW1P-14 (2.9 wt.%). The B_4C synthesized from MW1P at 1673 K was found to contain a boron, total carbon and free carbon content of 78.2, 20.8 and 2.9 wt.% respectively. The chemical analyses results of the products obtained from MW2P are given in Table 3.10. The free carbon content in the product obtained from MW2P even at 1473 K was found to be <2 wt.%. The boron content was found to be >79 wt.% for all the products obtained from MW2P in the temperature range of 1473 to 1873 K. The chemical analyses results of the products obtained from MW3P are given in Table 3.11. The free carbon contents in the products (MW3P-12 to MW3P-16) were found to be in the range of 1 to 2.9 wt.%. The chemical analyses results of MW5P are given in Table 3.12. The amount of free carbon in all the products (MW5P-12 to MW5P-16) were higher than those in the products obtained by the heat-treatment of MW2P and MW3P indicating that thermal decomposition temperature of 773 K is not sufficient to remove the excess carbon especially from the carbon-rich condensed product, MW5P. However, a higher thermal decomposition temperature of 873 K resulted in lowering the free carbon content as can be seen from Table 3.13. Based on the results of chemical analyses, the thermal decomposition temperature of 773 K was found to be suitable for a condensed product with CBMR 3.38 (C/B wt.% ratio 1.87). Condensed products with higher CBMR 6 (C/B wt.% ratio 3.33) required a higher temperature for the thermal decomposition to remove the excess carbon from the condensed product.

Table 3.9. Results of chemical analyses of the products obtained from MW1P

Sample	Boron (wt. %)	Total C (wt.%)	Free C (wt.%)
MW1P-16	77.6	23.8	3.8
MW1P-15	77.1	23.3	4.3
MW1P-14	78.2	20.8	2.9
MW1P-13	77.4	23.7	5.5
MW1P-12	78.1	22.3	4.7

Expanded uncertainty in B is ± 1.5 wt.%, total C is ± 0.5 wt.% and free C is ± 0.8 wt.% with 0.95 level of confidence.

Table 3.10. Results of chemical analyses of the products obtained from MW2P

Sample	Boron (wt.%)	Total C (wt.%)	Free C (wt.%)
MW2P-16	81.1	20.0	0.4
MW2P-15	80.7	19.7	0.9
MW2P-14	80.5	20.5	0.9
MW2P-13	80.4	19.7	1.6
MW2P-12	79.8	19.7	1.9

Expanded uncertainty in B is ± 1.5 wt.%, total C is ± 0.5 wt.% and free C is ± 0.8 wt.% with 0.95 level of confidence.

Table 3.11. Results of chemical analyses of the products obtained from MW3P

Sample	Boron (wt.%)	Total C (wt.%)	Free C (wt.%)
MW3P-16	80.5	18.6	1.1
MW3P-15	80.2	19.8	1.2
MW3P-14	79.7	20.0	2.0
MW3P-13	80.4	18.9	2.9
MW3P-12	75.8	18.8	1.9

Expanded uncertainty in B is ± 1.5 wt.%, total C is ± 0.5 wt.% and free C is ± 0.8 wt.% with 0.95 level of confidence.

Table 3.12. Results of chemical analyses of the products obtained from MW5P

Sample	Boron (wt.%)	Total C (wt.%)	Free C (wt.%)
MW5P-16	76.4	24.1	3.9
MW5P-15	75.6	24.4	4.3
MW5P-14	77.3	21.2	2.4
MW5P-13	77.0	17.9	2.6
MW5P-12	69.3	16.6	3.6

Expanded uncertainty in B is ± 1.5 wt.%, total C is ± 0.5 wt.% and free C is ± 0.8 wt.% with 0.95 level of confidence.

Table 3.13. Results of chemical analyses of the products obtained from MW6P

Sample	Boron (wt.%)	Total C (wt.%)	Free C (wt.%)
MW6P-16	80.1	21.0	1.3
MW6P-15	78.6	19.6	2.0
MW6P-14	77.8	20.2	2.1
MW6P-13	77.3	18.7	1.2
MW6P-12	72.3	20.3	2.8

Expanded uncertainty in B is ± 1.5 wt.%, total C is ± 0.5 wt.% and free C is ± 0.8 wt.% with 0.95 level of confidence.

3.3.6 Morphology of the products obtained from MW2P: SEM

The SEM images of the products obtained from MW2P are shown in Fig. 3.27. The sizes of the particles are <1 µm in these samples heat-treated at all the temperatures (1473 to 1873 K). Two different sized particles are seen in the images: one with smaller equiaxed particles and the other with larger equiaxed particles. Fig. 3.27a is the SEM image of MW2P-16 and Fig. 3.27b is the magnified image of the smaller particles. The larger particles are of <0.5 µm size and smaller particles are of <0.1 µm. The morphology of MW2P-15 and the magnified image of smaller particles are shown in Fig. 3.27c and Fig. 3.27d, respectively. In the case of MW2P-15, the sizes of larger particles and smaller particles respectively are <0.8 and 0.1 µm. The SEM image of MW2P-14 and the magnified image of smaller particles are shown in Fig. 3.27e and Fig. 3.27f, respectively. The two different particle sizes observed in MW2P-14 are <0.5 µm and <0.1 µm. The morphology of MW2P-13 is shown in Fig. 3.27g and the magnified image is shown in Fig. 3.27h. In this case, sizes of the larger particles are <1 µm and smaller particles are <0.1 µm. The smaller particle size could be due to more nucleation sites in the case of highly dispersed reactants in a homogeneous precursor. Even at 1873 K, the particle sizes are low perhaps due to the shorter duration of heating (10 min). Figs. 3.27i and 3.27j show the morphologies of MW2P-12 and the magnified image of smaller particles respectively. The fine particles are <0.2 µm. It is observed that at temperatures below 1273 K, the growth of particles is not significant. Hence, in this study nanocrystalline boron carbide was synthesized which does not require further processing such as grinding to reduce the particle size for sintering studies.

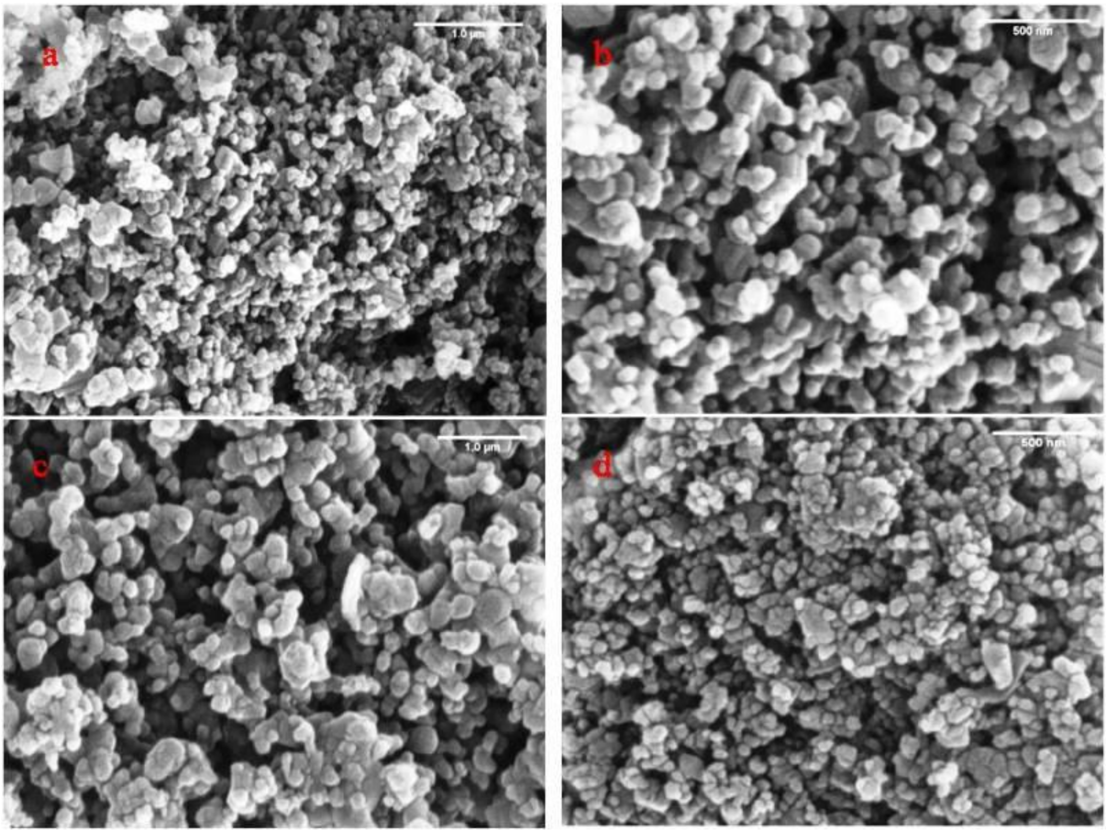

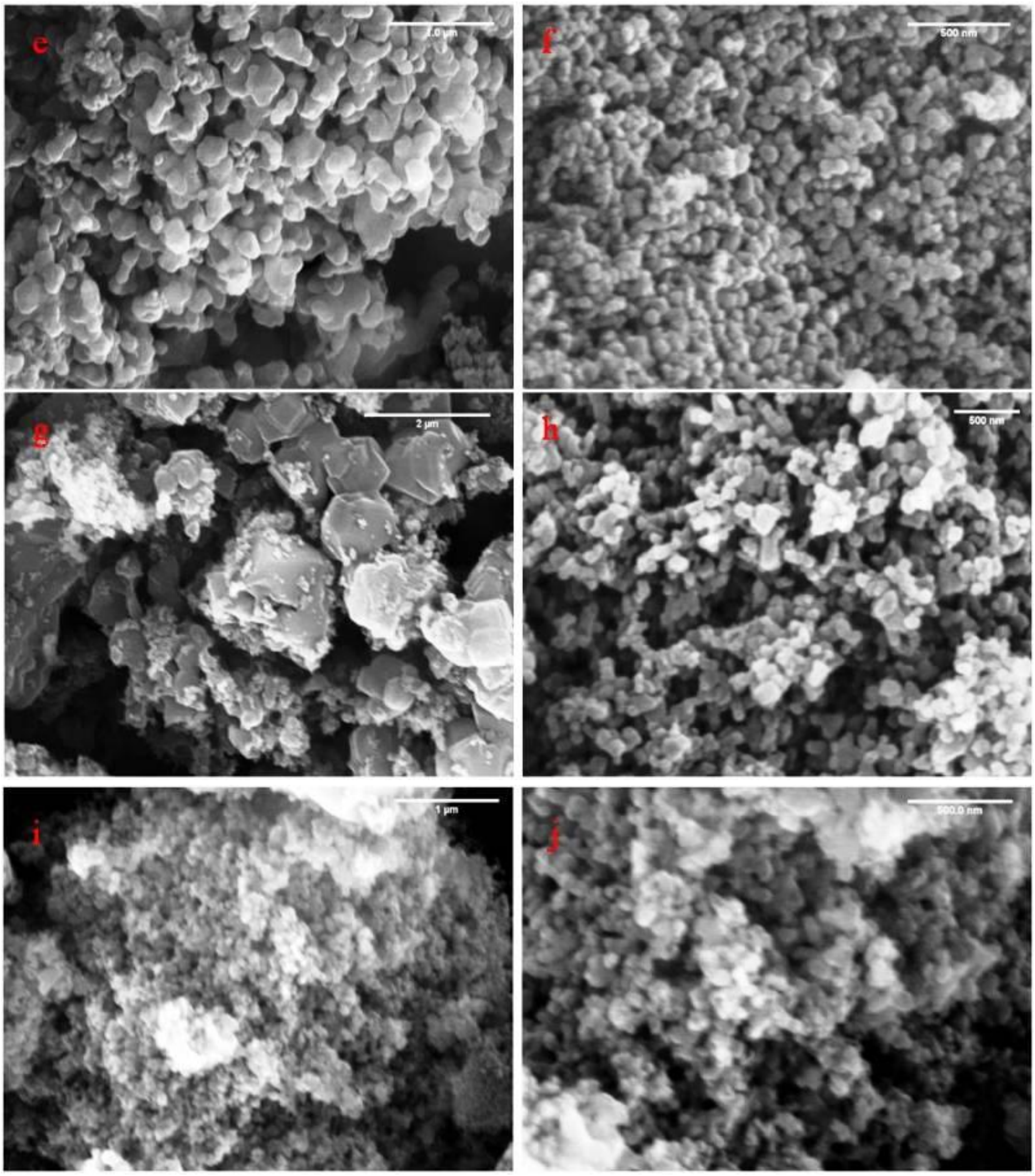

Figure 3.27. SEM images: a) MW2P-16, c) MW2P-15, e) MW2P-14, g) MW2P-13, i) MW2P-12 and b, d, f, h and j are the magnified images of smaller particles

3.4 Summary of the studies carried out on the synthesis of nanocrystalline B_4C

Table 3.14 compares the results of chemical analyses of the B_4C synthesized in the present study using different precursors.

Table 3.14. Summary of the results of chemical analyses of boron carbide products carried out in the present study

Precursor, CBMR	T (K)	t (min)	B (wt.%)	C_T (wt.%)	C_f (wt.%)	XCS (nm)
B_2O_3-sucrose; solid state, 3.5	1873	10	73.5	27.6	3.3	33
B_2O_3-sucrose; solid state, 3.38	1873	10	76.6	25.4	2.5	32
B_2O_3-Sucrose; Freeze-drying, 3.38	1873	10	80.2	21.7	1.6	28
H_3BO_3-Mannitol, 3.38	1873	10	81.1	20.0	0.4	34

T is the temperature in Kelvin, t is the time in min, B is boron content in wt.%, C_T is total carbon in wt.%, C_f is free carbon in wt.% and XCS is X-ray crystallite size in nm.

The amount of free carbon in the product mixture of B_4C with free carbon synthesized by the precursor method is a measure of the homogeneity of the reactants in the precursors. A homogeneous precursor results in a product containing boron carbide with lower free carbon impurity if the temperature and heating rate are properly chosen. In the present study, even though the free carbon content was <3 wt.% in the boron carbide samples prepared at 1873 K using boric oxide-sucrose precursor, the solid state mixing of the reactants perhaps resulted in the inhomogeneity of the reactant mixture. The mixing of the reactants in a suitable medium helps to improve the homogeneity of the reactant mixture. The precursor obtained from freeze-drying of reactants (slurry in water) was found to be more homogeneous than that of a reactant mixture obtained by physical mixing of the solid reactant components. The boron carbide product obtained by heating the precursor prepared using the freeze-dried reactant mixture at 1873 K was found to contain a lower free carbon content of 1.6 wt.%. Ethanol is not a suitable medium for the preparation of precursor. Homogeneity was further improved with the use of mannitol and boric acid for the preparation of precursor. The optimized thermal decomposition temperature for the preparation of precursor from the mannitol-boric acid condensed product with C/B wt.% ratio of 1.87 (CBMR 3.38) was found to be 773 K. The amount of free carbon in the product boron carbide synthesized from this precursor was found to be low, 0.4 wt.%.

Chapter 4

Studies on sintering of nc-B_4C by Spark Plasma Sintering Technique

Nanocrystalline boron carbide was synthesized by the precursor method using boric oxide and sucrose for studying sinterability of compacts prepared from the samples. The nc-B_4C thus obtained was characterized for phase purity, chemical composition, specific surface area, particle size distribution and microstructure. Boron carbide samples procured from M/s. Sigma Aldrich was also characterized for phase purity, chemical composition, specific surface area, particle size distribution and microstructure. Spark plasma sintering studies were carried out on the nc-B_4C and the sample procured from the above vendor. This chapter presents the results of these studies. Results of densification of B_4C powder compacts by spark plasma sintering are discussed in detail. The density, microstructure and microhardness of the sintered compacts are presented in this chapter.

4.1 Results and Discussion

4.1.1 Synthesis of nc-B_4C for SPS

nc-B_4C was prepared by using the B_2O_3-sucrose precursor. The methods of preparation of the precursor and B_4C are detailed in Section 2.3.1 of Chapter 2. B_4C was synthesized by heat-treatment of the precursor at 1873 K for 20 min in order to ensure completion of the reaction. The bulk preparation of B_4C was carried out using the furnace described in Section 2.2.2 of Chapter 2.

4.1.2 Characterization of the nc-B_4C powders

4.1.2.1 XRD analysis of nc-B_4C and c-B_4C powder

It is reported that the presence of the B_2O_3 layer on B_4C delays the onset of sintering until it completely volatilizes. It also leads to coarsening of the grains in the sintered B_4C [202-204]. B_2O_3 melts at 723 K and this molten B_2O_3 surrounding the B_4C particles restrict the particle to particle contact in B_4C powder thereby affecting the diffusion of boron and carbon during sintering. Methanol washing helps to remove the B_2O_3 impurity [205, 206, 126, 128]. Hence, nc-B_4C synthesized in the present study was thoroughly washed with methanol. The sample designation of B_4C powder employed for spark plasma sintering studies are given in Table 4.1.

Table 4.1. Sample designation of B_4C powder used for spark plasma sintering studies

Sample	Remarks
nc-B_4CBW1	nanocrystalline boron carbide powder before methanol washing
nc-B_4CAW1	nanocrystalline boron carbide powder after methanol washing
c-B_4CBW	commercial boron carbide powder before methanol washing
c-B_4CAW	commercial boron carbide powder after methanol washing

The XRD patterns of nc-B_4CBW1 and nc-B_4CAW1 are shown in Fig. 4.1. B_2O_3 peaks were seen in the XRD pattern of nc-B_4CBW1 powder and the peaks were absent in the XRD pattern of nc-B_4CAW1 powder. This clearly shows that washing of the B_4C powder using methanol helps to remove B_2O_3 impurity present in the powder. The peaks corresponding to that of carbon were absent in the XRD patterns of nc-B_4CBW1 and nc-B_4CAW1; perhaps the free carbon present in the powder was below the detection limit of XRD. B_2O_3 peaks were absent in the c-B_4CBW and c-B_4CAW and the XRD patterns are shown in Fig. 4.2. Peak pertaining to carbon was seen in the XRD pattern of c-B_4CBW and c-B_4CAW; perhaps the method of preparation of c-B_4CBW (carbothermic reduction at high temperature) might have resulted in high crystallinity of the free carbon present in the powder. Average X-ray crystallite sizes of all the samples were <31 nm.

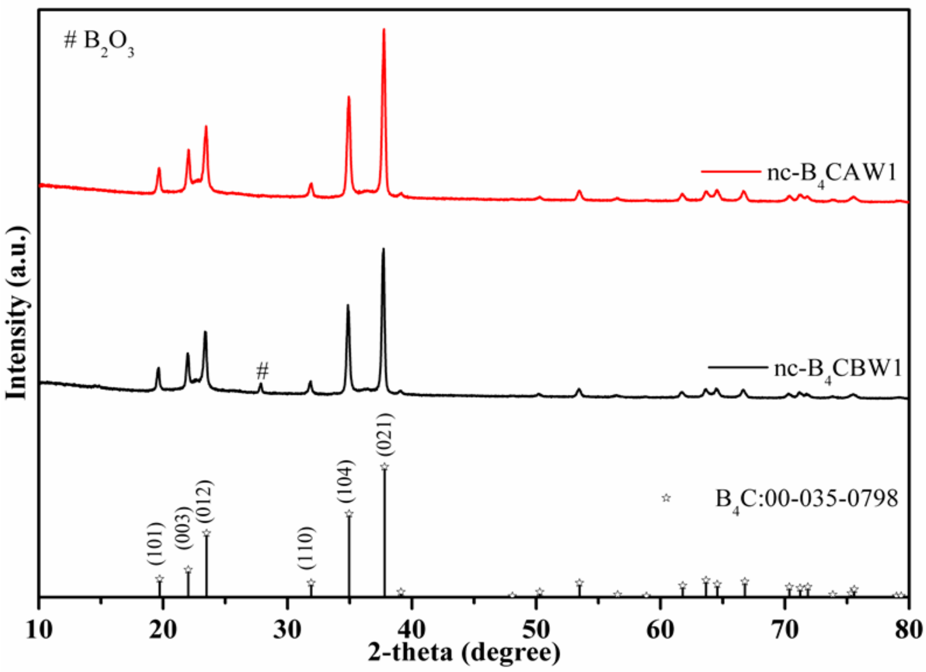

Figure 4.1. XRD patterns of nc-B_4CBW1 and nc-B_4CAW1

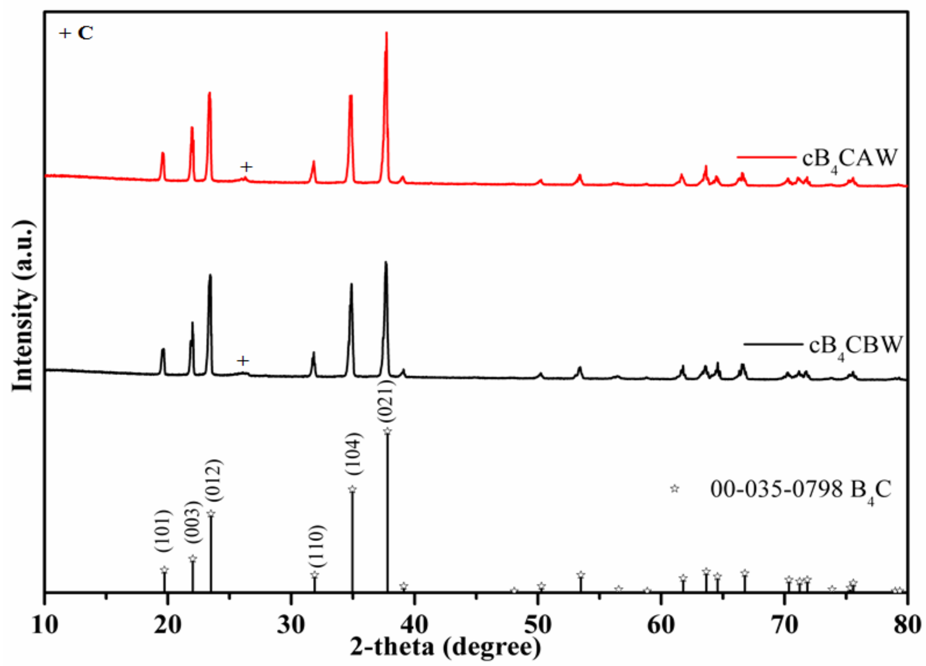

Figure 4.2. XRD patterns of c-B_4CBW and c-B_4CAW

4.1.2.2 Results of chemical analyses, specific surface area and particle size distribution of nc-B_4C and c-B_4C powders

The results of chemical analyses and specific surface area of nc-B_4CBW1, nc-B_4CAW1 and c-B_4CBW are given in Table 4.2. The free carbon content in nc-

B_4CBW1 and nc-B_4CAW1 powder was less than 1 wt.%. The free carbon content in the c-B_4CBW was also less than 1 wt.% (0.7 wt.%). The estimated boron, total carbon and free carbon content in the nc-B_4CBW1 and nc-B_4CAW1 powders were found to be almost similar. Boron, total carbon and free carbon content in nc-B_4CBW1 powders were found to be 78.5, 21.9 and 1.0 wt.% respectively whereas that of nc-B_4CAW1 were 78.1, 22.1 and 0.9 wt.% respectively. The specific surface area of nc-B_4CAW1 powder was found to be 63 m^2g^{-1}. The c-B_4CBW had a specific surface area of 28 m^2g^{-1}. The nc-B_4CAW1 had a higher specific surface area as compared to the c-B_4CBW.

Table 4.2. Results of chemical analyses of nc-B_4CBW1, nc-B_4CAW1 and c-B_4CBW

Sample	Boron (wt.%)	Total C (wt.%)	Free C (wt.%)	SSA (m^2g^{-1})	XCS (nm)
nc-B_4CBW1	78.5	21.9	1.0	134	31
nc-B_4CAW1	78.1	22.1	0.9	63	28
c-B_4CBW	79.5	19.7	0.7	28	30

Expanded uncertainty in B is ± 1.5 wt.%, total C is ± 0.16 wt.% and free C is ± 0.50 wt.% with 0.95 level of confidence.

The particle size distribution results indicated that 10% of the particles in the nc-B_4CBW1 powder were <3 µm. 50% of the particles were in the size range of <9 µm and 90% of the particles were <25 µm in size range. Similarly 10% of the particles in nc-B_4CAW1 powder were <3 µm. 50% of the particles were in the size range of <8 µm and 90% of the particles were <19 µm in size range. This indicates that the size distribution of the particles in nc-B_4CBW1 and nc-B_4CAW1 are similar; perhaps, there is no agglomeration in the nanocrystalline boron carbide powder synthesized in the present study. 10% of the particles were in the size range of <42 µm in the c-B_4CBW powder. 50% of the particles were <61 µm and 90% of the particles were <87 µm in size range. In the case of c-B_4CBW and c-B_4CAW also, the size distribution remains the same; perhaps, there is no agglomeration in c-B_4CAW powder also. The particle size distributions of the nc-B_4CBW1, nc-B_4CAW1, c-B_4CBW and c-B_4CAW are given in Table 4.3. The particle size distribution of nc-B_4CBW1 and nc-B_4CAW1 are shown in Fig. 4.3 and those of c-B_4CBW and c-B_4CAW are shown in Fig. 4.4, respectively.

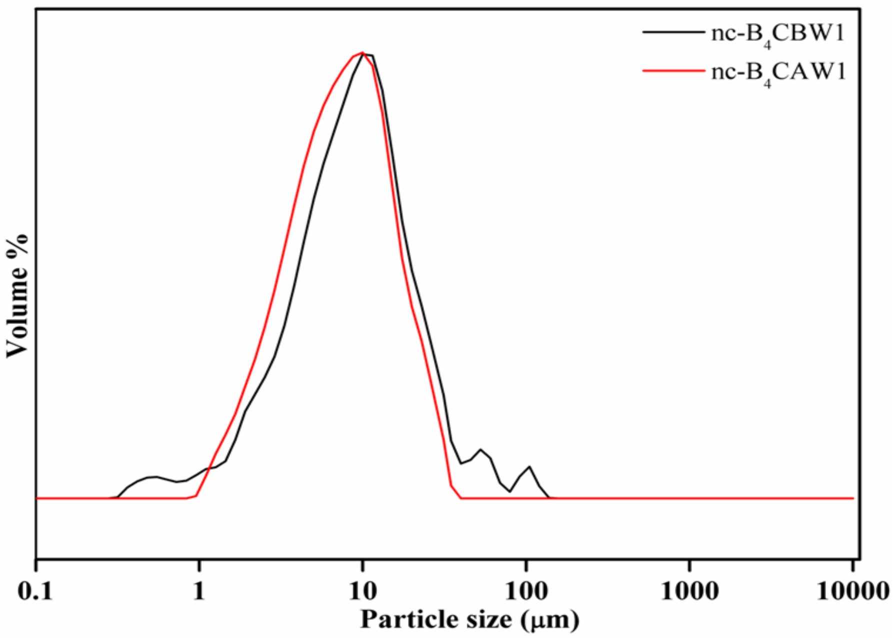

Figure 4.3 Particle size distribution of nc-B_4CBW1 and nc-B_4CAW1

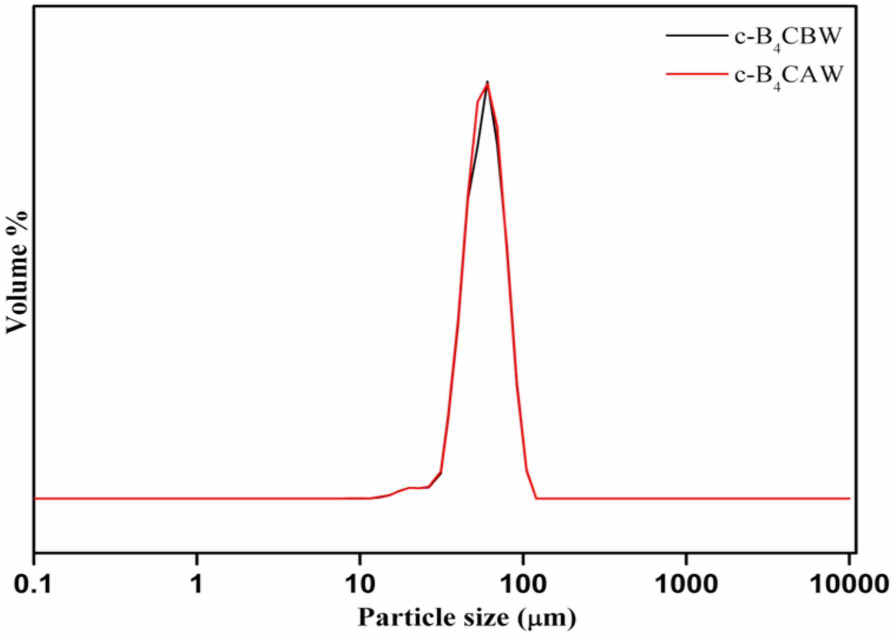

Figure 4.4 Particle size distribution of c-B_4CBW and c-B_4CAW

Table 4.3. Particle size distribution of nc-B_4C and c-B_4C

Sample	d (0.1) µm	d (0.5) µm	d (0.9) µm
nc-B_4CBW1	2.9	9.5	25.4
nc-B_4CAW1	2.8	8.0	19.0
c-B_4CBW	42.3	61.8	86.9
c-B_4CAW	42.0	61.4	86.6

4.1.2.3 Morphology of nc-B_4CAW1 and c-B_4CAW powder: SEM

The morphologies of the nc-B_4CAW1 and c-B_4CAW powders are shown in Fig. 4.5. Fig. 4.5a is the SEM image of nc-B_4CAW1, showing both larger particles and smaller particles. Fig. 4.5b is the SEM image of nc-B_4CAW1 and Fig. 4.5c is the magnified image of finer particles in the nc-B_4CAW1. Both larger particles and finer particles are equiaxed with a size of ~1 µm and <0.1 µm respectively. The morphology of c-B_4C looks like large flakes (Fig. 4.5d and Fig. 4.5e), perhaps the c-B_4C synthesized by carbothermic reduction using an Acheson type furnace resulted in flaky morphology.

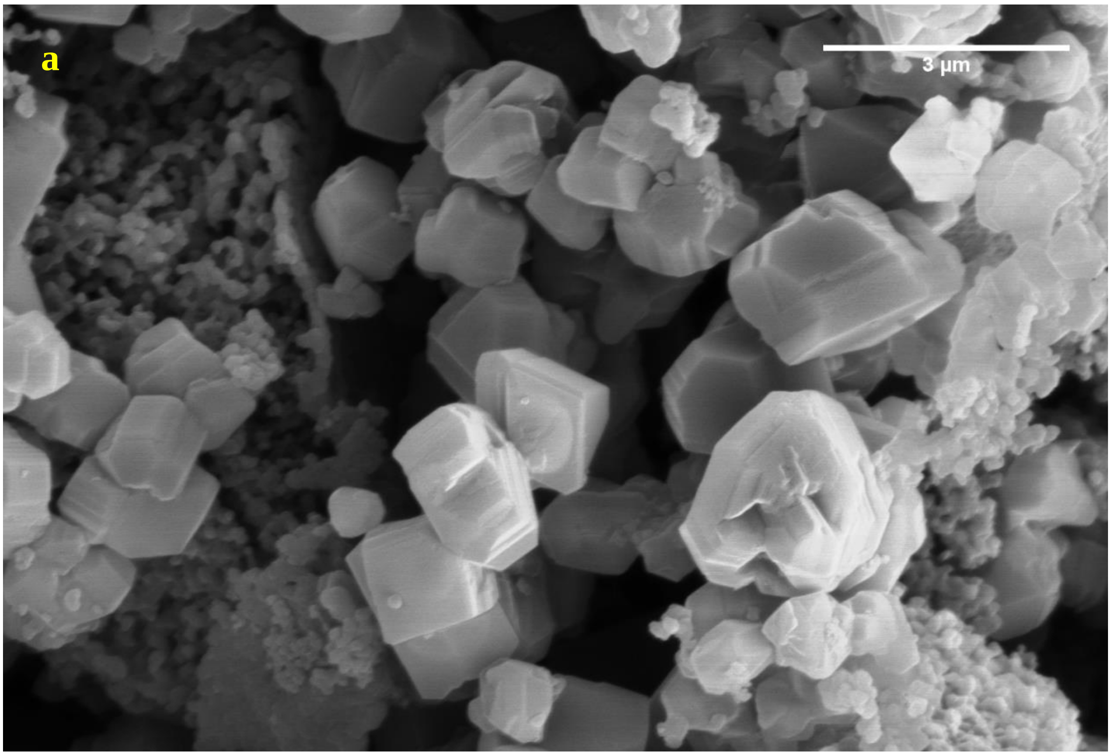

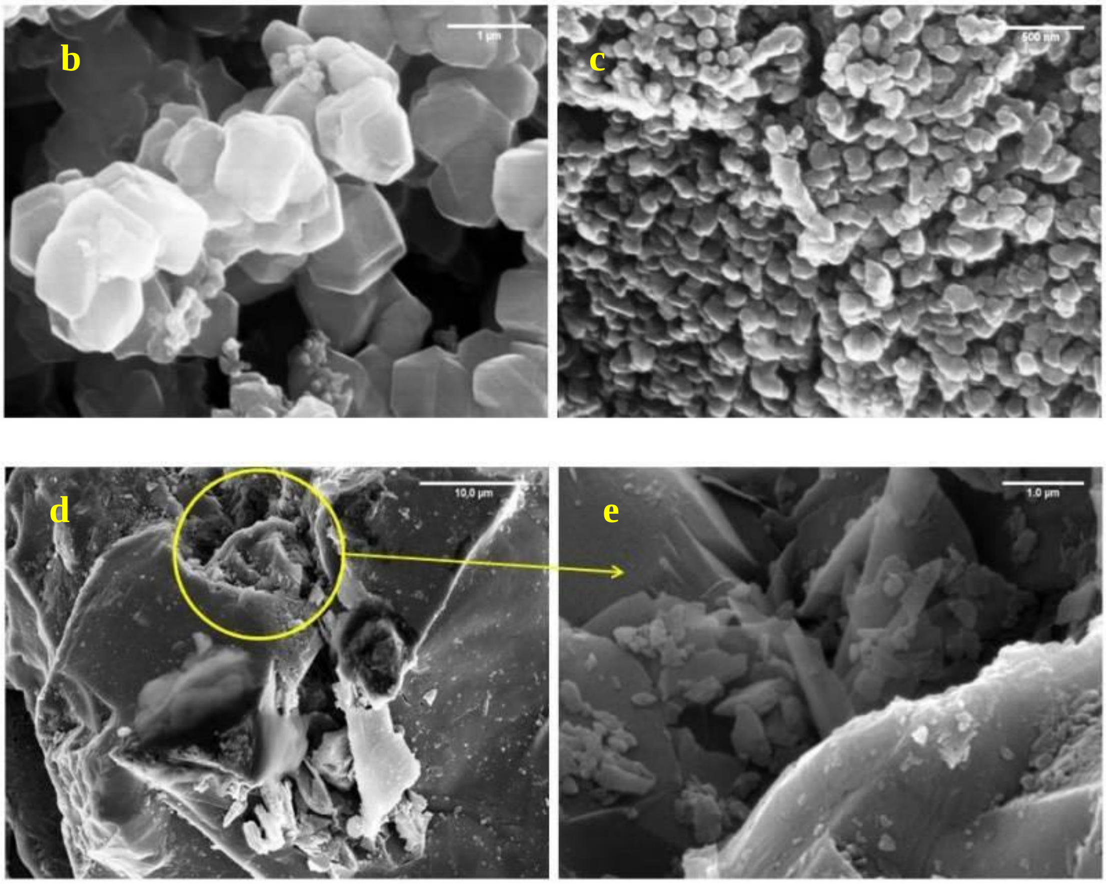

Figure 4.5. SEM images: a, b, c) nc-B_4CAW1 and d, e) c-B_4CAW

4.2 Spark plasma sintering of nc-B_4CAW1 and c-B_4CAW

Spark plasma sintering of the nc-B_4CAW1 was carried out at 1873, 1973 and 2073 K whereas c-B_4CAW was sintered at 1973 K in order to compare the densification of both the powders. The densification procedure is detailed in Section 2.4 of Chapter 2. The sample designation of all the samples are given in Table 4.4.

Table 4.4. Sample designation of spark plasma sintered samples

Sample	Temp. (K)	Duration of heating (min)	Pressure (MPa)
nc-B_4C16	1873	5	50
nc-B_4C17	1973	5	50
nc-B_4C18	2073	5	50
c-B_4C17	1973	5	50

nc = nanocrystalline, c = commercial, Temp.-sintering temperature

4.2.1 Characterization of the spark plasma sintered compacts

4.2.1.1 Spark plasma sintered compacts

A typical photograph of the sintered compacts before removing the graphite foil is shown in Fig. 4.6. It was found that the compact, nc-B_4C18 was partially melted and was stuck to the plunger. Perhaps, the passing of high current would have caused direct heating of the powders based on Joule heating. The contact point of particles offer high resistance to the current flow and hence, resulted in increased heating in the region of contact between the particles as explained in Ref. [121]. The temperature of the localized heating zones often exceeds the melting point of the material. It is surmised that the localized heating would have resulted in the partial melting of the compact at 2073 K.

Figure 4.6. Photograph of the sintered compacts before removing the graphite foil. From left: nc-B_4C16, nc-B_4C17, c-B_4C17 and nc-B_4C18

4.2.1.2 XRD analysis of spark plasma sintered compacts

The XRD patterns of the sintered compacts are shown in Fig. 4.7. The XRD patterns matched with the ICDD database file number 00-035-0798. The XRD patterns of the sintered compacts indicated the absence of impurity phases. B_2O_3 peak was seen in the nc-B_4C16, perhaps resulting from the surface oxidation of the sintered sample after removing the graphite foil.

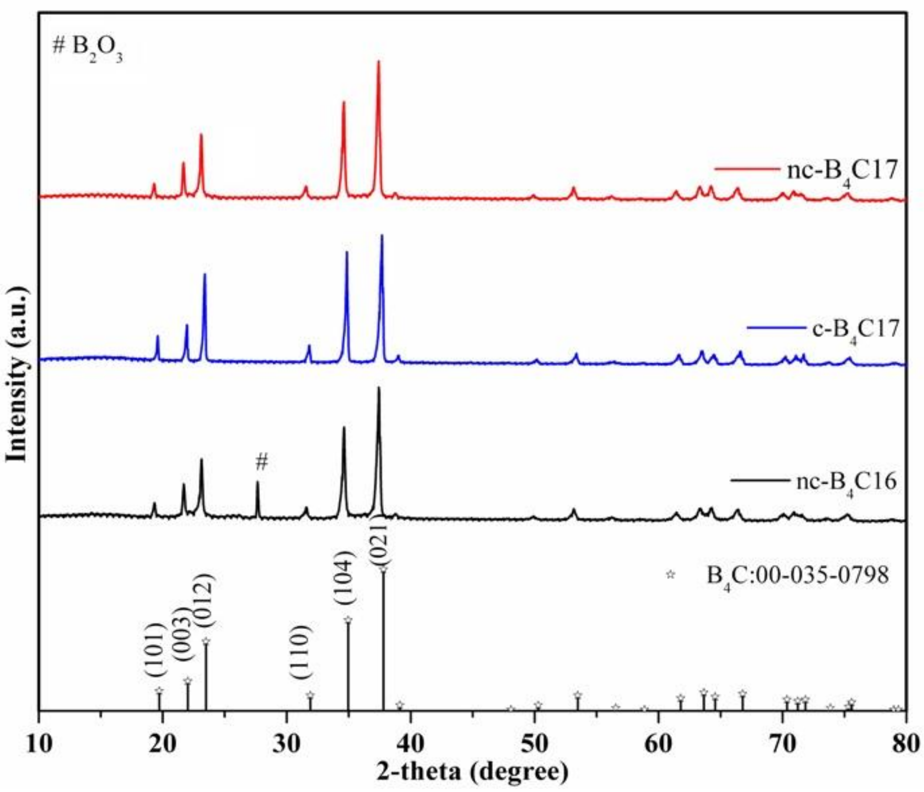

Figure 4.7. XRD patterns of the spark plasma sintered samples

4.2.1.3 Densities of the spark plasma sintered compacts

The densities of the sintered compacts were measured using the Archimedes principle with distilled water as the immersion medium. The densities of all the sintered compacts are shown in Fig. 4.8. With the increase in temperature, the density of the compacts increased. The c-B_4C17 had a relatively lower density as compared to the nc-B_4C17 at the same temperature, probably because of the larger particle size in the c-B_4C17 as compared to the sample synthesized in the present study. The comparison of density values reported in literature is given in Table 4.5. At 1973 K, the density of the spark plasma sintered nanocrystalline boron carbide (nc-B_4C17) was found to be ~95% TD. The density obtained in the present study is comparable to the density of boron carbide reported by Sairam et al. [121]. However, in the present study, the duration of heating (5 min) was less compared to that employed by Sairam et al. (15 min). Moshtaghioun et al. [122] have reported a density of 97% TD for the

B_4C sintered at 1973 K. This could be due to the higher pressure (75 MPa) used compared to that in the present study (50 MPa). These authors have also reported [124] a density of ~95% TD for the B_4C sintered with the similar conditions as reported in Ref. [122]. The density of spark plasma sintered compact at 1873 K was ~92% TD which is higher than the density reported by Moshtaghioun et al. [117] (~90% TD) even though the pressure used by these authors was higher (75 MPa) than that in the present study (50 MPa).

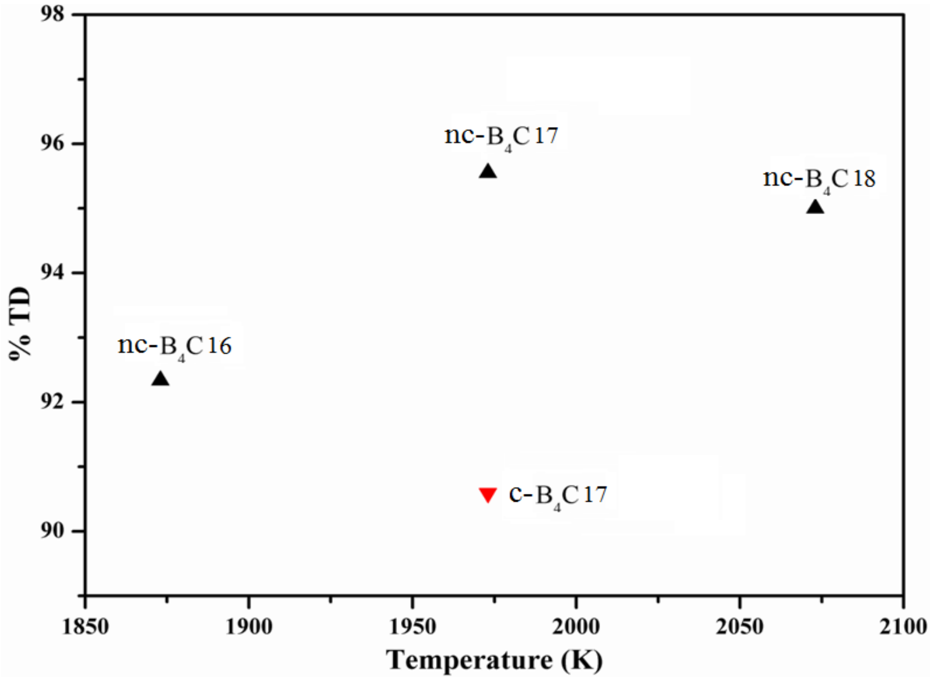

Figure 4.8 Densities of the spark plasma sintered compacts

Table 4.5. Density and microhardness of the sintered B_4C reported in literature

Author	Sample details	[1]Temp. (K)	Heating rate (K min^{-1})	[2]Time (min)	Pressure (MPa)	Density (%TD)	Hardness (GPa)	Ref.
Zhang et al.	B_4C powders (97.1% purity, Shanghai ChaoWei Nanotechnology Co., Ltd., China), d(50) = 1.21 µm	2173	100	6	40	~94	26.4 ± 4.3	[106]
Hayun et al.	grade HS, H.C. Starck Company, Germany	2173-2473			32		32 ± 2	[114]
Hayun et al.	grade HS, H.C. Starck Company, Germany, SSA = 15–20, B = 75.05 wt.%, C = 21.8 wt.%, d (50) ≤ 8mm	2173	50	6	50	89		[115]
Cengiz et al.	P = 2.95 µm HP grade	1923	100	5	40	98.6	31.04 ± 0.5	[116]
	P = 1.78 µm HS grade H.C. Starck Company, Germany	1943	100	5	40	99.1	30.67 ± 0.5	
Moshtaghioun et al.	P = 500 nm, Grade HD20, H. C. Starck, Germany	1873	100	5	75	90.3	22.8	[117]
		1973	100	3	75	100	36.4	
Moshtaghioun et al.	P = ∼ 0.5 µm; Grade HD20, H.C. Starck, Germany	1973	100	3	75	> 98.5	~38	[118]
Badica et al.	HD 20, H. C. Starck, SSA = 22-27	1873	50	20	300	95.6	27.6 ±1.8	[119]
		2373	50	10	50	97.8	35.3 ± 2.6	
Li et al.	P = 493.8 nm, Mudanjiang Jingangzuan boron carbide Co. Ltd., Mudanjiang, China)	1873	100	3		98.33	31	[120]
Sairam et al.	P = d (50) =2.4, B = 77.7 wt.%, C = 22 wt.%, O = 0.2 wt.%	1973	100	15	50	94.4	32	[121]
		2073	100	15	50	100	37.2	

Moshtaghioun et al.	P = Avg. ~40 nm, Tekna Plasma System Inc., Canada	[a]1873	100	3	75	94.6	22.8 ± 3	[122]
		[a]1973	100	3	75	97.1	-	
		[b]1873	100	3	75	97.5	32.5 ± 3	
		[b]1973	100	3	75	98.5	-	
Ji et al.	P = 2.36, 97% purity, Mudanjiang Diamond Boron Carbide Co., Ltd., China	1973	100	5	> 80	99.7	37.8	[123]
Moshtaghioun et al.	P = 500 nm	1973	100	3	75	100	36 ± 2	[124]
	P = 220 nm	1973	100	3	75	98.5	36 ± 1	
	P = 40 nm, Grade HD20, H. C. Starck,Germany and Tekna Plasma System Inc., Canada	1973	100	3	75	94.7	28 ± 2	
Moshtaghioun et al.	P = 40 nm, Tekna Plasma System Inc., Canada	1873	100	3	75	~98	31	[126]
Belon et al.	P = 0.2, grade HD20, H.C. Starck, Germany, SSA = 17.8	1923	200	5	100	98	39.6 ± 3.1	[127]
Asadikiya et al.	P = d (50) = 0.6-0.9, Grade HD 15, H.C. Starck, Germany	2073	100	20	60	[c]88	18 ± 0.75	[128]
		2073	100	20	60	[d]92.1	26.77 ± 0.66	
Moskovskikh et al.	Amorphous boron (99.5 %, d < 45 µm) graphite (99.5 %, d < 45 µm)	2223	100	60	50	98.1	36.34 ± 0.32	[130]
Ortiz et al.	P = 0.6, Grade HD20, H.C. Starck	1973	100	3	75			[131]
Present study	P = d (50) = 8	1973	100	5	50	95.55	24.08 ± 1.5	

[a]-as-received commercial powder, [b]-annealed at 1423 K , 8h, [c]-as-received powder, [d]-alcohol-washed powder, SSA-specific surface area (m^{2}g^{-1}), P = , Particle size (µm) [1]and [2] -sintering temperature and duration of heating

4.2.1.4 Morphology of the spark plasma sintered compacts: SEM

The sintered compacts were ground using silicon carbide paper (grit size 80 to 1000) and polished using diamond paste (6 and 1µm) before taking SEM images. All the samples were coated with gold prior to SEM analysis. SEM images of nc-B_4C16, nc-B_4C17 and c-B_4C17 are shown in Fig. 4.9. Homogeneous microstructures with numerous open pores at the surface of the sintered compact are observed in the SEM images of nanocrystalline boron carbide sintered at 1873 and 1973 K. The pores would have been originated from the chipping-off of the loose particles during the grinding and polishing of the samples. The microstructure with well-sintered regions are clearly seen in the SEM images. This kind of morphology was observed for the boron carbide sintered at 2173 K by Zhang et al. [106]. The SEM image of the c-B_4C17 is shown in Fig. 4.9c. The morphology of the c-B_4C powder is shown as the inset in the same figure. The SEM image of the c-B_4C17 appeared as if the powders were just compressed. Abnormal grain growth was not observed in the SEM images. In the SEM image of c-B_4C17, the portion marked inside black circles indicates chipping during the sample preparation stage. This kind of chipping was also observed by Moshtaghioun et al. [118] and Hayun et al. [115].

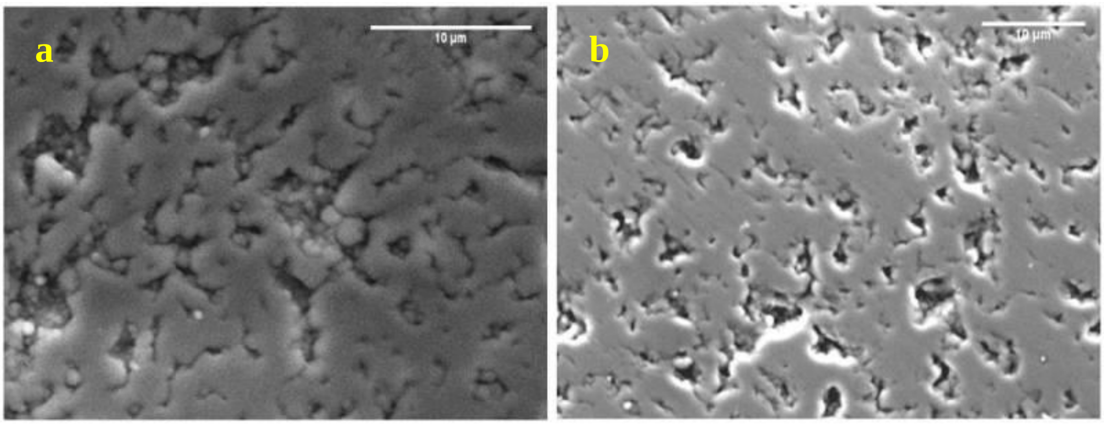

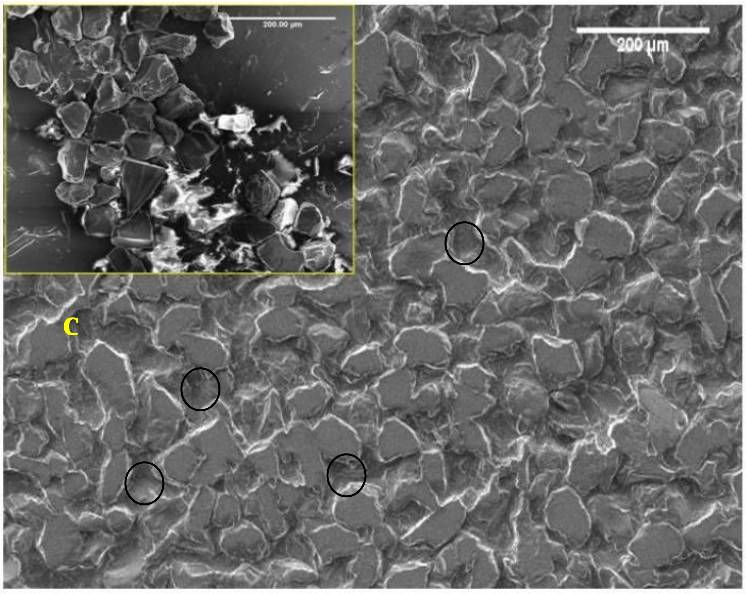

Figure 4.9. SEM images of spark plasma sintered samples: a) nc-B_4C16, b) nc-B_4C17 and c) c-B_4C17- the inset shows the morphology of the powder

4.2.1.5 Microhardness of the sintered compacts

The microhardness number reported here is an average of five measurements. The microhardness of nc-B_4C16 was found to be 9.7±0.9 GPa and that of nc-B_4C17 was found to be 24.1±1.2 GPa. The microhardness of c-B_4C17 was found to be 3.8±0.3 GPa. The microhardness values of the B_4C sintered by spark plasma sintering technique reported in the literature are given in Table 4.5. Sairam et al. [121] have reported a microhardness of 6.7 GPa for the B_4C sintered by SPS at 1873 K for 15 min. At the same temperature, the hardness value obtained in the present study is higher than that reported by these authors even though the duration of heating was lower (5 min) in the present study. Moshtaghioun et al. [122] have reported a microhardness value of ~23 GPa for the boron carbide sintered at 1873 K using SPS. Even though the density of the sintered compact is almost similar (~95% TD) to the density reported in the present study (~95% TD at 1973 K), the hardness value obtained in the present study is slightly higher (~24 GPa) than that reported by these authors.

4.3 Summary

The nc-B_4C powder synthesized in this study for sintering studies was found to contain B_2O_3 as an impurity phase. The methanol washing of the nc-B_4C powder helped to remove the B_2O_3 from the surface of the powder particles. This was confirmed by the absence of peaks pertaining to that of B_2O_3 in the XRD pattern of ncB$_4$CAW1. Both nc-B$_4$CAW1 and c-B$_4$CAW showed a unimodal particle size distribution. The specific surface area of nc-B$_4$CAW1 was higher as compared to that of c-B$_4$CBW. The method of preparations of nc-B$_4$CAW1 and c-B$_4$CBW were different and this would have resulted in the variation of the specific surface areas in nc-B$_4$CAW1 and c-B$_4$CBW. The morphology of nc-B$_4$CAW1 was equiaxed and that of c-B$_4$CBW was flaky. The XRD patterns of the sintered compacts indicated the absence of impurity phases. The density of the nc-B$_4$C17 was higher as compared to that of c-B$_4$C17. The microhardness of nc-B$_4$C17 was also higher than that of c-B$_4$C17.

4.4 Conclusion

Nanocrystalline boron carbide prepared in the present study was sintered using the spark plasma sintering technique. The density of the nc-B$_4$C17 was found to be ~95% TD compared to the density of c-B$_4$C17 (~90% TD). Hence, nanocrystalline B_4C powder was found to be better sinterable as compared to the sample prepared by carbothermic reduction at higher temperatures (commercial sample procured from a vendor). The hardness of nc-B$_4$C17 was found to be ~24.08 GPa. Hence, the nanocrystalline boron carbide powder synthesized by a precursor method at low-temperature is superior in powder characteristics for the sintering, than that synthesized at high temperatures by carbothermic reduction.

Chapter 5

Studies on sintering of nc-B_4C by Hot Pressing Technique

Nanocrystalline boron carbide was synthesized by the precursor method using boric oxide and sucrose for studies on sintering of nc-B_4C compacts. nc-B_4C powder synthesized by precursor method was characterized for phase purity, chemical composition, specific surface area, particle size distribution and microstructure. Boron carbide samples procured from M/s. Sigma Aldrich were also characterized for phase purity, chemical composition, specific surface area, particle size distribution and microstructure. The sinterability of these powders by hot pressing was studied in detail and the results are presented in this chapter.

5.1 Results and Discussion

5.1.1 Synthesis of nc-B_4C for hot pressing

nc-B_4C was prepared by using the B_2O_3-sucrose precursor. The method of preparation of the precursor and B_4C are detailed in Section 2.3.1 of Chapter 2. Essentially, B_4C was synthesized by heat-treatment of the precursor at 1873 K for 20 min in order to ensure completion of the reaction. B_4C was prepared in bulk using the furnace described in Section 2.2.2 of Chapter 2 for sintering studies.

5.1.2 Characterization of the nc-B_4C powders

5.1.2.1 XRD analysis of nc-B_4C and c-B_4C powders

nc-B_4C powder synthesized was thoroughly washed with methanol. The sample designation of B_4C powder before and after washing with methanol are given in Table 5.1.

Table 5.1. nc-B_4C powders used for hot pressing studies

Sample	Remarks
nc-B_4CBW2	nanocrystalline boron carbide powder before methanol washing
nc-B_4CAW2	nanocrystalline boron carbide powder after methanol washing
c-B_4CBW	commercial boron carbide powder before methanol washing
c-B_4CAW	commercial boron carbide powder after methanol washing

The XRD patterns of nc-B_4CBW2 and nc-B_4CAW2 are shown in Fig. 5.1. B_2O_3 peaks were seen in the XRD pattern of nc-B_4CBW2 powder and the peaks were absent in the XRD pattern of nc-B_4CAW2 powder. This clearly shows that washing of the B_4C powder with methanol helps to remove the B_2O_3 impurity present in the powder. The peaks corresponding to that of carbon were absent in the XRD patterns of nc-B_4CBW2 and nc-B_4CAW2; perhaps the free carbon present in the powder was below the detection limit of XRD. The c-B_4CBW and c-B_4CAW did not contain B_2O_3 impurity phase as can be seen from the XRD pattern shown in Fig. 5.2. Peak pertaining to carbon was seen in the XRD pattern of c-B_4CBW and c-B_4CAW; perhaps the method of preparation of c-B_4C (carbothermic reduction at high temperature) might have resulted in the high crystallinity of the free carbon present in the powder. Average X-ray crystallite sizes of all the samples were <31 nm.

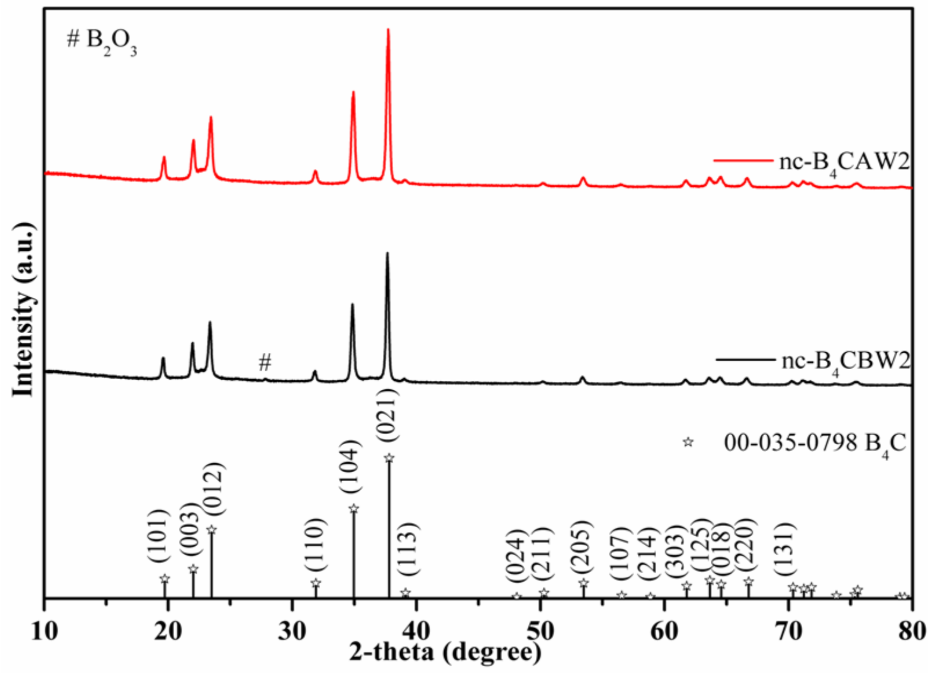

Figure 5.1. XRD patterns of nc-B_4CBW2 and nc-B_4CAW2

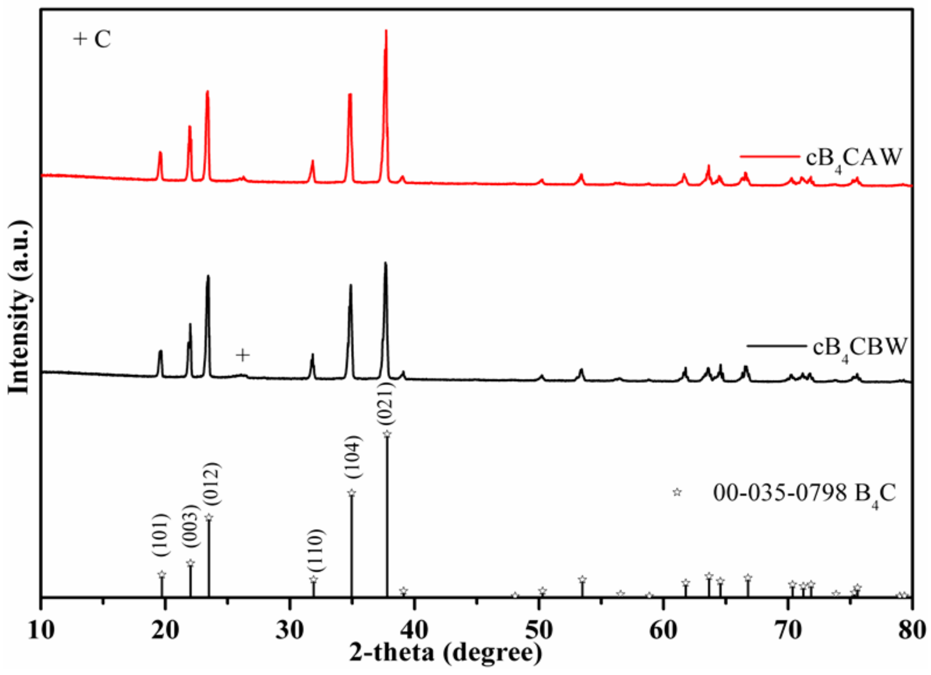

Figure 5.2. XRD patterns of c-B_4CBW and c-B_4CAW

5.1.2.2 Results of chemical analyses, specific surface area and particle size distribution of nc-B_4C and c-B_4C

The results of the chemical analyses and specific surface area of nc-B_4CBW2, nc-B_4CAW2 and c-B_4CBW are given in Table 5.2. The free carbon content in the nc-

B_4CBW2 and nc-B_4CAW2 powders were less than 1 wt.%. The free carbon content in c-B_4CBW was also less than 1 wt.% (0.7 wt.%). The estimated boron, total carbon and free carbon content in the nc-B_4CBW2 and nc-B_4CAW2 powders were found to be almost similar. Boron, total carbon and free carbon content in the nc-B_4CBW2 powder were found to be 79.5, 21.7 and 0.6 wt.% respectively whereas that of nc-B_4CAW2 were 79.7, 21.6 and 0.7 wt.% respectively. The specific surface area of nc-B_4CAW2 powder was found to be 58 m^2g^{-1}. The c-B_4CBW had a specific surface area of 28 m^2g^{-1}. The nc-B_4CAW2 had a higher specific surface area as compared to that of c-B_4CBW.

Table 5.2 Results of chemical analyses of nc-B_4CBW2, nc-B_4CAW2 and c-B_4CBW

Sample	Boron (wt.%)	Total C (wt.%)	Free C (wt.%)	SSA (m^2g^{-1})	XCS (nm)
nc-B_4CBW2	79.5	21.7	0.6	102	31
nc-B_4CAW2	79.7	21.6	0.7	58	27
c-B_4CBW	79.5	19.7	0.7	28	30

Expanded uncertainty in B is ± 1.5 wt.%, total C is ± 0.16 wt.% and free C is ± 0.50 wt.% with 0.95 level of confidence.

The particle size distribution results indicated that 10% of the particles in the nc-B_4CBW2 powder prepared in the present study were <3 µm. 50% of the particles were in the size range of <9 µm and 90% of the particles were <20 µm in size range. The particle size distribution results indicated that 10% of the particles in the nc-B_4CAW2 powder prepared in the present study were <3 µm. 50% of the particles were in the size range of <8 µm and 90% of the particles were <24 µm in size range. This indicates that the size distribution of the particles in nc-B_4CBW2 and nc-B_4CAW2 are similar; perhaps, there is no agglomeration in the nanocrystalline boron carbide powder synthesized in the present study. 10% of the particles were in the size range of <42 µm in the c-B_4CBW powder. 50% of the particles were <61 µm and 90% of the particles were <87 µm in size range. In the case of c-B_4CBW and c-B_4CAW also, the size distribution remains the same; perhaps, there is no agglomeration in c-B_4C powder also. The particle size distributions of the nc-B_4CBW2, nc-B_4CAW2, c-B_4CBW and c-B_4CAW are given in Table 5.3. The particle size distribution of nc-B_4CBW2 and nc-B_4CAW2 are shown in Fig. 5.3 whereas that of c-B_4CBW and c-B_4CAW are shown in Fig. 5.4, respectively.

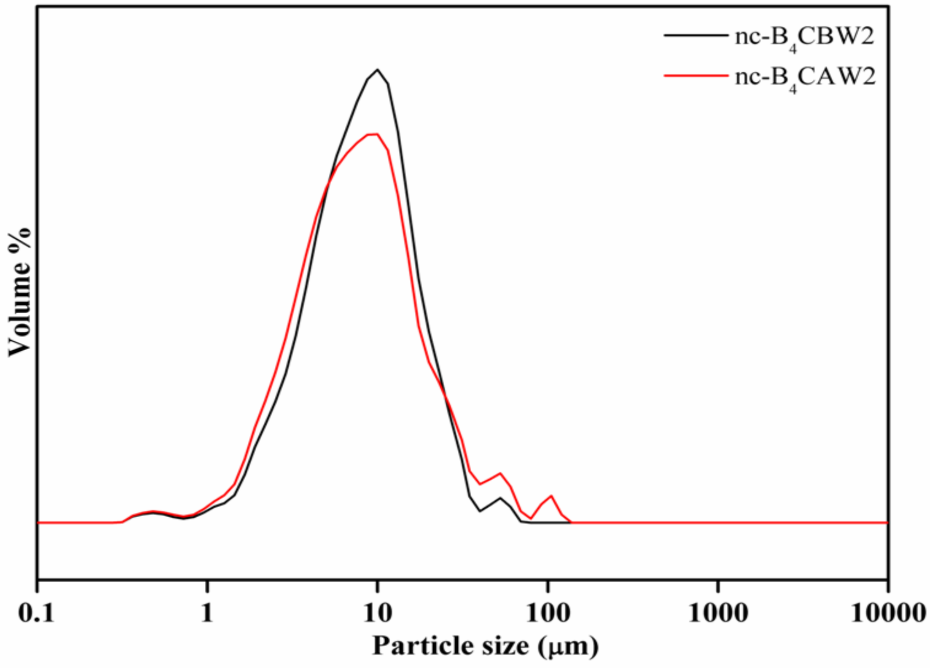

Figure 5.3. Particle size distribution of nc-B_4CBW2 and nc-B_4CAW2

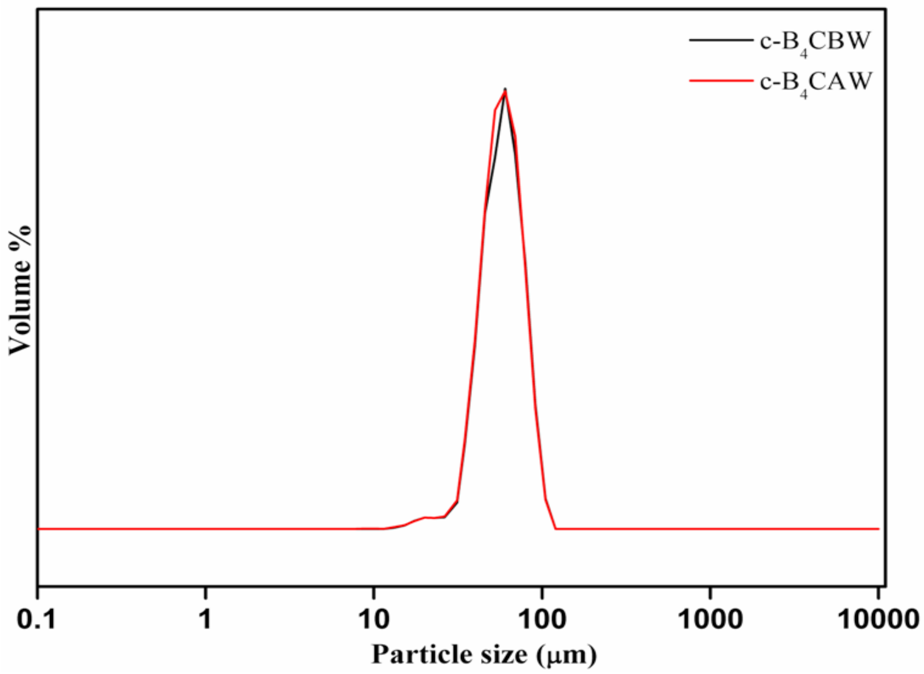

Figure 5.4. Particle size distribution of c-B_4CBW and c-B_4CAW

Table 5.3. Particle size distribution of nc-B_4CBW2, nc-B_4CAW2, c-B_4CBW and c-B_4CAW

Sample	d (0.1) μm	d (0.5) μm	d (0.9) μm
nc-B_4CBW2	3.2	8.9	20.5
nc-B_4CAW2	2.8	8.2	24.1
c-B_4CBW	42.3	61.8	86.9
c-B_4CAW	42.0	61.4	86.6

5.1.2.3 Morphology of nc-B_4CAW2 and c-B_4CAW powder: SEM

The morphologies of nc-B_4CAW2 and c-B_4CAW powders are shown in Fig. 5.5. Fig. 5.5a is the SEM image of nc-B_4CAW2 and Fig. 5.5b is the magnified image of finer particles in the nc-B_4CAW2. Both larger particles and finer particles are equiaxed with a size of ~1 μm and <0.2 μm respectively. The c-B_4C sample has a flaky morphology. This sample perhaps synthesized by carbothermic reduction using an Acheson type furnace, resulted in the flaky morphology.

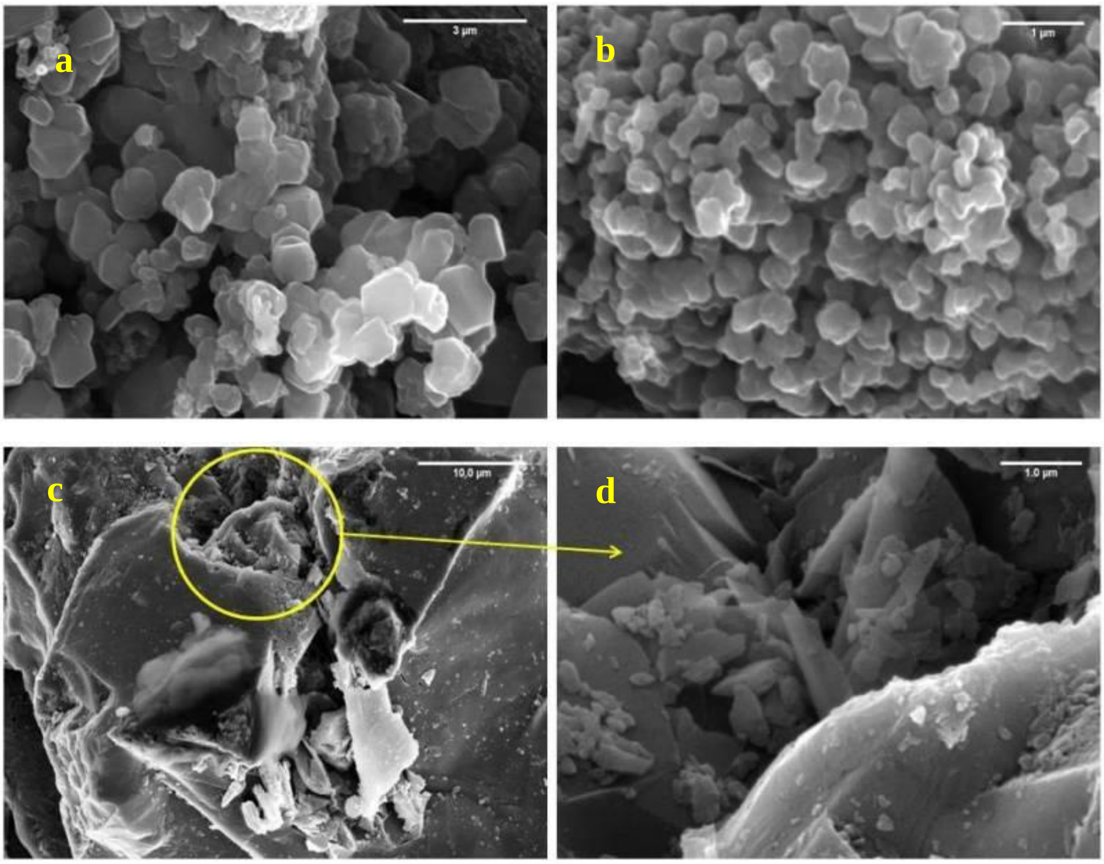

Figure 5.5. SEM images: a and b) nc-B_4CAW2, c and d) c-B_4CAW

5.2 Hot pressing of nc-B_4CAW2 and c-B_4CAW

Hot pressing of nc-B_4CAW2 and c-B_4CAW was carried out at 1973 and 2073 K in order to compare the densification of both samples. The densification procedure is detailed in Section 2.3 of Chapter 2. The sample designation of the hot pressed boron carbide are given in Table 5.4.

Table 5.4. Sample designation of hot pressed B_4C samples

Sample	Temp. (K)	Duration of heating (min)	Pressure (MPa)
nc-B_4CHP17	1973	60	35
c-B_4CHP17	1973	60	35
nc-B_4CHP18	2073	60	35
c-B_4CHP18	2073	60	35

nc-nanocrystalline, HP-hot pressed, c-commercial, Temp.-sintering temperature

5.2.1 Characterization of the hot pressed samples

Typical photograph of the nc-B_4CHP17 and c-B_4CHP18 are shown in Fig. 5.6. The diameter of the sintered compact was 60 mm. The photograph was taken before removing the graphite foil from the c-B_4CHP18 and the photograph of nc-B_4CHP17 was taken after removing the graphite foil.

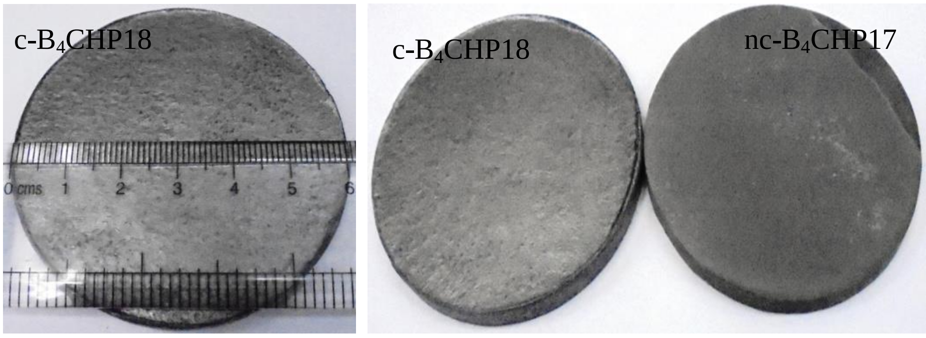

Figure 5.6. Photographs of c-B_4CHP18 and nc-B_4CHP17

5.2.1.1 XRD analysis of the hot pressed samples

The XRD patterns of the sintered compacts are shown in Fig. 5.7. The XRD patterns matched with the ICDD database file number 00-035-0798. The XRD patterns of the sintered compacts indicated the absence of impurity phases.

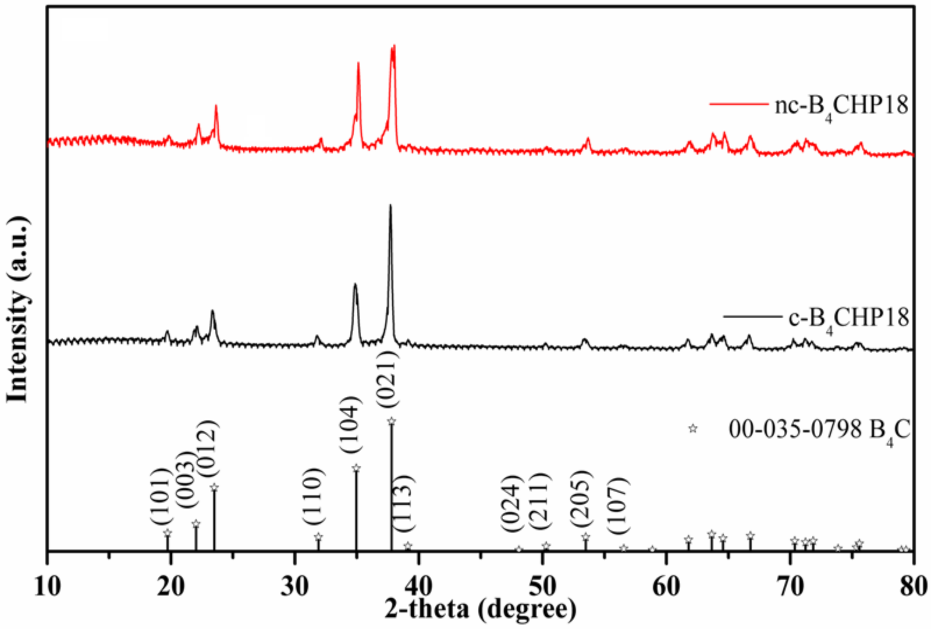

Figure 5.7. XRD patterns of nc-B_4CHP18 and c-B_4CHP18

5.2.1.2 Densities of the hot pressed compacts

The densities of the sintered compacts were measured using the Archimedes principle with distilled water as the immersion medium. The densities of all the sintered compacts are shown in Fig. 5.8. It is found that with an increase in the sintering temperature, the densities of both nc-B_4C and c-B_4C hot pressed compacts increased. The comparison of density values reported in literature is given in Table 5.5. A lower density value obtained in the present study may be due to the lower sintering temperature and pressure used in the present study as compared to that reported in literature. The rate of heating was also less in the present study compared to that reported in literature.

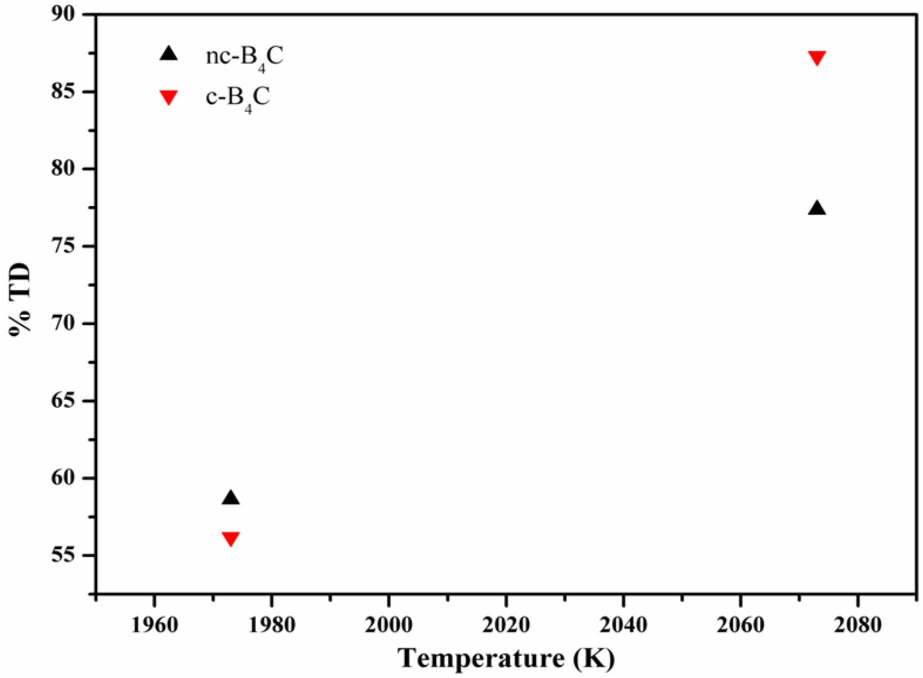

Figure 5.8. Densities of the hot pressed compacts

Table 5.5. Density and hardness of the sintered B_4C reported in literature

Author	Sample details, Particle size (µm)	^{1}Temp. (K)	Heating rate (K min^{-1})	^{1}Time (min)	Pressure (MPa)	Density (% TD)	Hardness GPa	Ref.
Kalandadze et al.	Synthesized from elements at 2273 K	2173-2373			20-40			[101]
Du et al.	B_4C powder, Mudanjiang Jinganzuan Boron carbide Co.Ltd., B = 76.43 wt.%, C = 20.71 wt.%, d (50) ≤1.52 µm	2073-2223	20 up to 1473 K and 10 after wards	5-100	15-30			[102]
		2123		60	30	<90%		
Angers et al.	B_4C powder from 7 suppliers	1775-2575	56 and 330		20.7-68.9			[103]
		1975			34.4	72.4		
Zhang et al.	B_4C powders (97.1% purity, Shanghai ChaoWei Nanotechnology Co., Ltd., China), d(50) = 1.60 µm	2173	10	60	75	98.49	32.48 ± 1.01	[105]
				60	100	99.76	35.56 ± 0.83	
Zhang et al.	B_4C powders (97.1% purity, Shanghai ChaoWei Nanotechnology Co., Ltd., China), d (50) = 1.21 µm	2173	10	60	40	91	21.8 ± 1.1	[106]
Present study	nc-B_4C	2073	up to 1273 K- 400 Kh^{-1} above this 200 Kh^{-1}	60	35	<80	11.07	

^{1}and ^{2} -sintering temperature and duration of sintering

5.2.1.3 Morphologies of the hot pressed compacts: SEM

The sintered compacts were ground using silicon carbide paper (grit size 80 to 1000) and polished using diamond paste (6 and 1 µm) before taking SEM images. All the samples were coated with gold prior to SEM analysis. SEM images of nc-B_4CHP18 and c-B_4CHP18 are shown in Fig. 5.9. The nc-B_4CHP18 shows smaller grains compared to that of c-B_4CHP18. The neck formation of the particles are clearly seen in both the images. Homogeneous microstructures with numerous open pores at the surface of the sintered compact are observed in the SEM images. The microstructure with well-sintered regions are clearly seen in the SEM images. Porosities are also seen in both the images which is reflected in the low density (~ 87% TD for c-B_4CHP18 and <80% TD for nc-B_4CHP18) of the hot pressed samples.

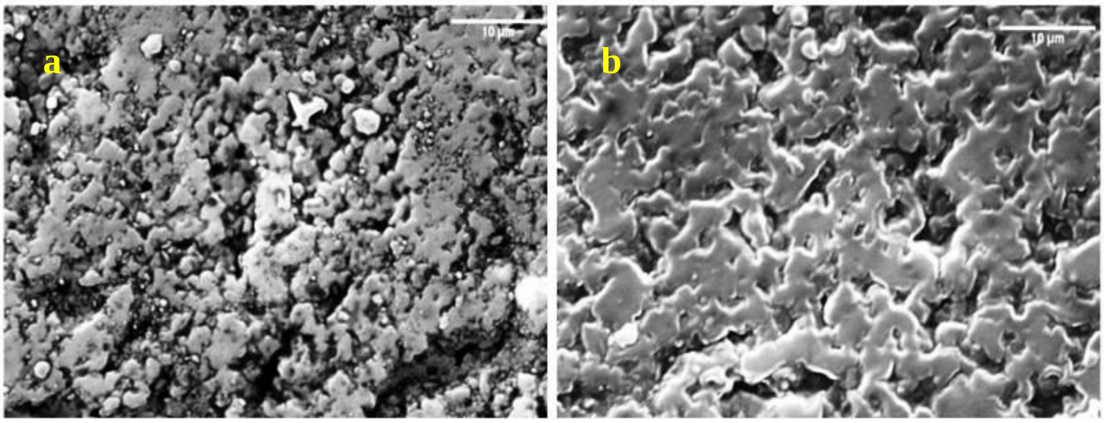

Figure 5.9. SEM images: a) nc-B_4CHP18 and b) c-B_4CHP18

5.2.1.4 Microhardness of the hot pressed compacts

The microhardness number reported here is an average of five measurements. The microhardness of nc-B_4CHP18 was found to be 11.0±0.5 GPa and that of c-B_4CHP18 was found to be 12.34±0.5 GPa. Both nc-B_4CHP18 and c-B_4CHP18 had comparable microhardness.

5.3 Summary

The nc-B_4C powder synthesized and employed in sintering studies was found to contain B_2O_3 as an impurity phase. Washing of the nc-B_4C powder with methanol helped to remove B_2O_3 from the powder. This was confirmed by the absence of peaks pertaining to that of B_2O_3 in the XRD patterns. Both nc-B_4CAW2 and c-B_4CAW showed a unimodal particle size distribution. The specific surface area of nc-B_4CAW2 was higher as compared to that of c-B_4CBW. The methods of preparation of nc-B_4CAW2 and c-B_4CBW were different and this would have resulted in the variation of the specific surface areas. The morphology of nc-B_4CAW2 was equiaxed and that of c-B_4CBW was flaky. Based on the results of the XRD analysis of hot pressed compacts of nc-B_4C and c-B_4C samples, it was found that there was no formation of impurity phases in the sintered compacts. The density of c-B_4C18 was higher as compared to that of nc-B_4C18. The microhardness of nc-B_4C18 and c-B_4C18 were comparable. The morphologies of nc-B_4C18and c-B_4C18 were homogeneous with no abnormal grain growth.

5.4 Conclusion

Studies on the sintering of nanocrystalline B_4C using hot pressing was carried out using boron carbide powder prepared by the precursor method. Boron carbide powder procured from M/s. Sigma Aldrich (commercially available) was also used for comparison of the sintering with the nanocrystalline B_4C powder. The density of the nanocrystalline B_4C powder prepared in the present study was found to be <80% TD at 2073 K, probably requiring further optimizations (temperature and pressure) during hot pressing.

Chapter 6

Studies on the synthesis of yttria-stabilized zirconia

This chapter discusses the results of the studies on the synthesis of nanocrystalline 8 mol.% yttria-stabilized zirconia. Two different heating methods (microwave-assisted and hot plate) were used for the synthesis. Three different fuels citric acid, glycine and urea were used for the combustion reaction. Microwave-assisted combustion synthesis of yttria-stabilized zirconia was carried out by fixing the fuel to oxidant mole ratio equal to 1. The powders obtained were calcined and then sintered. Conventional heating using a hot-plate was also carried out by fixing the fuel to oxidant mole ratio as 1. The powder synthesized using microwave-assisted heating was characterized for phase purity, specific surface area, phase content by Raman spectroscopic technique, particle size distribution and microstructural analysis. The ionic conductivity of the sintered compacts were determined using ac-impedance spectroscopy.

6.1 Results and discussion

6.1.1 Combustion process

6.1.1.1 Citric acid (CA) as fuel

During microwave heating of the combustion mixture consisting of the aqueous solution of yttrium nitrate, zirconyl nitrate and CA, evaporation of water resulted in the formation of a viscous gel. A large amount of brownish fumes were released upon further heating. Continued heating after the brownish fumes died down did not lead to ignition of the resultant gel. This indicated that the gel did not couple with microwave. Hence, the product was only a porous gel, perhaps requiring higher temperatures to get ignited. The product thus obtained ('as-prepared') was light brown in colour. The photograph of the gel and 'as-prepared' product are shown in Fig. 6.1.

Figure 6.1. Photograph of the gel formed using CA as the fuel and the 'as-prepared' product

6.1.1.2 Glycine as fuel

When glycine was used as the combustion fuel, after the formation of the gel, further heating resulted in the ignition. Brownish fumes were evolved during the ignition. The combustion reaction was violent in this case as compared to the case where citric acid was used as the fuel. The 'as-prepared' product obtained using glycine as the fuel was pale grey in colour and fluffy. The photograph of the 'as-prepared' product is shown in Fig. 6.2.

Figure 6.2. Photograph of the 'as-prepared' product obtained using glycine as the fuel

6.1.1.3 Urea as fuel

When urea was used as the combustion fuel, after the formation of the gel, further heating resulted in smouldering with the continuous evolution of small amount of brownish fumes. The ‘as-prepared’ powder was found to be agglomerated and white in colour. The photograph of combustion using urea as fuel is shown in Fig. 6.3.

Figure 6.3. Photograph of the combustion using urea as the fuel

6.1.2 Phase analysis: XRD

6.1.2.1 XRD: Citric acid as the fuel

Fig. 6.4 shows typical XRD patterns of the ‘as-prepared’ powder, calcined powder and powder of sintered compacts obtained using CA as the fuel by both heating methods. The ‘as-prepared’ powder obtained by microwave heating did not have the characteristic peaks corresponding to that of YSZ implying that only denitration took place and the Zr-Y-CA did not react further to form YSZ. However, the hot-plate derived ‘as-prepared’ product showed crystallinity and formation of YSZ. In the microwave heating, water acts as the coupling agent to denitrate the mixture. However, once the water was removed, the gel did not couple with the microwave to take the reaction to completion. The XRD patterns of the calcined samples ZACM and ZACH indicated the complete formation of a solid solution between Y_2O_3 and ZrO_2. The peaks present in the calcined samples were broader compared to that of sintered samples, suggesting a smaller size of crystallites. The patterns of the sintered samples, ZASH and ZASM, also showed the presence of only YSZ solid solution. The solid solution could be either cubic or tetragonal. However, it was difficult to assign the exact structure from the XRD pattern alone due to the similarity in the d-spacing values or lattice parameter values. This was also observed by earlier authors [143, 146-147, 177]. The d-spacing values of both cubic and tetragonal phases of YSZ are given in Table 6.1. The data were taken from ICDD database, 00-030-1468 for cubic YSZ and 00-060-0501 for tetragonal YSZ.

Table 6.1. Comparison of d-spacing values of cubic and tetragonal yttria-stabilized zirconia

Cubic yttria-stabilized zirconia lattice parameter, a = 5.139 Å PDF number: 00-030-1468				Tetragonal yttria-stabilized zirconia a = 3.6237 Å and c = 5.148 Å PDF number: 00-060-0501			
2θ	d (Å)	I	Miller indices	2θ	d (Å)	I	Miller indices
30.0842	2.968	100	111	30.1458	2.9620	999	101
34.8676	2.571	25	200	34.8346	2.5733	77	002
50.1364	1.818	55	220	35.0013	2.5615	144	110
59.5975	1.550	40	311	43.0835	2.0978	4	102
62.5380	1.484	6	222	50.2152	1.8153	389	112
73.6596	1.285	5	400	50.3374	1.8112	196	200
81.5868	1.179	10	331	59.5776	1.5504	148	103
-			-	59.8023	1.5452	295	211
-			-	62.6738	1.4811	82	202
-			-	68.3694	1.3709	<1	212
-			-	73.5475	1.2867	25	004
-			-	73.9507	1.2806	50	220
-			-	78.8842	1.2125	<1	104

d-‘d’ spacing

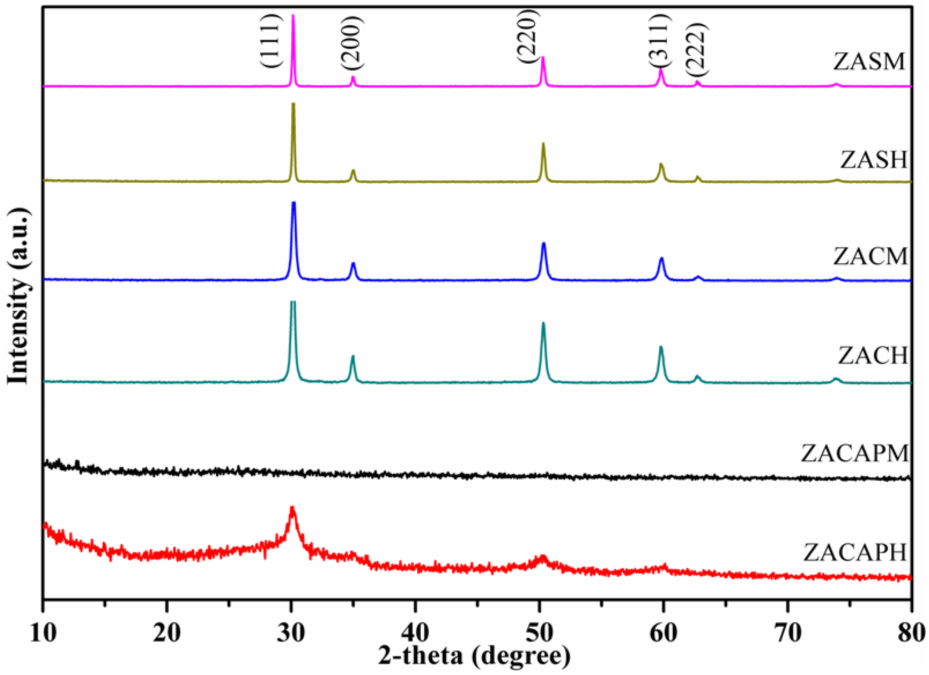

Figure 6.4. Typical XRD patterns of the 'as-prepared', calcined and sintered samples. Combustion fuel: citric acid

6.1.2.2 XRD: Glycine as the fuel

Typical XRD patterns of the 'as-prepared', calcined and sintered samples obtained using glycine as fuel by both the heating methods are shown in Fig. 6.5. The peaks in the XRD pattern of the 'as-prepared' powder obtained by hot-plate heating was broader as compared to that of microwave-derived 'as-prepared' powders which indicated smaller size crystallites in hot-plate derived powders. The XRD patterns of calcined powders, ZGCH and ZGCM, were also broad and it clearly reveals the nanocrystallinity in the calcined powders also. The width of the peaks in the sintered samples was relatively smaller compared to that of calcined sample. This clearly indicated that there was an increase in the crystallite size upon sintering.

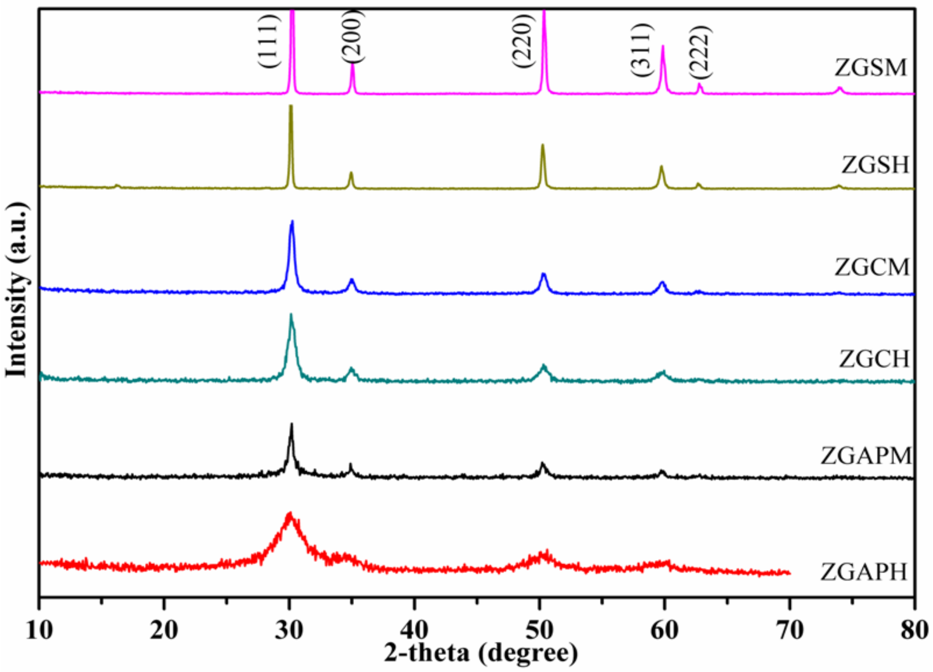

Figure 6.5. Typical XRD patterns of the 'as-prepared', calcined and sintered samples. Combustion fuel: glycine

6.1.2.3 XRD: Urea as the fuel

Typical XRD patterns of 'as-prepared', calcined and sintered products obtained using urea as the fuel by both heating methods are shown in Fig. 6.6. The urea-derived 'as-prepared' powders obtained using both heating methods were found to be nanocrystalline. The calcined and sintered products were highly crystalline. The XRD patterns indicated the formation of a solid solution of Y_2O_3 and ZrO_2. The width of the peaks in the XRD patterns of ZUSM and ZUSH were relatively smaller as compared to that of calcined samples indicating an increase in the crystallite size as a result of sintering. The sintering was carried out at 1873 K and this high temperature could have resulted in the growth of crystallites.

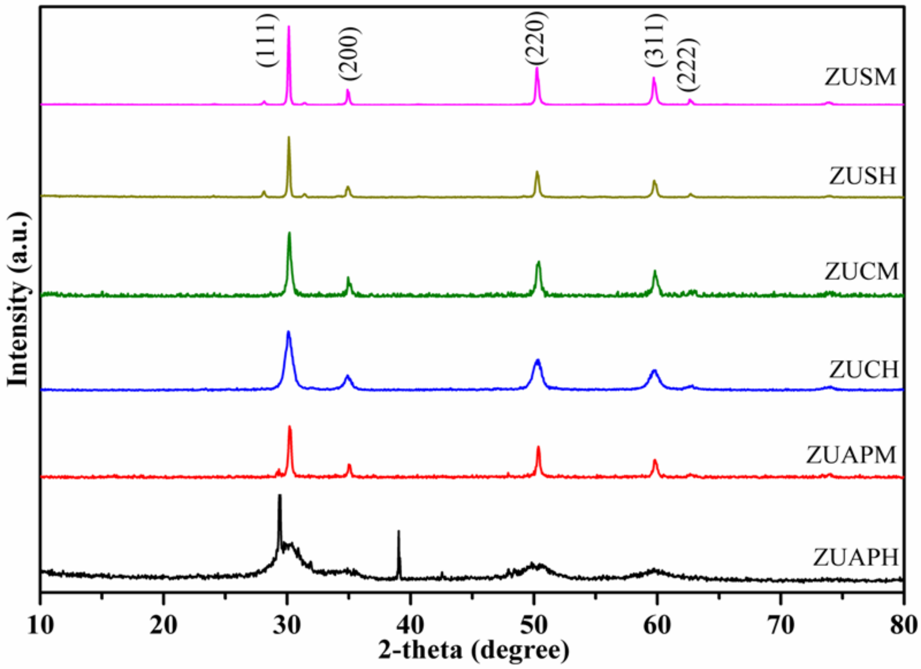

Figure 6.6. Typical XRD patterns of the 'as-prepared', calcined and sintered samples. Combustion fuel: urea

The average X-ray crystallite sizes (XCS) of the calcined and sintered samples are summarized in Table 6.2. The average crystallite sizes of ZACM and ZACH were comparable and were found to be 22 and 29 nm respectively. The average crystallite sizes of ZGCM and ZGCH were comparable and found to be in the range of 12 to 15 nm. The smaller crystallite size obtained using glycine as the fuel by both the heating methods could be due to rapid combustion coupled with gas evolution which in turn resulted in a fine and fluffy product. The average crystallite size of ZUCM was 25 nm and that of ZUCH was 12 nm. The crystallite size of all the sintered samples was in the range of 51 to 59 nm. The sintering resulted in an increase in the crystallite size of all the samples irrespective of the fuel used. Wang et al. [156] have reported that the X-ray crystallite size varied with the ignition temperature and amount of glycine for the synthesis of 8 mol.% YSZ by the glycine-nitrate process.

Table 6.2. X-ray crystallite sizes of calcined and sintered YSZ samples

No.	Sample name	XCS (nm)
1	ZACM	22
2	ZASM	59
3	ZACH	29
4	ZASH	55
5	ZGCM	15
6	ZGSM	51
7	ZGCH	12
8	ZGSH	56
9	ZUCM	25
10	ZUSM	57
11	ZUCH	12
12	ZUSH	54

6.1.3 TEM analysis

TEM bright field images and corresponding selected area electron diffraction (SAED) patterns of the calcined samples ('as-prepared' powder prepared by microwave heating) are shown in Fig. 6.7. It is seen that the particles even in calcined samples were in the nanometer size range. Fig. 6.7a shows the bright field image and corresponding SAED pattern of ZACM. It is seen that in the case of ZACM, the particles were in the size range of 10 to 55 nm and equiaxed. Discontinuous rings in the SAED pattern indicated a larger size of particles. Fig. 6.7b shows the bright field image and corresponding SAED pattern of the ZGCM. In this case the particles were equiaxed and in 5 to 60 nm range. More particles were in lower size range and continuous rings in the SAED pattern indicated the presence of finer size particles. Fig. 6.7c shows the bright field images and the corresponding SAED patterns of

ZUCM. Two kinds of morphologies were observed in this sample, polygonal coarse particles having a size range of 70 to 150 nm and equiaxed fine particles with a size range of 10 to 25 nm. Corresponding SAED patterns also indicated the bi-modal size distribution of particles. In the case of urea as fuel, the localized heating could have resulted in the sintering of agglomerates which gave rise to larger size particles. Similar behaviour was observed in the preparation of ThO_2 using urea as fuel [175].

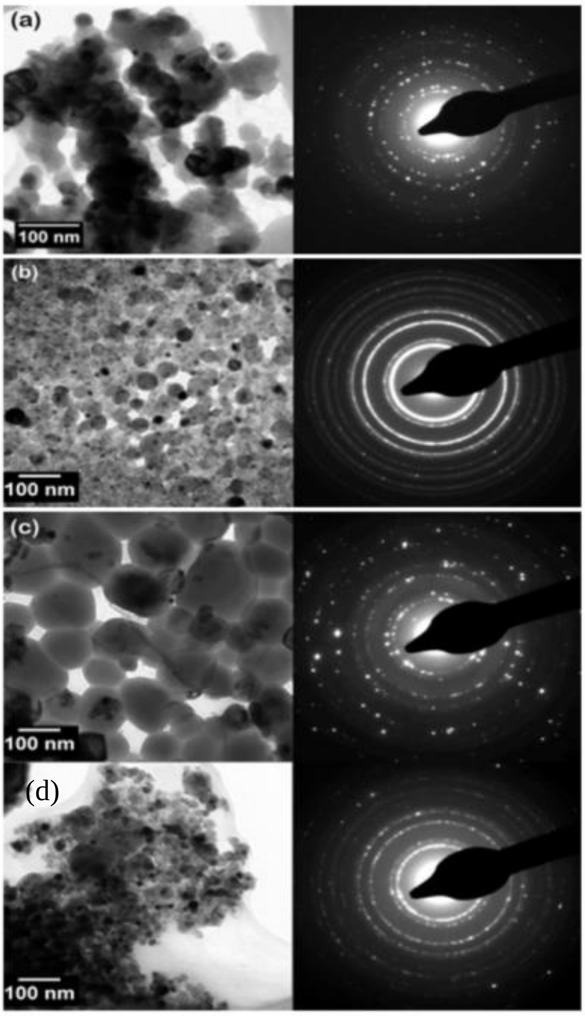

Figure 6.7. TEM Bright field images and corresponding selected area electron diffraction patterns of the calcined samples prepared by microwave heating method using different fuels: (a) ZACM, (b) ZGCM, (c) ZUCM (larger particles) and (d) ZUCM (smaller particles).

The average crystallite sizes complement these observations. d-spacing for cubic as well as tetragonal YSZ are very close that in the present study it is difficult to index SAED patterns uniquely to cubic or tetragonal phase. In all the cases, the diffraction patterns may be described as due to a mixture of both cubic and tetragonal phases.

6.1.4 Raman spectra analysis

Raman scattering is one of the powerful tools used for distinguishing cubic and tetragonal phases [207-220]. Fig. 6.8 shows the Raman spectra of the calcined samples obtained using the microwave heating method. The spectra of all the calcined samples were broad, perhaps due to very small crystallite sizes [215]. The spectra of the calcined samples obtained using glycine and citric acid as fuel showed four distinct broad peaks. The urea derived calcined powder showed two peaks at 586 and 149 cm^{-1}. The citric acid derived calcined powders gave a spectrum with four peaks at 148, 256, 472 and 618 cm^{-1}. The glycine derived calcined powders also showed four peaks at 149, 289, 490 and 591 cm^{-1}. Presence of four peaks shows the existence of both tetragonal and cubic phases. The peak at 618 cm^{-1} is assigned to the cubic phase, and other peaks can be attributed to the tetragonal phase. The broad peak at 618 cm^{-1} could be due to the merger of the peak at 640 cm^{-1} assigned for the tetragonal phase. Frison et al. [214] have reported that, the particle size, crystallinity, defects, stress, micro-strain etc. have an effect on the position, width and shape of the peaks in the Raman spectra. The peaks at wave numbers ranging from 618 to 630 cm^{-1} could be due to the presence of the cubic phase. Fig. 6.9 shows the Raman spectra of the sintered samples obtained using the microwave heating method. The sintered samples showed five distinct peaks which can be assigned to that of tetragonal and cubic phases. Lopez et al. [215] have also confirmed that the tetragonal peaks could not be detected by XRD but were observed in the Raman spectra of the samples. Quantification of the phases present in the prepared samples was not carried out in the present study.

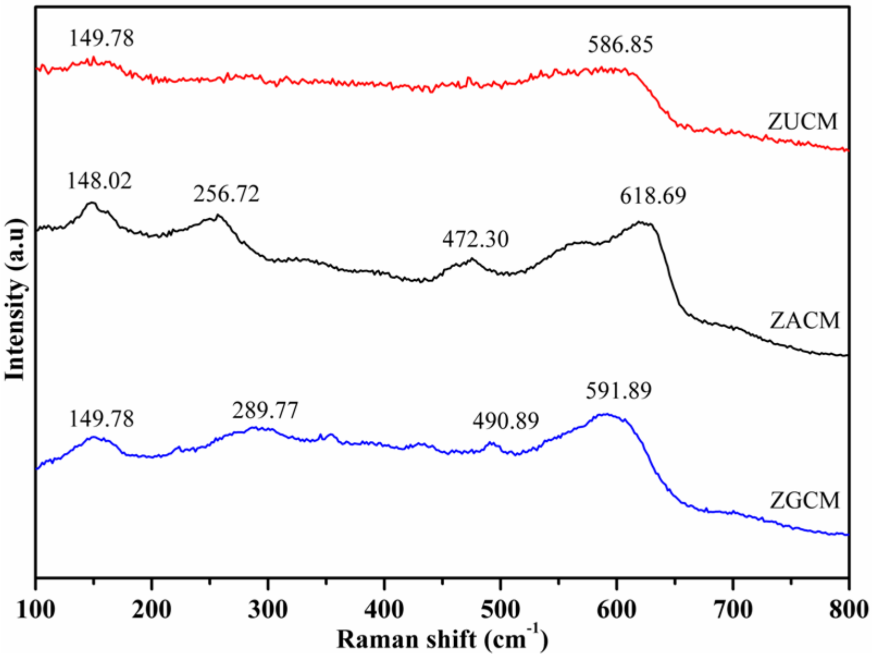

Figure 6.8. Raman spectra of the calcined powders obtained from microwave-assisted synthesis using glycine, citric acid and urea as fuels

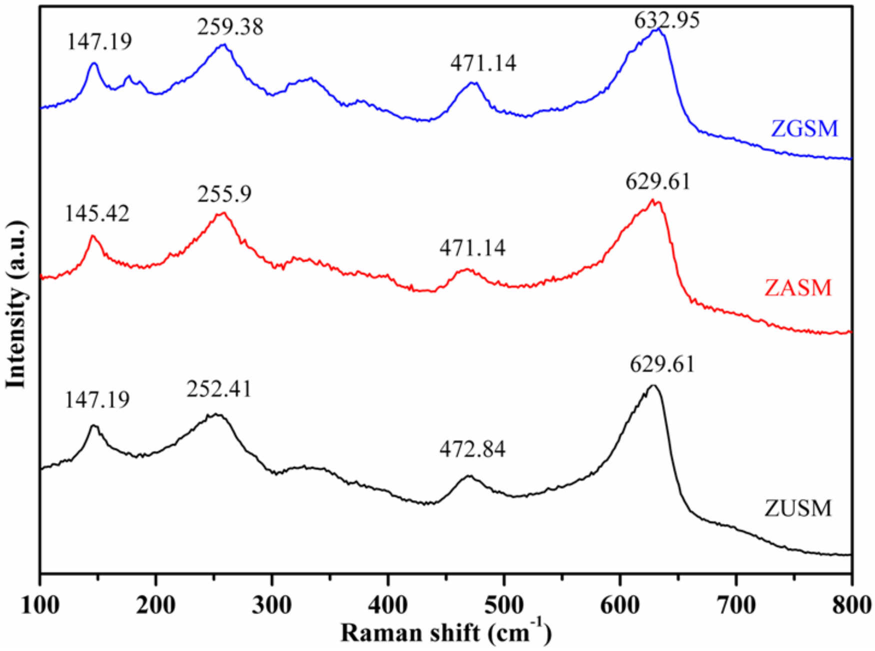

Figure 6.9. Raman spectra of the sintered powders obtained from microwave-assisted synthesis using glycine, citric acid and urea as fuels

6.1.5 Morphology of the sintered compacts: SEM

SEM images of the sintered compacts obtained from microwave-assisted heating method are shown in Fig. 6.10. All the samples show a distinct grain boundary. The presence of pores is clearly seen in all the images. Two types of grains are present in ZASM-one with size ~10 µm and the other with size <10 µm. The image of the sintered sample obtained using citric acid as fuel shows interconnected porosity. The ZGSM sample shows the presence of closed porosity (as circled in the SEM image (b)). Two different grains are present in the case of ZGSM also, finer grains with size <5 µm and larger grains of ~15 µm. The sintered sample ZUSM shows grains of two different sizes-larger grains of ~15 µm size and <10 µm grain size. This could be due to the presence of agglomerates that resulted in differential densification during sintering.

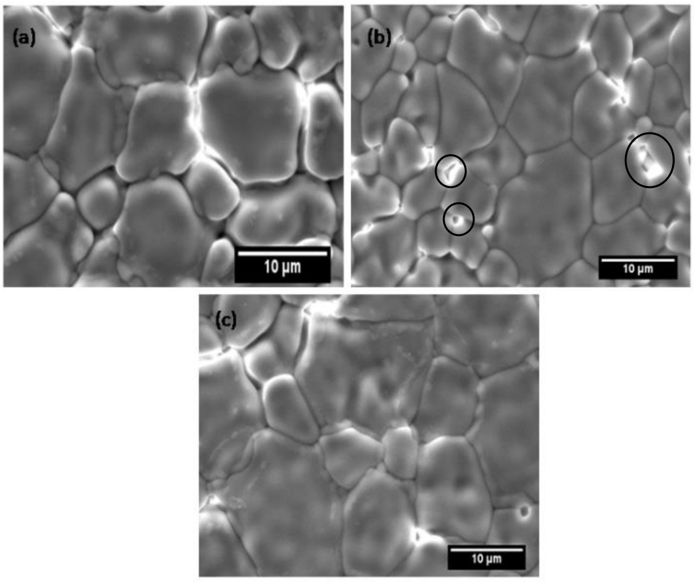

Figure 6.10. SEM images of the sintered pellets: (a) ZASM, (b) ZGSM, and (c) ZUSM

Cross-sectional images of the sintered compacts obtained from the hot-plate heating method are also shown in Fig. 6.11. ZASH shows a grain size of ~10 µm. ZGSH shows irregular finer grains in the size range of 1 to 10 µm. Perhaps, the compacts prepared using the glycine-derived powder would have resulted in faster sintering at the periphery of the compacts and relatively less sintering at the interior. This differential densification could be the reason for finer grains in the cross-sectional images of ZGSH. SEM image of ZUSH shows that the grain formation is incomplete and densification is with irregular grains. The particle size distribution of the urea-derived powder shows a bimodal distribution and this could have resulted in differential densification which is also reflected in the low density of the sintered samples.

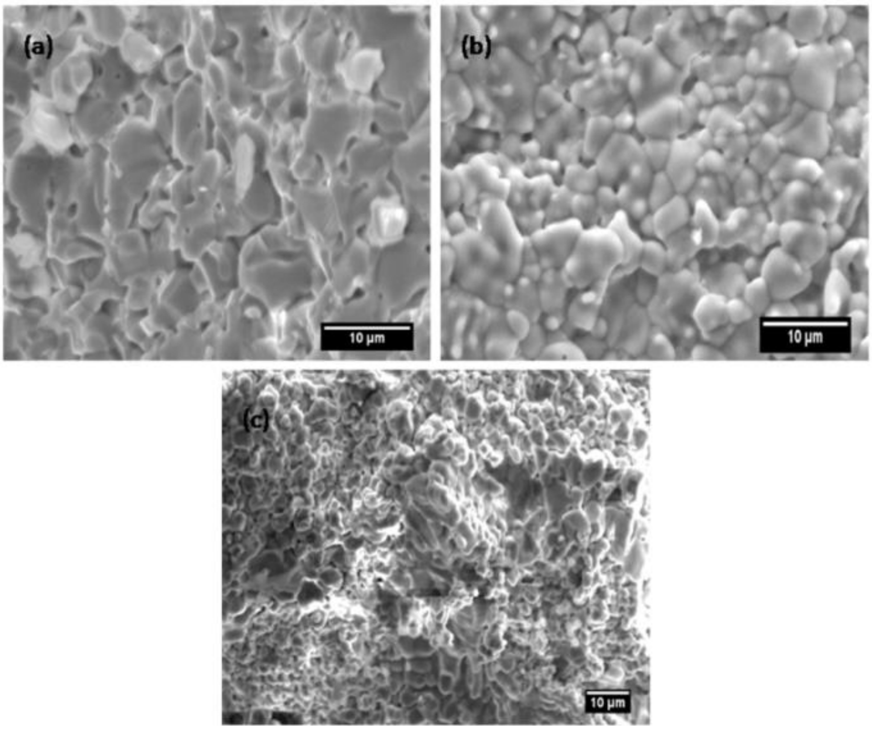

Figure 6.11. SEM cross-sectional images: (a) ZASH, (b) ZGSH and (c) ZUSH.

6.1.6 Particle size distribution

Dynamic laser scattering investigations were carried out for the 'as-prepared' and the calcined powders obtained in both the heating methods. The particle size distribution of 'as-prepared' and calcined powder obtained by using citric acid as fuel are shown in Fig. 6.12. The 'as-prepared' and calcined powders showed unimodal distribution. 50% of the particles were in the size range <115 and 112 µm for ZACM and ZACH respectively. Fig. 6.13 shows the particle size distribution of 'as-prepared' and calcined powders obtained using glycine as fuel. The calcined powders, ZGCM and ZGCH showed particle size of <84 and 133 μm respectively for 50% particles. The distribution was unimodal with narrower distribution as compared to the powders obtained using citric acid as the fuel. The lower particle size of the calcined powders obtained using microwave heating was due to the fast combustion which would have resulted in more gas evolution within a short time. The particle size distribution of the 'as-prepared' and the calcined powder obtained by using urea as fuel are shown in Fig. 6.14. 50% of the particles were in the size range of <274 and 262 μm for ZUCM and ZUCH, respectively. The 'as-prepared' and the calcined powder obtained by hot-plate heating using urea as fuel showed a bimodal distribution while that obtained using microwave heating showed a unimodal distribution. This might be due to the localized heating and would have resulted in partial sintering of the powder in the case of hot-plate heating compared to the uniform heating in the case of microwave. The particle sizes of the 'as-prepared' and calcined samples are given in Table 6.3.

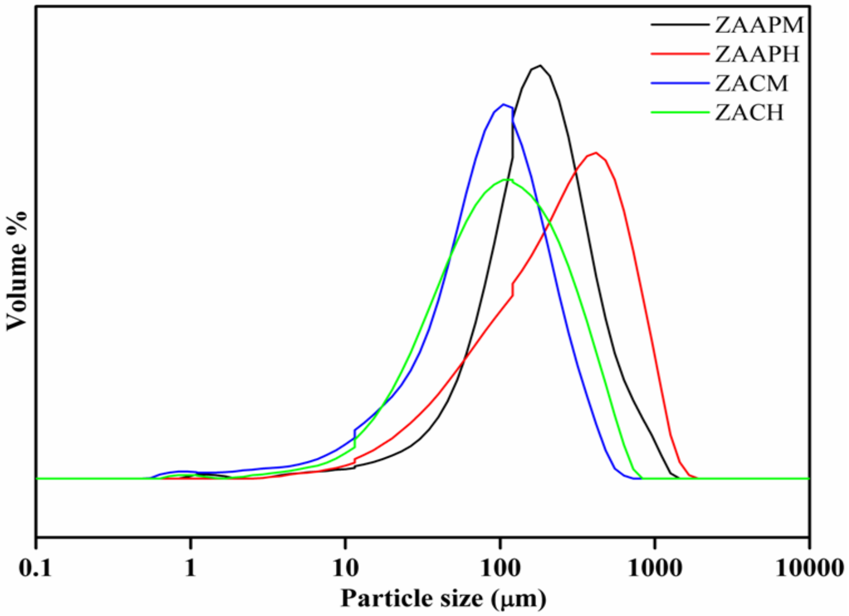

Figure 6.12. Particle size distribution of 'as-prepared' and calcined powders prepared using citric acid as fuel

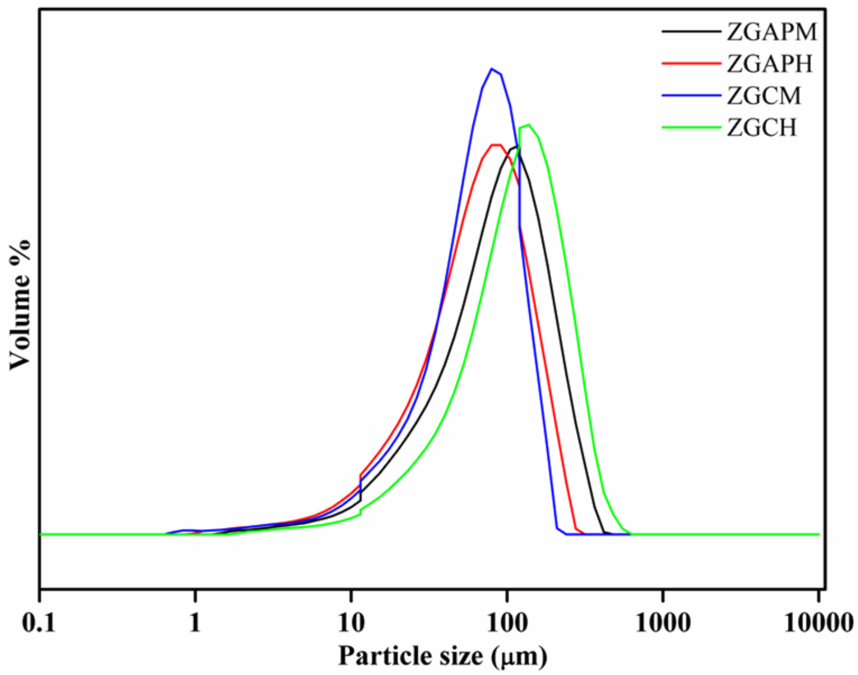

Figure 6.13. Particle size distribution of 'as-prepared' and calcined powders prepared using glycine as fuel

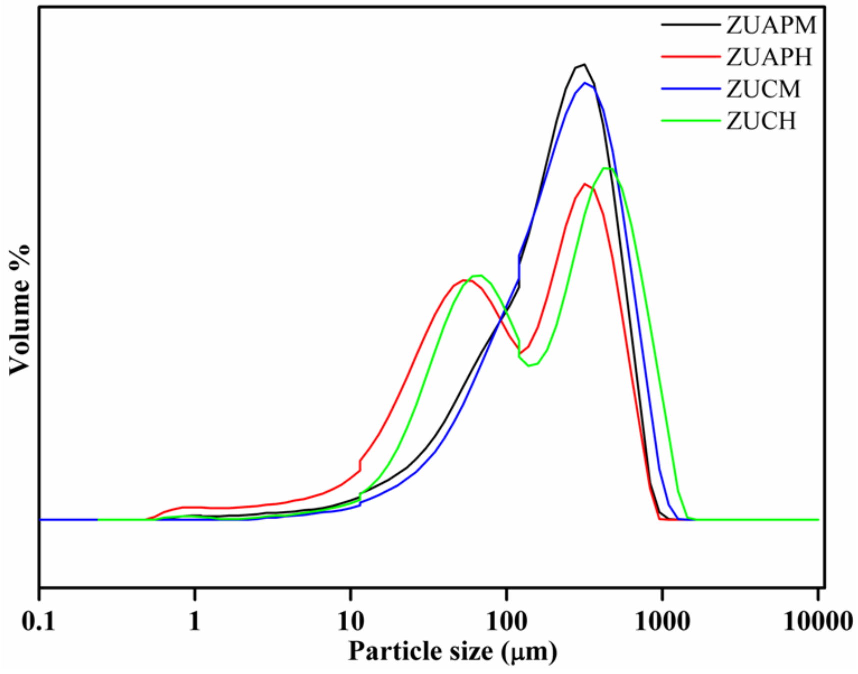

Figure 6.14. Particle size distribution of 'as-prepared' and calcined powders prepared using urea as fuel

Table 6.3. Particle size distribution of the 'as-prepared' and calcined powders.

Sample	d (0.1) µm	d (0.5) µm	d (0.9) µm
ZAAPM	32.5	268.8	726.8
ZAAPH	48.8	299.2	887.2
ZACM	24.9	115.6	322.9
ZACH	26.3	112.9	384.6
ZGAPM	24.7	101.4	244.3
ZGCM	23.2	84.4	175.1
ZGCH	36.0	133.8	307.5
ZUAPM	20.9	147.1	646.3
ZUAPH	50.1	284.4	699.7
ZUCM	58.6	274.0	700.1
ZUCH	39.2	262.5	962.2

6.1.7 Specific surface area of calcined powders

The values of the specific surface area of the calcined powders are given in Table 6.4. The specific surface area of powders in all the cases were comparable except in the case of urea-derived powder. When urea was used as the fuel, microwave-assisted synthesis yielded powders with a lower surface area, perhaps due to agglomeration. Similar result was obtained by Silva et al. [157] who have reported a specific surface area of 1.3 m^2g^{-1} for 8 mol.% YSZ prepared by combustion method (hot-plate heating) using urea as the fuel, which is lower compared to the values for the samples obtained using urea as fuel in the present study. However, the specific surface area of the powders prepared using glycine as the fuel by combustion method was reported to be 21.6 m^2g^{-1} [157], which is higher compared to the results obtained in the present study. Biswas et al. [163] have also reported a lower specific surface area of 2.66 m^2g^{-1} for the powders synthesized using urea as fuel similar to the value reported by Silva et al. [157]. This could be due to the higher combustion temperature with urea as fuel as reported by Silva et al. [157].

Table 6.4. Specific surface area and residual carbon content of YSZ samples

Sample name	SSA (m^2g^{-1})	Residual carbon content (ppm)
ZACM	6	5800 ± 514
ZASM	-	170 ± 18
ZACH	7.11	1600 ± 68
ZASH	-	-
ZGCM	7.18	5000 ± 760
ZGSM	-	100 ± 3
ZGCH	7.76	1750 ± 212
ZGSH	-	-
ZUCM	4.48	700 ± 82
ZUSM	-	160 ± 32
ZUCH	6	260 ± 30
ZUSH	-	-

6.1.8 Residual carbon in the samples

The residual carbon content of the calcined and sintered samples are given in Table 6.4. Kaus et al. [162] have reported that the presence of residual carbonaceous species would affect the sinterability of the powder. The amount of carbon in the citric acid-derived ‘as-prepared’ powders was found to be in the range of 20 to 30 wt.%. The amount of residual carbon in the ‘as-prepared’ powders was found to be very high, perhaps the carbonaceous material was not fully removed by combustion reaction. The amount of residual carbon in ZACM and ZACH was 5800 and 1600 ppm, respectively. In the case of ZGCM and ZGCH, the residual carbon contents were 5000 and 1750 ppm, respectively. The lower residual carbon content in the hot-plate derived calcined powders could be due to the longer duration of heating. The residual carbon contents in ZUCM and ZUCH were 700 and 260 ppm, respectively. It is seen that the amount of residual carbon in the calcined samples mainly depends on the type of fuel used. The carbon content in the fuel decreases in the order of citric acid > glycine > urea. Accordingly, the amount of residual carbon in ZACM was more compared to that of ZGCM. The amount of residual carbon was least in ZUCM. Carbon content in all the sintered samples was found to be less than 200 ppm.

6.1.9 Density of the sintered compacts

The densities of the sintered compacts ZASM and ZASH were in the range of 94 to 96% of TD and those of ZGSM and ZGSH were in the range of 95 to 97% TD. The samples ZUSM and ZUSH showed a density of 90% TD. Silva et al. [157] have reported a similar trend in the densities of YSZ compacts obtained from glycine and urea derived powders. The lower density of the sintered compacts obtained using powders prepared using urea as the fuel could be due to the presence of hard agglomerates, which resulted in differential densification during sintering.

6.1.10 Impedance measurement and ionic conductivity

Typical Nyquist plot of the impedance measured at different temperatures for the sample ZASM is shown in Fig. 6.15. In the present study the total pellet resistance was taken as the low frequency intercept of the combined arc on the real Z′-axis as mentioned in Ref. [159]. The total pellet resistances comprise the bulk resistance (R_b) and resistance due to grain boundary (R_{gb}). The total ionic conductivity obtained at 956 K was 3.15×10^{-3} Scm^{-1} for ZASM and that for ZASH at 905 K was 1.8×10^{-3} Scm^{-1}. The total ionic conductivity obtained for ZGSM and ZGSH at 957 K were 2.7×10^{-3} and 1.7×10^{-3} Scm^{-1}, respectively. He et al. [160] have reported a conductivity of 1.6×10^{-2} Scm^{-1} and 2.4×10^{-2} Scm^{-1} at 1123 K for 8 mol.% YSZ powders obtained at two different pre-sintering temperatures 1273 and 1473 K, respectively using glycine-nitrate process. Rajeswari et al. [221] have reported an ionic conductivity of 9×10^{-2} Scm^{-1} at 1073 K for the commercially available YSZ powder (TZ-8Y) sintered by conventional ramp and hold method. The variation of oxide-ion conductivity for all the sintered samples in the temperature range 673 to 1073 K is shown in Fig. 6.16. The ionic conductivity of the citric acid derived powders was found to be slightly higher compared to that of glycine derived powders, despite the density of the later outweighed the density of the former. It is surmised that the difference in the amount of cubic / tetragonal phases between the samples and the difference in the morphology of these compacts could be the reason for this difference in ionic conductivity. Mondal et al. [222] have reported that if the concentration of Y_2O_3 exceeds more than 2.4 mol.%, the tetragonal phases also get stabilized by the presence of small grain sizes. The Arrhenius plots of all the compacts were linear. The activation energy was calculated from the slope of the fitted line. The activation energies were 1, 0.976, 1.02, 0.98 and 1.04 eV, respectively, for ZASM, ZASH, ZGSM, ZGSH and ZUSM. Even though the activation energy of ZUSM was similar to the samples ZASM and ZGSM, its ionic conductivity was lower due to its lower density. Shukla et al. [159] have reported the activation energy for the 8 mol.% YSZ as 1 eV in the temperature range 623 to 1073 K which is in agreement with the present study.

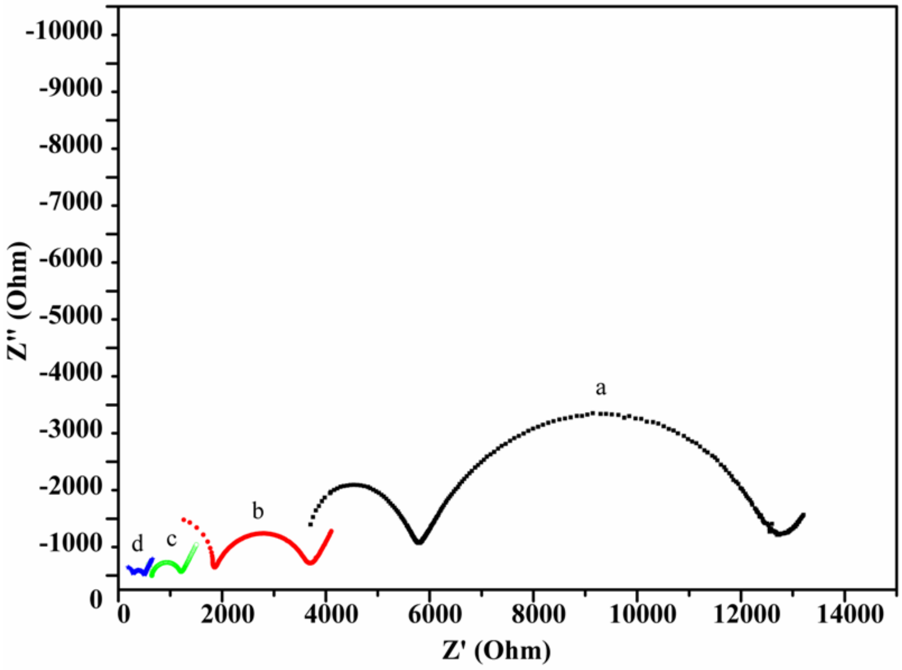

Figure 6.15. Typical Nyquist plot for ZASM at different temperatures: (a) 673, (b) 723, (c) 773, and (d) 823 K

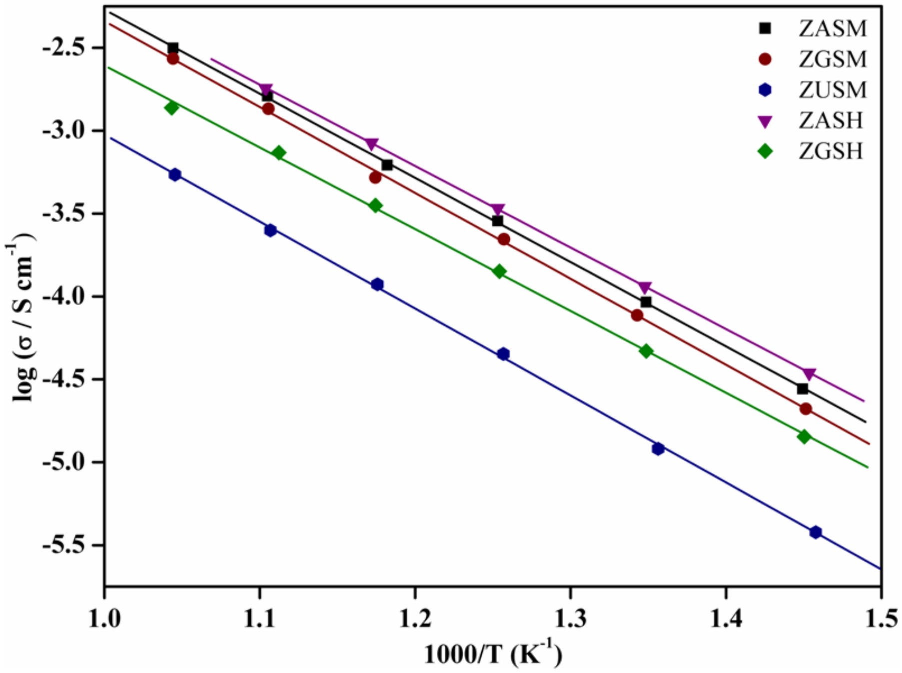

Figure 6.16. Arrhenius plots with corresponding linear fits of ZASM, ZGSM, ZUSM, ZASH and ZGSH

6.2 Conclusion

Nanocrystalline 8 mol.% YSZ was synthesized by gel combustion method using three different fuels-citric acid, glycine and urea. The crystallite size, microstructure and ionic conductivity of the samples depended on the nature of the fuel used. The sintered compacts prepared from powders obtained using citric acid or glycine as combustion fuel yielded density in the range of 94 to 97% TD. The TD of the compacts prepared from the powder obtained using urea as the fuel was in the range of 90% TD. The activation energies for the oxide ion conduction of the sintered pellets obtained from microwave-derived powders using citric acid, glycine or urea as fuels were 1, 1.02 and 1.04 eV respectively. However, the compacts from hot-plate derived powders using citric acid and glycine as fuels were 0.976 and 0.98 eV respectively. The ionic conductivity of the sintered compacts obtained using hot-plate heated and urea-derived powders showed a lower conductivity compared to the other samples. The present study showed that 8 mol.% YSZ powder suitable for solid electrolyte application can be easily prepared by microwave assisted gel-combustion synthesis using either citric acid or glycine as the combustion fuel.

Chapter 7

Summary and conclusions

In the present study, nanocrystalline sinteractive boron carbide powder was synthesized by the precursor method. The amount of free carbon present as an impurity in the synthesized product was minimized by suitable modification in the preparation of precursor. The important factors influencing the presence of free carbon in the B_4C product synthesized by precursor method are the homogeneity of the reactants (such as B_2O_3/H_3BO_3 and C components in the precursor), temperature and rate of reaction. Improving the homogeneity of the components in the precursor helps to reduce the amount of free carbon impurity in the final product of B_4C. In order to improve the homogeneity of the reactants in the precursor, two different methods were adopted: a) mixing boric oxide-sucrose in a suitable dispersion medium and removal of the dispersion medium by freeze-drying followed by heat-treatment and b) preparation of a condensed product by microwave-assisted heating of a solution containing mannitol and boric acid followed by thermal decomposition of the condensed product.

The sintering of boron carbide ceramic compacts is generally influenced by the powder characteristics such as surface area, particle size distribution, the presence of free carbon as the impurity phase etc. The present study has been carried out to optimize the process parameters to obtain nanocrystalline boron carbide with desired powder characteristics for sintering at relatively lower temperatures using advanced sintering techniques. The nanocrystalline boron carbide thus prepared in the present study was sintered using two advanced techniques viz., spark plasma sintering and hot pressing.

A new method based on microwave-assisted combustion synthesis was also developed to prepare nanocrystalline yttria-stabilized zirconia in the present study.

7.1 Studies on the synthesis of nc-B_4C by the precursor method

Nanocrystalline boron carbide was synthesized by employing the precursor method in the present study. Precursors were prepared using three different methods:

a) Direct solid-state mixing of the reactants B_2O_3 and sucrose followed by heat-treatment of this reactant mixture to optimize the temperature of preparation of precursor. The reactants, B_2O_3 and sucrose, were taken in such a way that CBMR was equal to 3.38 (C/B wt.% ratio = 1.87). The precursor was also prepared using B_2O_3 and sucrose with the stoichiometric CBMR of 3.5 (C/B. wt.% ratio = 1.94) at the optimized temperature.

b) Mixing B_2O_3 and sucrose (CBMR = 3.38) in a suitable medium followed by freeze-drying of the slurry to remove the medium. Subsequently, the freeze-dried powder was heat-treated to get the precursor.

c) Preparation of a condensed product by microwave-assisted heating of a solution containing mannitol and boric acid. The condensed product was thermally decomposed to obtain the precursor. Precursors were prepared from mannitol and boric acid with CBMR = 3.38 (C/B wt.% ratio = 1.87) and CBMR = 6 (C/B wt.% ratio = 3.33).

In the present study, the preparation and further processing of the precursor with CBMR 3.38 were carried out systematically using B_2O_3 and sucrose with the objective to synthesize nanocrystalline boron carbide which is suitable for sintering at a relatively lower temperature as compared to that synthesized by the conventional carbothermic reduction process. The temperature and duration of reaction were optimized to get a final product of boron carbide with a minimum amount of free carbon as the impurity phase. The optimized results obtained with CBMR equal to 3.38 were compared with those obtained with the stoichiometric reactants, i.e. CBMR equal to 3.5. Systematic studies were carried out to optimize the temperature of preparation of precursor using boric oxide as the boron source and sucrose as the carbon source.

A graphite resistance heating furnace was made in-house to study the synthesis of boron carbide from the precursor. The graphite serves as the heating element and also as the container material for the reactants. In the precursor method, reactants were mixed in solid state; the mixture tends to be inhomogeneous. This often results in a product mixture of B_4C and a significant amount of free carbon, necessitating a suitable modification in the process. Improving the homogeneity of the components in the precursor helps to reduce the free carbon content in the final product significantly. In the present study, the B_2O_3 and sucrose were made into a slurry in media such as water or ethanol and freeze-dried to remove the medium. The precursor for the synthesis of boron carbide was prepared by heat-treatment of this dried product. The homogeneity of the precursor can also be improved if the components are mixed on a molecular scale, say by complexation. Mannitol forms a stable 2:1 complex with boric acid via B-O-C bonds. The product formed by the thermal decomposition of the condensed product was the precursor for the synthesis of boron carbide. The excess carbon than that required to form B-O-C bond was removed by the thermal decomposition of the condensed product. In this study, two complexes were prepared by taking mannitol and boric acid with different carbon to B_2O_3 mole ratio: a) CBMR of 3.38 (C/B wt%. ratio = 1.87) and b) CBMR of 6 (excess carbon, C/B wt.% ratio = 3.33). A higher CMBR was chosen to explore the effect of thermal decomposition of the condensed product on the removal of excess carbon than that required for the stoichiometric reaction as per Eq. (3.2). The mannitol-boric acid condensed product was prepared by microwave-assisted heating of the solution of mannitol and boric acid. The precursors and the boron carbide synthesized from these precursors were characterized for chemical composition, phase purity and morphology. The conclusions from these studies are:

- The free carbon content in the product was used as a measure of homogeneity of the reactants in the precursor.
- Boron carbide synthesized from all these precursors was found to be nanocrystalline.
- The optimized temperature for the preparation of precursor using boric oxide and sucrose (CBMR = 3.38, C/B wt%. ratio = 1.87) was found to be 873 K. The free carbon content in the product obtained from this precursor at 1873 K (10 min) was found to be 2.5 wt.%. The boron and total carbon contents were found to be 76.6 wt.% and 25.4 wt.% respectively.
- A lower carbon to B_2O_3 mole ratio (3.38) as compared to the stoichiometric ratio (3.5) was found to be suitable for the synthesis of B_4C using a precursor method as it resulted in nc-B_4C with lower free carbon content compared to that obtained from stoichiometric reactants.
- The precursor was also prepared by freeze-drying of (B_2O_3 + sucrose) slurry followed by heat-treatment at 873 K. The free carbon content in the product obtained from this precursor at 1873 K (10 min) was found to be ~1.5 wt.%. The boron and total carbon contents were found to be 80.2 wt.% and 21.7 wt.% respectively.

- Ethanol was found to be not suitable as the solvent for the freeze-drying of the slurry prepared using B_2O_3 and sucrose as it resulted in the loss of B_2O_3 during freeze-drying.
- Use of mannitol as a complexing agent was found to be beneficial compared to sucrose as this resulted in the formation of B-O-C bonds and thereby improved the dispersion of boron and carbon components.
- The optimized precursor preparation temperature in the case of the mannitol-boric acid complex with CBMR equal to 3.38 (C/B wt.% ratio = 1.87) was found to be 773 K. The free carbon content in the product obtained at 1873 K (10 min) from this precursor was found to be <0.5 wt.%.
- The optimized precursor preparation temperature was 873 K in the case of the mannitol-boric acid complex with CBMR equal to 6 (C/B wt.% ratio = 3.33). The free carbon content in the product obtained at 1873 K (10 min) from this precursor was found to be 1.3 wt.%.

7.2 Studies on the sintering of nc-B_4C by SPS technique

Consolidation of B_4C powder into high-density compacts is difficult due to the high melting point, low self-diffusion coefficient and the presence of covalent bonding. The present study explores the effect of powder characteristics of nanocrystalline boron carbide prepared by the precursor method on densification of B_4C compacts by SPS technique. A furnace was made in-house for the bulk synthesis of nc-B_4C by the precursor method. nc-B_4C synthesized using B_2O_3-sucrose precursor was used for spark plasma sintering studies. The spark plasma sintering of nc-B_4CAW1 was carried out at 1873, 1973 and 2073 K. Sintering of c-B_4CAW (procured from a vendor) was also carried out at 1973 K. The microstructure of the sintered compacts was studied using SEM. Microhardness of the sintered compacts were measured using the Vickers indentation method. The conclusions from these studies are:

- The nanocrystalline boron carbide synthesized in the present study showed better densification as compared to the microcrystalline boron carbide.
- The density of the nc-B_4C sintered at 1973 K (nc-B_4C17) was found to be ~95% TD as compared to the density of c-B_4C17 (~90% TD)
- The microhardness of nc-B_4C17 was found to be ~24 GPa.
- The nanocrystalline B_4C sintered using SPS showed a homogeneous microstructure without abnormal grain growth.

7.3 Studies on the sintering of nc-B_4C by the hot pressing technique

The present study explores the effect of powder characteristics of nanocrystalline boron carbide synthesized using the precursor method on hot pressing. nc-B_4C synthesized using B_2O_3-sucrose precursor was used for hot pressing. The hot pressing of nc-B_4CAW2 was carried out at 1973 and 2073 K. Sintering of c-B_4CAW (from a commercial source) was also carried out at 1973 and 2073 K. The microstructure of the sintered compacts was studied using SEM. Microhardness of the hot pressed compacts were measured by Vickers indentation method. The conclusions from these studies are:

- The densification was not effective at 1973 K for nc-B_4CHP17 and c-B_4CHP17. The density achieved at 1973 K was low (<60% TD for both nc-B_4CHP17 and c-B_4CHP17).
- The density of nanocrystalline boron carbide sintered at 2073 K (nc-B_4CHP18) was found to be <80% TD and that of c-B_4CHP18 was found to be ~87% TD.

- The microhardness of nc-B_4CHP18 and c-B_4CHP18 were comparable (~11.1 and 12.3 GPa respectively).
- Both sintered compacts (nc-B_4CHP18 and c-B_4CHP18) showed a homogeneous microstructure.

7.4 Studies on the synthesis of yttria-stabilized zirconia

Yttria-stabilized zirconia was synthesized by combustion method. Two different heating methods (microwave-assisted and hot-plate) were used for the synthesis. Three different fuels citric acid, glycine and urea were used for the combustion. Microwave-assisted combustion synthesis of yttria-stabilized zirconia was carried out by fixing the fuel to oxidant mole ratio in the combustion mixture equal to 1. The powders obtained were calcined and then sintered. Conventional heating using hot-plate was also carried out by fixing the fuel to oxidant mole ratio of the reactants in the combustion mixture as equal to 1. The powder synthesized using microwave-assisted heating was characterized for phase purity, specific surface area, phase content by Raman spectroscopic technique, particle size distribution and microstructural analysis. The ionic conductivity of the sintered compacts was determined using ac-impedance spectroscopy. The conclusions from these studies are:

- The crystallite size, microstructure and ionic conductivity of the samples depend on the nature of the fuel used for combustion synthesis.
- The sintered compacts of YSZ prepared from powders obtained by combustion synthesis using citric acid or glycine as combustion fuel yielded density in the range of 94 to 97% TD.
- The TD of the compacts of YSZ prepared from the powder obtained by combustion synthesis using urea as the combustion fuel was in the range of 90% TD.

- The activation energies for the oxide ion conduction of the sintered pellets obtained from microwave-derived powders using citric acid, glycine or urea as fuels were 1, 1.02 and 1.04 eV respectively.
- The activation energies for the oxide ion conduction of the sintered pellets obtained from hot-plate derived powders using citric acid and glycine as fuels were 0.976 and 0.98 eV respectively.
- The present study showed that 8 mol.% YSZ powder suitable for solid electrolyte application can be easily prepared by microwave-assisted gel-combustion synthesis using either citric acid or glycine as the combustion fuel.

Chapter 8

Scope for future studies

In the present study, nanocrystalline boron carbide was synthesized using the precursor method by taking two different boron sources (boric oxide and boric acid) and carbon sources (sucrose and mannitol). The B_2O_3 and sucrose were taken in such a way that the carbon to B_2O_3 mole ratio is 3.38 compared to the stoichiometric ratio, 3.5. The precursor was prepared from B_2O_3 and sucrose and B_4C was synthesized from this precursor. It was found that lower carbon to B_2O_3 mole ratio resulted in a product with lower free carbon impurity as compared to the stoichiometric ratio. A systematic study of the preparation of precursor and processing of the precursor using different carbon sources and boron sources by varying the carbon to B_2O_3 mole ratios can be carried out. The present study was focused on the minimization of free carbon in the final product. Studies should be carried out to maximize the yield of B_4C using various precursors.

Precursor using mannitol-boric acid was prepared by microwave-assisted heating in the present study. The H_3BO_3 and mannitol were taken in such a way that the carbon to B_2O_3 mole ratio is 3.38 and 6 for the preparation of precursor. However, studies on the synthesis of B_4C using microwave energy are limited in the literature. Studies can be carried out to explore the advantages of microwave-assisted synthesis of B_4C with different carbon sources and boron sources. The effect of various carbon sources and boron sources on the purity and yield of boron carbide may be studied systematically.

In the present study, spark plasma sintering of nanocrystalline boron carbide obtained by the precursor method using boric oxide-sucrose precursor was carried out at 1873, 1973 and 2073 K by fixing the heating rate and applied pressure. Hence, one can study the influence of sintering parameters such as temperature, pressure and heating rate on the densification, microstructure and mechanical properties of nc-B_4C by varying the particle size of boron carbide powder. The kinetics of sintering of nc-B_4C and the mechanism of densification using SPS can also be taken up. SPS of boron carbide synthesized using other precursors also can be studied. Spark plasma sintering of nanocrystalline boron carbide was carried out without sintering additive in the present study. Different sintering additive and their role in the densification of boron carbide synthesized using the precursor method can also be studied.

Sintering of nc-B_4C was also carried out in this study by using hot pressing at different temperatures, 1973 and 2073 K and compared the results with that of sinterability of commercially available B_4C (perhaps prepared by carbothermic reduction route). Heating rate, applied pressure and duration of heating were constant in the present study. One can study the influence of applied pressure on the densification by keeping the temperature constant and influence of heating rate by keeping the applied pressure and temperature constant. Studies can be carried out to optimize the temperature to get high-density boron carbide compacts using nc-B_4C synthesized from different precursors.

Nanocrystalline materials can be densified at a lower temperature compared to microcrystalline materials. Hence, conventional pressureless sintering of nc-B_4C can be studied. Sintering using dilatometer can be carried out to study the kinetics of sintering of nc-B_4C synthesized by using precursors prepared from different sources of carbon and boron.

Nanocrystalline yttria-stabilized zirconia was synthesized using the combustion method by employing two different heating methods (microwave and hot-plate) in the present study. Three different fuels such as citric acid, glycine and urea were used as the fuel by fixing the fuel to oxidant mole ratio as 1. Studies can be carried out by varying the fuel to oxidant ratio and also using mixed fuels. The effect of fuel to oxidant ratio on the conductivity of the YSZ solid electrolyte prepared by combustion synthesis can be studied.

References

[1] M.R. Kolhe, P.G. Khot, India's energy scenario-current and future, Int. J. Manage., 6 (2015) 47-66.

[2] http://www.world-nuclear.org/information-library/country-profiles/countries-g-n/india.aspx (accessed 2 February 2018).

[3] http://www.npcil.nic.in/content/302_1_AllPlants.aspx (accessed 4 February 2018).

[4] S. Banerjee, H.P. Gupta, The evolution of the Indian nuclear power programme, Prog. Nucl. Energy, 101 (2017) 4-18.

[5] S.A. Bhardwaj, Indian nuclear power programme-past, present and future, Sadhana, 38 (October 2013) 775-794.

[6] http://www.barc.gov.in/about/anushakti_sne.html (accessed 5 February 2018).

[7] http://dae.nic.in/?q=node/212 (accessed 5 February 2018).

[8] P.N. Prasad, An introduction to nuclear reactors, IANCAS bulletin, Vol. 1, No. 1 (2002) 3-8.

[9] S. Glasstone, A. Sesonske, Nuclear reactor engineering-Reactor design basics, Ed. 4, CBS publishers and distributors Pvt. Ltd., India, (2004).

[10] http://dae.nic.in/?q=node/179 (accessed 5 February 2018).

[11] D.E. Mahagin, R.E. Dahl, "Nuclear applications of boron and the borides", pp. 612-630 in: Boron and refractory borides, Ed. V.I. Matkovich, Springer-Verlag, Berlin, Heidelberg, New York (1977).

[12] D.E. Mahagin, Fast reactor neutron absorber materials, The American Ceramic Society, (1979), HEDL-SA-1690-FP.

[13] IAEA-TECDOC-884, Absorber Materials, control rods and designs of shutdown systems for advanced liquid metal fast reactors, Proceeding of technical committee meeting held in Obninsk, Russian Federation, 3-7 July, (1995).

[14] V.R. Babu, R. Veerasamy, S. Patri, S.I.S. Raj, S.C.S.P.K. Krovvidi, S.K. Dash, C. Meikandamurthy, K.K. Rajan, P. Puthiyavinayagam, P. Chellapandi, G. Vaidyanathan, S.C. Chetal, Testing and qualification of control and safety rod and its drive mechanism of fast breeder reactor, Nucl.

Eng. Des., 240 (2010) 1728-1738.

[15] S. Patri, R. Vijayashree, S.S. Kumar, P.A. Kumar, M. Sabih, S. Chandramouli, P.N. Rao, C. Meikandamurthy, V. Prakash, P. Selvaraj, Investigations on the availability of second shutdown system of Indian FBR, Nucl. Eng. Des., 319 (2017) 91-105.

[16] R. Dheenadhayalan, A. Venkatesan, K. Madhusoodanan, P. Chellapandi, Design of instrumentation for control and safety rod drive mechanisms of prototype fast breeder reactor, Int. J. Nucl. Energy Sci. Technol., 7 (2013) 380-395.

[17] K. Devan, A. Riyas, M. Alagan, P. Mohanakrishnan, A new physics design of control safety rods for prototype fast breeder reactor, Ann. Nucl. Energy, 35 (2008) 1484-1491.

[18] B. Kryger, J. M. Escleine, pp.533-565 in: The nuclear fuel of pressurized water reactors and fast reactors design and behaviour, Ed. H. Bailly, D. Menessier, C. Prunier, Lavoisier Publishing, France (1999).

[19] G.N. Makarenko, "Borides of the IVb Group", pp. 310 in: Boron and refractory borides, Ed. V.I. Matkovich Springer-Verlag, Berlin, Heidelberg, New York (1977).

[20] F. Thevenot, Boron carbide: a comprehensive review, J. Eur. Ceram. Soc., 6 (1990) 205-225.

[21] P.F. Rogl, J. Vřešťál, T. Tanaka, S. Takenouchi, The B-rich side of the B–C phase diagram, Calphad, 44 (2014) 3-9.

[22] M. Beauvy, Stoichiometric limit of carbon-rich boron carbide phases, J. Less-Common Met., 90 (1983) 169-175.

[23] H.O. Pierson, Handbook of refractory carbides and nitrides-Properties, characteristics, processing and applications, Noyes Publications Westwood, New Jersey, U.S.A, (1996) 142-143.

[24] R. Lazzari, N. Vast, J.M. Besson, S. Baroni, A.D. Corso, Atomic structure and vibrational properties of icosahedral B_4C boron carbide, Phy. Rev. Lett., 83 (1999) 3230-3233.

[25] A.K. Suri, C. Subramanian, J.K. Sonber, T.S.R.Ch. Murthy, Synthesis and consolidation of boron carbide: a review, Int. Mater. Rev., 55 (2010) 4-40.

[26] A. Alizadeh, E.T. Nassaj, N. Ehsani, Synthesis of boron carbide powder by a

carbothermic reduction method, J. Eur. Ceram. Soc., 24 (2004) 3227-3234.

[27] C.H. Jung, M.J. Lee, C.J. Kim, Preparation of carbon-free B_4C powder from B_2O_3 oxide by carbothermal reduction process, Mater. Lett., 58 (2004) 609-614.

[28] T. Kobayashi, K. Yoshida, T. Yano, Effects of addition of seed grains on morphology and yield of boron carbide powders synthesized by carbothermal reduction, Ceram. Int., 39 (2013) 3849-3856.

[29] T. Kobayashi, K. Yoshida, T. Yano, Effects of heat-treatment temperature and starting composition on morphology of boron carbide particles synthesized by carbothermal reduction, Ceram. Int., 39 (2013) 597-603.

[30] S. Herth, W.J. Joost, R.H. Doremus, R.W. Siegel, New Approach to the synthesis of nanocrystalline boron carbide, J. Nanosci. Nanotechnol., 6 (2006) 954-959.

[31] M.P.L.N. Rao, G.S. Gupta, P. Manjunath, S. Kumar, A.K. Suri, N. Krishnamurthy, C. Subramanian, Temperature measurements in the boron carbide manufacturing process-a hot model study, Int. J. Refract. Met. Hard Mater., 27 (2009) 621-628.

[32] M.P.L.N. Rao, G.S. Gupta, P. Manjunath, S. Kumar, A.K. Suri, N. Krishnamurthy, C. Subramanian, Core temperature measurement in carbothermal reduction processes, Thermochim. Acta, 482 (2009) 66-71.

[33] Y.N. Tumanov, The synthesis of boron carbide in a high frequency electromagnetic field, J. Less-Common Met., 67 (1979) 521-529.

[34] G. Goller, C. Toy, A. Tekin, C.K. Gupta, The Production of boron carbide by carbothermic reduction, High Temp. Mater. Processes, 15 (1996) 117-122.

[35] A. Alizadeh, E. Taheri-Nassaj, N. Ehsani, H.R. Baharvandi, Production of boron carbide powder by carbothermic reduction from boron oxide and petroleum coke or carbon active, Adv. Appl. Ceram., 105 (2006) 291-296.

[36] Y. Gao, A. Etzold, T. Munhollon, W. Rafaniello, R. Haber, Processing factors influencing the free carbon contents in boron carbide powder by rapid carbothermal reduction, Diamond Relat. Mater., 61 (2016) 14-20.

[37] R.F.K. Gunnewiek, P.M. Souto, R.H.G.A. Kiminami, Synthesis of nanocrystalline boron carbide by direct microwave carbothermal reduction

of boric acid, J. Nanomater., volume (2017), Article ID 3983468, 1-8.

[38] F. Farzaneh, F. Golestanifard, M.S. Sheikhaleslami, A.A. Nourbakhsh, New route for preparing nanosized boron carbide powder via magnesiothermic reduction using mesoporous carbon, Ceram. Int., 41(2015)13658-13662.

[39] R.M. Mohanty, K. Balasubramanian, S.K. Seshadri, Multiphase formation of boron carbide in B_2O_3-Mg-C based micropyretic process, J. Alloys Compd., 441 (2007) 85-93.

[40] M. Alkan, M.S. Sonmez, B. Derin, O. Yücel, Effect of initial composition on boron carbide production by SHS process followed by acid leaching, Solid State Sci., 14 (2012) 1688-1691.

[41] P. Asgarian, A. Nourbakhsh, P. Amin, R.E. Kahrizsangi, K.J.D. MacKenzie, The effect of different sources of porous carbon on the synthesis of nanostructured boron carbide by magnesiothermic reduction, Ceram. Int., 40 (2014) 16399-16408.

[42] P. Singh, B. Singh, M. Kumar, A. Kumar, One step reduction of boric acid to boron carbide nanoparticles, Ceram. Int., 40 (2014) 15331-15334.

[43] C. Subramanian, A.K. Suri, T.S.R.Ch. Murthy, Development of boron-based materials for nuclear applications, BARC Newsletter, Issue No. 313, Mar-Apr, (2010) 14-22.

[44] K.U. Nair, D.K. Bose, C.K. Gupta, The production of elemental boron by fused salt electrolysis, Miner. Process. Extr. Metall. Rev., 9 (1992) 283-291.

[45] A. Jain, S. Anthonysamy, G.S. Gupta, V. Ganesan, Processing of enriched elemental boron (^{10}B 65 at. %), Mater. Chem. Phys., 140 (2013) 335-342.

[46] A. Jain, C. Ghosh, T.R. Ravindran, S Anthonysamy, R. Divakar, E. Mohandas, G.S. Gupta, Structural characterization of electrodeposited boron, Bull. Mater. Sci., 36 (2013) 1323-1329.

[47] B. Chang, B.L. Gersten, S.T. Szewczyk, J.W. Adams, Characterization of boron carbide nanoparticles prepared by a solid state thermal reaction, Appl. Phys. A, 86 (2007) 83-87.

[48] J.K. Sonber, T.S.R.Ch. Murthy, C. Subramanian, R.K. Fotedar, R.C. Hubli, A.K. Suri, Synthesis, densification and characterization of boron carbide, Trans. Ind. Ceram. Soc., 72 (2013) 100-107.

[49] U.A. Tamburini, Z.A. Munir, Influence of synthesis temperature on the

defect structure of boron carbide: experimental and modeling sudies, J. Am. Ceram. Soc., 88 (2005) 1382-1387.

[50] A.S. Ramos, S.P. Taguchi, E.C.T. Ramos, V.L. Arantes, S. Ribeiro, High-energy ball milling of powder B-C mixtures, Mater. Sci. Eng. A, 422 (2006) 184-188.

[51] Rafi-ud-din, G.H. Zahid, E. Ahmad, M. Maqbool, T. Subhani, W.A dil Syed, S.Z. Hussain, Effect of cellulose-derived structural homogeneity of precursor on the synthesis and morphology of boron carbide, J. Inorg. Organomet. Polym., 25 (2015) 995-999.

[52] M. Maqbool, Rafi-ud-din, G.H. Zahid, E. Ahmad, Z. Asghar, T. Subhani, M. Shahzad, I. Kaleem, Effect of saccharides as carbon source on the synthesis and morphology of B_4C fine particles from carbothermal synthesis precursors, Mater. Express, 5 (2015) 390-400.

[53] N. Tahara, M. Kakiage, I. Yanase, H. Kobayashi, Effect of addition of tartaric acid on synthesis of boron carbide powder from condensed boric acid-glycerin product, J. Alloys Compd., 573 (2013) 58-64.

[54] M. Kakiage, N. Tahara, I. Yanase, H. Kobayashi, Low-temperature synthesis of boron carbide powder from condensed boric acid-glycerin product, Mater. Lett., 65 (2011) 1839-1841.

[55] S. Corradetti, S. Carturan, L. Biasetto, A. Andrighetto, P. Colombo, Boron carbide as a target for the SPES project, J. Nucl. Mater., 432 (2013) 212-221.

[56] Rafi-ud-din, G.H. Zahid, Z. Asghar, M. Maqbool, E. Ahmad, T. Azhar, T. Subhani, M. Shahzad, Ethylene glycol assisted low-temperature synthesis of boron carbide powder from borate citrate precursors, J. Asian Ceram. Soc., 2 (2014) 268-274.

[57] A.K. Khanra, Production of boron carbide powder by carbothermal synthesis of gel material, Bull. Mater. Sci., 30 (2007) 93-96.

[58] A. Sinha, T. Mahata, B.P. Sharma, Carbothermal route for preparation of boron carbide powder from boric acid-citric acid gel precursor, J. Nucl. Mater., 301 (2002) 165-169.

[59] M. Kakiage, Y. Tominaga, I. Yanase, H. Kobayashi, Synthesis of boron carbide powder in relation to composition and structural homogeneity of

precursor using condensed boric acid-polyol product, Powder Technol., 221 (2012) 257-263.

[60] S. Mondal, A.K. Banthia, Low-temperature synthetic route for boron carbide, J. Eur. Ceram. Soc., 25 (2005) 287-291.

[61] P.M. Barros, I. Valeria, P. Yoshida, M.A. Schiavon, Boron-containing poly(vinyl alcohol) as a ceramic precursor, J. Non-Cryst. Solids, 352 (2006) 3444-3450.

[62] M. Kakiage, N. Tahara, R. Watanabe, I. Yanase, H. Kobayashi, Microstructure in precursor formed by controlling composition of condensed boric acid-poly(vinyl alcohol) product for low-temperature synthesis of boron carbide powder, J. Ceram. Soc. Jpn., 121 (2013) 40-44.

[63] I. Yanase, R. Ogawara, H. Kobayashi, Synthesis of boron carbide powder from polyvinyl borate precursor, Mater. Lett., 63 (2009) 91-93.

[64] M. Kakiage, N. Tahara, S. Yanagidani, I. Yanase, H. Kobayashi, Effect of boron oxide/carbon arrangement of precursor derived from condensed polymer-boric acid product on low-temperature synthesis of boron carbide powder, J. Ceram. Soc. Jpn., 119 (2011) 422-425.

[65] T.R. Pilladi, K. Ananthasivan, S. Anthonysamy, Synthesis of boron carbide from boric oxide-sucrose gel precursor, Powder Technol., 246 (2013) 247-251.

[66] P. Foroughi, Z. Cheng, From micron-sized particles to nanoparticles and nanobelts: structural non-uniformity in the synthesis of boron carbide by carbothermal reduction, Adv. Ceram. Armour XI, (2016) 51-62.

[67] K. Zakharova, A. Mednikova, V. Rumyantsev, T. Genusova, Synthesis of boroncarbide from boric acid and carbon-containing precursors, pp.4 in: Proc. Int. Conf. Nanomater. Appl. Prop., 2 (2013) (03AET09) .

[68] T.R. Pilladi, K. Ananthasivan, S. Anthonysamy, V. Ganesan, Synthesis of nanocrystalline boron carbide from boric acid-sucrose gel precursor, J. Mater. Sci., 47 (2012) 1710-1718.

[69] P. Foroughi, Z. Cheng, Understanding the morphological variation in the formation of B_4C via carbothermal reduction reaction, Ceram. Int., 42 (2016) 15189-15198.

[70] O. Avciata, C. Ergun, I. Erden, C. Ustundag, S. Yilmaz, S. Cihangir,

Synthesis of B_4C from sugar based precursor, in: Global Roadmap for Ceramics-ICC2 Proc., Verona, (2008) June 29-July 4. DOI:10.13140/RG.2.1.1508.5927.

[71] J.L. Watts, P.C. Talbot, J.A. Alarco, I.D.R. Mackinnon, Morphology control in high yield boron carbide, Ceram. Int., 43 (2017) 2650-2657.

[72] S.K. Vijay, R.K. Prabhu, V. Chandramouli, S. Anthonysamy, Synthesis of nanocrystalline boron carbide by sucrose precursor method: optimization of process conditions, Ceram. Int., 44 (2018) 4676-4684.

[73] T.R. Pilladi, Studies on the Synthesis and characterization of nanocrystalline boron carbide (Thesis) (2012) 59-78.

[74] R.S. Roth, T.A. Vanderah, "Experimental determination of phase equilibria diagrams in ceramics systems", pp. 3-18 in: Proceedings of the 9th Asian conference on Solid State Ionics: The science and technology of ions in motion, Ed. B. V. R. Chowdari, H.L. Yoo, G.M. Choi and J.H. Lee, (2004).

[75] S. Windisch, H. Nowotny, "Preparation of transition metal carbides and related compounds", pp. 533-559 in: Preparative methods in solid state chemistry, Ed. P. Hagenmuller, Academic Press, Newyork & London, (1972).

[76] M.D. Rasmussen, M. Akin, M.F. Berard, Effect of precursor freeze-drying conditions on the sinterability of hydroxide-derived Y_2O_3 powders, Ceram. Int., 10 (1984) 99-104.

[77] S. Shukla, Freeze-drying process: A review, Int. J. Pharm. Sci. Res., 2 (2011) 3061-3068.

[78] F.K. Roehrig, T.R. Wright, Freeze-drying: A unique approach to the synthesis of ultrafine powders, J. Vac. Sci. Technol., 9 (1972) 1368-1372.

[79] G.W. Oetjen, P. Haseley, Freeze-drying, Ed.2, Wiley-VCH GmbH & Co., (2004).

[80] Wei-ling Luan, L. Gao, J.K. Guo, Study on drying stage of nano scale powder preparation, Nanostruct. Mat., 10 (1998) 1119-1125.

[81] T. Fukasawa, Z.Y. Deng, M. Ando, Pore structure of porous ceramics synthesized from water-based slurry by freeze-dry process, J. Mater. Sci., 36 (2001) 2523-2527.

[82] F.K. Roehrig, T.R. Wright, Carbide synthesis by freeze-drying, J. Am.

Ceram. Soc., Discussions and Notes 55 (1972) 58-58.

[83] S.W. Sofie, F. Dogan, Freeze casting of aqueous alumina slurries with glycerol, J. Am. Ceram. Soc., 84 (2001) 1459-64.

[84] S. Ding, Y.P. Zeng, D. Jiang, Fabrication of mullite ceramics with ultrahigh porosity by gel freeze-drying, J. Am. Ceram. Soc., 90 (2007) 2276-2279.

[85] T. Fukasawa, Z.Y. Deng, M. Ando, Synthesis of porous silicon nitride with unidirectionally aligned channels using freeze-drying process, J. Am. Ceram. Soc., 85 (2002) 2151-55.

[86] D. Pérez-Coll, P. Nu´n˜ez, J.R. Frade, J.C.C. Abrantes, Conductivity of CGO and CSO ceramics obtained from freeze-dried precursors, Electrochim. Acta, 48 (2003) 1551-1557.

[87] J. Zhao, Y. He, L. Zhang, K. Lu, Preparation of porous TiO_2 powder with mesoporous structure by freeze-drying method, J. Alloys Compd., 678 (2016) 36-41.

[88] Y. Wang, M.D. Gawryla, D.A. Schiraldi, Effects of freezing conditions on the morphology and mechanical properties of clay and polymer/clay aerogels, J. Appl. Polym. Sci., doi: 10.1002/APP.39143, (2013) 1637.

[89] S. Farhan, R. Wang, H. Jiang, K. Li, C. Wang, A novel combination of simple foaming and freeze-drying processes for making carbon foam containing multiwalled carbon nanotubes, Ceram. Int., 42 (2016) 8980-8989.

[90] E.T. Thostenson, T.W. Chou, Microwave processing: fundamentals and applications, Composites: Part A, 30 (1999) 1055-1071.

[91] D.K Agrawal, Microwave processing of ceramics, Curr. Opin. Solid State Mater. Sci., 3 (1998) 480-485.

[92] R.R. Mishra, A.K. Sharma, Microwave-material interaction phenomena: Heating mechanisms, challenges and opportunities in material processing, Composites: Part A, 81 (2016) 78-97.

[93] K. Chandran, S. Anthonysamy, M. Lavanya, R. Sudha, P.R. Reshmi, D. Annie, R.R. Madhavan, T.N. Prasanthi, C. Sudha, S. Saroja, V. Ganesan, Studies on the chemical compatibility of alloy D9 with B_4C in the presence of sodium, Procedia Eng., 86 (2014) 631-638.

[94] H.J. Heuvel, P. Holler, P. Dunner, Absorber material cladding chemical interaction in vented fast breeder reactor absorber pins. B_4C/stainless steel

chemical interaction in sodium environment and effect of metallic Nb and Cr^4 layers, J. Nuclr. Mater., 130 (1985) 517.

[95] IGC Newsletter, Internal report, IGCAR, Kalpakkam, 3 December, 1986.

[96] R.M. German, Sintering theory and practice, John Wiley and Sons, INC. (1996).

[97] K. Lu, Sintering of nanoceramics, Int. Mater. Rev., 53 (2008) 21-38.

[98] C. Subramanian, A.K. Suri, Development of boron based neutron absorber materials, Met. Mater. Processes, 16 (2004) 39-52.

[99] A.G. Thomas, H.J. Jones, Hot pressing of ceramic powders, Powder Metall., 6 (1960) 160-169.

[100] M.N. Rahaman, Sintering of ceramics, CRC press, Taylor and Francis group, (2007).

[101] G.I. Kalandadze, S.O. Shalamberidze, A.B. Peikrishvili, Sintering of boron and boron carbide, J. Solid State Chem., 154 (2000) 194-198.

[102] X. Du, Z. Zhang, Y. Wang, J. Wang, W. Wang, H. Wang, Z. Fu, Hot-pressing kinetics and densification mechanisms of boron carbide, J. Am. Ceram. Soc., 1-7 (2015) 1-7.

[103] R. Angers, M. Beauvy, Hot-pressing of boron carbide, Ceram. Int., 10 (1983) 49-55.

[104] M.W. Chen, Microstructural characterization of commercial hot-pressed boron carbide ceramics, J. Am. Ceram. Soc., 88 (2005) 1935-1942.

[105] X. Zhang, H. Gao, Z. Zhang, R. Wen, G. Wang, J. Mu, H. Che, X. Zhang, Effects of pressure on densification behaviour, microstructures and mechanical properties of boron carbide ceramics fabricated by hot pressing, Ceram. Int., 43 (2017) 6345-6352.

[106] X. Zhang, Z. Zhang, R. Wen, G. Wang, X. Zhang, J. Mu, H. Che, W. Wang, Comparisons of the densification, microstructure and mechanical properties of boron carbide sintered by hot pressing and spark plasma sintering, Ceram. Int., 44 (2018) 2615-2619.

[107] S.L. Dole, S. Prochazka, R.H. Doremus, Microstructural coarsening during sintering of boron carbide, J. Am. Ceram. Soc., 72 (1989) 958-966.

[108] M.A. Kuzenkova, P.S. Kislyi, B.L. Grabchuk, N.I. Bodnaruk, The structure and properties of sintered boron carbide, J. Less-common Met., 67 (1979)

217-223.

[109] S. Roszeitis, B. Feng, H.P. Martin, A. Michaelis, Reactive sintering process and thermoelectric properties of boron rich boron carbides, J. Eur. Ceram. Soc., 34 (2014) 327-336.

[110] M. Suárez, A. Fernández, J.L. Menéndez, R. Torrecillas, H.U. Kessel, J. Hennicke, R. Kirchner, T. Kessel, Challenges and opportunities for spark plasma sintering: A key technology for a new generation of materials, http://www.intechopen.com/books/sintering-applications, http://dx.doi.org/10.5772/53706, INTECH Publications.

[111] D.V. Dudina, A.K. Mukherjee, Reactive spark plasma sintering: successes and challenges of nanomaterial synthesis, J. Nanomater., (2013), Article ID 625218, 1-12.

[112] O. Guillon, J.G. Julian, B. Dargatz, T. Kessel, G. Schierning, J. Räthel, M. Herrmann, Field-assisted sintering technology/spark plasma sintering: mechanisms, materials, and technology developments, Adv. Eng. Mater., 16 (2014) 830-849.

[113] Z.A. Munir, U.A. Tamburini, M. Ohyanagi, The effect of electric field and pressure on the synthesis and consolidation of materials: A review of the spark plasma sintering method, J. Mater. Sci., 41 (2006) 763-777.

[114] S. Hayun, V. Paris, M.P. Dariel, N. Frage, E. Zaretzky, Static and dynamic mechanical properties of boron carbide processed by spark plasma sintering, J. Eur. Ceram.Soc., 29 (2009) 3395-3400.

[115] S. Hayun, S. Kalabukhov, V. Ezersky, M.P. Dariel, N. Frage, Microstructural characterization of spark plasma sintered boron carbide ceramics, Ceram. Int., 36 (2010) 451-457.

[116] M. Cengiz, B. Yavas, Y. Celik, G. Goller, O. Yucel, F.C. Sahin, Spark plasma sintering of boron carbide ceramics using different sample geometries and dimensions, Proc. of the 3rd Int. Cong. APMAS2013, April 24-28, (2013), Antalya, Turkey, Acta Phys. Pol. A, 125 (2014) 260-262.

[117] B.M. Moshtaghioun, F.L. Cumbrera-Hernández, D. Gómez-García, S. de Bernardi-Martín, A. Domínguez-Rodríguez, A. Monshi, M.H. Abbasi, Effect of spark plasma sintering parameters on microstructure and room-temperature hardness and toughness of fine-grained boron carbide (B_4C), J.

Eur. Ceram. Soc., 33 (2013) 361-369.

[118] B.M. Moshtaghioun, F.L. Cumbrera, A.L. Ortiz, M.C. Rodríguez, D. Gómez-García, Additive-free superhard B_4C with ultrafine-grained dense microstructures, J. Eur. Ceram. Soc., 34 (2014) 841-848.

[119] P. Badica, S. Grasso, H. Borodianska, S.S. Xie, P. Li, P. Tatarko, M.J. Reece, Y. Sakka, O. Vasylkiv, Tough and dense boron carbide obtained by high-pressure (300 MPa) and low-temperature (1600 °C) spark plasma sintering, J. Ceram. Soc. Jap., 122 (2014) 271-275.

[120] X. Li, D. Jiang, J. Zhang, Q. Lin, Z. Chen, Z. Huang, Densification behaviour and related phenomena of spark plasma sintered boron carbide, Ceram. Int., 40 (2014) 4359-4366.

[121] K. Sairam, J.K. Sonber, T.S.R.Ch. Murthy, C. Subramanian, R.K. Fotedar, P. Nanekar, R.C. Hubli, Influence of spark plasma sintering parameters on densification and mechanical properties of boron carbide, Int. J. Refract. Met. Hard Mater., 42 (2014) 185-192.

[122] B.M. Moshtaghioun, A.L. Ortiz, D. Gómez-García, A. Domínguez-Rodríguez, Densification of B_4C nanopowder with nanograin retention by spark-plasma sintering, J. Eur. Ceram. Soc., 35 (2015) 1991-1998.

[123] W. Ji, S.S. Rehman, W. Wang, H. Wang, Y. Wang, J. Zhang, F. Zhang, Z. Fu, Sintering boron carbide ceramics without grain growth by plastic deformation as the dominant densification mechanism, Sci. Rep., 5, article number 15827, 1-8.

[124] B.M. Moshtaghioun, D. Gomez-Garcia, A. Dominguez-Rodriguez, R.I. Todd, Grain size dependence of hardness and fracture toughness in pure near fully-dense boron carbide ceramics, J. Eur. Ceram. Soc., 36 (2016) 1829-1834.

[125] R. Chaim, On densification mechanisms of ceramic particles during spark plasma sintering, Scr. Mater., 115 (2016) 84-86.

[126] B.M. Moshtaghioun, D. Gómez-García, A. Domínguez-Rodríguez, A.L. Ortiz, Enhancing the spark-plasma sinterability of B_4C nanopowders via room-temperature methylation induced purification, J. Eur. Ceram. Soc., 36 (2016) 2843-2848.

[127] R. Belon, G. Antou, N. Pradeilles, A. Maître, D. Gosset, Mechanical

behaviour at high temperature of spark plasma sintered boron carbide ceramics, Ceram. Int., 43 (2017) 6631-6635.

[128] M. Asadikiya, C. Rudolf, C. Zhang, B. Boesl, A. Agarwal, Y. Zhong, Thermodynamic modeling and investigation of the oxygen effect on the sintering of B_4C, J. Alloys Compd., 699 (2017) 1022-1029.

[129] M. Asadikiya, C. Zhang, C. Rudolf, B. Boesl, A. Agarwal, Y. Zhong, The effect of sintering parameters on spark plasma sintering of B_4C, Ceram. Int., 43 (2017) 11182-11188.

[130] D.O. Moskovskikh, K.A. Paramonov, A.A. Nepapushev, N.F. Shkodich, A.S. Mukasyan, Bulk boron carbide nanostructured ceramics by reactive spark plasma sintering, Ceram. Int., 43 (2017) 8190-8194.

[131] A.L. Ortiz, F. Sánchez-Bajo, V.M. Candelario, F. Guiberteau, Comminution of B_4C powders with a high-energy mill operated in air in dry or wet conditions and its effect on their spark-plasma sinterability, J. Eur. Ceram. Soc., 37 (2017) 3873-3884.

[132] M.F. Toksoy, W. Rafaniello, K.Y. Xie, L. Ma, K.J. Hemker, R.A. Haber, Densification and characterization of rapid carbothermal synthesized boron carbide, Int. J. Appl. Ceram. Technol., 14 (2017) 443-453.

[133] M. Zhang, T. Yuan, R. Li, S. Xie, M. Wang, Q. Weng, Densification mechanisms and microstructural evolution during spark plasma sintering of boron carbide powders, Ceram. Int., 44 (2018) 3571-3579.

[134] S.P.S. Badwal, Zirconia-based solid electrolytes: microstructure, stability and ionic conductivity, Solid State Ionics, 52 (1992) 23-32.

[135] E.C.S Rao, H.S. Maiti, Solid electrolytes with oxygen ion conduction, Solid State Ionics, 11 (1984) 317-338.

[136] H.G. Scott, Phase relationships in the zirconia-yttria system, J. Mater. Sci., 10 (1975) 1527-1535.

[137] C. Pascual, P. Duran, Subsolidus phase equilibria and ordering in the system ZrO_2-Y_2O_3, J. Am. Ceram. Soc., 66 (1983) 23-27.

[138] V.S. Stubican, Phase equilibria and metastabilities in the systems zirconia–magnesia, zirconia-calcia, and zirconia-yttria, S. Somiya, N. Yamamoto, H. Yanagida (Eds.), Sci. and Technol. Zirconia III, Adv. Ceram. 24A, The Am. Ceram. Soc., Ohio, Westerville (1988) 71-82.

[139] Y. Suzuki, Phase transition temperature of fluorite-type ZrO_2-Y_2O_3 solid solutions containing 8-44 mol.% Y_2O_3, Solid State Ionics, 81 (1995) 211-216.

[140] M. Yashima, M. Kakihana, M. Yoshimura, Metastable-stable phase diagrams in the zirconia-containing systems utilized in solid-oxide fuel cell application, Solid State Ionics, 86-88 (pt.2) (1996) 1131-1149.

[141] L. Li, O.V.D. Biest, P.L. Wang, J. Vleugels, W.W. Chen, S.G. Huang, Estimation of the phase diagram for the ZrO_2-Y_2O_3-CeO_2 system, J. Eur. Ceram. Soc., 21 (2001) 2903-2910.

[142] T.H. Etsell, S.N. Flengas, The electrical properties of solid oxide electrolytes, Chem. Rev., 70 (1970) 339-376.

[143] I.G. Juan, B. Ferrari, M.T. Colomer, Influence of the urea content on the YSZ hydrothermal synthesis under dilute conditions and its role as dispersant agent in the post-reaction medium, J. Eur. Ceram. Soc., 29 (2009) 3185-3195.

[144] Y.B. Khollam, A.S. Deshpande, A.J. Patil, H.S. Potdar, S.B. Deshpande, S.K. Date, Synthesis of yttria stabilized cubic zirconia (YSZ) powders by microwave-hydrothermal route, Mater. Chem. Phys., 71 (2001) 235-241.

[145] X. Xin, L.U. Zhe, Z. Ding, X. Huang, Z. Liu, X. Sha, Y. Zhang, W. Su, Synthesis and characteristics of nanocrystalline YSZ by homogeneous precipitation and its electrical properties, J. Alloys Compd., 425 (2006) 69-75.

[146] R. Srinivasan, R.J.D. Angelis, G.I. Burtron, Identification of tetragonal and cubic structures of zirconia using synchrotron X-radiation source, J. Mater. Res., 6 (1991) 1287-1292.

[147] M.M. Kashani-Motlagh, A. Maghsoudipour, L. Majidzadeh Gorjani, F. Hashemzadeh, Synthesis and characterization of cubic yttria-stabilized zirconia (8YSZ) nanoparticles by a modified sol-gel route using sucrose and pectin as organic precursors, Int. J. Phys. Sci., 6 (2011) 2518-2525.

[148] K. Haberko, A. Ciesla, A. Pron, Sintering behaviour of yttria-stabilized zirconia powders prepared from gels, Ceramurg. Int., 1 (1975) 111-116.

[149] C. Suciu, A.C. Hoffmann, A. Vik, F. Goga, Effect of calcination conditions and precursor proportions on the properties of YSZ nanoparticles obtained

by modified sol-gel route, J. Chem. Eng., 138 (2008) 608-615.

[150] Z. Wang, R. Hui, N. Bogdanovic, Z. Tang, S. Yick, Y. Xie, I. Yaroslavski, A. Burgess, R. Maric, D. Ghosh, Plasma spray synthesis of ultra-fine YSZ powder, J. Power Sources, 170 (2007) 145-149.

[151] S.T. Aruna, N. Balaji, K.S. Rajam, Phase transformation and wear studies of plasma sprayed yttria-stabilized zirconia coatings containing various mol.% of yttria, Mater. Charact., 62 (2011) 697-705.

[152] D.S. Patil, K. Prabhakaran, R. Dayal, C.D. Prasad, N.M. Gokhale, A.B. Samui, S.C. Sharma, Eight mole percent yttria stabilized zirconia powders by organic precursor route, Ceram. Int., 34 (2008) 1195-1199.

[153] S. Vatansever, F. Oksuzomer, S.N. Koc, M. Somer, H. Deligoz, M.A. Gurkaynak, Fabrication of yttria-stabilized zirconia nanoparticles by the reverse microemulsion method for SOFC applications, Mater. Sci. Poland, 28 (2010) 85-91.

[154] A. Ringuede, J.A. Labrincha, J.R. Frade, A combustion synthesis method to obtain alternative cermet materials for SOFC anodes, Solid State Ionics, 141-142 (2001) 549-557.

[155] R.E. Juarez, D.G. Lamas, G.E. Lascalea, N.E.W. de Reca, Synthesis of nanocrystalline zirconia powders for TZP ceramics by nitrate-citrate combustion route, J. Eur. Ceram. Soc., 20 (2000) 133-138.

[156] Q. Wang, R. Peng, C. Xia, W. Zhu, H. Wang, Characteristics of YSZ synthesized with a glycine-nitrate process, Ceram. Int., 34 (2008) 1773-1778.

[157] C.A. da Silva, N.F.P. Ribeiro, M.M.V.M. Souza, Effect of the fuel type on the synthesis of yttria-stabilized zirconia by combustion method, Ceram. Int., 35 (2009) 3441-3446.

[158] K.A. Singh, L.C. Pathak, S.K. Roy, Effect of citric acid on the synthesis of nano-crystalline yttria-stabilized zirconia powders by nitrate-citrate process, Ceram. Int., 33 (2007) 1463-1468.

[159] A.K. Shukla, V. Sharma, N.A.l Dhas, K.C. Patil, Oxide-ion conductivity of calcia- and yttria-stabilized zirconias prepared by rapid-combustion route, Mater. Sci. Eng., B, 40 (1996) 153-157.

[160] T. He, Q. He, N. Wang, Synthesis of nano-sized YSZ powders from glycine-

nitrate process and optimization of their properties, J. Alloys Compd., 396 (2005) 309-315.

[161] J. Yang, J. Lian, Q. Dong, Q. Guan, J. Chen, Z. Guo, Synthesis of YSZ nanocrystalline particles via the nitrate-citrate combustion route using diester phosphate (PE) as dispersant, Mater. Lett., 57 (2003) 2792-2797.

[162] I. Kaus, P.I. Dahl, J. Mastin, T. Grande, M.A. Einarsrud, Synthesis and characterization of nanocrystalline YSZ powder by smoldering combustion synthesis, J. Nanomater., 206 (2006) 1-7.

[163] M. Biswas, P.K. Ohja, E.M. Jayasingh, C.D. Prasad, Synthesis of nanocrystalline yttria-stabilized zirconia for SOFC, Nanomater. Nanotehnol., 1 (2011) 55-58.

[164] K. Nomura, Y. Mizutani, M. Kawai, Y. Nakamura, O. Yamamoto, Aging and Raman scattering study of scandia and yttria doped zirconia, Solid State Ionics, 132 (2000) 235-239.

[165] https://www.intechopen.com/books/developments-in-combustion-technology/solution-combustion-synthesis-applications-in-oxide-electronics,

[166] K.C. Patil, M.S. Hegde, T. Rattan, S.T. Aruna, Chemistry of nanocrystalline oxide materials-combustion synthesis, properties and applications, World scientific publishing Co. Pte. Ltd., (2008).

[167] S.T. Aruna, A.S. Mukasyan, Combustion synthesis and nanomaterials, Curr. Opin. Solid State Mater. Sci., 12 (2008) 44-50.

[168] A.S. Mukasyan, P. Epstein, P. Dinka, Solution combustion synthesis of nanomaterials, Proc. Combust. Inst., 31 (2007) 1789-1795.

[169] G. Liu, K.C. Jiangtao, Combustion synthesis of refractory and hard materials: a review, Int. J. Refract. Met. Hard Mater., 39 (2013) 90-102.

[170] K.C. Patil, S.T. Aruna, T. Mimani, Combustion synthesis: an update, Curr. Opin. Solid State Mater. Sci., 6 (2002) 507-512.

[171] K.C. Patil, S.T Aruna, S. Ekambaram, Combustion synthesis, Curr. Opin. Solid State Mater. Sci., 2 (1997) 158-165.

[172] K. Laishram, R. Mann, N. Malhan, A novel microwave combustion approach for single step synthesis of α-Al_2O_3 nanopowders, Ceram. Int., 38 (2012) 1703-1706.

[173] L.C. Nehru, V. Swaminathan, C. Sanjeeviraja, Rapid synthesis of

nanocrystalline ZnO by a microwave-assisted combustion method, Powder Technol., 226 (2012) 29-33.

[174] R.V. Mangalaraja, J. Mouzon, P. Hedstorm, C.P. Camurri, S. Ananthakumar, M. Oden, Microwave-assisted combustion synthesis of nanocrystalline yttria and its powder characteristics, Powder Technol., 191 (2009) 309-314.

[175] V. Chandramouli, S. Anthonysamy, P.R.V. Rao, R. Divakar, D. Sundararaman, PVA aided microwave synthesis: a novel route for the production of nanocrystalline thoria powders, J. Nucl. Mater., 231 (1996) 213-220.

[176] V.P. Pakharukova, E.M. Moroz, D.A. Zyuzin, V.I. Zaikovskii, F.V. Tuzikov, G.R. Kosmambetova, P.E. Strizhak, Structure characterization of nanocrystalline yttria-stabilized zirconia powders prepared via microwave-assisted synthesis, J. Phys. Chem. C, 116 (2012) 9762-9768.

[177] L. Combemale, G. Caboche, D. Stuerga, D. Chaumont, Microwave synthesis of yttria-stabilized zirconia, Mater. Res. Bull., 40 (2005) 529-536.

[178] Standard test methods for chemical, mass spectrometric and spectrochemical analysis of nuclear grade boron carbide, ASTM C791-12 (2012) 1-26.

[179] N.N. Greenwood, A. Earnshaw, Chemistry of elements, Ed. 2, Butterworth Heinemann, Elsevier, India, (1997) 203-204.

[180] V.K. Manchanda, M.S. Subramanian, Volumetric Determination of Boron in Boron Carbide, BARC Report no.1017 (1979).

[181] J. Mendham, R.C. Denney, J.D. Barnes, M.J.K. Thomas, VOGEL’S text book of quantitative chemical analysis, Ed. 6, Pearson Education Limited, Dorling Kindersley (India) Pvt. Ltd., (2007), 384-385.

[182] D. Annie, V. Chandramouli, S. Anthonysamy, Wet chemical method for determination of free carbon content in boron carbide, Int. J. Chem. Anal. Sci., 7 (2016) 1-4.

[183] B.D. Cullity, Elements of X-ray diffraction, Ed. 2, Addison-Wesley publishing Company INC, (1978), 102.

[184] C. Suryanarayana, M. Grant Norton, X-ray diffraction a practical approach, Plenum Press, Newyork and London, (1998).

[185] Technical note, Malvern Instruments, Dynamic light scattering: an

introduction in 30 minutes, MRK656-01

[186] R. Pecora, Dynamic light scattering measurement of nanometer particles in liquids, J. Nanopart. Res., 2 (2000) 123-131

[187] J.B. Condon, Surface area and porosity determinations by physisorption measurements and theory, Ed. 1, Elsevier, (2006).

[188] S. Lowell, J.E. Shields, Powder surface area and porosity, Ed. 2, Powder technology series, Ed. B. Scarlet, Chapman and Hall Ltd., (1984).

[189] Practical scanning electron microscopy: Electron and ion microprobe analysis, Ed. 1, Ed. J.I. Goldstein, H. Yakowitz, D.E. Newbury, E. Lilshin, J.W. Colby, J.R. Coleman, Plenum Press, New York, (1975).

[190] Electron Microscopy: The Basics, written by B. Voutou, Eleni-Chrysanthi Stefanaki based on the lecture of Dr. Konstantinos Giannakopoulos National Center for Scientific Research 'Demokritos', Greece. Physics of Advanced Materials Winter School (2008).

[191] P.F. Kane, G.B. Larrabee, Characterizations of solid surfaces, Plenum press, London, (1978).

[192] D.B. Williams, C.B. Carter, Transmission electron microscopy, Springer, Plenum press, Newyork and London, (1996).

[193] S. Wartewig, IR and Raman spectroscopy: fundamental processing, WILEY-VCH GmbH & Co. KGaA, Weinheim, (2003).

[194] G.S. Bumbrah, R.M. Sharma, Raman spectroscopy-Basic principle, instrumentation and selected applications for the characterization of drugs of abuse, Egypt. J. Forensic Sci., 6 (2016) 209-215.

[195] G.D. Quinn, R. Gettings, L.K. Ives, A standard reference material for Vickers hardness of ceramics and hard materials, HARDMEKO 2004, Hardness measurements theory and application in laboratories and industries, 11-12 November, (2004), Washington, D.C., USA

[196] E. Barsoukov, J.R. Macdonald, Impedance spectroscopy theory, experiment, and applications, Ed. 2, A John Wiley & Sons, Inc., (2005).

[197] A.R. West, Solid state chemistry and its applications, John Wiley and Sons PTE. Ltd., Singapore, Indian edition, (2009).

[198] V.F. Lvovich, Impedance spectroscopy- Applications to electrochemical and dielectric phenomena, John Wiley & Sons, Inc., (2012).

[199] Y.H. Roos, M. Karel, T.P. Labuza, H. Levine, M. Mathlouthi, D. Reid, E. Shalaev, L. Slade, Melting and crystallization of sugars in high-solids systems, J. Agric. Food Chem., 61 (2013) 3167-3178.

[200] J.J. Donoghue, D. Hubbard, Thermal expansion studies of boric oxide glass and of crystalline boric oxide, Natl. Bur. Stand., Res. Pap. RP1425, Part J. Res. J.'Xational Bur. Stand., 27 (1941) 371-379.

[201] A.W. Weimer, W.G. Moore, R.P. Roach, J.E. Hitt, R.S. Dixit, Kinetics of carbothermal reduction synthesis of boron carbide, J. Am. Ceram. Soc., 75 (1992) 2509-2514

[202] N. Cho, K.G. Silver, Y. Berta, R.F. Speyer, Densification of carbon-rich boron carbide nanopowder compacts, J. Mater. Res., 22 (2007) 1354-1359.

[203] H. Lee, R.F. Speyer, Sintering of boron carbide heat-treated with hydrogen, J. Am. Ceram. Soc., 85 (2002) 2131-33.

[204] H. Lee, R.F. Speyer, Pressureless sintering of boron carbide, J. Am. Ceram. Soc., 86 (2003)1468-73.

[205] P.D. Williams, D.D. Hawn, Aqueous dispersion and slip casting of boron carbide powder: Effect of pH and oxygen content, J. Am. Ceram. Soc., 74 (1991) 1614-18.

[206] K.H. Kim, J.H. Chae, J.S. Park, D.K. Kim, K.B. Shim, B.H. Lee, Methanol washing effects on spark plasma sintering behaviour and mechanical properties of B_4C ceramics, J. Ceram. Process. Res., 8 (2007) 238-242.

[207] M.B. Pomfret, C. Stoltz, B. Varughese, R.A. Walker, Structural and compositional characterization of yttria-stabilized zirconia: evidence of surface-stabilized, low-valence metal species, Anal. Chem., 77 (2005) 1791-1795.

[208] M. Mazaheri, A.M. Zahedi, M.M. Hejazi, Processing of nanocrystalline 8 mol.% yttria-stabilized zirconia by conventional, microwave-assisted and two-step sintering, Mater. Sci. Eng., A, 492 (2008) 261-267.

[209] C.C. Chen, M.M. Nasrallah, H.U. Anderson, Synthesis and characterization of YSZ thin film electrolytes, Solid State Ionics, 70/71 (1994) 101-108.

[210] J.M. Calderon-Moreno, M. Yoshimura, Characterization by Raman spectroscopy of solid solutions in the yttria-rich side of the zirconia-yttria system, Solid State Ionics, 154-155 (2002) 125-133.

[211] B.P. Michael, J.C. Owrutsky, R.A. Walker, High-temperature Raman spectroscopy of solid oxide fuel cell materials and processes, J. Phys. Chem. B, 110 (2006) 17305-17308.

[212] A. Paul, B. Vaidhyanathan, J. Binner, Micro-Raman spectroscopy of indentation induced phase transformation in nanozirconia ceramics, Adv. Appl. Ceram., 110 (2011) 114-119.

[213] A.J. Semjonow, E. Anastassakis, Asymmetry of defect-induced Raman spectra in yttria-stabilized zirconia, Physica A, 201 (1993) 416-420.

[214] R. Frison, S. Heiroth, J.L.M. Rupp, K. Conder, E.J. Barthazy, E. Muller, M. Horisberger, M. Dobeli, L.J. Gauckler, Crystallization of 8 mol.% yttria-stabilized zirconia thin-films deposited by RF-sputtering, Solid State Ionics, 232 (2013) 29-36.

[215] E.F. Lopez, V.S. Escribano, M. Panizza, M.M. Carnasciali, G. Busca, Vibrational and electronic spectroscopic properties of zirconia powders, J. Mater. Chem., 11 (2001) 1891-1897.

[216] B.P. Michael, C. Stoltz, B. Varughese, R.A. Walker, Structural and compositional characterization of yttria-stabilized zirconia: evidence of surface stabilized, low-valence metal species, Anal. Chem., 77 (2005) 1791-1795.

[217] I. Kosacki, V. Petrovsky, H.U. Anderson, Raman spectroscopy of nanocrystalline ceria and zirconia thin films, J. Am. Ceram. Soc., 85 (2002) 2646-2650.

[218] C.M. Phillippi, K.S. Mazdiyasni, Infrared and Raman spectra of zirconia polymorphs, J. Am. Ceram. Soc., 54 (1971) 254-258.

[219] V.G. Keramidas, W.B. White, Raman scattering study of the crystallization and phase transformations of $ZrO_{2,}$ J. Am. Ceram. Soc., 57 (1974) 22-24.

[220] A. Feinberg, C.H. Perry, Structural disorder and phase transitions in ZrO_2-Y_2O_3 system, J. Phys. Chem. Solids, 42 (1981) 513-518.

[221] K. Rajeswari, M.B. Suresh, U.S. Hareesh, Y.S Rao, D. Das, R. Johnson, Studies on ionic conductivity of stabilized zirconia ceramics (8YSZ) densified through conventional and non-conventional sintering methodologies, Ceram. Int., 37 (2011) 3557-3564.

[222] P. Mondal, A. Klein, W. Jaegermann, H. Hahn, Enhanced specific grain

boundary conductivity in nanocrystalline Y_2O_3-stabilized zirconia, Solid State Ionics, 118 (1999) 331-339.